



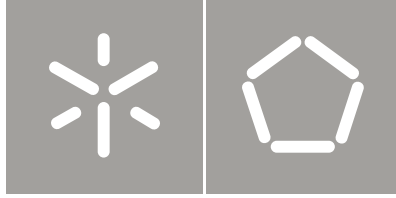
Universidade do Minho
Escola de Engenharia

Nguyen Trong Quyen

Macro-mechanical modelling and simulation
of textile fabric and clothing with S-FEM

Nguyen Trong Quyen | Macro-mechanical modelling and simulation
of textile fabric and clothing with S-FEM





Universidade do Minho
Escola de Engenharia

Nguyen Trong Quyen

Macro-mechanical modelling and simulation
of textile fabric and clothing with S-FEM

Tese de Doutoramento
Programa Doutoral em Engenharia Têxtil

Trabalho efectuado sob a orientação do
Professor Doutor Fernando Batista Nunes Ferreira
Universidade do Minho

Professor Doutor Abel João Padrão Gomes
Universidade da Beira Interior - Departamento de Informática

DECLARAÇÃO

Nome

Nguyen Trong Quyen

Endereço electrónico: quyenum@gmail.com Telefone: _____ / _____

Número do Bilhete de Identidade: B3647207 (Passport ID)

Título dissertação /tese

Macro-mechanical modelling and simulation of textile fabric and clothing with S-FEM

Orientador(es):

Professor Doutor Fernando Batista Nunes Ferreira

Professor Doutor Abel João Padrão Gomes Ano de conclusão: 2014

Designação do Mestrado ou do Ramo de Conhecimento do Doutoramento:

Programa Doutoral em Engenharia Têxtil

DE ACORDO COM A LEGISLAÇÃO EM VIGOR, NÃO É PERMITIDA A REPRODUÇÃO DE QUALQUER PARTE DESTA TESE.

Universidade do Minho, 03 / 03 / 2014

Assinatura: _____

Acknowledgements

First of all, I would like to give thanks for all things unto God and the Father in the name of our Lord Jesus Christ, who is and who was and who has listened to my prayers and given me with the strength and resolve to embark on this on-going academic path.

First and foremost, I would like to take this opportunity to express my profound gratitude and deep regards to my supervisors, Professor Fernando Batista Nunes Ferreira (Department of Textile Engineering, University of Minho, Portugal), Professor Abel Gomes (Department of Informatics, University of Beira Interior, Portugal), and Professor Ngo Chi Trung (Department of International Cooperation, Hanoi University of Science and Technology, Vietnam) for their exemplary guidance, monitoring and constant encouragement throughout the course of this thesis. Their help, support and guidance allowed me to learn a lot from their great scientific skills during my PhD period, between 2010 and 2014, at University of Minho, Guimarães, Portugal, what shall carry me a long way in the journey of life on which I am about to embark after finishing up this academic stage.

I am very grateful to my colleagues and friends at University of Minho for giving me very enjoyable moments both in private and scientific life in Portugal. It is also an occasion to thank my Vietnamese friends and the Vietnamese community who have encouraged and helped me during my period in Portugal.

I would like to give my special thanks to my parents Tuyen and Quyen, my wife Thanh, my daughters Nha Thy and Khanh Thy, my sister Tuyen and my brother Quoc for their patient love and their stimulating support. They have encouraged me to go ahead with my research, what enabled me to complete this work.

Finally, this study would not have been possible without the support of the BRIDGING THE GAP Erasmus Mundus project funded by the European Commission programme Erasmus Mundus External Cooperation Windows - Lot 12 and implemented by the University of Trento. This project has given me invaluable opportunities to daily experience new ways of thinking, studying and living in Europe.

Campus of Azurém, Guimarães, Portugal, March 03, 2014

Nguyen Trong Quyen

EMECW L12 MOBILITY GRANT AWARD CONTRACT BTG_559

Grant agreement n 2009/1661-001 001ECW

Resumo

Esta tese propõe um método de elementos finitos, designado por S-FEM (*Smoothed Finite Element Method*), para modelação e análise mecânica de estruturas têxteis planas. Neste enquadramento teórico, supõe-se que a estrutura têxtil não-tecida é um material isotrópico elástico, enquanto a estrutura têxtil tecida é um material elástico com anisotropia ortotrópica, para os quais as leis constitutivas utilizam propriedades mecânicas de baixa pressão (*low stress*) com base na Medição Objetiva de Tecidos (FOM - *Fabric Objective Measurement*).

As formulações de elementos finitos de baixa ordem baseadas em deslocamento quando aplicadas a elementos finitos de placas (*plate/shell*) quadriláteras de 4 nós, incluindo campos de tensão de cisalhamento transversal, baseiam-se nas contribuições de Raymond Mindlin e por Eric Reissner, no que agora se designa teoria de deformação por cisalhamento de primeira ordem (*first-order shear deformation*, do inglês, ou FSDT de forma abreviada), ou simplesmente teoria de Mindlin-Reissner, e nas abordagens MITC (*Mixed Interpolation of Tensorial Components*), são nesta tese combinadas com a técnica de suavização do/da gradiente/tensão nos termos dos modelos S-FEM por forma a mitigar problemas como são o caso da distorção de elementos finitos, da granularidade grosseira da malha, bem como dos bem conhecidos fenómenos de bloqueio. As malhas de quadriláteros são utilizadas nesta tese devido à sua capacidade de representar geometrias complexas de tecidos em resultado de deformações mecânicas como são os casos da recuperação face à pressão planar, flexão, deformação, vibração, drapejamento, etc.

Refira-se que foi desenvolvido e implementado em Matlab um software para os novos modelos de elementos finitos, em grande medida devido à inexistência de modelos S-FEM em softwares de análise de elementos finitos (*finite element analysis* ou FEA), lacuna esta que ocorre quer em softwares comerciais, quer não comerciais, e até em códigos abertos. Exemplos numéricos para as aplicações básicas de engenharia no que respeita à modelação mecânica de folhas de tecido fino e de folhas de tecido de espessura média em estudos de casos típicos, como é o caso da recuperação face a pressão planar, flexão, deformação e comportamento livre de vibrações, indicam que os elementos finitos (*plate/shell*) desenvolvidos com a técnica de suavização de tensão e MITC acabam por aliviar os efeitos de distorção dos elementos, a granularidade grosseira da malha e efeito de bloqueio na modelação e análise mecânica de tecidos muito finos e até mesmo de tecidos de espessura média.

Os modelos de elementos finitos de placas (*plate/shell*) desenvolvidos durante o trajeto desta tese, bem como as suas propriedades mecânicas de baixa tensão em termos de FOM, são, portanto, bem adaptados à modelação e análise numérica de deformação macro-mecânica de folhas de tecido muito fino e de folhas de tecido de espessura média, incluindo ao mesmo tempo análise de deformação mecânica simples e complexa.

Abstract

An S-FEM (Smoothed Finite Element Method) for mechanical analysis and modelling of the textile fabrics is proposed. In this theoretical framework, one assumes that the non-woven fabric is an elastic isotropic material, while the woven fabric is an elastic with orthotropic anisotropy for which the constitutive laws formulated are using low-stress mechanical properties based on FOM (Fabric Objective Measurement). The displacement-based low-order finite element formulations for four-node quadrilateral plate/shell finite element, including assumed transverse shear strain fields, are based on the contributions of Raymond Mindlin and by Eric Reissner as FSDT (first-order shear deformation theory and so-called the Mindlin-Reissner theory) together with MITC (Mixed Interpolation of Tensorial Components) approaches, which are combined with the gradient/strain smoothing technique in terms of S-FEM models contributed by G. R. Liu et al. in order to mitigate problems as element distortion, mesh coarseness as well as the well-known locking phenomena. Quadrilateral meshes are used due to ability to represent complicated geometries of complex mechanical deformation of the fabric such as plane stress recovery, bending, buckling, vibration, draping behavior, etc. The finite element computer codes were developed in MATLAB for the new formulated plate/shell finite element models due to the lack of FEM (Finite Element Method) packages for S-FEM models in both commercial and non-commercial FEA (Finite Element Analysis) computer applications, and even from open-source platforms. Numerical examples for the basic engineering applications of mechanical modelling of thin to moderately thick fabric sheet in the typical case studies such as in-plane stress recovery, bending, buckling and free-vibration behavior, indicate that the developed plate/shell finite elements with assumed strain smoothing technique and MITC, do alleviate element distortion, mesh coarseness, and locking effect even for mechanical analysis and modelling very thin to moderately thick fabric. The developed plate/shell finite element models and low-stress mechanic properties in terms of FOM are, therefore, well adapted for numerical analysis and modelling of macro-mechanical deformation of the thin to moderately thick fabric sheet including both simple and complex mechanical deformation analysis.

Contents

Acknowledgements.....	i
Resumo.....	iii
Abstract.....	v
Contents.....	vi
List of abbreviations.....	ix
List of figures.....	x
List of tables.....	xv
List of symbols	xvii
1 Introduction.....	1
1.1 Overview.....	1
1.2 Cloth simulation approaches	4
1.3 Analytic and numerical methods in cloth simulation.....	10
1.4 Thesis statement	17
1.5 Objectives.....	17
1.6 Organization of the thesis.....	19
1.7 Contribution of the thesis	20
1.8 References.....	21
2 Fabric objective measurement and Constitutive equation formulations.....	30
2.1 Introduction	30
2.1.1 Roles of fabric objective measurement.....	30
2.1.2 Fabric objective measurement, KES-FB and SiroFAST system	33
2.1.3 The configuration of KES-FB system.....	36
2.1.4 The configuration of SiroFAST system.....	37
2.2 Mechanical parameters.....	38
2.3 Experimental analysis of fabric properties with KES-FB system.....	40
2.3.1 Tensile and shear test (KES-FB1).....	40
2.3.2 Pure bending test (KES-FB2)	43

2.3.3	<i>Compression test (KES-FB3)</i>	43
2.3.4	<i>Surface test (KES-FB4)</i>	44
2.4	Formulation of constitutive laws for fabric deformations	45
2.4.1	<i>Tensile stress and tensile strain, uniaxial applied force</i>	46
2.4.2	<i>Tensile stress and tensile strain, plane stress and bending</i>	47
2.4.3	<i>The transverse shear strain</i>	50
2.4.4	<i>Coordinate transformation of warp yarns and weft yarns for the loading direction</i>	51
2.5	Final remarks.....	54
2.6	References.....	56
3	Theoretical formulations of S-FEM for textile fabrics	59
3.1	Introduction	60
3.2	Preliminaries.....	61
3.2.1	<i>Domains and boundaries</i>	61
3.2.2	<i>Governing equations</i>	61
3.2.3	<i>Domain discretization and continuity conditions</i>	63
3.2.4	<i>Integration in space</i>	64
3.2.5	<i>Integration in time</i>	67
3.3	The strain/gradient smoothing technique	69
3.3.1	<i>Introduction</i>	69
3.3.2	<i>The smoothing operator</i>	71
3.4	Analysis of bending, buckling and vibrational behavior of plate	74
3.4.1	<i>Introduction</i>	74
3.4.2	<i>Kinetic equations</i>	74
3.4.3	<i>Four-node quadrilateral plate bending element</i>	77
3.4.4	<i>Strain-smoothing operation</i>	80
3.5	Analysis of plane-stress problems	85
3.5.1	<i>Introduction</i>	85
3.5.2	<i>Four-node quadrilateral membrane element with normal rotation</i>	85
3.5.3	<i>Strain-smoothing operation</i>	87
3.6	Analysis of shell structures	88
3.6.1	<i>Four-node quadrilateral flat shell element</i>	88

3.6.2	<i>The warped configuration</i>	92
3.6.3	<i>Elements in the global coordinate system</i>	93
3.7	Final remarks.....	95
3.8	References.....	97
4	Numerical examples and discussions.....	102
4.1	Numerical examples	102
4.1.1	<i>Buckling behavior of woven fabric</i>	104
4.1.2	<i>Buckling behavior of woven fabric in terms of free-vibration behavior</i>	118
4.1.3	<i>Bending behavior of woven fabric</i>	131
4.1.4	<i>Plane-stress problems of woven fabric</i>	135
4.2	Discussions	143
4.2.1	<i>Number of smoothing domains</i>	143
4.2.2	<i>CPU time variation</i>	144
4.3	Final remarks.....	145
4.4	References.....	147
5	Conclusions	149
5.1	Research outcomes	149
5.2	Limitations.....	150
5.3	Future works.....	151
5.4	Final remarks.....	151

List of abbreviations

AEM	Applied Element Method
ASTM	American Society for Testing and Materials
CAA	Computer-Aided Analysis
CAD	Computer-Aided Design
CAE	Computer-Aided Engineering
CAM	Computer-Aided Manufacturing
CAP	Computer-Aided Planning
CIM	Computer-Integrated Manufacturing
CS-FEM	Cell-Based Smoothed Finite Element Method
DOF	Degrees of Freedom
ES-FEM	Edge-Based Smoothed Finite Element Method
FAST/SiroFAST	Fabric Assurance by Simple Testing
FDM	Finite-Difference Method
FEA	Finite Element Analysis
FEM	Finite Element Method
FOM	Fabric Objective Measurement
FSDT	First-order Shear Deformation Theory
FS-FEM	Face-Based Smoothed Finite Element Method
FVM	Finite-Volume Method
GFEM	Generalized Finite Element Method
KES-FB	Kawabata Evaluation System for Fabric
MRP	Material Requirements Planning
MSD	Mass-Spring-Damper
NS-FEM	Node-based Smoothed Finite Element Method
ODE	Ordinary Differential Equations
PDE	Partial Differential Equation
PIM	Point Interpolation Methods
S-FEM	Smoothed Finite Element Methods
XFEM	Extended Finite Element Method
α FEM	Alpha Finite Element Method

List of figures

Figure 1.1: Finite element predictions of the ballistic impact of Kevlar® woven fabric at high initial projectile velocities, yarn slip increases the time to failure and the deflection of the fabric by decreasing the warp yarn tension at the point of impact. Images of experiment (top) and simulated contours of the warp yarn tension (middle and bottom) at time after impact.....	2
Figure 1.2: Modelling of the damage mechanism of woven fabric composite model using CAE.....	3
Figure 1.3: Spring-mass models via particle system for anisotropic bending stiffness, with possible rest curvature defined on the surface (left), along precise lines (center) and additional stiffness with their own custom rest length (right).....	7
Figure 1.4: Examples of spring/mass models via particle system approach (from left to right): Maya nCloth simulation, Blender's built in cloth dynamics and Havok cloth simulation	8
Figure 1.5: Finite element modeling and control of flexible fabric parts	12
Figure 1.6: A finite-volume method for contact drape simulation of woven fabrics and garments....	12
Figure 1.7: Prediction of the ballistic impact on a Kevlar® woven fabric: Yarn slip in an unloaded specimen that was tested at $v = 362$ m/s (top) and simulation of the test (bottom): (a), (a') Slip displacement in the direction of the weft yarns predicts unraveling of the weave at the free edges of the fabric, (b), (b ') Yarn slip in the direction of the weft yarns increases the warp yarn pitch at the edge of the fabric.....	13
Figure 1.8: (a) Top; (b) Isometric; (c) Zoomed isometric views of a 40×40 cm wool fabric of which a quadrant is fixed over a 20×20 cm pedestal. The bottom element edges are portrayed by chained lines	14
Figure 1.9: Pressure distribution of the body wearing the cotton one-piece dress, front (left) and back (right)	14
Figure 2.1: Relationship between the three primary hand values and the mechanical properties....	34
Figure 2.2: The KES-FB system for measuring fabric mechanical properties.....	36
Figure 2.3: The principal directions of warp yarns, weft yarns and bias of woven fabric.	39
Figure 2.4: Graph chart with typical curves of tensile test, plot of tensile stress–strain.....	41
Figure 2.5: Graph chart with typical curves of shear test, plot of shear stress against shear strain.	42
Figure 2.6: Graph chart with typical curves of bending test, plot of bending moment against curvature.	43
Figure 2.7: Graph chart with typical curves of compression test.	44
Figure 2.8: Graph chart with typical curves of surface frictional (a) and surface roughness (b).	44

Figure 2.9: The warp and weft directions of woven fabrics due to their yarn-based structure denoted with 1 and 2 in orthotropic axes of sheet material and the transverse direction denoted with 3.....	46
Figure 2.10: Definition of shearing strains.	48
Figure 2.11: The free-body diagrams for the in-plane stresses in the warp yarns direction.	52
Figure 3.1: Domain, Neumann and Dirichlet boundaries.....	61
Figure 3.2: Example of finite elements and Neumann and Dirichlet boundaries.....	63
Figure 3.3: Example of the division of a four-node quadrilateral element into the smoothing domains in CS-FEM by connecting between the opposite mid-segment points of smoothing domains: a) 1 SD; b) 2 SDs; c) 3 SDs; and d) 4 SDs.....	71
Figure 3.4: A four-node quadrilateral plate bending element.	74
Figure 3.5: The problem domain is divided into quadrilateral elements, each discretized element of domain is further divided into SD smoothing domains: a) 1 SD; b) 2 SDs; c) 3 SDs; d) 4 SDs.	80
Figure 3.6: The shape function of local point in the element. l_1 is the proportion of b to a and similarly to l_2	82
Figure 3.7: A four-node quadrilateral membrane element with normal rotation.....	85
Figure 3.8: Formation of the four-node shell element.....	88
Figure 3.9: A four-node quadrilateral flat shell element undergoes bending and twisting, as well as in-plane deformation.	89
Figure 3.10: Warped and projected quadrilateral shell element to flat geometric transformation. ...	92
Figure 4.1: General configuration of geometrical and mechanical properties of fabric sample.....	102
Figure 4.2: Numerical results for strain energy of twelve buckling modes of a CSCS plain-woven fabric sheet h_1/l with different mesh density subjected uniform load.	106
Figure 4.3: Numerical results for strain energy of twelve buckling modes of a SCSF plain-woven fabric sheet h_1/l with different mesh density subjected uniform load.	107
Figure 4.4: Numerical results for strain energy of twelve buckling modes of a CFFF plain-woven fabric sheet h_1/l with different mesh density subjected uniform load.	107
Figure 4.5: Numerical results for strain energy of twelve buckling modes of a CSCS plain-woven fabric sheet h_2/l with different mesh density subjected uniform load.	108
Figure 4.6: Numerical results for strain energy of twelve buckling modes of a SCSF plain-woven fabric sheet h_2/l with different mesh density subjected uniform load.	108
Figure 4.7: Numerical results for strain energy of twelve buckling modes of a CFFF plain-woven fabric sheet h_2/l with different mesh density subjected uniform load.	109
Figure 4.8: Buckling modes of a CFFF plain-woven fabric sheet with h_1/l , using 20×20 Q4 elements and 1 smoothing domain per element.	110

Figure 4.9: Resultant displacement magnitude for buckling modes of a CFFF plain-woven fabric sheet with $h1/l$	111
Figure 4.10: Buckling modes of a CSCS plain-woven fabric sheet with $h1/l$, using 20×20 Q4 elements and 1 smoothing domains per element.	112
Figure 4.11: Resultant displacement magnitude for buckling modes of a CSCS plain-woven fabric sheet with $h1/l$	113
Figure 4.12: Buckling modes of a SCSF plain-woven fabric sheet with $h2/l$, using 20×20 Q4 elements and 1 smoothing domains per element.	114
Figure 4.13: Resultant displacement magnitude for modes of buckling of a SCSF plain-woven fabric sheet with $h2/l$	115
Figure 4.14: Buckling modes of a CFFF plain-woven fabric sheet with $h2/l$, using 20×20 Q4 elements and 1 smoothing domains per element.	116
Figure 4.15: Resultant displacement magnitude for modes of buckling of a CFFF plain-woven fabric sheet with $h2/l$	117
Figure 4.16: Numerical results for strain energy of twelve vibration modes of a CSCS plain-woven fabric sheet $h1/l$ with different mesh density subjected natural frequency.	120
Figure 4.17: Numerical results for strain energy of twelve vibration modes of a SCSF plain-woven fabric sheet $h1/l$ with different mesh density subjected natural frequency.....	120
Figure 4.18: Numerical results for strain energy of twelve vibration modes of a CFFF plain-woven fabric sheet $h1/l$ with different mesh density subjected natural frequency.....	121
Figure 4.19: Numerical results for strain energy of twelve vibration modes of a CSCS plain-woven fabric sheet $h2/l$ with different mesh density subjected natural frequency.	121
Figure 4.20: Numerical results for strain energy of twelve vibration modes of a SCSF plain-woven fabric sheet $h2/l$ with different mesh density subjected natural frequency.....	122
Figure 4.21: Numerical results for strain energy of twelve vibration modes of a CFFF plain-woven fabric sheet $h2/l$ with different mesh density subjected natural frequency.....	122
Figure 4.22: Modes of vibration for a CFFF plain-woven fabric sheet with $h1/l$, using 20×20 Q4 elements and 1 smoothing domains per element.	123
Figure 4.23: Resultant displacement magnitude for modes of free-vibration for a CFFF plain-woven fabric sheet with $h1/l$	124
Figure 4.24: Modes of vibration for a CSCS plain-woven fabric sheet with $h1/l$, using 20×20 Q4 elements and 1 smoothing domains per element.	125
Figure 4.25: Resultant displacement magnitude for modes of free-vibration for a CSCS plain-woven fabric sheet with $h1/l$	126

Figure 4.26: Modes of vibration for a SCSF plain-woven fabric sheet with $h2/l$, using 20×20 Q4 elements and 1 smoothing domains per element.	127
Figure 4.27: Resultant displacement magnitude for modes of free-vibration of a SCSF plain-woven fabric sheet with $h2/l$	128
Figure 4.28: Modes of vibration for a CFFF plain-woven fabric sheet with $h2/l$, using 20×20 Q4 elements and 1 smoothing domains per element.	129
Figure 4.29: Resultant displacement magnitude for modes of free-vibration of a CFFF plain-woven fabric sheet with $h2/l$	130
Figure 4.30: Numerical results for strain energy of non-dimensional transverse displacements of the plain-woven fabric sheet $h1/l$ with different mesh density and boundary conditions subjected uniform load.....	133
Figure 4.31: Numerical results for strain energy of non-dimensional transverse displacements of a plain-woven fabric sheet $h2/l$ with different mesh density and boundary conditions subjected uniform load.....	133
Figure 4.32: Bending behavior of plain-woven fabric sheet with $h2/l$, using 20×20 Q4 elements and 1 smoothing domains per element with different boundaries.....	134
Figure 4.33: Resultant displacement magnitude for bending behavior of plain-woven fabric sheet with $h2/l$	134
Figure 4.34: Configuration of tensile stress and tensile strain, uniaxial applied force in the direction of warp and weft yarns.	136
Figure 4.35: The plane-stress deformation of a plain-woven fabric sheet with $h1/l$, under uniaxial applied force in warp direction, using 70×70 Q4 elements and 1 smoothing domains per element.	137
Figure 4.36: Resultant load vector for plane-stress deformation of a plain-woven fabric sheet with $h1/l$, under uniaxial applied force in warp direction.....	138
Figure 4.37: The magnitude of the stress of a plain-woven fabric sheet with $h1/l$, under uniaxial applied force in warp direction.	138
Figure 4.38: The plane-stress deformation of a plain-woven fabric sheet with $h1/l$, under uniaxial applied force in weft direction, using 70×70 Q4 elements and 1 smoothing domains per element.	139
Figure 4.39: Resultant load vector for plane-stress deformation of a plain-woven fabric sheet with $h1/l$, under uniaxial applied force in weft direction.....	139
Figure 4.40: The magnitude of the stress of a plain-woven fabric sheet with $h1/l$, under uniaxial applied force in weft direction.	140

Figure 4.41: The plane-stress deformation of a plain-woven fabric sheet with $h2/l$, under uniaxial applied force in warp direction, using 70×70 Q4 elements and 1 smoothing domains per element.	140
Figure 4.42: Resultant load vector for plane-stress deformation of a plain-woven fabric sheet with $h2/l$, under uniaxial applied force in warp direction.	141
Figure 4.43: The magnitude of the stress of a plain-woven fabric sheet with $h2/l$, under uniaxial applied force in warp direction.	141
Figure 4.44: The plane-stress deformation of a plain-woven fabric sheet with $h2/l$, under uniaxial applied force in weft direction, using 40×40 Q4 elements and 1 smoothing domains per element.	142
Figure 4.45: Resultant load vector for plane-stress deformation of a plain-woven fabric sheet with $h2/l$, under uniaxial applied force in weft direction.	142
Figure 4.46: The magnitude of the stress of a plain-woven fabric sheet with $h2/l$, under uniaxial applied force in weft direction.	143
Figure 4.47: Recorded of CPU time on the numerical simulation results of bending behavior of a plain-woven fabric sheet using S-FEM and standard FEM.	144

List of tables

Table 1.1: Features summary of cloth-modeling work	5
Table 2.1: The six basic fabric mechanical properties and corresponding quality and performance attributes of fabrics and garments	31
Table 2.2: Typical fabric properties measured in FOM	32
Table 2.3: The possibility application of fabric objective measurement technology	32
Table 2.4: Primary fabric handle	35
Table 2.5: The parameters describing fabric mechanical and surface properties	37
Table 2.6: The low-stress mechanical parameters measured on the FAST system	38
Table 2.7: The major elasticity parameters of the fabric used in the mechanical modelling and simulation.	39
Table 2.8: The addition of elasticity parameters according to the transverse direction of the fabric needed to develop the numerical models in this research in this research.....	39
Table 2.9: Options of instruments for measuring the low-stress mechanical properties of fabric of which results used for calculating elasticity parameters.	40
Table 2.10: The physical parameters of fabric	40
Table 2.11: Constitutive equations for displacement-based low-order finite element formulations of plate and shell finite element	54
Table 3.1 Versions of S-FEM Models and Properties.	70
Table 3.2 Typical types of smoothing domains	72
Table 3.3: List of space-discretized equations of motions.....	95
Table 4.1: Mechanical properties of plain-woven fabric samples	103
Table 4.2: Geometrical configurations for numerical examples.....	103
Table 4.3: Dirichlet boundary conditions	104
Table 4.4: Numerical output of twelve eigenbuckling modes for a CCCC/SSSS/SCSF/CFFF plain-woven fabric sheet with $h1/l$, using 20×20 Q4 elements and 1 smoothing domain per element (Q4SD1)	105
Table 4.5: Numerical output of twelve eigenbuckling modes for a CCCC/SSSS/SCSF/CFFF plain-woven fabric sheet with $h2/l$, using 20×20 Q4 elements and 1 smoothing domain per element (Q4SD1)	105

Table 4.6: Numerical output of twelve eigenvibration modes for a CSCS/SCSF/CFFF plain-woven fabric sheet with $h1/l$, using 20×20 Q4 elements and $SDs = 1,4$ smoothing domains per element.....	118
Table 4.7: Numerical output of twelve eigenvibration modes for a CSCS/SCSF/CFFF plain-woven fabric sheet with $h2/l$, using 20×20 Q4 elements and $SDs = 1,4$ smoothing domains per element.....	119
Table 4.8: Non-dimensional bending displacement of a square fabric sheet with various mesh densities, under uniform pressure, simply-supported (SSSS), clamped (CCCC) and (SCSF) boundary conditions.....	132

List of symbols

General symbols, vector, matrices and tensors

∇_s	Symmetric-gradient operator
∇	Gradient operator
$\nabla \cdot$	Divergence operator
Γ	Boundary of the medium
Γ_t	Neumann boundary of the medium
Γ_u	Dirichlet boundary of the medium
Ω	Domain of the medium
Ω^e	The discretized finite element domain
Ω^s	The smoothing domain
Φ	The smoothing or weight function
F	System load vector
f	Finite element load vector
B	Strain-displacement matrix or so-called gradient matrix
D	Material matrix
K	System stiffness matrix
M	System mass matrix
N	Shape function matrix
k	Finite element stiffness matrix
m	Finite element mass matrix
q	Nodal degrees of freedom vector
\dot{q}	Generalized nodal velocity vector
\ddot{q}	Generalized nodal accelerations vector
t	Time
Δt	Time increment
u	Generalized displacement vector
λ	Critical buckling load
ω	Frequency
γ	Shear vector

ϵ	Strain vector
κ	Curvature strain vector
σ	Stress vector

Material characteristics

E	Young's modulus
G	Shear modulus, or rigidity modulus, expressing the shearing rigidity
B	Bending rigidity
K	Bulk's modulus
ν	Poisson's ratios
ρ	Mass per unit area (also known as basis weight and grammage)
h	Thickness

Superscripts

b	Curvature/bending element
g	Geometric element
m	Membrane element
p	Plate bending element
s	Transverse shear element

Subscripts

1, 2, 3	The principal directions of orthotropic material corresponding to the 1-, 2-, and 3-axes
<i>warp, weft, bias</i>	The principal directions of woven fabric sheet corresponding to directions of warp yarns, weft yarns and bias
x, y, z	The principal directions of Cartesian coordinate system corresponding to the x -, y -, and z -axes
12, xy	The double subscript for shear stress, the first subscript indicates the direction normal to the surface/selvedge over which the shear stress is acting and the second subscript indicates the direction in which the stress is acting

1.1 Overview

Analytic modelling and numerical simulation have played important roles in science and engineering of textiles and clothing. In fact, together with the development of the fabric objective measurement technology (FOM) and the revolution of computers, they are recognized as one of the major technological transformations to mankind [1-8]. The engineering design is the procedure of definition of the dimensional and physical characteristics of a textile fabric product for the achievement of the desirable handle, performance and appearance [9, 10], which correspond closely to a synthesis of functional specifications, mechanical properties, aesthetic effects, etc., depending on the wearing process [2, 9, 11, 12]. Nowadays, textile materials are also being used in a broad range of technical products, such as the production of fibrous and reinforcements in composites in automotive, aerospace, marine and civil engineering applications [13, 14], smart textiles for protection [15, 16], textiles for medical applications, etc. [17, 18]. Therefore, the prediction of the end-product's mechanical properties and the aesthetic features of the textile fabrics before the actual fabrication is of major importance in the automation and integration of processes in the textile and clothing industry [19-21]. In most of the engineering sectors, advanced computational approaches in which numerical methods have been widely developed are applied in modelling and simulation of complex problems of engineering and mathematical physics to predict how a product reacts to real-world forces, vibration, heat, fluid flow and other physical effects, etc. [22]. This is important to verify the feasibility, benefits and drawbacks of the product, in terms of time, quality and cost improvements and in terms of capability to establish a better collaborative working approaches [7, 23]. These principal tasks have been analyzed, designed and implemented as computer applications, in particular CAE (Computer-Aided Engineering) systems, which provide services and facilities to foster the intelligent and efficient use of the computing technologies in engineering tasks such as textile, garment and fashion [7, 19, 24, 25]. Note that CAE solutions comprise CAD (Computer-Aided Design), FEA (Finite Element Analysis), CAA (Computer-Aided Analysis), CIM (Computer-Integrated Manufacturing), CAM (Computer-Aided Manufacturing), MRP (Material Requirements Planning) and CAP (Computer-Aided Planning).

Nowadays, CAE is an essential analysis tool in many engineering fields, namely aero engineering, civil engineering, medical engineering, textile and cloth engineering, in large because this technology enables to accurately predict the deformation behaviour of specific engineering structures under specific loading conditions, as illustrated in Figures 1.1 and 1.2. In this respect, FEM (Finite Element Method) plays an essential role in CAE systems, because it allows us to find the efficient analytical and numerical solution of variational problems in science and engineering, particularly in the textile area. Examples of FEM/FEA systems are ANSYS, ABAQUS, COMSOL, MSC Nastran, etc. [26-28]. In practice, FEM is also known as Finite Element Analysis (FEA), being thus considered as a computerized method for predicting how a product reacts to real-world forces, vibration, heat, fluid flow and other physical effects.

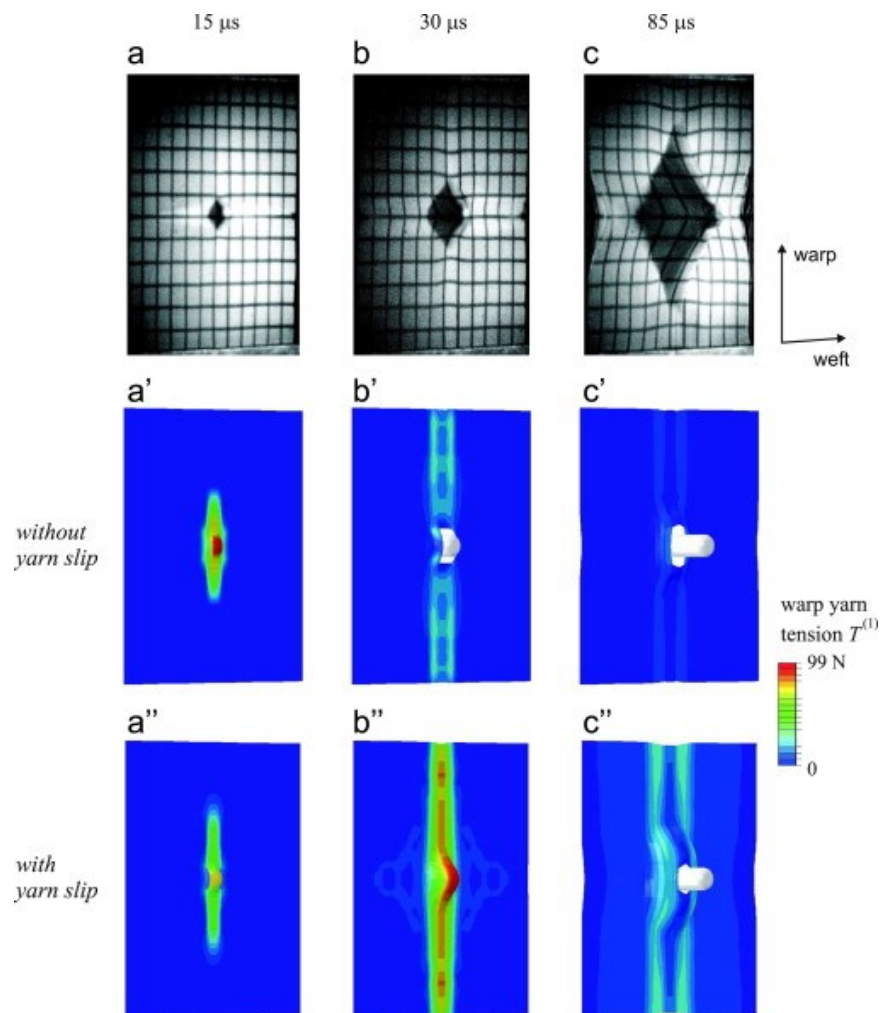


Figure 1.1: Finite element predictions of the ballistic impact of Kevlar® woven fabric at high initial projectile velocities, yarn slip increases the time to failure and the deflection of the fabric by decreasing the warp yarn tension at the point of impact. Images of experiment (top) and simulated contours of the warp yarn tension (middle and bottom) at time after impact. [29]

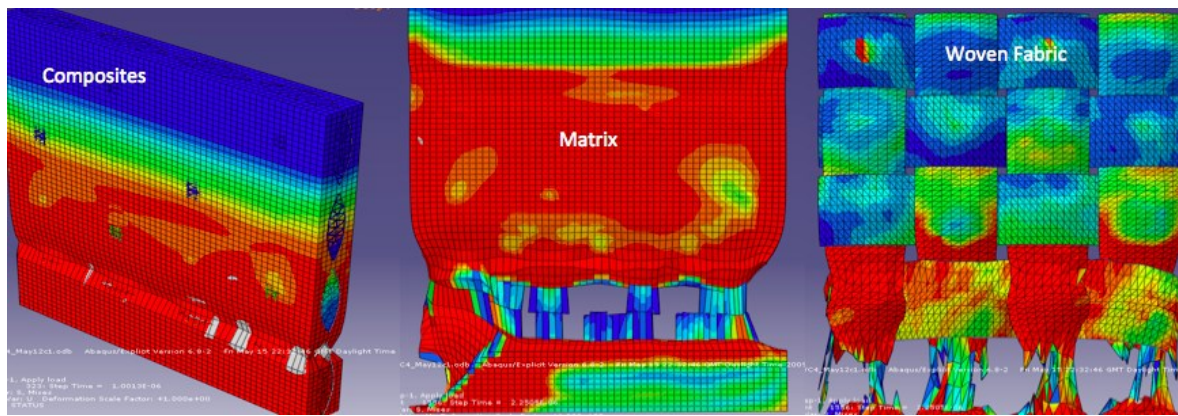


Figure 1.2: Modelling of the damage mechanism of woven fabric composite model using CAE. [30]

FEA shows whether a product will break, wear out or work the way it was designed. It is called analysis, but in the product development process, it is used to predict what is going to happen when the product is used. FEA works by breaking down a real object into a large number (thousands to hundreds of thousands) of finite elements, such as little cubes. Mathematical equations help to predict the behaviour of each element. A computer then adds up all the individual behaviours to predict the behaviour of the actual object as a whole.

FEM is one of the most efficient numerical solutions to predict the mechanical behaviours of textile fabric products affected by many physical effects, including the following ones:

- Mechanical stress
- Mechanical vibration
- Fatigue
- Motion
- Heat transfer
- Fluid absorption
- Electrostatics

On the other hand, the textile fabrics are flexible, either homogeneous or inhomogeneous, and porous materials with elastic orthotropic anisotropy. These unique characteristics make textile structures to be able to deform differently when compared with other engineering sheet materials. Besides, the textile fabrics are characterized by an increased structural complexity because of the complex combination of their structural units and their interactions. These complex characteristics of the textiles' mechanics and their application in many engineering areas make them ideal objects for the mechanical modelling and simulation using FEM/FEA, as well as computer-based methods.

This introductory chapter focuses on the investigation of mechanical modelling and simulation approaches for the textile fabrics and cloth. A brief state-of-the-art of the computational models for the mechanical deformation of fabric, as well as the development of quadrilateral plate and shell finite element models, are presented. Based on these models, the difficulties towards a comprehensive finite element model for modelling and simulation of the textile fabrics are highlighted in order to give room to motivation, scope and objectives of the present work.

1.2 Cloth simulation approaches

One of the first attempts at analytic modelling of woven fabric structures was reported by R. Haas [31] in the aerodynamic literature in German early 1910s, in the period of worldwide development of airships. However, it was Peirce [32] who first started off research in the bending behaviour of fabric and the measurement of its material properties in 1930s, having in that time presented a geometrical and a mathematical force model of the plain-weave structure that is today considered as the pioneering work in the analytical mechanical modelling of the textile fabrics [33]. These two models due to Haas and Peirce were extensively used and considerably developed by subsequent researchers and most advanced features can be found in surveys and publications [34-36].

In general, the analytical modelling and numerical simulation of the textile fabric products on both experimental and theoretical research can be subjected to simple or complex deformation behaviours to predict fabric performance. In case of simple deformations, the principal tests include tensile, shearing, bending, compression and surface, while buckling, draping behaviour and mechanical vibration are complex deformations [37]. Regardless of deformation of fabric be simple or complex, the low-stress mechanical properties play an important role, especially in handle, performance and appearance of fabric and is particularly indispensable in modelling and simulation of the textile fabrics [38-40]. It is a well-known fact that the KES-FB and SiroFAST [10] systems are based on the development of fabric objective measurement related to fabric hand principle and govern the low-stress mechanical properties of fabric to meet industry's needs for a reliable method of predicting fabric handle, performance and appearance [1, 2].

Unlike the mechanical models that are used in solving mechanical engineering problems, as needed to make the analysis of deformable structures, a large amount of new challenges arise from the highly versatile nature of the textile fabrics, several approaches for modelling and simulation were proposed,

from which a large number of combination of methods that have emerged and evolved as those shown in Table 1.1.

Table 1.1: Features summary of cloth-modeling work

Approach	Authors	Methods	Time	Parameters
Geometrical	Weil [41]	Curve fitting, subdivision, relaxation	Fast*	Positions of constraint points
	Agui et al. [42]	Polygonization, relaxation	Fast*	Bending angle, thresholds
	Hinds et al. [43]	3D interaction, interpolation	Fast*	Geometrical offset from object
	Ng et al. [44]	Mapping	Fast	Various functions
Physical	Feynman [45]	Energy minimization, multigrid method	Fast	Elasticity, bending, gravity
	Terzopoulos et al. [46]	Elasticity theory, Lagrange's theory	Medium*	Density, damping, metric, curvature tensor
	Aono [47]	Elasticity theory, D'Alembert's principle, finite difference	Medium*	Stress, strain, Young's modulus, rigidity, Poisson's ratio, density, damping, Lamé constant
	Thalmann et al. [48]	Deformable model, Newtonian dynamics	Medium	Deformable model's parameters
	Volino et al. [49]	Newtonian dynamics, elasticity theory	Medium on SCI	Stress, strain, Young's modulus, rigidity, Poisson's coefficient, density, thickness
	Breen et al. [50]	Energy minimization, Newtonian dynamics	Long on IBM RS6000/320	Repulsion, stretching, bending, trellis, gravity
	Okabe et al. [51]	Energy minimization, elasticity theory	Medium on IBM RS6000/320	Elongation, shearing, bending, twisting, density
	Li et al. [52]	Simplified Navier-Stokes equation, Bernoulli's equation, deformable model	Fast on SGI Power	Air velocity, deformable model's parameters

	Provot [53]	Newtonian dynamics, Euler integration	Fast on Sparc 10	Mass, stiffness, damping, viscosity
	Ng et al. [54]	Energy minimization, multigrid method	Fast	Elasticity, bending, gravity
	Hearle et al. [55]	Energy-based approach	Fast*	Elasticity, extension, bending, friction
Hybrid	Rudomin [56]	Convex hull, deformable model	Medium*	Shape of the object, deformable model's parameters
	Kunii et al. [57]	Energy minimization, singularity theory, curve fitting	Medium*	Mass, stiffness, positions of characteristic points
	Taillefer [58]	Curve fitting, relaxation	Fast*	Positions of hanging points, stretching, bending, weight, self-repulsion
	Tsopelas [59]	Thin-wall deformation, elastica, NURBS fitting	Medium on Sparc 2	Thickness, diameter, rigidity
	Dhande et al. [60]	Swept surface generation	Fast*	Directrix curve, generatrix curve

* is estimated.

Source: Hing et al [36].

The textile cloth modeling approaches can be therefore classified into three following categories [5, 8, 9, 34, 36, 45, 61-66]:

- Geometrically-based – This approach has to do with cloth appearance rather than performance, particularly folds and creases represented by a set of geometrical equations. However, it is lacked of optional parameters on simulation due to not consider the physical properties of cloth. It requires a considerable manipulation and intervention from user that can be regarded as an advanced drawing tool. [67, 68]
- Physically-based – This approach applies to both static and dynamic simulation of cloth and is considered as the most efficient approach (Figure 1.3). Cloth can be modeled using triangular or rectangular meshes of finite mass points as vertices or nodes. Physically-based approaches include energy-minimization and force calculation methods. The energy-based method represent the distributed energies on meshes as a set of equations and achieve a local minimum energy state by moving the discrete mass points of the mesh. The force-based

method computes forces acting between the discrete points and integrate over the resulting differential equations using numerical methods to calculate the displacement of each point at each time step. [54, 69-72]

- Hybrid-based – It is the combination of physical and geometrical methods. [56, 59, 60, 73]

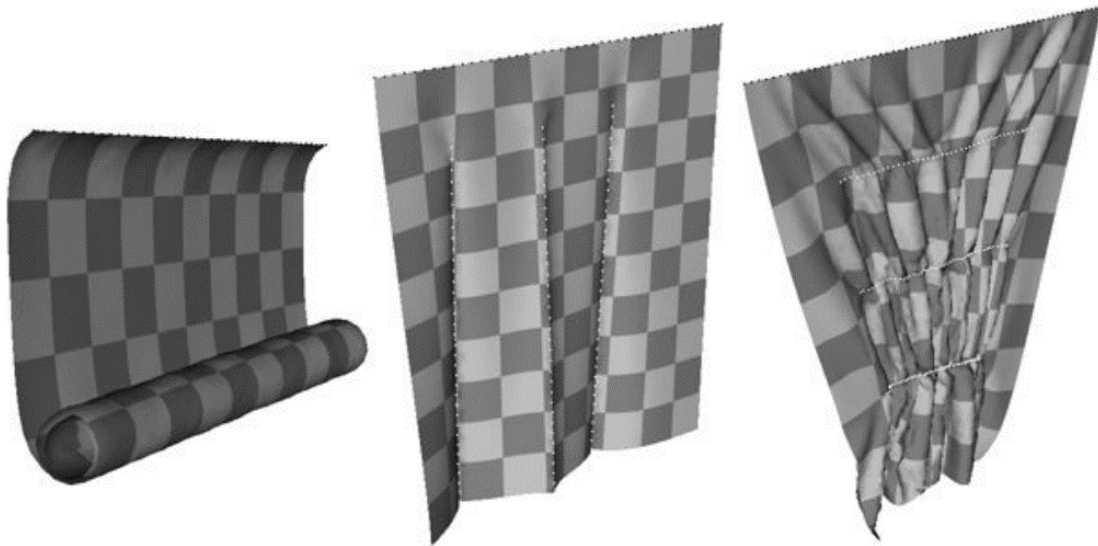


Figure 1.3: Spring-mass models via particle system for anisotropic bending stiffness, with possible rest curvature defined on the surface (left), along precise lines (center) and additional stiffness with their own custom rest length (right). [71]

Since the early 1980's, cloth simulation has been an important topic in computer graphics in which modelling and simulation of the textile fabrics generally refers to the simulation of soft-body dynamics [74-76]. It focuses on visually realistic physical simulations and can be done by using a variety of approaches such as energy minimization methods [46, 77], shape matching [72, 78] and rigid-body based deformation [79]. Rendering effects produce a visually plausible emulation of textiles and clothing, which is used in a variety of contexts, e.g., video games, animation, film, etc. Many real-time graphics engines are provided by either commercial source code or open source code for soft-body and rigid-body dynamics simulation that may be used in collision detection and response algorithms; for example, Autodesk Maya nCloth, Havok Cloth, NVIDIA PhysX Technology are examples of commercial software, while Blender (Stichting Blender Foundation), OpenCloth are known as open source software and so forth as illustrated in Figure 1.4. The applicable scope of soft body dynamics is quite broad, not only simulation deformable materials such as clothing and fabric but also simulation of soft organic materials such as muscle, fat, hair and vegetation, etc.



Figure 1.4: Examples of spring/mass models via particle system approach (from left to right): Maya nCloth simulation, Blender's built in cloth dynamics and Havok cloth simulation. [80-82]

Up to date, there are two main methods that have been extensively used for decades to present as:

- Mass-Spring-Damper system – It has been successfully applied to simulate many kinds of soft things, such as creatures and clothes via particle systems, but the actual structure of real cloth at the yarn level can be ignored [83-87]. They have been used extensively in cloth simulation [66, 88-92] since the pioneering work of Terzopoulos et al [93]. Much effort has been made to improve this model to address the anisotropic property of cloth in computer aided garment prototyping, such as the inverse dynamics procedure to eliminate super-elongation of the springs [53]; the heuristic method of handling post-buckling instability to achieve stable but responsive simulation [91]; the implicit integration method to take large time steps [76]. However, there are several publications concerning the selection of spring constant for a given behaviour [94-96]. Unfortunately, it can be shown that mass-spring-damper systems fail to describe a continuum mechanical solid because of difficulty to control efficiently realistic physically-based behaviors [97]. In spring/mass models, finite mass points act as a system of particles connected with elastic springs obeying Hooke's law. There is a distinction between the two solvers for spring-mass models that can be expressed as follows:
 - Force-based techniques are to determine the internal spring forces and external forces (due to contact, gravity, air resistance, wind, etc.) acting on the nodes at each time step and Newton's second law gives differential equations for the motion of the nodes. The simple explicit solvers, e.g. Euler integration, are appropriate to create high resolution cloth with realistic stiffness.

-
- Position-based dynamics techniques are based on constraint relaxation in which the distance between the connected nodes will be equal to the initial distance to avoid an expensive implicit solution of a system of ordinary differential equations, which is solved sequentially and iteratively, by directly moving nodes to satisfy each constraint, until cloth gains sufficiently stiffness. Many real-time graphics engines use position based dynamics as PhysX, Havok Cloth, Maya nCloth, etc. [98].
 - Finite element simulation – This a more physically accurate approach, which uses a finite element based numerical method to solve the partial differential equations (PDE) and compute component displacements, strains and stresses under internal and external loads [99-101]. A body is required to be subdivided into finite elements, which has several advantages such as accurate representation of complex geometry, inclusion of dissimilar material properties, easy representation of the total solution and capture of local effects [27, 102]. The cloth/fabric is modeled as a three-dimensional elastic continuum by breaking its surface into a large number of connected finite elements and solving for the energy principles in structural mechanics of the fabric (e.g. stresses-strains relation, Hooke's law, bending stiffness and other mechanical properties) under the specific boundary conditions. The equations of motions are obtained by integrating the stress fields over each of elements and relating this, via Newton's second law, to the nodal accelerations and velocities. The finite element based numerical methods has been extensively used in mechanical modelling and simulation of the textile fabrics for many modelling scales: yarns, fabric unit cell and either single or multi fabric layer [64, 103-108]. However, FEM has only had a marginal role in cloth simulation compared with spring/mass models via particle systems [107, 109, 110].

In view of the above classification of approaches, physically-based simulation has been widely accepted as the most effective approach, which divides into two subcategories of models: simplified models and analysis and numerical models.

In general, the simplified models (e.g. in case of soft body dynamics) conform to visually plausible emulations rather than accurate scientific/engineering simulations in order to satisfy real-time requirements, while analytic and numerical models are concerned with the simulation of the actual mechanical behavior of materials and not tied that much about time. In this thesis, we are mainly interested in analytic and numerical methods for the textile fabric material simulation.

1.3 Analytic and numerical methods in cloth simulation

There is quite a large number of numerical methods used in the literature. The most popular methods for continuum modelling are FEM (Finite Element Method), FDM (Finite Difference Method) and Boundary Element Method (BEM). In discontinuum modelling, the most known methods are DEM (Distinct Element Method), DDA (Discontinuous Deformation Analysis) and BPM (Bonded Particle Model). There are more two other methods, MM (Meshless Methods) and Artificial Neural Networks (ANN) that do not fit in previous two categories. The physical and mathematical settings generally lead to a set of PDE (Partial Differential Equation), which are then turned into ODE (Ordinary Differential Equations), for which standard methods for numerical integration exist. To solve PDEs, either inside the continuum or on the boundaries of the discretization, they have to be discretized in space by finite elements, yielding a set of ODEs, which are then solved using suitable numerical time integration schemes [111]. Implicit integration methods require the solution of possibly large systems of equations that may be linear or nonlinear in space-time. Therefore, FEM emerged as a more physically accurate approach, which uses the widely used finite element based model to solve the PDEs which govern the dynamics of an elastic material [112].

The application of the numerical methods in the textile mechanics, in particular those concerning FEM (Finite Element Method), firstly appeared in the late 1960's, when a project using computer programs were initiated by Hearle, Konopasek and Newton at University of Manchester Institute of Science and Technology (UMIST) [113]. Recent studies about the numerical analysis and modelling of textile fabrics implemented a modelling hierarchy based on modelling scales as follows [114-121]:

- The micro-mechanical modelling: generally for yarn-level simulation [122-124]
- The meso-mechanical modelling: generally for simulation at the fabric unit cell level [125-128]
- The macro-mechanical modelling: usually for simulation at the fabric sheet level [64, 103, 129]

In the context of FEA in textile fabric engineering, there are many publications about analysis and modelling of either simple or complex deformations of woven fabric and this specific area has attracted the interest of many researchers from many engineering sectors. In early 1980's, Lloyd [130, 131] presented a finite element model to analysis of the complex deformations of the textile fabrics, such as the ballistic deformation of a knitted fabric. The NONSAP finite element programs were used for computing the model. However, this model only considers in-plane deformations and neglected bending, twisting deformations and transverse shear-strain fields. During 1980's, there was very few

noticeable works on finite element simulation of textile cloth. The limitation of computer hardware and software in addition with the traditional of textile could be the reason.

The finite element modelling of the textile fabrics has increasingly received attention since the late 1980's and early 1990's. Most of the existing approaches in mechanical modelling of the textile fabrics are based on or related to the geometrically exact thin shell formulation proposed by Simo et al. [132, 133]. Collier et al. [110] used geometric nonlinear shell membrane finite elements to predicted the draping performance. They treated the draping behaviour of fabric as an orthotropic material whose tensile moduli in the warp and weft direction of fabric were obtained by using the Tensile and Shear Tester of KES-FB (Kawabata Evaluation System for Fabric) and literature values of Poisson's ratio also were determined. The resulted approach agreed between experimental and predicted drape coefficients.

Gan et al. [107] also used geometric nonlinear shell/plate elements to model large fabric deformation, such as drape. They assumed fabrics as linear elastic orthotropic material and their modelling results are in agreement compared with experimental data. Chen and Govindaraj [134] applied a shear flexible shell theory to predict fabric drape. The fabric is taken to be a continuous orthotropic medium and used finite element formulations to solve the governing equations under particular boundary conditions. Characteristics of fabric include Young's modulus in the warp and weft directions, shear modulus in bias direction and Poisson's ratio.

Kang and Yu [135] developed a nonlinear finite element code in order to simulate the 3D drape shapes of woven fabrics. The fabric was assumed as an elastic material with orthotropic anisotropy and fabric drape was considered to be a geometric nonlinear phenomenon. Unlike former finite element formulations, Etmuss et al. [136] presented a linear finite element approach based on a plane-stress assumption. The corotational strain formulation is used to account for arbitrary rigid body transformations, while bending behavior is treated separately from in-plane deformation. The resulting equation system is solved by using an efficient implicit time integration scheme.

Eischen et al. [109] used software based on nonlinear shell theory to simulate 3D motions related to real fabric-manufacturing processes (Figure 1.5). This model is bounded to rectangular cloth surfaces and built from experimental curves of fabric characteristics obtained by using KES-FB. Their study focuses on the accuracy model by precisely simulating mechanical behavior of fabric and then comparing the bending and buckling properties with the mechanical property values from real fabric experiments.

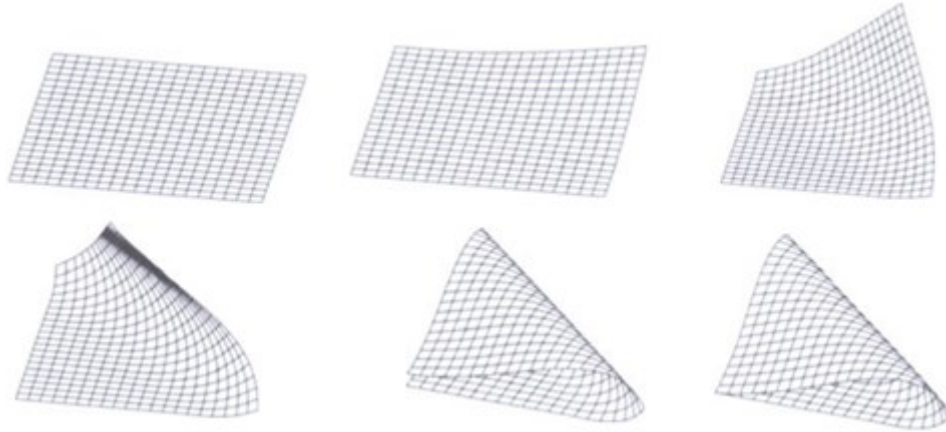


Figure 1.5: Finite element modeling and control of flexible fabric parts [109]

Chen and his coworkers [129] presented extended work of a geometrically nonlinear FVM (Finite-Volume Method) developed by themselves to predict contact drape deformations of woven fabrics. This model includes the computing of the out-of-plane bending and in-plane membrane strain energies of the fabric sheet, which is divided into a number of structured finite volumes based on mesh lines along the warp and weft directions. The equilibrium equations of the fabric sheet are derived from employing the principle of stationary total potential energy and solved by using the Newton-Raphson method. They compared numerical simulation of two square fabric sheets with available experimental results showing a close match between them (Figure 1.6). However, the main disadvantage of a finite-volume method is much more computations required compared to a FDM (Finite-Difference Method) or FEM. Thus it costs much more than numerical solutions delivered by a FDM or FEM.

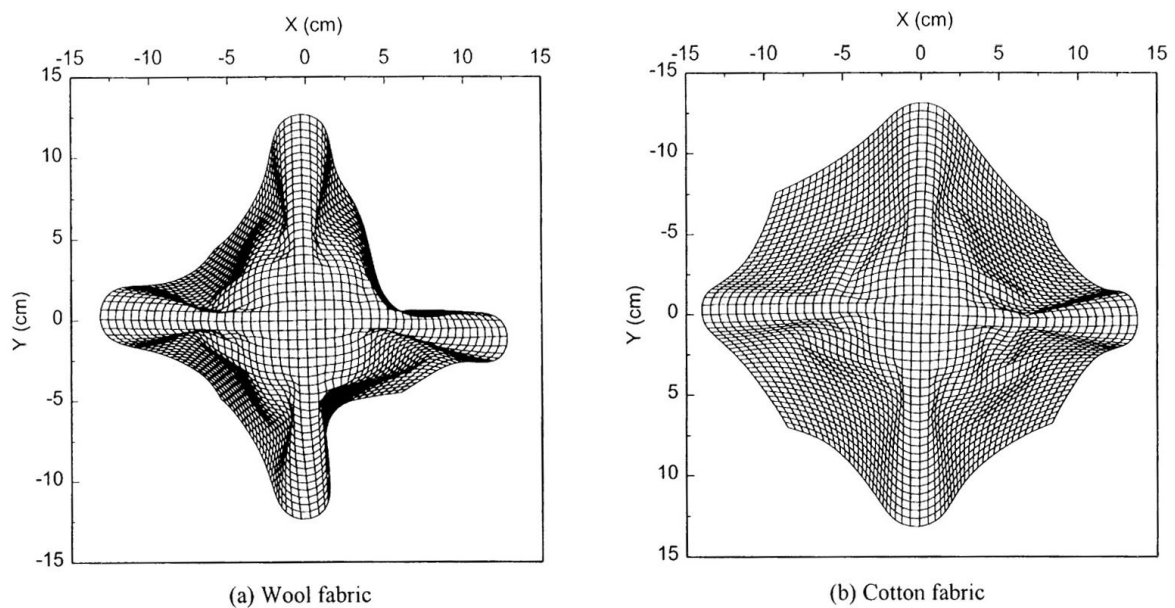


Figure 1.6: A finite-volume method for contact drape simulation of woven fabrics and garments. [129]

King et al. [137] developed a continuum model that can both simulate existing fabrics and predict the behavior of novel fabrics in-plane loading. They related the fabric structural configuration to the macroscopic deformation through an energy minimization method and used the internal forces using equilibrium arguments to determine the macroscopic stresses. Using this approach, authors developed a model for plain weave ballistic fabrics based on a pin-jointed beam geometry and implemented this model using Abaqus FEA environment to simulate fabrics under different modes of deformation as illustrated in Figure 1.7.

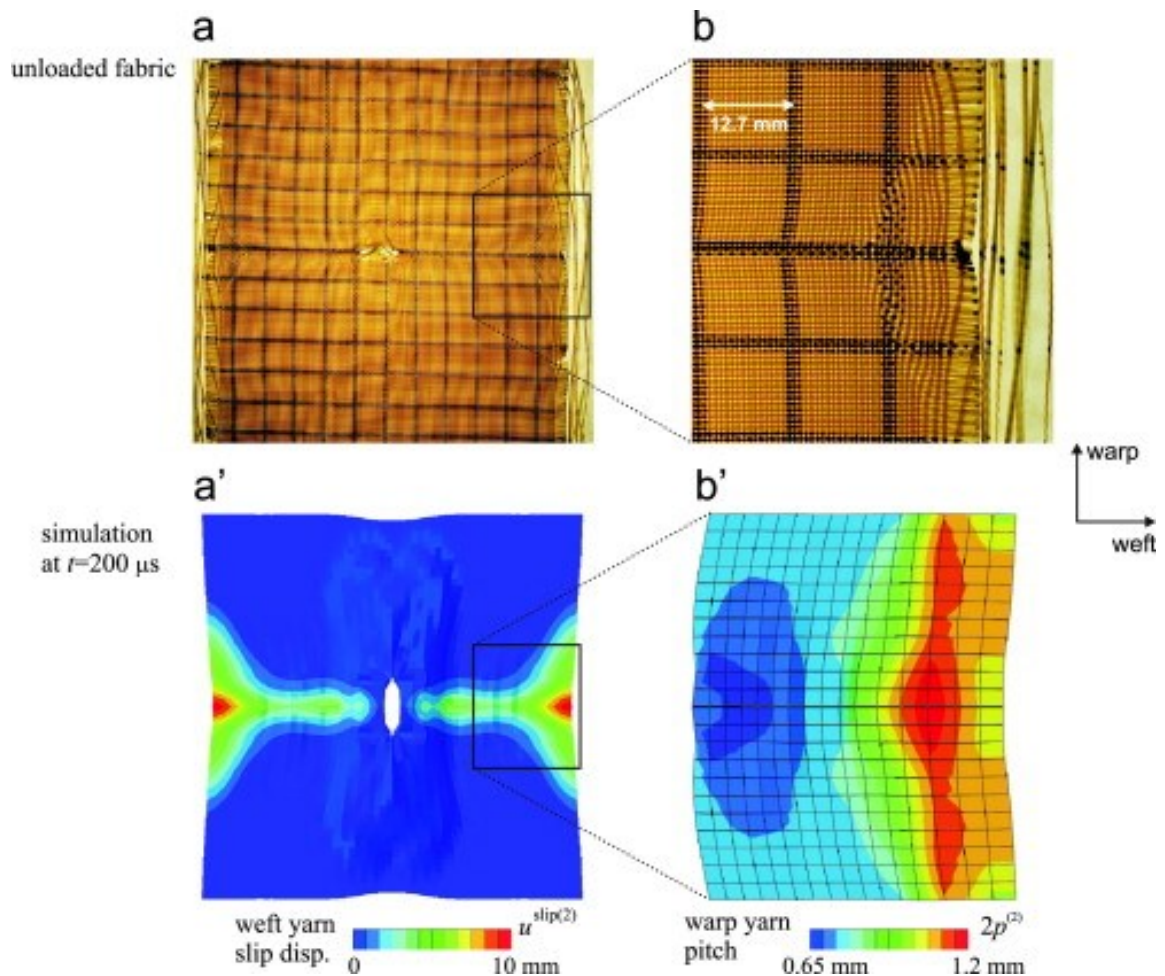


Figure 1.7: Prediction of the ballistic impact on a Kevlar® woven fabric: Yarn slip in an unloaded specimen that was tested at $v = 362 \text{ m/s}$ (top) and simulation of the test (bottom): (a), (a') Slip displacement in the direction of the weft yarns predicts unraveling of the weave at the free edges of the fabric, (b), (b') Yarn slip in the direction of the weft yarns increases the warp yarn pitch at the edge of the fabric. [29]

Sze and Liu [138] presented a bilinear stress-resultant solid-shell element with assumed natural transverse shear and thickness strains for drape analyses (Figure 1.8). The solid-shell element is partitioned into a surface, four line and four point sub-elements to reduce the computational burden of interpolating the assumed strain field. However, the converged solutions are non-physical.

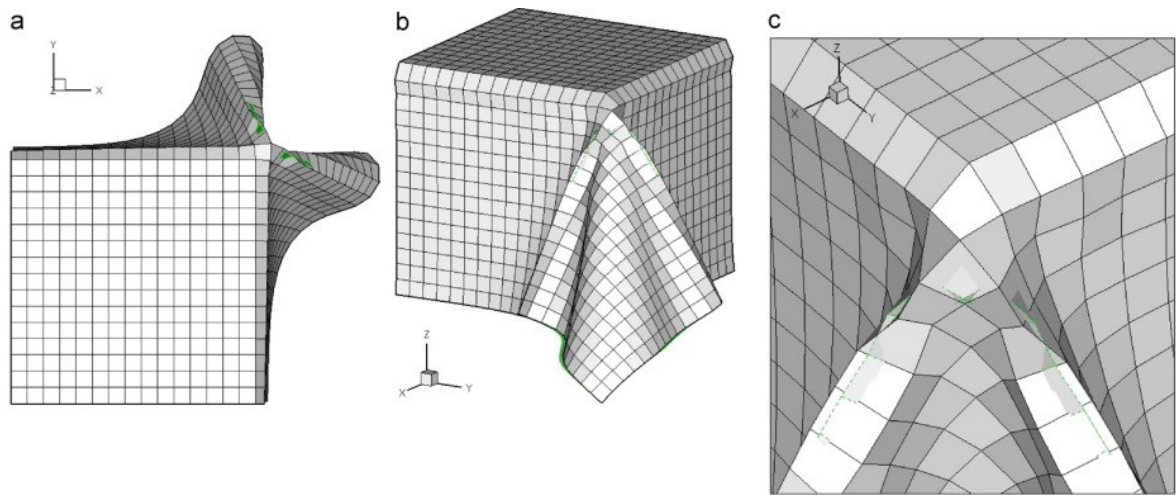


Figure 1.8: (a) Top; (b) Isometric; (c) Zoomed isometric views of a 40×40 cm wool fabric of which a quadrant is fixed over a 20×20 cm pedestal. The bottom element edges are portrayed by chained lines. [138]

Wang et al. [139] presented a finite-element mechanical contact model based on FSDT (Mindlin–Reissner shell theory) for a three-dimensional garment and human body (Figure 1.9). In this model, the mathematical formulation of the finite-element model using 4-node thin plate shell elements is defined to describe the strain–stress performance of the three-dimensional garment. The mechanical parameters of fabric samples were obtained by using KES-FB. Due to be based on FSDT, assumed the existence of the transverse shear strains in the model. However, authors did not present the technique to mitigate shear-locking effect that may appear in thin shell finite elements based on FSDT.

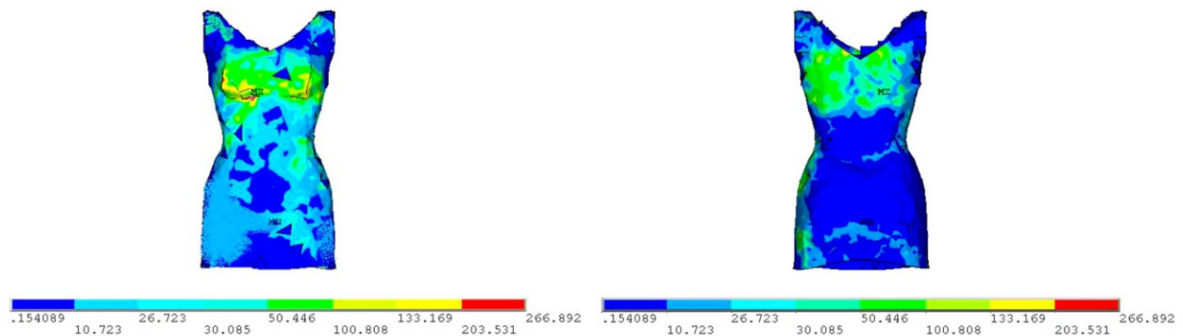


Figure 1.9: Pressure distribution of the body wearing the cotton one-piece dress, front (left) and back (right). [139]

More recent reviews on mechanical analysis of woven fabrics based on FEM can be found in the literature [7, 8, 62, 63, 140]. The above-referenced works can indicate that membrane and plate/shell finite element models are most appropriate for precise mechanical analysis and modelling of the textile fabrics, especially for complex deformation of the textile fabrics and cloth. The fabric objective measurement (FOM) technology has approved the important role in the field. Thus, mechanical realism is of paramount importance in a clothing modeling framework in which the mechanics of

woven fabrics is capturing realistic in-plane stress and out-of-plane transverse shear strains as well as bending behaviors. These mechanical properties of the fabrics aim to establish constitutive equations for FEM models including linear and nonlinear FEA.

From the past five decades, the development of simple and efficient low-order plate/shell elements have been principally based on FDST (Mindlin-Reissner theory, also so-called the first-order shear deformation theory) due to simplicity of mesh generation and robustness (e.g. against mesh entanglement during large deformations) in linear and nonlinear analysis, such as the case of either simple or complex fabric deformations. These attempts make the FSDT more convenient and reasonable in practical applications. However, the well-known problem of low-order elements is the appearance of shear-locking effect because the thickness-to-span ratio of plate/shell becomes too small as it is the case of fabric sheet, where the dimensional thickness is too small to compare with other length or width dimensions. There have been many techniques proposed to overcome this phenomenon with varying success. Various approaches can be found in published works [23, 27, 141-144]. Thus only the most recent advanced works are mentioned in sequel.

Zienkiewicz et al. [145] and Hughes et al. [146, 147] proposed the application of selective/reduced integration techniques. However, thin plate elements based on these techniques are not effective in certain cases due to be found that extra zero energy modes caused by rank deficiency may exist. However, the work of MacNeal et al. [148] motivated Hughes and Tezduyar [149] to present a scheme in which the rank deficiency was refined by using 2x2 quadrature and the interpolation of the transverse shear strains, but one-point quadrature integration was the drawback of these schemes. Another approach by Belytschko et al. [150] and Belytschko and Tsay [151] was the stabilization procedure with one-point quadrature integration. Also working along the same lines, several mixed/hybrid elements based on the FSDT may be efficient in remedying the shear-locking effect such as the shear-flexible element by Wilt et al. [152] and the shear-locking-free element by Auricchio and Sacco [153]. However, they are usually more complex formulation and implementation in theory and high computational time cost in rendering, so their usage is less attractive.

The famous discrete Kirchhoff triangular element (DKT) and discrete Kirchhoff quadrilateral element (DKQ) proposed by Batoz et al. [154] is a robust plate/shell bending element, which can give efficient results for analyzing bending problems. However, the transverse shear strain fields are regarded as zero, so these plate/shell elements are therefore efficient for thin plate/shell element only. Katili et al. [155, 156] proposed an extended DKQ element for thick plate/shell analysis is the discrete Kirchhoff-

Mindlin elements (DKM) based on Mindlin–Reissner theory with assumed shear strain fields. A new concept was introduced via the work of Macneal [157], namely assumed natural strain (ANS) method. In this concept, the shear strains are computed through the kinematic variables at discrete collocation points of the element instead of using nodes of element. There were many successful models that are based on this new approach, being the mixed interpolation tensorial component elements (MITC) proposed by Bathe and his coworkers [158] one of the most popular; Bathe and Dvorkin [159] also proposed a well-known 4-node quadrilateral plate element based on Mindlin-Reissner theory using MITC; Zienkiewicz's teamwork [160] proposed the linked interpolation for Mindlin-Reissner plate elements and so forth. The reader is referred to [161, 162] for more details about this subject.

In parallel with the above developments, several recent formulations of plate elements have been based on the Timoshenko's beam whose displacement function was used to develop locking-free plate finite elements. In the work of Ibrahimbegović [163, 164], the kinematic variables and shear strains along sides of element were approximated by using Timoshenko's beam theory and then, using the mixed interpolation method to develop three thin and thick plate elements PQ1, PQ2, PQ3. Also, based on Timoshenko's beam function method, Soh et al. [165] presented a 9-DOF triangular plate bending element with a scheme similar to those of DKT and DKQ elements for analysis of thick and thin plate and a 12-DOF quadrilateral element (ARS-Q12) was also presented [166]. Later, Cen et al. [167] modified the element ARS-Q12 to formulate a 4-node 20-DOF quadrilateral element (CTMQ20) by adding a bilinear in-plane displacement field of the mid-plane. Once again, based on the same Timoshenko's beam theory, several elements were later developed e.g. a 9-DOF triangular element (RDKTM) [168], a 20-DOF quadrilateral Mindlin plate element (RDKQM) [169], a 20-DOF and 24-DOF quadrilateral elements (RDKQ-L20)[170] and (RDKQ-L24) [171] and so on. Recent reviews for the shear deformable plate and shell finite elements can be found in several surveys e.g. Gal et al. [161], Zhang et al. [172].

In addition to the appearance of the locking phenomenon in displacement-based low-order finite element formulations for thin plate and shell finite element models, such formulations also have the other shortcomings with regard to low accuracy due to element distortion, mesh coarseness, etc. The development of computational approaches based on numerical methods, in particular with FEM, have allowed the development of more versatile computer applications in research, design and production activities. Among various types of finite element methods such as AEM (Applied Element Method), GFEM (Generalized Finite Element Method), XFEM (Extended Finite Element Method), Spectral Method, etc., the new literature S-FEM (Smoothed Finite Element Methods) has been recently

presented in applied mechanics [173]. The application of S-FEM models to thin plate/shell finite element models to overcome the shear-locking phenomena, element distortion and mesh coarseness has been proven [173-178]. These models offer more efficient approximate solutions that are stable and convergent to the exact solution [174, 175, 179-185]. They have been also proven to have more accuracy, precision, reliability and of more practical importance. At the period of this study, the S-FEM models has been being developed in many engineering areas, but not yet fully developed and applied in textile engineering [186]. Therefore, the smoothed finite element methods, together with fabric objective measurement technology that respects to low-stress mechanical properties of fabric are the main objects and objectives in this study in order to find a numerical solution that offer a lower computational cost but effective performance in comparison with more conventional finite elements for modelling and simulation of mechanical behavior of thin to moderately thick textile fabric.

1.4 Thesis statement

Taking into account the existing knowledge FOM (Fabric Objective Measurement) and the new developments in finite element methods, in particular S-FEM (Smoothed Finite Element Methods), we state that application of FOM and S-FEM to displacement-based low-order finite element formulations based on quadrilateral plate/shell finite element models are well appropriate for numerical modelling and simulation in predicting the mechanical deformation behaviour of the textile fabrics, as needed in cloth simulation, which will lead to the perspective of widely accepted and integrated S-FEM models into FEA/CAE environment for textile fabric engineering.

1.5 Objectives

As introduced above, the scope of this study is the mechanical modelling and simulation of the textile fabrics based on the plate/shell finite element models. Therefore, three general objectives in this work are pursued. The first one is to come up to the formulation of constitutive equations based on the low-stress mechanical properties. The second one is the study of mechanical modelling of the textile fabrics using finite element methods and the strain/gradient smoothing technique through S-FEM models. These two general objectives must lead to an efficient, robust and accurate computational technique based on the finite element technology to provide means to the engineering analysis of both simply and complex mechanical behavior of the textile fabrics, e.g. tensile, bending, buckling and vibration. The last objective is developing a computational tool that exchanges data for the solution of these objectives with other separate solvers.

In respect to fabric objective measurement (FOM), we have the following goal (or specific objectives):

- To review the state of the art on fabric objective measurement and low-stress mechanical properties of the textile fabrics.
- To present the major elasticity parameters of the fabric and the additional elasticity parameters used in this research. The KES-FB (Kawabata Evaluation System for Fabrics) system and low-stress mechanical parameters from which the major elasticity parameters of the fabric can be computed is presented.
- To propose a technique for approximating the transverse shear modulus, which acts through the fabric thickness.
- To formulate the constitutive laws using low-stress mechanical properties that are applicable for macro-mechanical modelling of the textile fabrics of both non-woven and woven fabrics in terms of elastic material with both isotropy and orthotropic anisotropy.

In the numerical modelling and simulation of the textile fabrics, the goals are:

- To review a brief state-of-the-art on modelling and simulation of the textile fabrics particularly based on plate/shell finite element models and a brief state-of-the-art on the displacement-based low-order finite element formulations for plate/shell finite element models.
- To develop S-FEM models for modelling and simulation of the textile fabrics to predict the simple and complex mechanical deformation behavior.
- To explore existing time integration schemes for dynamic deformations and to work with the best choice for long time analysis periods.
- To develop finite element computer codes for the developed S-FEM models due to the lack of supported FEM packages for S-FEM models in the current FEA/CAE systems.
- To demonstrate the developed and implemented S-FEM models for the basic engineering applications of modelling and simulation of the textile fabrics such as plane stress recovery, bending, buckling and free-vibration behavior.

All these objectives are oriented to improve and to combine the most advances of fabric objective measurement technology with the development of smoothed finite element methods into the textile engineering sector, i.e. the low-stress mechanical properties together with a stabilized conforming nodal integration and mesh moving algorithms, to perform the analysis of the mechanical deformation behaviour involving tensile, shear as well as bending properties. Besides, since the time when this study was initiated, S-FEM has not yet support by vast of FEA/CAE systems, applications. Thus, the

finite element computer codes for S-FEM models will be programmed in order to better sustain in practice the research described in this thesis. This also give a better interactive between theoretical works and practical works rather than using FEA/CAE systems, applications.

1.6 Organization of the thesis

The principal research topic approached in this thesis is numerical modelling for predicting the mechanical deformation behavior of thin to moderately thick fabrics. Thus, the development and implementation of this theoretical framework covers the literature of FOM (Fabric Objective Measurement), S-FEM (Smoothed Finite Element Methods) and FSDT (Reissner-Mindlin theory). Taking into consideration the thesis statement and the objectives mentioned above, the thesis here presented is organized as follows:

Chapter 1 – Introduction and outline of the thesis. In this chapter, it is presented the most recent advances in the investigation of mechanical modelling and simulation approaches of the textile fabrics and cloth, in particular with numerical methods, from which the difficulties towards a comprehensive finite element model for modelling and simulation of the textile fabrics are highlighted in order to give room to motivation, scope and objectives of the present work.

Chapter 2 – An understanding of the objective measurement of fabrics (FOM) is the key role of the success and efficiency of the theoretical work in the fields of both analytical modelling and numerical simulation to predict the mechanical deformation behavior of the textile fabrics and cloth. This chapter presents a formulation of the constitutive laws of the textile fabrics using low-stress mechanic properties via FOM. These constitutive equations are applicable to the formulation of plate/shell finite element models based on Reissner-Mindlin theory.

Chapter 3 – This chapter begins with the definition of elastic static and dynamic analysis of the textile fabrics, then the discretization of dynamics equilibrium equations in space-time will yields the equations of motion as well as the time integration schemes. Here the concept of gradient (strain) smoothing technique via S-FEM models is introduced. In the context of continuum mechanics, the formulation of plate and shell finite element models based on FSDT together with the strain-smoothing operation are presented.

Chapter 4 – In order to demonstrate and evaluate the developed and implemented S-FEM models, this chapter presents numerical modelling examples in predicting the mechanical deformation behavior of the textile fabrics including plane-stress, bending and buckling and free-vibration behavior.

Chapter 5 – This chapter concludes the thesis with the main advantages and disadvantages of the formulated and implemented numerical models, being also presented suggestions for future research to be developed as a direct consequence of this work.

1.7 Contribution of the thesis

This thesis has a few contributions to the advance of knowledge relative to textile engineering, applied mechanics and applied computer science, namely:

- Computation of the transverse shear modulus of the textile fabrics base on the objective measurement technology via using mechanical parameters of compression test. This shear modulus is needed to formulate of fabric constitutive laws for transverse shear strain relation, which act through the fabric thickness.
- In textile fabric engineering, this is the first time that one applies the strain/gradient smoothing technique via S-FEM to displacement-based 4-node quadrilateral finite element model for general plate and shell structures based on FSDT in order to enhance accuracy and to alleviate shear locking phenomena as well as element distortion effect. These results enhance the capabilities of low-order flat elements in the case of quadrilateral plate/shell finite element to perform efficiency the mechanical analysis and modelling of thin to moderately thick fabric sheet as well as the numerical computational model.
- Given the above insufficiencies of current FEA/CAE systems, this is the first time that research work incorporate the designs, implementation and development of the finite element computer codes for the developed plate/shell element model to demonstrate the basic engineering applications of mechanical modelling of thin to moderately thick fabric sheet in the typical case studies such as in-plane stress recovery, bending behavior and buckling and free-vibration behavior. The codes have been implemented with MATLAB v12.

1.8 References

1. Hu, J., *Fabric Testing*. Woodhead Textiles Series. 2008: Woodhead Publishing Ltd.
2. Saville, B.P., *Physical testing of textiles*. Woodhead Textiles Series. 1999: Woodhead Publishing Ltd.
3. Kawabata, S. and M. Niwa. *Influence of fibre process parameters on product performance*. in *Fibres to Finished Fabrics: Fibre Science/Dyeing & Finishing Groups Joint Conference*. 1998. The Textile Institute.
4. Postle, R., *Fabric objective measurement technology: present status and future potential*. International Journal of Clothing Science and Technology, 1990. **2**(3): p. 7-17.
5. Han, F., Stylos, G.K., *3D modelling, simulation and visualisation techniques for drape textiles and garments*, in *Modelling and predicting textile behaviour*. 2009, Woodhead Publishing Limited in association with The Textile Institute.
6. Patanaik, A., *Modeling and Simulation in Fibrous Materials*. 1 ed. 2012: Nova Science Publishers, Inc.
7. Veit, D., *Simulation in textile technology: Theory and applications*. 1 ed. Woodhead Publishing Series in Textiles. 2012: Woodhead Publishing.
8. Magnenat-Thalmann, N., *Modeling and Simulating Bodies and Garments*. 2010: Springer-Verlag London Limited.
9. Fan, J., W. Yu, and L. Hunter, *Clothing appearance and fit: Science and technology*. Woodhead Publishing in Textiles. 2004: CRC.
10. Behery, H.M., *Effect of mechanical and physical properties on fabric hand*. 2005, North America by CRC Press LLC: Woodhead Publishing Limited
11. Hu, J., *Structure and mechanics of woven fabrics*. 2004, Cambridge: Woodhead Publishing Ltd.
12. Amirbayat, J. and J.W.S. Hearle, *The complex buckling of flexible sheet materials—Part I. Theoretical approach*. International Journal of Mechanical Sciences, 1986. **28**(6): p. 339-358.
13. Shishoo, R., *Textile Advances in the Automotive Industry*. Woodhead Textiles Series. 2008: Woodhead Publishing Ltd.
14. Fangueiro, R., *Fibrous and Composite Materials for Civil Engineering Applications*. Woodhead Textiles Series. 2011: Woodhead Publishing Ltd.
15. Chapman, R., *Smart Textiles for Protection*. Woodhead Textiles Series. 2012: Woodhead Publishing Ltd.
16. Mattila, H.R., *Intelligent textiles and clothing*. 1 ed. Woodhead Publishing Series in Textiles. 2006: Woodhead Publishing.
17. Anand, S.C., J.F. Kennedy, and M. Mirafteb, *Medical and healthcare textiles*. Woodhead Textiles Series. 2010: Woodhead Publishing Ltd.
18. Bartels, V., *Handbook of Medical Textiles*. Woodhead Textiles Series. 2011: Woodhead Publishing Ltd.
19. Fairhurst, C., *Advances in Apparel Production*. Woodhead Publishing in Textiles. 2008: Woodhead Publishing Limited.
20. Majumdar, A., A. Das, and R. Alagirusamy, *Process control in textile manufacturing*. Woodhead Textiles Series. 2012: Woodhead Publishing Ltd.
21. Damyanov, G.B. and D. Germanova-Krasteva, *Textile Processes: Quality Control and Design of Experiments*. 1 ed. 2012: Momentum Press.

-
22. Klempous, R., et al., *Advanced Methods and Applications in Computational Intelligence*. 2013: Springer Publishing Company, Incorporated. 420.
 23. Cook, R.D., et al., *Concepts and applications of finite element analysis*. 4 ed. 2002: John Wiley & Sons, Inc.
 24. Liu, Y.-J., D.-L. Zhang, and M.M.-F. Yuen, *A survey on CAD methods in 3D garment design*. *Computers in Industry*, 2010. **61**(6): p. 576-593.
 25. Wang, C.C.L. and M.M.F. Yuen, *CAD methods in garment design*. *Computer-Aided Design*, 2005. **37**(6): p. 583-584.
 26. Zienkiewicz, O.C. and R.L. Taylor, *The Finite Element Method for Solid and Structural Mechanics*. 6 ed. Vol. 2. 2005: Butterworth-Heinemann Ltd.
 27. Reddy, J.N., *An Introduction to the Finite Element Method*. 2005: McGraw-Hill Education - Europe.
 28. Liu, G.R. and S.S. Quek, *The finite element method a practical course*. 2003, Oxford; Boston: Butterworth-Heinemann.
 29. Parsons, E.M., M.J. King, and S. Socrate, *Modeling yarn slip in woven fabric at the continuum level: Simulations of ballistic impact*. *Journal of the Mechanics and Physics of Solids*, 2013. **61**(1): p. 265-292.
 30. Yahya, M.F. *Damage mechanism of woven fabric composite model*. [cited 2013; Available from: <http://fsg.uitm.edu.my>].
 31. Haas, R. and A. Dietzius, *The stretching of the fabric and the shape of the envelope in non-rigid balloons*. National Advisory Committee for Aeronautics, 1918. **16**: p. 149-271.
 32. Peirce, F.T., *The Handle of Cloth as a Measurable Quantity*. *Journal of the Textile Institute*, 1930. **21**: p. 377-416.
 33. Peirce, F.T., *The geometry of cloth structure*. *Journal of the Textile Institute*, 1937. **28**: p. 43-77.
 34. Breen, D.E., *A survey of cloth modeling methods*, in *Cloth Modeling and Animation*, D. House and D. Breen, Editors. 2000, A.K. Peters. p. 19-53.
 35. Breen, D.E., *A Survey of Cloth Modeling Research*. Tech. Report TR-92030, Center for Advanced Technology, Rensselaer Polytechnic Inst., 1993.
 36. Ng, H.N. and R.L. Grimsdale, *Computer graphics techniques for modeling cloth*. *IEEE Computer Graphics and Applications*, 1996. **16**(5): p. 28-41.
 37. Shanahan, W.J., D.W. Lloyd, and J.W.S. Hearle, *Characterizing the Elastic Behavior of Textile Fabrics in Complex Deformations*. *Textile Research Journal*, 1978. **48**(9): p. 495-505.
 38. Kawabata, S., *The Standardization and Analysis of Hand Evaluation*. 1980, Osaka: Textile Machinery Society of Japan.
 39. Luible, C. and N. Magnenat-Thalmann, *The simulation of cloth using accurate physical parameters*. *Proceedings of the Tenth IASTED International Conference on Computer Graphics and Imaging*, 2008: p. 123-128.
 40. Potluri, P., I. Porat, and J. Atkinson, *Towards automated testing of fabrics*. *International Journal of Clothing Science and Technology*, 1995. **7**(2/3): p. 11-23.
 41. Weil, J., *The synthesis of cloth objects*. *SIGGRAPH Comput. Graph.*, 1986. **20**(4): p. 49-54.
 42. T. Agui, Y.N., M. Nakajma, *An Expression Method of Cylindrical Cloth Objects - An Expression of Folds of a Sleeve using Computer Graphics*. *Tens. Soc. of electronics, Information and Communications*, 1990. **J73-D-II**(7): p. 1095-1097.
 43. Hinds, B.K. and J. McCartney, *Interactive garment design*. *The Visual Computer*, 1990. **6**(2): p. 53-61.
-

-
44. Ng, H. and R. Grimsdale, *GEOFF - A geometrical editor for fold formation*. Image Analysis Applications and Computer Graphics, Third International Computer Science Conference, ICSC'95, 1995. **1024**: p. 124-131.
 45. Feynman, C., *Modeling the appearance of cloth*. 1986, Massachusetts Institute of Technology.
 46. Terzopoulos, D., et al., *Elastically deformable models*. SIGGRAPH Computer Graphics, 1987. **21**(4): p. 205-214.
 47. Aono, M., *A Wrinkle Propagation Model for Cloth*, in *CG International '90*, T.-S. Chua and T. Kunii, Editors. 1990, Springer Japan. p. 95-115.
 48. Magnenat-Thalmann, N. and Y. Yang, *Techniques for cloth animation*, in *New trends in animation and visualization*, M.-T. Nadia and T. Daniel, Editors. 1991, Wiley-Interscience. p. 242-256.
 49. Volino, P., M. Courchesne, and N.M. Thalmann, *Versatile and efficient techniques for simulating cloth and other deformable objects*, in *Proceedings of the 22nd annual conference on Computer graphics and interactive techniques*. 1995, ACM. p. 137-144.
 50. Breen, D.E., D.H. House, and M.J. Wozny, *A particle-based model for simulating the draping behavior of woven cloth*. Textile Research Journal, 1994. **64**(11): p. 663-685.
 51. Okabe, H., et al., *Three dimensional apparel CAD system*. SIGGRAPH Comput. Graph., 1992. **26**(2): p. 105-110.
 52. Ling, L., M. Damodaran, and R.L. Gay, *Aerodynamic force models for animating cloth motion in air flow*. The Visual Computer, 1996. **12**(2): p. 84-104.
 53. Provot, X. *Deformation constraints in a mass-spring model to describe rigid cloth behavior*. in *Proceedings of Graphics Interface (GI 1995)*. Canadian Computer-Human Communications Society.
 54. Ng, H., *Fast Techniques for the Modeling and Visualization of Cloth*, in *Centre for VLSI and Computer Graphics*. 1996, University of Sussex, UK.
 55. Hearle, J.W.S., P. Potluri, and V.S. Thammandra, *Modelling Fabric Mechanics*. Journal of The Textile Institute, 2001. **92**(3): p. 53-69.
 56. Rudomin, I.J., *Simulating cloth using a mixed geometric-physical method*. 1990, University of Pennsylvania. p. 132.
 57. Kunii, T. and H. Gotoda, *Singularity theoretical modeling and animation of garment wrinkle formation processes*. The Visual Computer, 1990. **6**(6): p. 326-336.
 58. Taillefer, F. *Mixed Modeling*. in *Proc. Compugraphics*.
 59. Tsopelas, N. *Animating the Crumpling Behavior of Garments*. in *Proc. 2nd Eurographics Workshop on Animation and Simulation*. 1991.
 60. Dhande, S.G., et al., *Geometric Modeling of Draped Fabric Surfaces*, in *Proceedings of the IFIP TC5/WG5.2/WG5.10 CSI International Conference on Computer Graphics: Graphics, Design and Visualization*. 1993, North-Holland Publishing Co. p. 349-356.
 61. Pascal Volino, N.M.-T., *Virtual Clothing: Theory and Practice*. 1 ed. 2000: Springer.
 62. Lutz Walter, G.-A.K., Stefano Carosio, *Transforming Clothing Production into a Demand-driven, Knowledge-based, High-tech Industry*. 2009: Springer-Verlag London Limited.
 63. Sherburn, M., *Geometric and Mechanical Modelling of Textiles*. 2007, University of Nottingham.
 64. Chen, M.X., Q.P. Sun, and M.F. Yuen, *Simulation of fabric drape using a thin plate element with finite rotation*. Acta Mechanica Sinica, 1998. **14**(3): p. 239-247.
 65. Dai, X., T. Furukawa, and S. Mitsui, *Drape formation based on geometric constraints and its application to skirt modelling*. International Journal, 2001. **13**: p. 23-37.
 66. Eberhardt, B., A. Weber, and W. Strasser, *A Fast, Flexible, Particle-System Model for Cloth Draping*. IEEE Comput. Graph. Appl., 1996. **16**(5): p. 52-59.
-

-
67. Hinds B, K. and J. McCartney, *Interactive garment design*. The Visual computer, 1990. **6**(2): p. 53-61.
 68. Huang, J., et al., *Geometrically based potential energy for simulating deformable objects*. The Visual Computer, 2006. **22**(9-11): p. 740-748.
 69. Terzopoulos, D. and K. Fleischer, *Deformable models*. The Visual computer, 1988. **4**(6): p. 306-331.
 70. Mezger, J., S. Kimmerle, and O. Eitzmuß, *Improved collision detection and response techniques for cloth animation*. 2002.
 71. Volino, P. and N. Magnenat-Thalmann, *Accurate Garment Prototyping and Simulation*. Computer-Aided Design and Applications, 2005. **2**(5): p. 645-654.
 72. Bender, J., D. Weber, and R. Dziol, *Fast and stable cloth simulation based on multi-resolution shape matching*. Computers & Graphics, 2013. **37**(8): p. 945-954.
 73. Kunii, T.L. and H. Gotoda, *Singularity theoretical modeling and animation of garment wrinkle formation processes*. Vis. Comput., 1990. **6**(6): p. 326-336.
 74. Nealen, A., et al., *Physically Based Deformable Models in Computer Graphics*. Computer Graphics Forum, 2006. **25**(4): p. 809-836.
 75. Magnenat-Thalmann, N., *Cloth Modeling and Simulation*, in *Modeling and Simulating Bodies and Garments*, N. Magnenat-Thalmann, Editor. 2010, Springer London. p. 71-137.
 76. Baraff, D. and A. Witkin. *Large steps in cloth simulation*. in *SIGGRAPH '98: Proceedings of the 25th annual conference on Computer graphics and interactive techniques*. ACM Press.
 77. Wardetzky, M., et al., *Discrete quadratic curvature energies*. Comput. Aided Geom. Des., 2007. **24**(8-9): p. 499-518.
 78. Steinemann, D., M.A. Otaduy, and M. Gross, *Fast adaptive shape matching deformations*, in *Proceedings of the 2008 ACM SIGGRAPH/Eurographics Symposium on Computer Animation*. 2008, Eurographics Association: Dublin, Ireland. p. 87-94.
 79. *PhysX*. [cited 2013; Available from: <https://developer.nvidia.com/physx>.
 80. *Maya nCloth*. [cited 2013; Available from: <http://www.autodesk.com>.
 81. *Havok Cloth*. [cited 2013; Available from: <http://www.havok.com>.
 82. *Blender*. [cited 2013; Available from: <http://www.blender.org>.
 83. Bro-Nielsen, M. and S. Cotin, *Real-time Volumetric Deformable Models for Surgery Simulation using Finite Elements and Condensation*. Computer Graphics Forum, 1996. **15**(3): p. 57-66.
 84. Howlett, P. and W.T. Hewitt, *Mass-spring simulation using adaptive non-active points*. Computer Graphics Forum (Eurographics 1998), 1998. **17**(3): p. 345-354.
 85. Ji, F., *Simulate the Dynamic Draping Behavior of Woven and Knitted Fabrics*. Journal of Industrial Textiles, 2006. **35**: p. 201-215.
 86. Eberhardt, B. and A. Weber, *A particle system approach to knitted textiles*. Computers & Graphics, 1999. **23**(4): p. 599-606.
 87. Volino, P., F. Cordier, and N. Magnenat-Thalmann, *From early virtual garment simulation to interactive fashion design*. Computer-Aided Design, 2005. **37**(6): p. 593-608.
 88. Breen, D.E., D.H. House, and M.J. Wozny, *Predicting the drape of woven cloth using interacting particles*. Proceedings of the 21st annual conference on Computer graphics and interactive techniques SIGGRAPH 94, 1994. **28**: p. 365-372.
 89. Chen, Y., et al., *Realistic Rendering and Animation of Knitwear*. IEEE Transactions on Visualization and Computer Graphics, 2003. **9**(1): p. 43-55.
 90. Carignan, M., et al. *Dressing animated synthetic actors with complex deformable clothes*. in *Computer Graphics (Proceedings of ACM SIGGRAPH 92)*. ACM Press.
 91. Choi, K.J. and H.S. Ko, *Stable but responsive cloth*. ACM Transactions on Graphics (ACM SIGGRAPH 2002), 2002. **21**(3): p. 604-611.
-

-
92. Vassilev, T., B. Spanlang, and Y. Chrysanthou, *Fast cloth animation on walking avatars*. Computer Graphics Forum, 2001. **20**(3): p. 260-267.
 93. Terzopoulos, D., et al. *Elastically deformable models*. in *Computer Graphics (Proceedings of ACM SIGGRAPH 87)*. ACM Press.
 94. Louchet, J., X. Provot, and D. Crochemore. *Evolutionary identification of cloth animation models*. in *Proceedings of the Eurographics Workshop on Computer Animation and Simulation (CAS 1995)*. Springer-Verlag.
 95. Deussen, O., L. Kobbelt, and P. Tücke. *Using Simulated Annealing to Obtain Good Nodal Approximations of Deformable Bodies*. in *In Sixth Eurographics Workshop on Simulation and Animation*. Springer.
 96. Maciel, A., R. Boulic, and D. Thalmann. *Deformable tissue parameterized by properties of real biological tissue*. in *Proceedings of the 2003 international conference on Surgery simulation and soft tissue modeling*. Springer-Verlag.
 97. van Gelder, A., *Approximate simulation of elastic membranes by triangulated spring meshes*. Journal of Graphics Tools, 1998. **3**(2): p. 21-41.
 98. Müller, M., et al., *Position based dynamics*. Journal of Visual Communication and Image Representation, 2007. **18**(2): p. 109-118.
 99. Zienkiewicz, O.C., R.L. Taylor, and J.Z. Zhu, *The Finite Element Method: Its Basis and Fundamentals*. Sixth ed. Vol. 1, 2, 3. 2005: Butterworth-Heinemann.
 100. Zienkiewicz, O. C. and R.L. Taylor, *The finite element method. Volume 1, The basis*. 2000, Oxford; Boston: Butterworth-Heinemann.
 101. Zienkiewicz, O.C. and R.L. Taylor, *The finite element method. Volume 2, Solid mechanics*. 2000, Oxford; Boston: Butterworth-Heinemann.
 102. Kaufmann, P., et al., *Flexible simulation of deformable models using discontinuous Galerkin FEM*. Graphical Models, 2009. **71**(4): p. 153-167.
 103. Sze, K.Y. and X.H. Liu, *Fabric drape simulation by solid-shell finite element method*. Finite Elements in Analysis and Design, 2007. **43**: p. 819 - 838.
 104. Creech, G. and A.K. Pickett, *Meso-modelling of Non-Crimp Fabric composites for coupled drape and failure analysis*. Journal of Materials Science, 2006. **41**: p. 6725-6736.
 105. Ascough, J., H. Bez, and A. Bricis, *A simple beam element, large displacement model for the finite element simulation of cloth drape*. Journal Of The Textile Institute, 1996. **87**(1): p. 152-165.
 106. Eischen, J.W., D. Shigan, and T.G. Clapp, *Finite-element modeling and control of flexible fabric parts*. Computer Graphics and Applications, IEEE, 1996. **16**(5): p. 71-80.
 107. Gan, L., N.G. Ly, and G.P. Steven, *A study of fabric deformation using nonlinear finite elements*. Textile Res J, 1995. **65**: p. 660-668.
 108. Collier, J.R., et al., *Drape prediction by means of finite-element analysis*. J Text Inst, 1991. **82**: p. 96-107.
 109. Eischen, J.W., D. Shigan, and T.G. Clapp, *Finite-element modeling and control of flexible fabric parts*. IEEE Computer Graphics and Applications, 1996. **16**(5): p. 71-80.
 110. Collier, J.R., et al., *Drape Prediction by Means of Finite-element Analysis*. Journal of The Textile Institute, 1991. **82**(1): p. 96-107.
 111. Claes Johnson, M., *Numerical Solution of Partial Differential Equations by the Finite Element Method*. January 15, 2009: Dover Publications.
 112. O. C. Zienkiewicz, R.L.T., J.Z. Zhu, *The Finite Element Method: Its Basis and Fundamentals*. Sixth ed. Vol. 1, 2, 3. May 2, 2005: Butterworth-Heinemann.
-

-
113. Hearle, J.W.S., M. Konopasek, and A. Newton, *On Some General Features of a Computer-Based System for Calculation of the Mechanics of Textile Structures*. Textile Research Journal, 1972. **42**(10): p. 613-626.
 114. Naoki, T., et al., *Hierarchical modelling of textile composite materials and structures by the homogenization method*. Modelling and Simulation in Materials Science and Engineering, 1999. **7**(2): p. 207.
 115. Bogdanovich, A.E., *Multi-scale modeling, stress and failure analyses of 3-D woven composites*. Journal of Materials Science, 2006. **41**(20): p. 6547-6590.
 116. Lomov, S.V., et al., *Textile geometry preprocessor for meso-mechanical models of woven composites*. Composites Science and Technology, 2000. **60**(11): p. 2083-2095.
 117. Lomov, S.V., et al., *Meso-FE modelling of textile composites: Road map, data flow and algorithms*. Composites Science and Technology, 2007. **67**(9): p. 1870-1891.
 118. Sagar, T.V., P. Potluri, and J.W.S. Hearle, *Mesoscale modelling of interlaced fibre assemblies using energy method*. Computational Materials Science, 2003. **28**(1): p. 49-62.
 119. Lin, H., et al., *Multi-scale integrated modelling for high performance flexible materials*. Computational Materials Science, 2012. **65**(0): p. 276-286.
 120. Naoki, T., Z. Masaru, and O. Yoshihiro, *Multi-scale finite element analysis of porous materials and components by asymptotic homogenization theory and enhanced mesh superposition method*. Modelling and Simulation in Materials Science and Engineering, 2003. **11**(2): p. 137.
 121. Nadler, B., P. Papadopoulos, and D.J. Steigmann, *Multiscale constitutive modeling and numerical simulation of fabric material*. International Journal of Solids and Structures, 2006. **43**(2): p. 206-221.
 122. Patnaik, A., et al., *Investigations on micro-mechanical and thermal characteristics of glass fiber reinforced epoxy based binary composite structure using finite element method*. Computational Materials Science, 2012. **62**(0): p. 142-151.
 123. Zhang, Y.T. and Y.B. Fu, *A micro-mechanical model of woven fabric and its application to the analysis of buckling under uniaxial tension. Part 2: buckling analysis*. International Journal of Engineering Science, 2001. **39**(1): p. 1-13.
 124. Tan, P., L. Tong, and G.P. Steven, *Micromechanics models for mechanical and thermomechanical properties of 3D through-the-thickness angle interlock woven composites*. Composites Part A: Applied Science and Manufacturing, 1999. **30**(5): p. 637-648.
 125. Hearle, J.W.S., R. Prakash, and M.A. Wilding, *Prediction of mechanical properties of nylon and polyester fibres as composites*. Polymer, 1987. **28**(3): p. 441-448.
 126. McBride, T.M. and J. Chen, *Unit-cell geometry in plain-weave fabrics during shear deformations*. Composites Science and Technology, 1997. **57**(3): p. 345-351.
 127. Grujicic, M., et al., *A meso-scale unit-cell based material model for the single-ply flexible-fabric armor*. Materials & Design, 2009. **30**(9): p. 3690-3704.
 128. Tan, P., L. Tong, and G.P. Steven, *A three-dimensional modelling technique for predicting the linear elastic property of opened-packing woven fabric unit cells*. Composite Structures, 1997. **38**(1-4): p. 261-271.
 129. Chen, S.F., J.L. Hu, and J.G. Teng, *A finite-volume method for contact drape simulation of woven fabrics and garments*. Finite Elements in Analysis and Design, 2001. **37**(6-7): p. 513-531.
 130. Lloyd, D.W., *The Analysis of Complex Fabric Deformations, in Mechanics of Flexible Fibre Assemblies*. The Netherlands, Alpen aan den Rijn, Sijthoff & Noordhoff Int'l Publishers B.B., 1980: p. 311-342.
-

-
131. Lloyd, D.W., *The Mechanics of Drape*, in *Flexible Shells*, E.L. Axelrad and F.A. Emmerling, Editors. 1984, Springer Berlin Heidelberg. p. 271-282.
 132. Simo, J.C. and D.D. Fox, *On a stress resultant geometrically exact shell model. Part I: Formulation and optimal parametrization*. Computer Methods in Applied Mechanics and Engineering, 1989. **72**(3): p. 267-304.
 133. Simo, J.C., D.D. Fox, and M.S. Rifai, *On a stress resultant geometrically exact shell model. Part II: The linear theory; Computational aspects*. Computer Methods in Applied Mechanics and Engineering, 1989. **73**(1): p. 53-92.
 134. Chen, B. and M. Govindaraj, *A physically based model of fabric drape using flexible shell theory*. Textile Res J, 1995. **65**: p. 324-330.
 135. Kang, T.J. and W.R. Yu, *Drape Simulation of Woven Fabric by Using the Finite-element Method*. Journal of The Textile Institute, 1995. **86**(4): p. 635-648.
 136. Etmuss, O., M. Keckeisen, and W. Strasser. *A fast finite element solution for cloth modelling*. in *Computer Graphics and Applications, 2003. Proceedings. 11th Pacific Conference on*. 2003.
 137. King, M.J., P. Jearanaisilawong, and S. Socrate, *A continuum constitutive model for the mechanical behavior of woven fabrics*. International Journal of Solids and Structures, 2005. **42**(13): p. 3867-3896.
 138. Sze, K.Y. and X.H. Liu, *Fabric drape simulation by solid-shell finite element method*. Finite Elements in Analysis and Design, 2007. **43**(11–12): p. 819-838.
 139. Wang, R., et al., *A finite-element mechanical contact model based on Mindlin–Reissner shell theory for a three-dimensional human body and garment*. Journal of Computational and Applied Mathematics, 2011. **236**(5): p. 867-877.
 140. Vassiliadis, S., *Advances in Modern Woven Fabrics Technology*. 2011: InTech.
 141. Zienkiewicz, O.C., R.L. Taylor, and J.Z. Zhu, *Shells as an assembly of flat elements*, in *The Finite Element Method Set (Sixth Edition)*. 2005, Butterworth-Heinemann: Oxford. p. 426-453.
 142. Zienkiewicz, O.C., R.L. Taylor, and J.Z. Zhu, *The Finite Element Method Set*. 6 ed. 2005, Oxford: Butterworth-Heinemann.
 143. Oñate, E., *Structural analysis with the finite element method. Linear statics: Beams, Plates and Shells*. Vol. 2. 2009, Dordrecht; London: Springer.
 144. Chapelle, D. and K.-J. Bathe, *The Finite Element Analysis of Shells - Fundamentals (Computational Fluid and Solid Mechanics)*. 2003, Berlin; New York: Springer.
 145. Zienkiewicz, O.C., R.L. Taylor, and J.M. Too, *Reduced integration technique in general analysis of plates and shells*. International Journal for Numerical Methods in Engineering, 1971. **3**(2): p. 275-290.
 146. Hughes, T.J.R., R.L. Taylor, and W. Kanoknukulchai, *A simple and efficient finite element for plate bending*. International Journal for Numerical Methods in Engineering, 1977. **11**(10): p. 1529-1543.
 147. Malkus, D.S. and T.J.R. Hughes, *Mixed finite element methods reduced and selective integration techniques: a unification of concepts*. Computer Methods in Applied Mechanics and Engineering, 1978. **15**: p. 63-81.
 148. Macneal, R.H., *A simple quadrilateral shell element*. Computers & Structures, 1978. **8**(2): p. 175-183.
 149. Hughes, T.J.R. and T.E. Tezduyar, *Finite elements based upon Mindlin plate theory with particular reference to the four-node bilinear isoparametric element*. 1981. p. 587–596.
 150. Belytschko, T., C.S. Tsay, and W.K. Liu, *A stabilization matrix for the bilinear mindlin plate element*. Computer Methods in Applied Mechanics and Engineering, 1981. **29**(3): p. 313-327.
-

-
151. Belytschko, T. and C.-S. Tsay, *A stabilization procedure for the quadrilateral plate element with one-point quadrature*. International Journal for Numerical Methods in Engineering, 1983. **19**(3): p. 405-419.
 152. Wilt, T.E., A.F. Saleeb, and T.Y. Chang, *A mixed element for laminated plates and shells*. Computers & Structures, 1990. **37**(4): p. 597-611.
 153. Auricchio, F. and E. Sacco, *A mixed-enhanced finite-element for the analysis of laminated composite plates*. International Journal for Numerical Methods in Engineering, 1999. **44**(10): p. 1481-1504.
 154. Batoz, et al., *Evaluation of a new quadrilateral thin plate bending element*. International Journal for Numerical Methods in Engineering, 1982. **8**(11): p. 1655-1677.
 155. Katili, I., *A new discrete Kirchhoff-Mindlin element based on Mindlin-Reissner plate theory and assumed shear strain fields—part I: An extended DKT element for thick-plate bending analysis*. International Journal for Numerical Methods in Engineering, 1993. **36**(11): p. 1859-1883.
 156. Katili, I., *A new discrete Kirchhoff-Mindlin element based on Mindlin-Reissner plate theory and assumed shear strain fields—part II: An extended DKQ element for thick-plate bending analysis*. International Journal for Numerical Methods in Engineering, 1993. **36**(11): p. 1885-1908.
 157. Macneal, R.H., *Derivation of element stiffness matrices by assumed strain distributions*. Nuclear Engineering and Design, 1982. **70**(1): p. 3-12.
 158. Dvorkin, E.N. and K.-J. Bathe, *A continuum mechanics based four-node shell element for general non-linear analysis*. Engineering Computations, 1984. **1**(1): p. 77-88.
 159. Bathe, K.-J. and E.N. Dvorkin, *A four-node plate bending element based on Mindlin/Reissner plate theory and a mixed interpolation*. International Journal for Numerical Methods in Engineering, 1985. **21**(2): p. 367-383.
 160. Zienkiewicz, O.C., et al., *Linked interpolation for Reissner-Mindlin plate elements: Part I—A simple quadrilateral*. International Journal for Numerical Methods in Engineering, 1993. **36**(18): p. 3043-3056.
 161. Gal, E. and R. Levy, *Geometrically nonlinear analysis of shell structures using a flat triangular shell finite element*. Archives of Computational Methods in Engineering, 2006. **13**(3): p. 331-388.
 162. Ayad, R. and A. Rigolot, *An improved four-node hybrid-mixed element based upon Mindlin's plate theory*. International Journal for Numerical Methods in Engineering, 2002. **55**(6): p. 705-731.
 163. Ibrahimbegović, A., *Plate quadrilateral finite element with incompatible modes*. Communications in Applied Numerical Methods, 1992. **8**(8): p. 497-504.
 164. Ibrahimbegović, A., *Quadrilateral finite elements for analysis of thick and thin plates*. Computer Methods in Applied Mechanics and Engineering, 1993. **110**(3-4): p. 195-209.
 165. Soh, A.K., Z.F. Long, and S. Cen, *A new nine DOF triangular element for analysis of thick and thin plates*. Computational Mechanics, 1999. **24**(5): p. 408-417.
 166. Soh, A.-K., et al., *A new twelve DOF quadrilateral element for analysis of thick and thin plates*. European Journal of Mechanics - A/Solids, 2001. **20**(2): p. 299-326.
 167. Cen, S., Y. Long, and Z. Yao, *A new hybrid-enhanced displacement-based element for the analysis of laminated composite plates*. Computers & Structures, 2002. **80**(9-10): p. 819-833.
 168. Wanji, C. and Y.K. Cheung, *Refined 9-Dof triangular Mindlin plate elements*. International Journal for Numerical Methods in Engineering, 2001. **51**(11): p. 1259-1281.
-

-
169. Wanji, C. and Y.K. Cheung, *Refined quadrilateral element based on Mindlin/Reissner plate theory*. International Journal for Numerical Methods in Engineering, 2000. **47**(1-3): p. 605-627.
170. Zhang, Y.X. and K.S. Kim, *Two simple and efficient displacement-based quadrilateral elements for the analysis of composite laminated plates*. International Journal for Numerical Methods in Engineering, 2004. **61**(11): p. 1771-1796.
171. Zhang, Y.X. and K.S. Kim, *Geometrically nonlinear analysis of laminated composite plates by two new displacement-based quadrilateral plate elements*. Composite Structures, 2006. **72**(3): p. 301-310.
172. Zhang, Y.X. and C.H. Yang, *Recent developments in finite element analysis for laminated composite plates*. Composite Structures, 2009. **88**(1): p. 147-157.
173. Liu, G.-R. and T. Nguyen-Thoi, *Smoothed finite element methods*. 2010: Taylor and Francis Group, LLC.
174. Liu, G., K. Dai, and T. Nguyen, *A Smoothed Finite Element Method for Mechanics Problems*. Computational Mechanics, 2007. **39**(6): p. 859-877.
175. Nguyen-Xuan, H., et al., *A smoothed finite element method for plate analysis*. Computer Methods in Applied Mechanics and Engineering, 2008. **197**(13-16): p. 1184-1203.
176. Nguyen-Thanh, N., et al., *An alternative alpha finite element method (AFEM) for free and forced structural vibration using triangular meshes*. Journal of Computational and Applied Mathematics, 2010. **233**(9): p. 2112-2135.
177. Nguyen-Thoi, T., et al., *A node-based smoothed finite element method (NS-FEM) for upper bound solution to visco-elastoplastic analyses of solids using triangular and tetrahedral meshes*. Computer Methods in Applied Mechanics and Engineering, 2010. **199**(45-48): p. 3005-3027.
178. Nguyen-Xuan, H., et al., *An edge-based smoothed finite element method (ES-FEM) with stabilized discrete shear gap technique for analysis of Reissner-Mindlin plates*. Computer Methods in Applied Mechanics and Engineering, 2010. **199**(9-12): p. 471-489.
179. Chen, L., et al., *A singular edge-based smoothed finite element method (ES-FEM) for crack analyses in anisotropic media*. Engineering Fracture Mechanics, 2011. **78**(1): p. 85-109.
180. Cui, X.Y. and G.Y. Li, *Smoothed Galerkin methods using cell-wise strain smoothing technique*. Engineering Analysis with Boundary Elements, 2012. **36**(5): p. 825-835.
181. Feng, S.Z., X.Y. Cui, and G.Y. Li, *Analysis of transient thermo-elastic problems using edge-based smoothed finite element method*. International Journal of Thermal Sciences, 2013. **65**(0): p. 127-135.
182. He, Z.C., et al., *An ES-FEM for accurate analysis of 3D mid-frequency acoustics using tetrahedron mesh*. Computers & Structures, 2012. **106-107**(0): p. 125-134.
183. Li, Y., G.R. Liu, and G.Y. Zhang, *An adaptive NS/ES-FEM approach for 2D contact problems using triangular elements*. Finite Elements in Analysis and Design, 2011. **47**(3): p. 256-275.
184. Nguyen-Thanh, N., et al., *A smoothed finite element method for shell analysis*. Computer Methods in Applied Mechanics and Engineering, 2008. **198**(2): p. 165-177.
185. Nguyen-Thoi, T., et al., *Static, free vibration and buckling analyses of stiffened plates by CS-FEM-DSG3 using triangular elements*. Computers & Structures, 2013. **125**(0): p. 100-113.
186. Nguyen, T.Q., F.N. Ferreira, and A. Gomes. *Modelling the bending behaviour of plain-woven fabric using flat shell element and strain smoothing technique*. in *13th AUTEX World Textile Conference*. 2013. Institute of Textile Machinery and High Performance Material Technology at TU Dresden.
-

Fabric objective measurement and Constitutive equation formulations

Abstract

This chapter focuses on the measurement of mechanical properties of fabric samples, which aims to provide physical and mechanical parameters for the formulation of fabrics constitutive laws corresponding to the mechanical deformation behavior of tensile, shear and bending properties. A brief development summary of objective measurement of fabric mechanical properties, as well as low-stress mechanical properties, is introduced. Among the fabric objective measurement instruments, the KES-FB instruments was chosen to measure the low-stress physical and mechanical parameters of fabric samples, being then the formulation of constitutive equations represented.

Keywords Woven fabric, non-woven fabric, fabric objective measurement, low-stress mechanics, KES-FB (Kawabata Evaluation System for Fabrics), SiroFAST (Fabric Assurance by Simple Testing), isotropic/orthotropic/anisotropic material, constitutive laws.

2.1 Introduction

2.1.1 Roles of fabric objective measurement

As outlined in the literature [1], the subjective measurement techniques are properly unable to meet the requirements of ever-changing marketplace of textile and clothing. Thus, the development of FOM (Fabric Objective Measurement) has been replacing the subjective measurement technique in use since the pioneering work of Peirce in the 1920s [2, 3]. Fabric objective measurement technology of mechanical, geometrical, surface and deformation properties, provides a scientific tool to measure the quality and performance characteristics of woven and non-woven fabrics [4-8]. The quality and performance attributes of fabrics related to the basic mechanical properties via the dimensional properties of fabric are shown in Table 2.1.

Test for fabric objective measurement can be broadly classified into two categories as follows [9-11]:

- High-stress mechanical tests: In order to measure tensile strength, tear strength and abrasion properties of fabrics, such tests normally being conducted until the fabric fail.

- Low-stress mechanical tests: Reflecting the level of stresses that a fabric can undergo during normal use, relates to fabric handle, making-up performance and garment appearance.

Table 2.1: The six basic fabric mechanical properties and corresponding quality and performance attributes of fabrics and garments

Fabric mechanical properties	Quality and mechanical performance
Uniaxial and biaxial tension	Fabric handle and drape Fabric formability and tailoring properties
Shear under tension	Garment appearance and seam pucker
Pure bending	Mechanical stability and shape retention
Lateral compression	Relaxation shrinkage, dimensional stability and hygral expansion
Longitudinal compression and buckling	Wrinkle recovery and crease retention Abrasion and pilling resistance
Surface roughness and friction	Mechanical and physiological comfort

Source: Fan et al. [12]

Nowadays, the FOM technology plays a key role in production principles for quality control of fabric manufacturing, finishing and refinishing operations to ensure that fabrics are easy to tailor, garments keep their shape during wear and provide information on fabric handle, as shown in Table 2.2, [1, 10, 11, 13-17]. Besides, it also plays important role in the development and application of the FEM/FEA/CAE systems in textile and cloth engineering as presented in Section 1.1.

The application of fabric objective measurement, as shown in Table 2.3, has become important due to the following main factors [8, 18, 19]:

- To meet the increasing level of automation in both textile and clothing manufacture.
- To carry out the production, research, development and quality control functions.
- To satisfy the need for quick response to maintain competitiveness in business.

Table 2.2: Typical fabric properties measured in FOM

Properties measured	Descriptions
Tensile and shear	Measured under low deformation forces are being also used to calculate properties such as deformability. This sometimes also called recovery and hysteresis (energy loss) properties.
Bending rigidity	Fabric bending length is generally measured and used to calculate the fabric rigidity.
Compression	This refers to the difference in fabric thickness under different loads, also termed the thickness of the surface layer and provides a measure of fabric softness or fullness.
Friction and roughness	They are measured either fabric-against-fabric or fabric-against-metal static and dynamic of friction. These properties are related to fabric handle.
Dimensional stability	Three main types of dimensional stability result from changes in the environment: relaxation, hygral, thermal. In practice, only the first two are generally considered important and measured.

Source: Kawabata et al. [4, 11, 12]

Table 2.3: The possibility application of fabric objective measurement technology

1.	Objective measurement of fabric quality and handle and their primary components for various textile products.
2.	Design and production of a diverse range of high quality yarns and fabrics using objective mechanical and surface-property data.
3.	Objective evaluation and control of textile processing and finishing sequences for the production of high quality yarns and fabrics.
4.	Objective evaluation of fabric tailorability and finished garment quality and appearance.
5.	Objective specifications by tailoring companies for fabric selection, production planning, process control and quality assurance, using fabric mechanical and dimensional property data.
6.	Measurement and control of the comfort, performance and stability of fabrics and clothing during use.
7.	Evaluation of the effect of changes in fabric finishing routines, including decatizing, on fabric tailor ability.

Source: Postle et al. [4, 12]

It also represents the possibility of incorporating the experience of numerous experts working in the textile and clothing industries into an integrated computerized scientific database in objective terms

[20], for example, a new database management system for improved clothing manufacturing proposed by Lee [21] who listed an excellent table of controllable parameters in the tailoring process.

The reader is referred to [1, 10-12, 20, 22] for more details about KES-FB and FAST system as well as the fabric properties, as presented in Tables 2.4 and 2.5, associated with problems in fabric performance and appearance as well as garment making and with potential poor garment appearance in wear.

In short, above notations can indicate the important and significant role of the FOM technology in providing the key for scientific, engineering and production principles, especially in the formulation of fabric constitutive laws as well as of the numerical models of this study.

2.1.2 Fabric objective measurement, KES-FB and SiroFAST system

The woven fabric mechanics was reported in the aerodynamic literature by the work of Haas, in German early 1912 [23], in the time of the worldwide development of airships. In parallel with the development of fabric mechanics, the development of objective measurement of fabric handle was introduced by the pioneering work of Peirce in United Kingdom, in 1930 [2, 3]. In 1937, Peirce [24] established the basic theory of fabric mechanics by investigating the basic equilibrium structure of a plain-weave fabric based upon the force equilibrium conditions and presented a geometrical and a mathematical force model of the plain-weave fabric. His work was further developed by subsequent researchers in the field, was towards the objective or quantitative assessment of fabric 'handle' and quality. The theoretical analysis of fabric mechanical properties such as tensile, shear, bending, compression and buckling came across in the work of Grosberg, Park and Swani and others during the 1960s [25-27]. Their contributions were on the physical and mechanical description as well as deformation properties of woven fabric. The extensive research in Sweden [28], Japan [4], UK [11] and Australia [12-16] has defined many of those mechanical, dimensional and other properties of fabrics that affect handle, performance in garment manufacture and the appearance of garments in wear. Considerable progress has been made during the last century in the development of the theory of geometrical structure and mechanical properties of fabrics. In order to meet demands from industry, the investigation of the geometry and mechanical deformation behaviour of fabrics have come off well through observation, explanation and prediction. Hearle, Thwaites and Amirbayat [29] presented the most important mechanical properties of fabric in the book entitled 'Mechanics of Flexible Fibre

Assemblies' edited by the leading researchers as Hearle, Grosberg, Backer, Thwaites, Amirbayat, Postle and Lloyd [22].

Much experimental techniques for the measurement of those mechanical properties evolved during those decades by many researchers. In order to develop an objective evaluation fabric hand system, Kawabata and Niwa [30] organized the Hand Evaluation and Standardisation Committee (HESK) in 1972, as a research committee of the Textile Machinery Society in Japan and 12 experts were invited to join this committee. Progress toward an objective evaluation system has been made possible by HESK and the term 'primary fabric handle' was defined, from which related to mechanical properties of the fabric, as listed in Table 2.2. The three primary handle values (PHV) comprising KOSHI (stiffness), NUMERI (smoothness) and FUKURAMI (fullness) were related to fabric properties measured with KES-FB as illustrated in Figure 2.1. However, the most important outcome at this period was an integrated system of fabric objective measurement, namely KES-F (Kawabata Evaluation System for Fabrics), which was designed to measure low-stress mechanical properties that determine fabric handle and garment making-up and appearance of fabrics [1, 10, 11, 20]. The KES-FB (the second version of KES-F) system enables a variety of fabric tests and is a sophisticated computer testing facility which became a standard textile test facility around the world [5, 31]. The development of an automatic version of the Kawabata system, called the KESFB-AUTO-A system was released in 1997 [32].

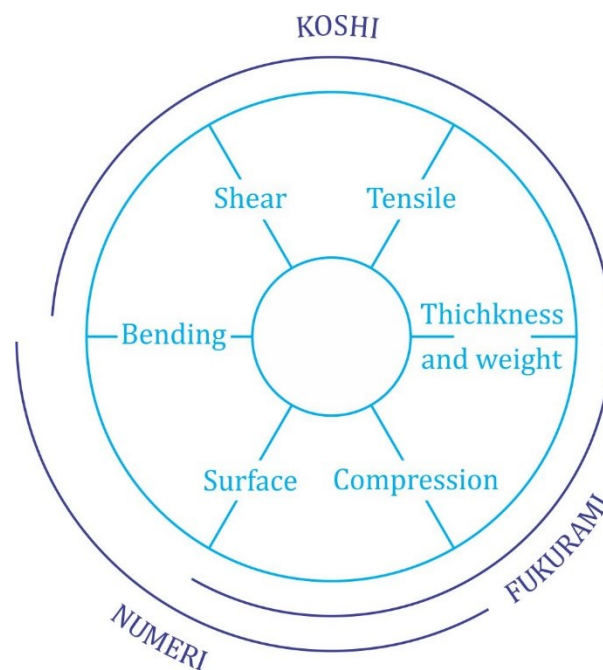


Figure 2.1: Relationship between the three primary hand values and the mechanical properties. [30]

The reader is referred to [1, 10-12, 22, 31] for more details about PHV, further handle values including SHARI (crispness) and HARI (anti-drape stiffness), as listed in Table 2.4 and diagnosis of tailoring problems on these PHV as well as THV (Total Handle Value) and TAV (Total Appearance Value). These references also including description of the KES-FB and SiroFAST system.

Table 2.4: Primary fabric handle

KOSHI	Stiffness	A measure of crispness in bending; springy flexural rigidity
NUMERI	Smoothness	A measure of smooth, supple and soft feel
FUKURAMI	Fullness and softness	A measure of bulk, with springiness in comparison; rich and warm
SHARI	Crispness	A measure of a crisp rigid fabric surface, with a cool feel
HARI	Antidrape stiffness	A measure of flare, the opposite of limp conformability

Source: Hearle [33, 34]

In late 1980s, the CSIRO, in Australia, developed the FAST (Fabric Assurance by Simple Testing) system [1, 35]. Similarly with KES-FB system, SiroFAST system can measure the low-stress mechanical and dimensional properties of fabric that can be used to predict performance in garment manufacture and the appearance of the garments in wear. It measures the resistance of fabric to deformation but not the recovery of the fabric from deformation. Besides, it is much cheaper than KES-F system and becoming more attractive to the industrial environment. These instruments also give information related to the fabric handle.

In practical terms, the extension or stress applied to woven fabrics in manufacturing, finishing, garment construction and wear process is generally governed by the low-stress scope of their characteristic stress-strain behaviour. The normal stresses related to fabric deformation behaviours under low-stress conditions are tensile, shear, bending and compression and both KES-FB and SiroFAST system are applicable devices to predict these low-stress deformations.

In general, both KES-FB and SiroFAST system can measure low-stress fabric mechanical properties, typically those in Table 2.2. Their results are basically similar on these two systems and can be plotted on control charts. Besides, both systems have been compared when applied to typical fabrics, as well as to diagnosis of tailoring problems [36].

2.1.3 The configuration of KES-FB system

The KES-FB system comprises of four precision instruments:

- KES-FB1: Tensile and shear tester
- KES-FB2: Pure bending tester
- KES-FB3: Compression tester
- KES-FB4: Surface characteristics tester

These instruments can test fabrics automatically and provide continuous stress-strain curves for the resistance of fabric to deformation and the recovery of the fabric from deformation, as illustrated in Figures 2.2 to 2.8. Load, deformation and recovery are measured using sensors and recorded using an *X-Y* recorder. There are five charts and 16 parameters in the warp and weft directions. The parameters describing mechanical and surface properties of fabric are shown in Table 2.5.

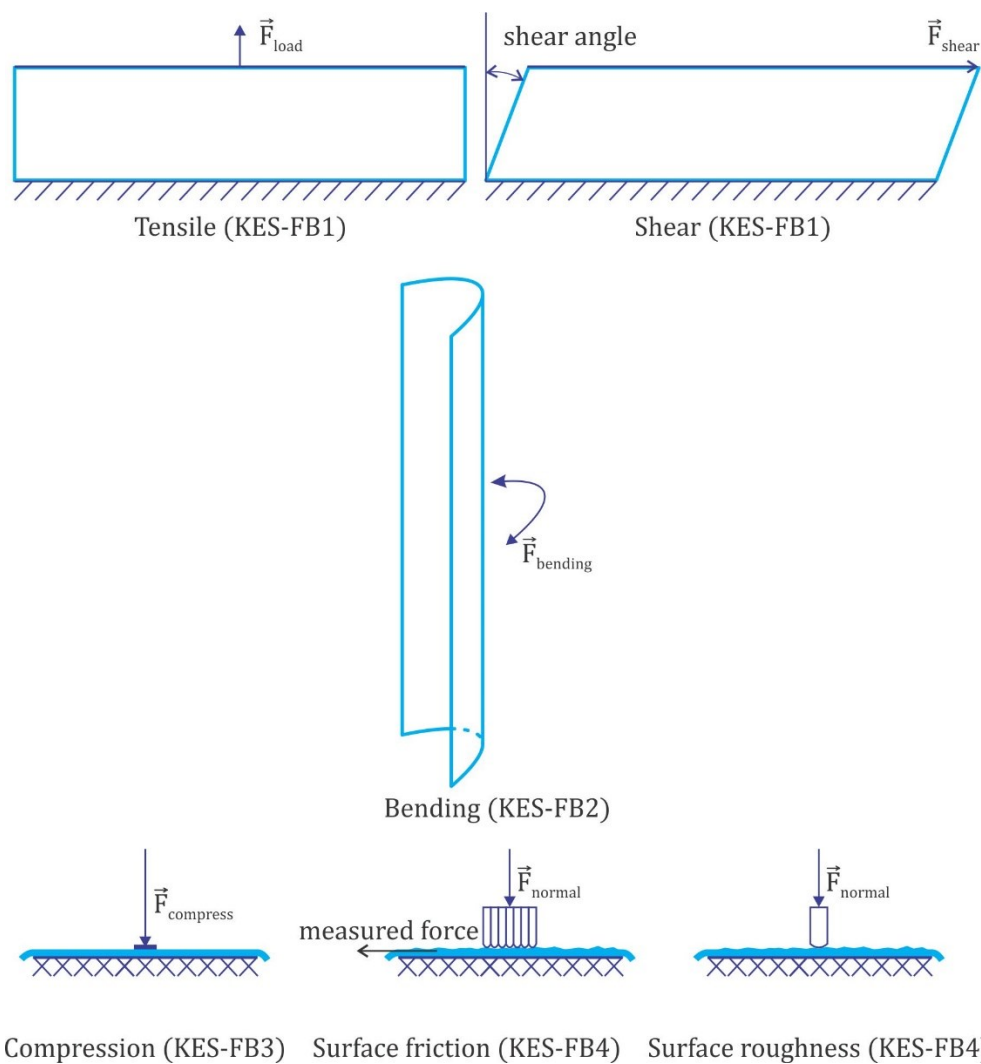


Figure 2.2: The KES-FB system for measuring fabric mechanical properties.

Table 2.5: The parameters describing fabric mechanical and surface properties

Instrument	Symbol	Notation	Unit
Tensile (KES-FB1)	<i>LT</i>	Linearity of tensile load-extension curve	
	<i>WT</i>	Tensile energy per unit area	<i>gf.cm/cm²</i>
	<i>RT</i>	Tensile resilience	%
	<i>EMT</i>	Extensibility, the strain at 500 <i>gf/cm</i> tensile load	%
Shear (KES-FB1)	<i>G</i>	Shear rigidity	<i>gf/cm.deg</i>
	<i>2HG</i>	Hysteresis of shear force at $\pm 0.5^0$ shear angle	<i>gf/cm</i>
	<i>2HG5</i>	Hysteresis of shear force at $\pm 5^0$ shear angle	<i>gf/cm</i>
Bending (KES-FB2)	<i>B</i>	Bending rigidity	<i>gf.cm²/cm</i>
	<i>2HB</i>	Hysteresis of bending moment	<i>gf.cm²/cm</i>
Compression (KES-FB3)	<i>LC</i>	Linearity of compression-thickness curve	
	<i>WC</i>	Compressional energy per unit area	<i>gf.cm²/cm</i>
	<i>RC</i>	Compressional resilience	%
	<i>T₀</i>	Fabric thickness at 0.5 <i>gf/cm²</i>	<i>mm</i>
	<i>T_m</i>	Fabric thickness at 50 <i>gf/cm²</i>	<i>mm</i>
Surface (KES-FB4)	<i>MIU</i>	Coefficient of fabric surface friction	
	<i>MMD</i>	Mean deviation of <i>MIU</i>	
	<i>SMD</i>	Geometrical roughness	<i>mm</i>
Weight	<i>W</i>	Fabric weight per unit area	<i>mg/cm²</i>

Source: Saville and others [1, 10-12, 20].

2.1.4 The configuration of SiroFAST system

The SiroFAST system consists of three individual instruments and a test method:

- SiroFAST-1: Compression tester
- SiroFAST-2: Bending tester
- SiroFAST-3: Extension tester
- SiroFAST-4: Dimensional stability (test method)

The FAST system provides 14 parameters that can be measured or calculated as listed in Table 2.6. Similarly to the KES-FB system, the measured parameters are plotted on a control chart from which the prediction of the fabric performance can be derived. Although the FAST system is technically less complicated than the KES-FB system, it is reliable and responsive information in order to control the finishing and tailoring progress of fabric and garment.

Table 2.6: The low-stress mechanical parameters measured on the FAST system

Instrument	Symbol	Notation	Unit
Tensile	<i>E5</i>	Extension at 5 <i>N/m</i>	%
	<i>E20</i>	Extension at 20 <i>N/m</i>	%
	<i>E100</i>	Extension at 100 <i>N/m</i>	%
	<i>EB5</i>	Bias extension	%
Shear	<i>G</i>	Shear rigidity	<i>N/m</i>
Bending	<i>C</i>	Bending length	<i>mm</i>
	<i>B</i>	Bending rigidity	$\mu N \cdot m$
Compression	<i>T2</i>	Thickness at 2 <i>gf/cm²</i>	<i>mm</i>
	<i>T100</i>	Thickness at 100 <i>gf/cm²</i>	<i>mm</i>
	<i>ST</i>	Surface thickness	<i>mm</i>
	<i>STR</i>	Released surface thickness	<i>mm</i>
Dimensional stability	<i>RS</i>	Relaxation shrinkage	%
	<i>RC</i>	Hygral expansion	%
Derived parameter	<i>F</i>	Formability	$\% \cdot mm^2$

Source: Saville and others [1, 10-12, 20].

The reader is referred to [1, 10-12, 20, 22] for more details about KES-FB and FAST system as well as the fabric properties, as presented in Tables 2.5 and 2.6, associated to fabric performance and appearance as well as garment making and with potential poor garment appearance in wear.

2.2 Mechanical parameters

In the modelling and simulation of the textile fabric products, the major elasticity parameters of the textile fabrics are those listed in Table 2.7. The addition of elasticity parameters according to the

transverse direction of the fabric, which are needed to develop the numerical models in this research, are listed in Table 2.8.

Table 2.7: The major elasticity parameters of the fabric used in the mechanical modelling and simulation.

Symbol	Notation
E	Young's modulus
G	Shear modulus, or rigidity modulus, expressing the shearing rigidity
B	Bending rigidity
ν	Poisson's ratio, significant for highly stretched fabric

Table 2.8: The addition of elasticity parameters according to the transverse direction of the fabric needed to develop the numerical models in this research in this research.

Symbol	Notation
K	Bulk's modulus
ν	Poisson's ratios related to transverse strain, or related to the anticlastic compression

The directions of applied forces according to principal directions of warp yarns and weft yarns and bias direction of woven fabric are shown in Figure 2.3. Note that there is no distinction of the directions of applied forces for the non-woven fabric due to be categorized as linear homogeneous isotropic material.

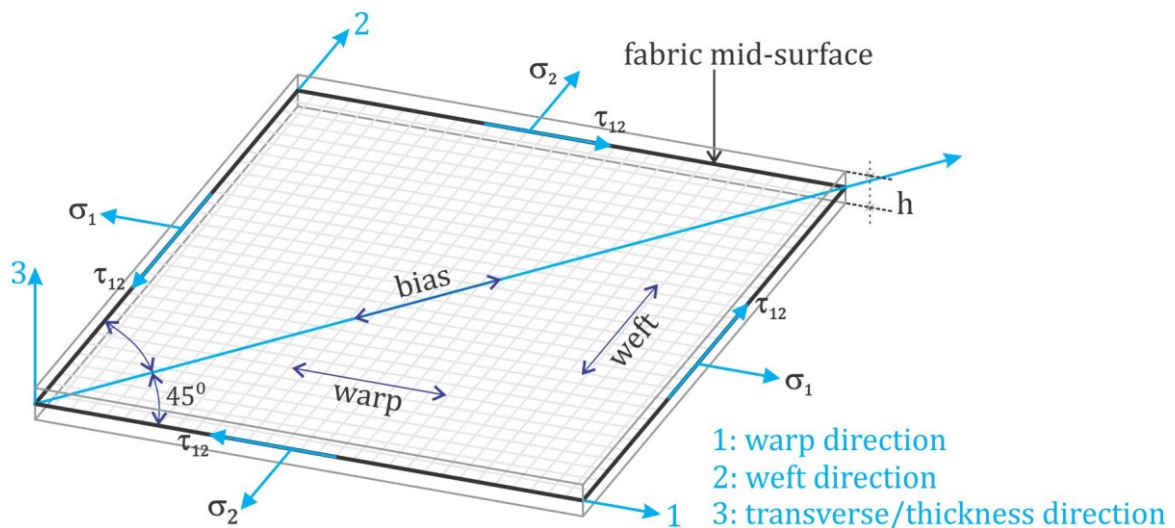


Figure 2.3: The principal directions of warp yarns, weft yarns and bias of woven fabric.

Depending on using the KES-FB or FAST instruments, almost elasticity parameters listed in Tables 2.7 and 2.8 can be obtained or calculated from the measured results, as shown in Table 2.9.

Table 2.9: Options of instruments for measuring the low-stress mechanical properties of fabric of which results used for calculating elasticity parameters.

Parameter	Mechanical properties	Instrument options	
		KES-FB	SiroFAST
E	Tensile stress-strain	KES-FB1	SiroFAST-3
G	Shear stress-strain	KES-FB1	SiroFAST-3
B	Pure bending	KES-FB2	SiroFAST-2
K	Compression	KES-FB3	SiroFAST-1

Together with mechanical parameters, there are two essential physical parameters, relating to dimension and weight, comprising fabric thickness and fabric weight, as listed in Table 2.10.

Table 2.10: The physical parameters of fabric

Symbol	Notation	Unit
h	Thickness	mm
ρ	Mass per unit area (also known as basis weight and grammage)	mg/cm^2

In order to measure the low-stress mechanical properties of specimen, the KES-FB system is used in this work. Section 2.3 provides a detailed explanation of the properties measured by the KES-FB system. Note that the measurement unit is defined according to the applied measurement standard or system. The reader is referred to [10, 11] for more details about the measurement standards and their corresponding measurement unit system applied for fabric testing.

2.3 Experimental analysis of fabric properties with KES-FB system

The descriptions in the following subsections were elaborated on those in [1, 10-12, 20, 22]. The corresponding figures were captured and noted from experimental analysis of fabric properties.

2.3.1 Tensile and shear test (KES-FB1)

The tensile properties are measured by applying the tensile-force to fabric sample clamped between chucks from zero to maximum preset at $10Kgf$ for the specimen of $20cm$ width and this is equivalent to $500 gf/cm$ ($4.9 N/cm$ or $490 N/m$) denoted by F_m . The force extension curve chart is plotted when applying the tensile-force from zero to maximum preset and vice versa to give

the pair of curves as shown in Figure 2.4, in which the recovery curve is plotted while the sample is being returned to its original length.

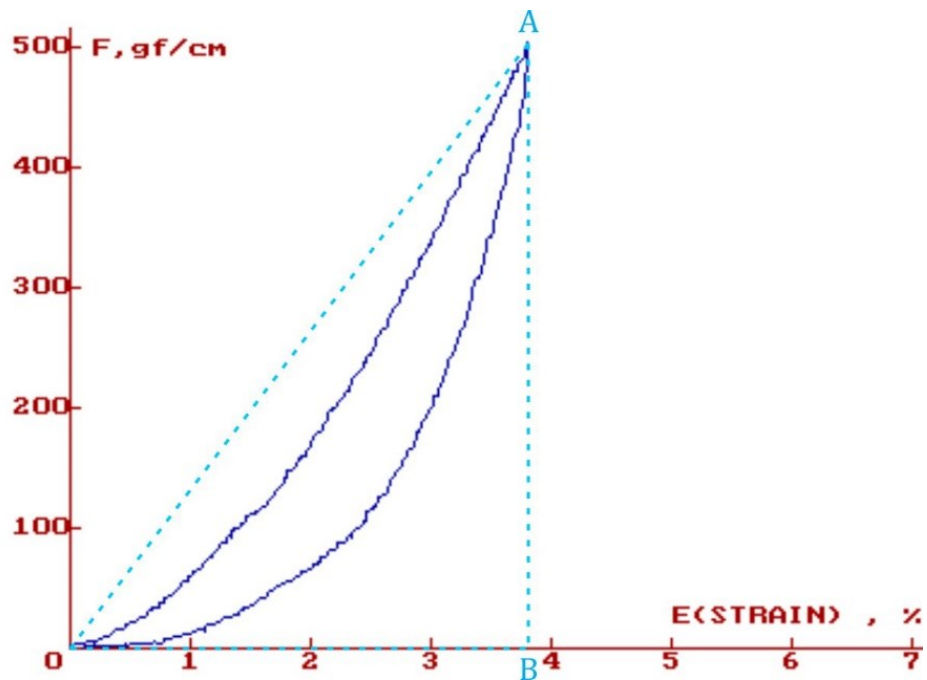


Figure 2.4: Graph chart with typical curves of tensile test, plot of tensile stress-strain.

From the control chart, tensile energy or the work done by the extension up to maximum force F_m was calculated as

$$WT = \int_0^{\varepsilon_m} F(\varepsilon) d\varepsilon = \text{the area under load strain curve} \quad (2.1)$$

where ε is the tensile strain, ε_m is the strain at the upper-limit load and F is tensile load as function of strain. The tensile resilience was given by

$$RT = \frac{WT'}{WT} = \frac{\text{the area under load decreasing curve}}{WT} \times 100 \quad (2.2)$$

in which WT' is the recovery work given by

$$WT' = \int_0^{\varepsilon_m} F'(\varepsilon) d\varepsilon = \text{the area under load decreasing curve} \quad (2.3)$$

where $F'(\varepsilon)$ is the tensile force at the recovering process. The linearity was computed by

$$LT = \frac{WT}{\frac{1}{2}F_m\varepsilon_m} = \frac{WT}{\text{the area of triangular } OAB} \quad (2.4)$$

From the above expression, the maximum value of tensile strain ε_m at maximum load 500 gf/cm can be written as

$$\varepsilon_m = \frac{2WT}{F_m LT} = \frac{WT}{250LT} = \frac{EMT}{100} \quad (2.5)$$

Shear properties are measured in a similar way as for tensile test, but the movement is performed transversally in cyclic shear deformation of $\pm 8^\circ$ shear angle under a constant tension force of 10 gf/cm or 98.1 mN/cm on the chuck.

A control chart is plotted during cyclic shear deformation as shown in Figure 2.5 and the following quantities are measured as

$$G = \text{slope of shear force – shear strain curve} \quad (2.6)$$

$$2HG = \text{hysteresis width of curve at } 0.5^\circ \quad (2.7)$$

$$2HG5 = \text{hysteresis width of curve at } 5^\circ \quad (2.8)$$

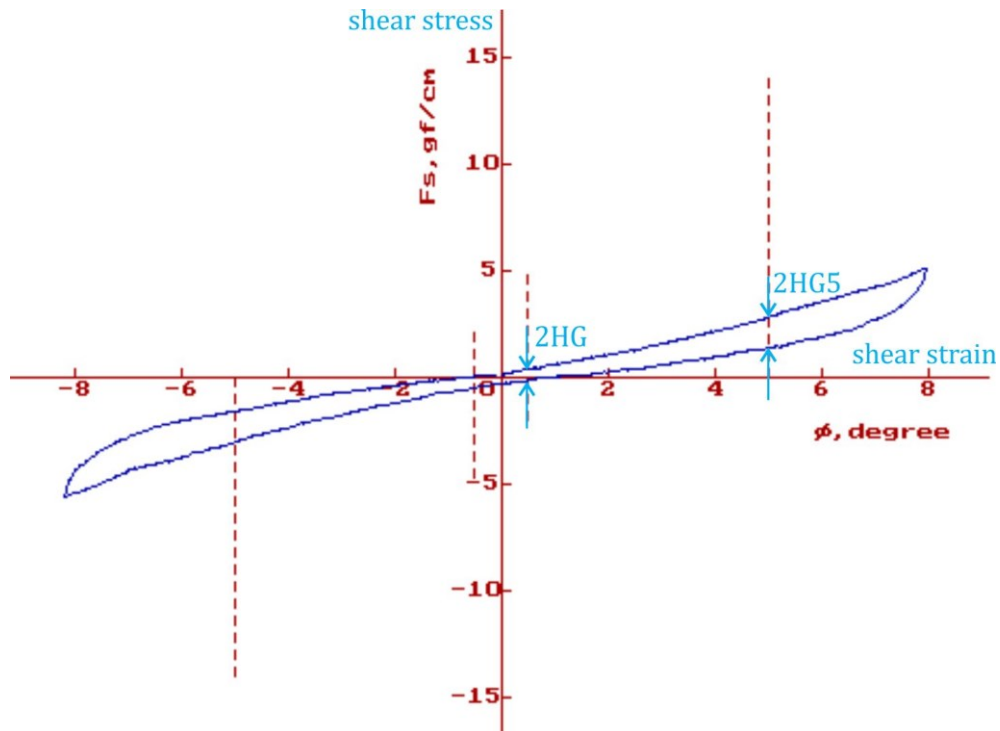


Figure 2.5: Graph chart with typical curves of shear test, plot of shear stress against shear strain.

2.3.2 Pure bending test (KES-FB2)

The bending properties is measured based on the principle of pure bending whereby the fabric sample is continuously bent in the curvature $\pm 2.5\text{cm}^{-1}$ in which the bend radius is $1/\text{curvature}$. The moment-curvature relationships is recorded on an X-Y recorder during the test operation as shown in Figure 2.6.

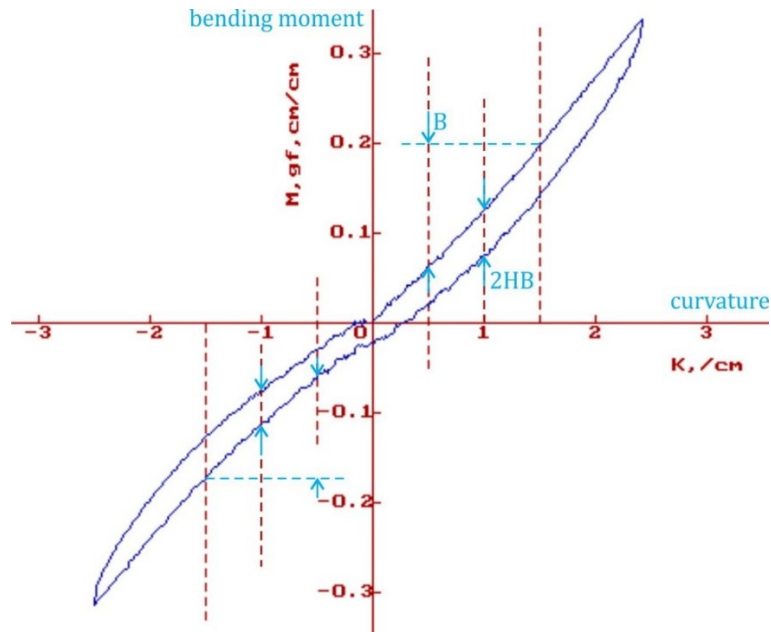


Figure 2.6: Graph chart with typical curves of bending test, plot of bending moment against curvature.

The bending rigidity B and moment of hysteresis $2HB$ are measured as follows

$$G = \text{slope of shear force} - \text{shear strain curve} \quad (2.9)$$

$$B = \text{slope of the bending moment} - \text{curvature curve} \quad (2.10)$$

$$2HB = \text{hysteresis width of the curve} \quad (2.11)$$

2.3.3 Compression test (KES-FB3)

To measure the compressional properties, the fabric sample is placed between two plates and compressed in its thickness (lateral) direction by a compression head. During this operation, the tester increases the pressure continuously until reaching the preset maximum pressure level at $50\text{ gf}/\text{cm}^2$ or $0.49\text{ N}/\text{cm}^2$ and vice versa for the recovery process, the load- deformation curve is recorded as shown in Figure 2.7.

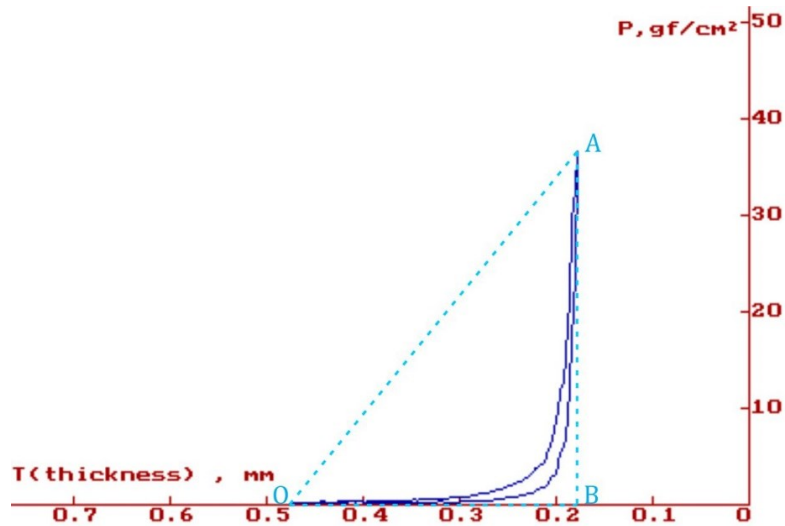


Figure 2.7: Graph chart with typical curves of compression test.

In the same manner as in the case of the tensile properties, the quantities LC, WC and RC are computed in a similarly way as for LT, WT and RT as shown in tensile test. A higher compressional resilience (RC) value indicates a better recovery from compression.

2.3.4 Surface test (KES-FB4)

The fabric surface properties can be measured by using two contact sensors under a constant tension, one for measuring frictional coefficient and the mean deviation of the coefficient of friction and the other for measuring geometrical surface roughness. While the fabric sample is being moved in a preset distance under the touch sensors with a constant tension, the parameters are recorded and computed directly from the calculation circuit of the instrument as shown in Figure 2.8.

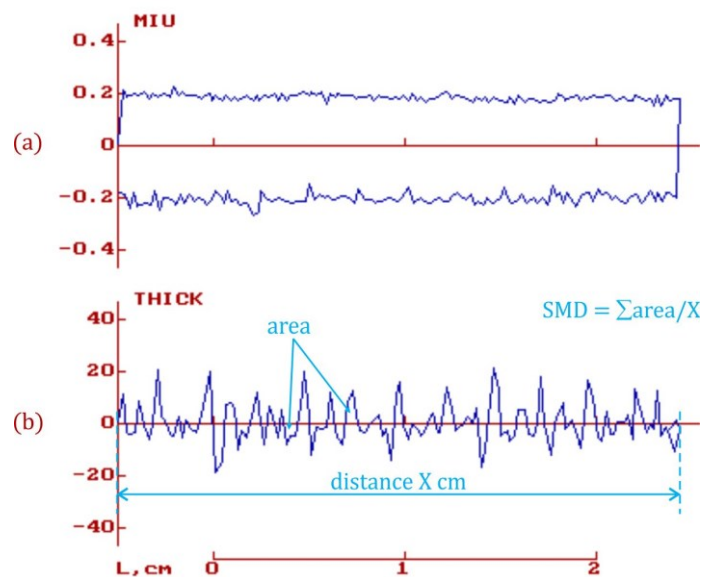


Figure 2.8: Graph chart with typical curves of surface frictional (a) and surface roughness (b).

A higher coefficient of friction (MIU) value represents a higher fabric friction, while a higher geometrical roughness (SMD) value indicates a rougher (i.e. less smooth) fabric surface.

2.4 Formulation of constitutive laws for fabric deformations

The fabric structures is in general classified into four categories as woven, nonwoven, knits and braid. For these types of structures, woven fabrics, whose theoretical structures and mechanical properties can be found in the literature [37-39], have demonstrated a greater dimensional stability in the warp and weft directions and highest packing density of yarn. Woven fabric is a type of textile material and it shares the complex deformation behaviour as other textile materials. It is not only the end products of spinning and weaving process, but raw materials for clothing and other industries such as composites and medical textiles. Every piece of woven fabric has two biases, perpendicular to each other and is an integration of warp and weft yarns through intersection. Thus, woven fabrics have been approximated as an elastic sheet material with orthotropic anisotropy in almost mathematical models in the field as presented in Section 1.2 and also in the present work. Besides, woven fabric is approximated to an elastica in some cases, which was discussed by Lloyd et al. [40].

Constitutive equations represent the relations between the deformations of the system and the internal stress-strain relationships, namely material law. The fabrics constitutive laws, which have been used to describe the mechanical deformation behaviours of fabrics, are indispensable to all numerical modeling and analysis of the fabric, virtual fabric simulation applications, computer-aided clothing engineering, computer-aided clothing design, etc. [41-44].

According to the objectives within this study, the formulation of fabric constitutive models using the mechanical properties via the fabric objective measurement techniques is applicable for both non-woven and woven fabric, as well as woven fabric composites. These models capture the primary features of both isotropy and orthotropic anisotropy according to linearity/nonlinearity that can be easily implemented in a linear/nonlinear plate/shell finite element framework for general clothing-wearer interaction modeling. The formulated constitutive equations are needed for developing displacement-based low-order finite elements based on quadrilateral plate/shell finite element model and S-FEM models via the gradient/strain smoothing technique, as presented in Chapter 3. In terms of the engineering constants, the plane-stress constitutive equations, as well as the constitutive equations for bending and out-of-plane transverse shear strain, are described the following sections.

2.4.1 Tensile stress and tensile strain, uniaxial applied force

In textile engineering, the normal stress can be generally defined as the force per unit length acting perpendicular to the side surface of fabric or selvage that produces normal strain, which is defined as the elongation (or stretch) of fabric per unit length responded to the direction of the applied force.

Let the warp and weft directions of woven fabrics due to their yarn-based structure be denoted with 1 and 2 and the direction normal to the 1-2 plane, also the transverse direction, be denoted with 3, as illustrated in Figure 2.3 and 2.9. According to material coordinates, the directions 1 and 2 coincide with the principal directions of orthotropic material, that is, the axes corresponding to the warp and weft direction of yarns of the fabric. These directions are used as indices adding to the stress, strain and elastic modulus indicate the direction of the applied force. Normal stress carries a single subscript to indicate that the stress acts on a plane normal to the axis in the subscript direction.

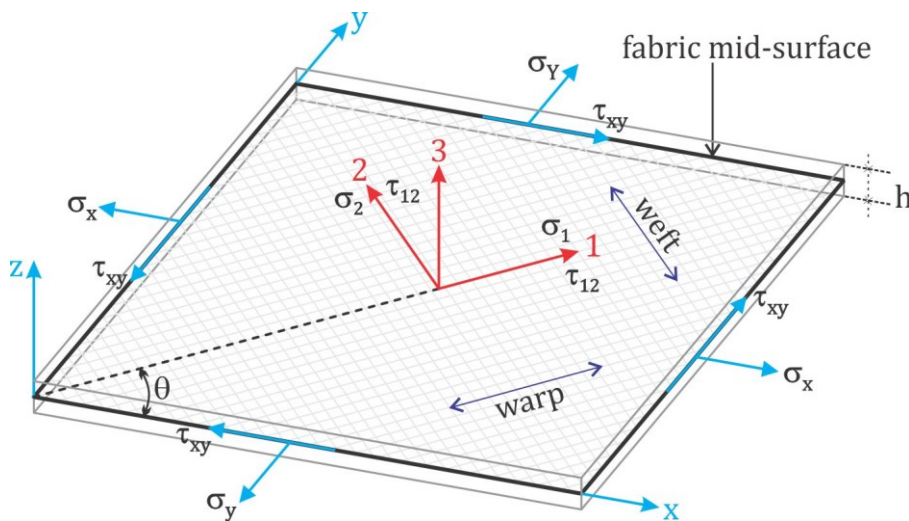


Figure 2.9: The warp and weft directions of woven fabrics due to their yarn-based structure denoted with 1 and 2 in orthotropic axes of sheet material and the transverse direction denoted with 3.

With the above assumption, the stress-strain relationship can be described by at least two elastic moduli as follows

$$\sigma_1 = E_1 \varepsilon_1 \quad (2.12)$$

$$\sigma_2 = E_2 \varepsilon_2 \quad (2.13)$$

where E_i is Young's modulus and σ_i and ε_i stand for stress and strain ($i = 1, 2$). Note that fabric thickness is too small when compare with fabric width and length that can be expressed as the thickness-to-span ratio indicated by $\frac{h}{L} = \frac{\text{thickness}}{\text{length}}$. Thus, for plane-stress in a sheet material such as

fabric, with respect to the 1-2 plane, the stress field is approximated such that $\sigma_{33} = \sigma_{23} = \sigma_{13} = 0$.

For the relationship between the bending moment and bending strain, the bending stiffness of woven fabric can be defined by two flexural moduli (so-called bending moduli) according to direction of load. The flexural moduli corresponding to the warp and weft direction are denoted by B_1 and B_2 .

For the non-woven fabrics, which are in general classified as an isotropic linear elastic material, the relationship between stress and strain is therefore independent of the direction of force such that $E = E_1 = E_2$ and $B = B_1 = B_2$.

2.4.2 Tensile stress and tensile strain, plane stress and bending

In the practical terms, fabrics will experience stresses in more than one direction within the plane. This is referred to as in-plane stress wherein yields the Poisson's ratio, being defined as the ratio between the strain perpendicular to the given loading direction and the strain parallel to this given loading direction. Poisson's ratios corresponding to the warp and weft directions of the woven fabrics are denoted by ν_{12} and ν_{21} , respectively, can be defined as

$$\frac{\varepsilon_{weft}}{\varepsilon_{warp}} = \nu_{12} = \frac{\varepsilon_2}{\varepsilon_1} \quad (2.14)$$

$$\frac{\varepsilon_{warp}}{\varepsilon_{weft}} = \nu_{21} = \frac{\varepsilon_1}{\varepsilon_2} \quad (2.15)$$

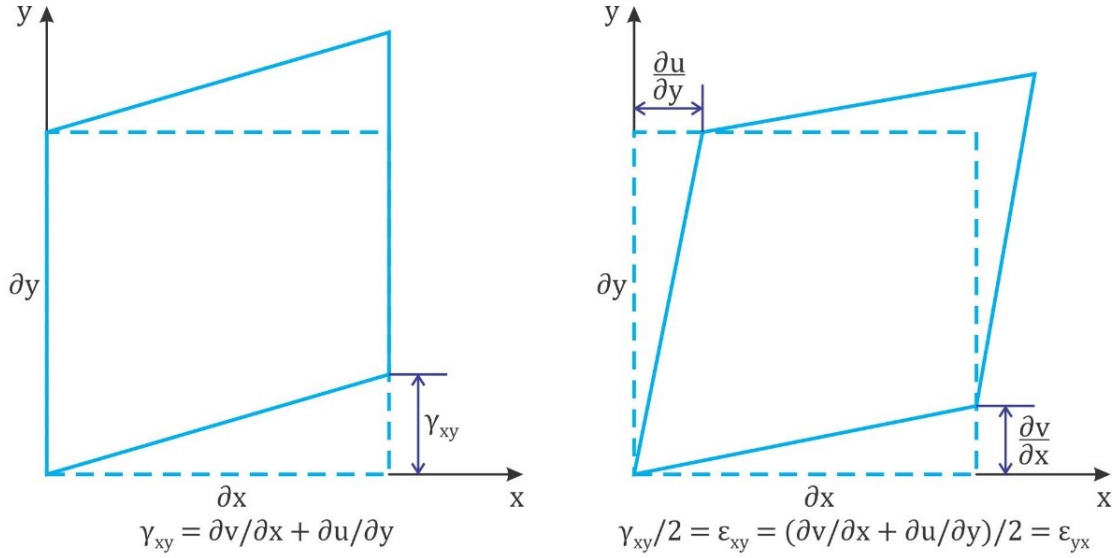
When a force is applied to a material, the strain fields are stretch in addition to the Poisson's contraction effect due to another force perpendicular to this applied force [45]. In the case of the textile fabric, by incorporating Equation (2.12, 2.13), the strain components are written as

$$\varepsilon_1 = \frac{\sigma_1}{E_1} - \nu_{21}\varepsilon_2 = \frac{\sigma_1}{E_1} - \nu_{21}\frac{\sigma_2}{E_2} \quad (2.16)$$

$$\varepsilon_2 = \frac{\sigma_2}{E_2} - \nu_{12}\varepsilon_1 = \frac{\sigma_2}{E_2} - \nu_{12}\frac{\sigma_1}{E_1} \quad (2.17)$$

Furthermore, the corresponding shear forces are also present. The shear stress τ_{12} and shear strain γ_{21} , as shown in Figure 2.10, are related by shear modulus G (so-called modulus of rigidity) in directions of warp and weft on surface of woven fabric, which gives

$$\tau_{12} = G\gamma_{12} \quad (2.18)$$



Engineer shear strain is the total shear strain Shear strain tensor is the average of two strain

Figure 2.10: Definition of shearing strains.

Note that the first numeral of the double subscript in Equation (2.18) indicates that the plane on which the stress acts is normal to the axis in the subscript direction; the second numeral designates the coordinate direction in which the stress acts. In each of the two axes directions, the relationship between Poisson's ratios and Young's modulus is expressed as $\nu_{21}E_1 = \nu_{12}E_2$ [46].

Equations (2.16, 2.17 and 2.18) can be written in the matrix form as

$$\begin{Bmatrix} \varepsilon_1 \\ \varepsilon_2 \\ \gamma_{12} \end{Bmatrix} = \begin{bmatrix} \frac{1}{E_1} & -\frac{\nu_{21}}{E_2} & 0 \\ -\frac{\nu_{12}}{E_1} & \frac{1}{E_2} & 0 \\ 0 & 0 & \frac{1}{G} \end{bmatrix} \begin{Bmatrix} \sigma_1 \\ \sigma_2 \\ \tau_{12} \end{Bmatrix} \quad (2.19)$$

Note that shear modulus G can be approximated by using the formulas defined in [11, 47]. It is expressed the relationship between the shear modulus and the extension of fabric in bias direction in terms of elastic moduli as follows

$$\frac{1}{G} = \frac{4}{E_{bias}} - \left(\frac{1 - \nu_2}{E_1} + \frac{1 - \nu_1}{E_2} \right) \quad (2.20)$$

in which E_{bias} stands for elastic modulus measured in the bias direction of warp yarns and weft yarns.

With appropriate constitutive relations, the stress-strain relation in terms of plane stress can be obtained by inverting the compliance matrix in constitutive Equation (2.19), which gives

$$\begin{bmatrix} \sigma_1 \\ \sigma_2 \\ \tau_{12} \end{bmatrix} = \begin{bmatrix} D_{11} & D_{12} & 0 \\ D_{21} & D_{22} & 0 \\ 0 & 0 & D_{66} \end{bmatrix} \begin{bmatrix} \varepsilon_1 \\ \varepsilon_2 \\ \gamma_{12} \end{bmatrix} \quad (2.21)$$

in which the stiffness components are defined as

$$D_{11} = \frac{E_1}{1 - \nu_{12}\nu_{21}} = \frac{E_{warp}}{1 - \nu_{warp}\nu_{weft}} \quad (2.22a)$$

$$D_{22} = \frac{E_2}{1 - \nu_{12}\nu_{21}} = \frac{E_{weft}}{1 - \nu_{warp}\nu_{weft}} \quad (2.22b)$$

$$D_{12} = D_{21} = \frac{E_2\nu_{12}}{1 - \nu_{12}\nu_{21}} = \frac{E_1\nu_{21}}{1 - \nu_{12}\nu_{21}} \quad (2.22c)$$

$$D_{66} = G \quad (2.22d)$$

Note that the engineering-tensor interchange matrix in Equations (2.18, 2.19 and 2.21) is defined by

$$\mathbf{R} = \begin{bmatrix} 1 & 0 & 0 \\ 0 & 1 & 0 \\ 0 & 0 & 2 \end{bmatrix} \quad (2.23)$$

such that

$$\begin{bmatrix} \varepsilon_1 \\ \varepsilon_2 \\ \gamma_{12} \end{bmatrix} = \mathbf{R} \begin{bmatrix} \varepsilon_1 \\ \varepsilon_2 \\ \varepsilon_{12} \end{bmatrix} \quad (2.24)$$

Similarly with the constitutive relations in Equation (2.19, 2.21), the relationship between bending moment and bending strain is given as

$$\begin{bmatrix} \sigma_1 \\ \sigma_2 \\ \tau_{12} \end{bmatrix} = \begin{bmatrix} D_{11} & D_{12} & 0 \\ D_{21} & D_{22} & 0 \\ 0 & 0 & D_{66} \end{bmatrix} \begin{bmatrix} \kappa_1 \\ \kappa_2 \\ \gamma_{12} \end{bmatrix} \quad (2.25)$$

In this case, σ_1 and σ_2 are bending stress, τ_{12} is bending strain, κ_1 and κ_2 are bending curvature, γ_{12} is twist strain and the stiffness components are defined as follows

$$D_{11} = B_1 \quad (2.26a)$$

$$D_{22} = B_2 \quad (2.26b)$$

$$D_{12} = B_2\nu_{12} = B_1\nu_{21} \quad (2.26c)$$

$$D_{66} = \varphi \quad (2.26d)$$

in which φ is torsional rigidity, ν_{12} and ν_{21} stand for the parameters analogous to Poisson's ratios related to the anticlastic curvature in the warp and weft directions. In the case of thin to moderately thick woven fabric, the anticlastic curvature is minimal, ν_{12} and ν_{21} are, therefore, approximated to zero.

The torsional rigidity φ can be calculated from the measured flexural moduli along the bias direction suggested by Kilby [47]. If the fabric is bent in a direction making an angle θ with direction 1, the bending rigidity B_1 is given by

$$B_\theta = B_1(\cos\theta)^4 + (4\tau + 2\nu_{12}B_2)(\cos\theta)^2(\sin\theta)^2 + B_2(\sin\theta)^4 \quad (2.27)$$

where $\theta = 45^\circ$ because it is taken in the bias direction, then $B_\theta = B_{45^\circ}$ stands for bending rigidity measured along bias direction. Therefore, the torsional rigidity is calculated by the following relationship

$$\varphi = B_{45^\circ} - \frac{1}{4}(B_1 + B_2) \quad (2.28)$$

2.4.3 The transverse shear strain

The thickness of thin to moderately thick fabric is generally too small to compare with other dimensions of fabric. Physically, this leads to the reaction of material when applied forces on the directional thickness of woven fabric are similar to the applied forces in the same direction of non-woven fabric, that is, the distinctions of mechanical properties between the warp yarns and the weft yarns in this direction is not necessary.

In fact, the configurations of the KES-FB system and the FAST system, as presented in the previous sections, do not distinguish the direction of warp yarns or weft yarns on compression test. Therefore, it can be assumed that the elasticity parameters corresponding to the dimensional thickness of fabric can be categorized as a linear homogeneous isotropic material. Then, the relationship between Bulk's modulus K and transverse shear modulus G is given in [45, 48], which expresses as

$$K = \frac{2G(1 + \nu)}{3(1 - 2\nu)} \quad (2.29a)$$

or

$$\rho \frac{\partial P}{\partial \rho} = \frac{2G(1 + \nu)}{3(1 - 2\nu)} \quad (2.29b)$$

where ρ is density of fabric, P is pressure and $\partial P/\partial \rho$ stands for the derivative of pressure with respect to density and ν is the ratio of Poisson related to transverse strain normal to the applied load. For thin to moderately thick fabric, the ratio of Poisson is minimal, so ν is approximated to zero.

The transverse shear constitutive equation for woven fabric and non-woven fabric is given as

$$D_0^s = \kappa G \begin{bmatrix} 1 & 0 \\ 0 & 1 \end{bmatrix} \quad (2.30)$$

where κ stands for the shear correction factor.

2.4.4 Coordinate transformation of warp yarns and weft yarns for the loading direction

In general, the loading direction does not coincide with the principal material directions. This required that the stresses and strains must be transformed into coordinates coinciding with the principal material directions via the coordinate transformation matrix. This matrix can be formulated by basing on summing forces acting along the warp or weft directions of the fabric, as shown in Figure 2.11.

The summing forces in the warp direction with respect to free body diagrams are defined in the [49], as illustrated in Figure 2.11.

Summing force in warp direction from free body diagram (a)

$$\begin{aligned} \sum F_{1a} = & \sigma_1 dA - \sigma_x(dA \cos \theta) \cos \theta - \sigma_y(dA \sin \theta) \sin \theta \\ & - \tau_{xy}(dA \cos \theta) \sin \theta - \tau_{xy}(dA \sin \theta) \cos \theta = 0 \end{aligned} \quad (2.31a)$$

Summing force in weft direction from free body diagram (b)

$$\begin{aligned} \sum F_{2b} = & \sigma_2 dA - \sigma_x(dA \sin \theta) \sin \theta - \sigma_y(dA \cos \theta) \cos \theta \\ & + \tau_{xy}(dA \cos \theta) \sin \theta + \tau_{xy}(dA \sin \theta) \cos \theta = 0 \end{aligned} \quad (2.31b)$$

Summing force in warp direction from free body diagram (b)

$$\begin{aligned} \sum F_{1b} = \tau_{12}dA + \sigma_x(dA\sin\theta)\cos\theta - \sigma_y(dA\cos\theta)\sin\theta \\ - \tau_{xy}(dA\cos\theta)\cos\theta + \tau_{xy}(dA\sin\theta)\sin\theta = 0 \end{aligned} \quad (2.31c)$$

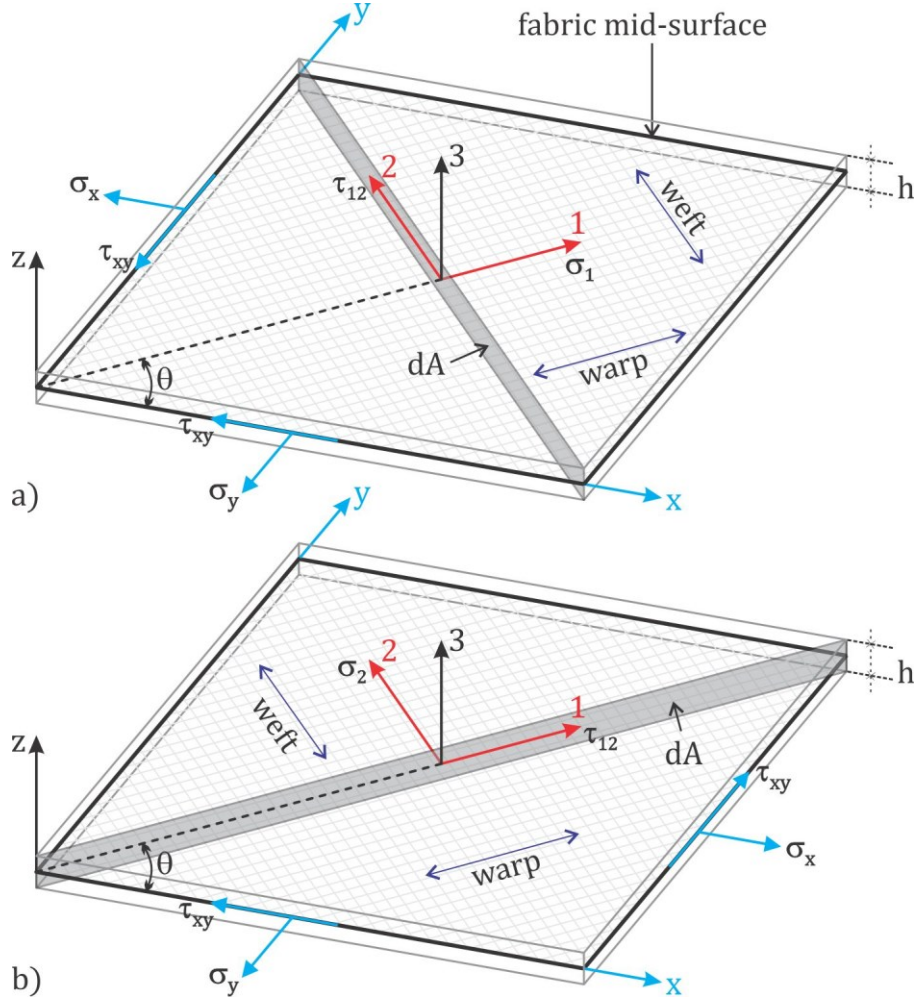


Figure 2.11: The free-body diagrams for the in-plane stresses in the warp yarns direction.

Simplifying these equations results in

$$\sigma_1 = \sigma_x \cos^2 \theta + \sigma_y \sin^2 \theta + 2\tau_{xy} \sin \theta \cos \theta \quad (2.32a)$$

$$\sigma_2 = \sigma_x \sin^2 \theta + \sigma_y \cos^2 \theta - 2\tau_{xy} \sin \theta \cos \theta \quad (2.32b)$$

$$\tau_{12} = -\sigma_x \sin \theta \cos \theta + \sigma_y \sin \theta \cos \theta + \tau_{xy} (\cos^2 \theta - \sin^2 \theta) \quad (2.32c)$$

Equations (2.32) can be rewritten in matrix form as follow

$$\begin{bmatrix} \sigma_1 \\ \sigma_2 \\ \tau_{12} \end{bmatrix} = \mathbf{T} \begin{bmatrix} \sigma_x \\ \sigma_y \\ \tau_{xy} \end{bmatrix} \quad (2.33)$$

or, equivalently, as

$$\begin{bmatrix} \sigma_x \\ \sigma_y \\ \tau_{xy} \end{bmatrix} = \mathbf{T}^{-1} \begin{bmatrix} \sigma_1 \\ \sigma_2 \\ \tau_{12} \end{bmatrix} \quad (2.34)$$

where \mathbf{T} is the coordinate transformation matrix defined as

$$\mathbf{T} = \begin{bmatrix} \cos^2\theta & \sin^2\theta & 2\sin\theta\cos\theta \\ \sin^2\theta & \cos^2\theta & -2\sin\theta\cos\theta \\ -\sin\theta\cos\theta & \sin\theta\cos\theta & (\cos^2\theta - \sin^2\theta) \end{bmatrix} \quad (2.35)$$

and \mathbf{T}^{-1} is the inverse matrix of \mathbf{T} , which is used for the transformation between the warp and weft directions of the fabric and the x and y directions within Cartesian coordinates (x, y, z) , written as

$$\mathbf{T}^{-1} = \begin{bmatrix} \cos^2\theta & \sin^2\theta & -2\sin\theta\cos\theta \\ \sin^2\theta & \cos^2\theta & 2\sin\theta\cos\theta \\ \sin\theta\cos\theta & -\sin\theta\cos\theta & (\cos^2\theta - \sin^2\theta) \end{bmatrix} \quad (2.36)$$

This coordinate transformation matrix is also applied for strain components which gives

$$\begin{bmatrix} \varepsilon_1 \\ \varepsilon_2 \\ \varepsilon_{12} \end{bmatrix} = \mathbf{T} \begin{bmatrix} \varepsilon_x \\ \varepsilon_y \\ \varepsilon_{xy} \end{bmatrix} \quad (2.37)$$

$$\begin{bmatrix} \varepsilon_x \\ \varepsilon_y \\ \varepsilon_{xy} \end{bmatrix} = \mathbf{T}^{-1} \begin{bmatrix} \varepsilon_1 \\ \varepsilon_2 \\ \varepsilon_{12} \end{bmatrix} \quad (2.38)$$

Combining Equations (2.21, 2.24, 2.33 to 2.38), the in-plane stiffness matrix in Cartesian coordinates (x, y, z) is given as

$$\begin{bmatrix} \sigma_x \\ \sigma_y \\ \tau_{xy} \end{bmatrix} = \tilde{\mathbf{D}} \begin{bmatrix} \varepsilon_x \\ \varepsilon_y \\ \gamma_{xy} \end{bmatrix} \quad (2.39)$$

where $\tilde{\mathbf{D}}$, the in-plane stiffness matrix is defined as

$$\tilde{\mathbf{D}} = \mathbf{T}^{-1} \mathbf{D} \mathbf{R} \mathbf{T} \mathbf{R}^{-1} = \begin{bmatrix} \tilde{D}_{11} & \tilde{D}_{12} & \tilde{D}_{16} \\ \tilde{D}_{12} & \tilde{D}_{22} & \tilde{D}_{26} \\ \tilde{D}_{16} & \tilde{D}_{26} & \tilde{D}_{66} \end{bmatrix} \quad (2.40)$$

in which, the components are

$$\tilde{D}_{11} = D_{11}\cos^4\theta + 2(D_{12} + 2D_{66})\cos^2\theta\sin^2\theta + D_{22}\sin^4\theta \quad (2.41a)$$

$$\tilde{D}_{22} = D_{11}\sin^4\theta + 2(D_{12} + 2D_{66})\cos^2\theta\sin^2\theta + D_{22}\cos^4\theta \quad (2.41b)$$

$$\tilde{D}_{12} = (D_{11} + D_{22} - 4D_{66})\cos^2\theta\sin^2\theta + D_{12}(\cos^4\theta + \sin^4\theta) \quad (2.41c)$$

$$\tilde{D}_{16} = (D_{11} - D_{12} - 2D_{66})\cos^3\theta\sin\theta + (D_{12} - D_{22} + 2D_{66})\cos\theta\sin^3\theta \quad (2.41d)$$

$$\tilde{D}_{26} = (D_{11} - D_{22} - 2D_{66})\cos\theta\sin^3\theta + (D_{12} - D_{22} + 2D_{66})\cos^3\theta\sin\theta \quad (2.41e)$$

$$\tilde{D}_{66} = (D_{11} + D_{22} - 2D_{12} - 2D_{66})\cos^2\theta\sin^2\theta + D_{66}(\cos^4\theta + \sin^4\theta) \quad (2.41f)$$

Note that the components $\tilde{D}_{16} \neq 0$ and $\tilde{D}_{26} \neq 0$ if only $\theta \neq 0$.

The bending stiffness matrix $\tilde{\mathbf{D}}$ is obtained by substituting the defined stiffness components as given in Equation (2.26) into Equations (2.41). It defines the relationship between bending moment and bending strain in Cartesian coordinates (x, y, z) .

2.5 Final remarks

Fabric constitutive laws for mechanical analysis and modelling of the textile fabrics based on the fabric objective measurement (FOM) technology via Kawabata evaluation system for fabrics (KES-FB) have been proposed in this chapter. These constitutive equations are formulated for both woven fabric and non-woven fabric.

In order to apply these constitutive equations to other sheet material, e.g. tissue, woven fabric composite, it is required that the major elasticity parameters, as introduced in Section 2.2, must be measured by an appropriate standard. For example, in the case of woven fabric composite, the high-stress mechanics via FOM can be applied.

The formulated constitutive equations \tilde{D}_0^m , \tilde{D}_0^b (Section 2.4.5) and D_0^s (Section 2.4.4) are applicable for both the existing standard FEM and S-FEM models comprising membrane finite element (for plane-stress problem) as well as plate/shell finite element based on either Kirchhoff–Love theory (classical plate theory) or Mindlin–Reissner theory (first-order shear deformation theory), as summarized in Table 2.11.

Table 2.11: Constitutive equations for displacement-based low-order finite element formulations of plate and shell finite element

Stiffness matrix	Plane-stress	Kirchhoff-Love theory		Mindlin-Reissner theory	
	Membrane	Plate	Shell	Plate	Shell
\tilde{D}_0^m	yes	no	yes	no	yes
\tilde{D}_0^b	no	yes	yes	yes	yes
D_0^s	no	no	no	yes	yes

Note that superscripts m , b and s stand for membrane, bending/curvature and shear element.

The reader is referred to Section 3.5 for the formulation of membrane finite element model, Section 3.4 for the formulation of plate bending finite element model with assumed transverse shear strain fields and Section 3.6 for the formulation of flat shell finite element model.

2.6 References

1. Behery, H.M., *Effect of mechanical and physical properties on fabric hand*. 2005, North America by CRC Press LLC: Woodhead Publishing Limited
2. Peirce, F.T., *26—THE “HANDLE” OF CLOTH AS A MEASURABLE QUANTITY*. *Journal of the Textile Institute Transactions*, 1930. **21**(9): p. T377-T416.
3. Postle, R., *Fabric objective measurement technology: present status and future potential*. *International Journal of Clothing Science and Technology*, 1990. **2**(3): p. 7-17.
4. Postle, R., S. Kawabata, and M. Niwa, *Objective Evaluation of Apparel Fabrics*. 1983: Textile Machinery Society of Japan.
5. Kawabata, S. and M. Niwa, *Objective measurement of fabric mechanical property and quality: its application to textile and clothing manufacturing*. *International Journal of Clothing Science and Technology*, 1991. **3**(1): p. 7-18.
6. Kawabata, S., *The Standardization and Analysis of Hand Evaluation*. *The Textile Machinery Society of Japan*. 1980.
7. Smuts, S., et al., *A Review of Fabric Objective Measurement*. *Tex Report*. 1991: CSIR Division of Textile Technology.
8. Damyanov, G.B. and D. Germanova-Krasteva, *Textile Processes: Quality Control and Design of Experiments*. 1 ed. 2012: Momentum Press.
9. Peterson, E.A., *Standardization of industrial garment fit*. *Industrial Launderer*, 1989. **31**: p. 81-89.
10. Hu, J., *Fabric Testing*. *Woodhead Textiles Series*. 2008: Woodhead Publishing Ltd.
11. Saville, B.P., *Physical testing of textiles*. *Woodhead Textiles Series*. 1999: Woodhead Publishing Ltd.
12. Fan, J., W. Yu, and L. Hunter, *Clothing appearance and fit: Science and technology*. *Woodhead Publishing in Textiles*. 2004: CRC.
13. Lutz Walter, G.-A.K., Stefano Carosio, *Transforming Clothing Production into a Demand-driven, Knowledge-based, High-tech Industry*. 2009: Springer-Verlag London Limited.
14. Fairhurst, C., *Advances in Apparel Production*. *Woodhead Publishing in Textiles*. 2008: Woodhead Publishing Limited.
15. Magnenat-Thalmann, N., *Modeling and Simulating Bodies and Garments*. 2010: Springer-Verlag London Limited.
16. Veit, D., *Simulation in textile technology: Theory and applications*. 1 ed. *Woodhead Publishing Series in Textiles*. 2012: Woodhead Publishing.
17. Horrocks, A.R. and S.C. Anand, *Handbook of Technical Textiles*. *Woodhead Publishing series in textiles*. 2000: Taylor & Francis.
18. Brady, P.R., *The objective measurement of finished fabric*, in *Finishing and Wool Fabric Properties: A Guide to the Theory and Practice of Finishing Woven Wool Fabrics*. 1997, CSIRO Wool Technology.
19. Majumdar, A., A. Das, and R. Alagirusamy, *Process control in textile manufacturing*. *Woodhead Textiles Series*. 2012: Woodhead Publishing Ltd.
20. Fan, J. and L. Hunter, *Engineering Apparel Fabrics and Garments*. *Woodhead Publishing in textiles*. 2009: Woodhead Publishing.
21. Lee, D.H., *Production in the market*. *Text Asia*, 2002. **33**: p. 42.
22. Hu, J., *Structure and mechanics of woven fabrics*. 2004, Cambridge: Woodhead Publishing Ltd.

-
23. Haas, R. and A. Dietzius, *The stretching of the fabric and the shape of the envelope in non-rigid balloons*. National Advisory Committee for Aeronautics, 1918. **16**: p. 149-271.
 24. Peirce, F.T., *The geometry of cloth structure*. Journal of the Textile Institute, 1937. **28**: p. 43-77.
 25. Grosberg, P. and N.M. Swani, *The Mechanical Properties of Woven Fabrics: Part III: The Buckling of Woven Fabrics*. Textile Research Journal, 1966. **36**(4): p. 332-338.
 26. Grosberg, P. and B.J. Park, *The Mechanical Properties of Woven Fabrics: Part V: The Initial Modulus and the Frictional Restraint in shearing of Plain Weave Fabrics*. Textile Research Journal, 1966. **36**(5): p. 420-431.
 27. Grosberg, P., *The Mechanical Properties of Woven Fabrics Part II: The Bending of Woven Fabrics*. Textile Research Journal, 1966. **36**(3): p. 205-211.
 28. Lindberg, J., L. Waesterberg, and R. Svenson, *108-Wool fabrics as garment construction materials*. Journal of the Textile Institute Transactions, 1960. **51**(12): p. T1475-T1493.
 29. Hearle, J.W., J.J. Thwaites, and J. Amirbayat, *Mechanics of Flexible Fibre Assemblies*. NATO Advanced Study Institute Series: E, Applied Sciences No. 38. 1980: Alpen aan den Rijn, The Netherlands, Sijthoff and Noordhoff.
 30. Kawabata, S., *The Standardization and Analysis of Hand Evaluation*. 1980, Osaka: Textile Machinery Society of Japan.
 31. Nihon Sen'i Kikai Gakkai. Hand, E. and C. Standardization, *H.E.S.C. Standard of Hand Evaluation: Men's winter suiting*. 1982: The Society.
 32. *Kawabata Evaluation System for Fabrics*. [cited 2014; Available from: <http://english.keskato.co.jp/>].
 33. Hearle, J.W.S., *Can fabric hand enter the dataspace? Part I*. Text Horizons, Int., 1993: p. 14-17.
 34. Hearle, J.W.S., *Can fabric hand enter the dataspace? Part II: Measuring the unmeasurable?* Text Horizons, Int., 1993: p. 16-20.
 35. *Fabric Assurance by Simple Testing*. [cited 2014; Available from: <http://www.csiro.au/>].
 36. Yick, K.-L., et al., *Comparison of Mechanical Properties of Shirting Materials Measured on the KES-F and FAST Instruments*. Textile Research Journal, 1996. **66**(10): p. 622-633.
 37. Alderman, S.D., *Mastering Weave Structures: Transforming Ideas Into Great Cloth*. 2004: Interweave Press, LLC.
 38. N, G., *Fabric Structure and Design*. 2009: New Age International (P) Limited.
 39. Behera, B.K. and P.K. Hari, *Woven Textile Structure: Theory And Applications*. Woodhead Publishing Series in Textiles. 2010: Elsevier Science.
 40. Lloyd, D.W., W.J. Shanahan, and M. Konopasek, *The folding of heavy fabric sheets*. International Journal of Mechanical Sciences, 1978. **20**(8): p. 521-527.
 41. Beaussart, A.J., J.W.S. Hearle, and R.B. Pipes, *Constitutive relationships for anisotropic viscous materials*. Composites Science and Technology, 1993. **49**(4): p. 335-339.
 42. Collier, J.R., et al., *Drape prediction by means of finite-element analysis*. J Text Inst, 1991. **82**: p. 96-107.
 43. Gan, L., N.G. Ly, and G.P. Steven, *A study of fabric deformation using nonlinear finite elements*. Textile Res J, 1995. **65**: p. 660-668.
 44. Eischen, J.W., D. Shigan, and T.G. Clapp, *Finite-element modeling and control of flexible fabric parts*. IEEE Computer Graphics and Applications, 1996. **16**(5): p. 71-80.
 45. Ferdinand Beer, J., E. Russell Johnston, John DeWolf, David Mazurek, *Mechanics of Materials*. 6th ed. 2012: McGraw-Hill Companies, Inc.
 46. Marc André Meyers, K.K.C., *Mechanical Behavior of Materials*. 2 ed. 2008: Cambridge University Press.
-

-
47. Kilby, W.F., *Planar Stress-Strain Relationships in Woven Fabrics*. Journal of the Textile Institute Transactions, 1963. **54**(1): p. T9-T27.
 48. Hibbeler, R.C., *Mechanics of Materials*. 8 ed. 2010: Prentice Hall.
 49. Nettles, A.T., *Basic mechanics of laminated composite plates*. NASA Reference Publication 1351. 1994, Marshall Space Flight Center, Alabama.

Theoretical formulations of S-FEM for textile fabrics

Abstract

An S-FEM (Smoothed Finite Element Method) for mechanical analysis and modelling of the textile fabrics is proposed in this chapter. In this theoretical framework, one assumes that the non-woven fabric is an elastic isotropic material, while the woven fabric is an elastic with orthotropic anisotropy for which the constitutive laws are formulated using low-stress mechanical properties based on FOM (Fabric Objective Measurement). The displacement-based low-order finite element formulations for four-node quadrilateral plate/shell finite element, including assumed transverse shear strain fields, are based on the contributions due to Raymond Mindlin [1] and by Eric Reissner [2], namely Mindlin-Reissner theory and so-called first-order shear deformation theory (FSDT), which are combined with the gradient/strain smoothing technique in terms of S-FEM models due to contributed by G. R. Liu et al. [3] in order to mitigate problems as element distortion, mesh coarseness as well as the well-known locking phenomena. Quadrilateral meshes are used due to ability to generate complicated geometries of complex mechanical deformation of the fabric such as plane stress recovery, bending, buckling, vibration, draping behavior, etc. The developed plate/shell finite element models and low-stress mechanic properties in terms of FOM are, therefore, well adapted for numerical analysis and modelling of macro-mechanical deformation of the very thin to moderately thick fabric sheet, including both simple and complex mechanical deformation analysis. In fact, numerical examples, as those shown in the next chapter, indicate that the developed plate/shell elements with assumed the strain/gradient smoothing technique, do alleviate element distortion, mesh coarseness and locking effect even for modelling thin to moderately thick fabric.

Keywords Woven fabric, non-woven fabric, Mindlin-Reissner theory, transverse shear strain, strain/gradient smoothing technique, smoothed finite element methods, shear-locking, element distortion, mesh coarseness, plate bending finite element, flat shell finite element.

3.1 Introduction

A brief definition of the static and dynamic problems for elastic systems, being appropriate to finite element analysis and modelling of mechanical deformation of the textile fabrics, is presented in Section 3.2, where the dynamic equilibrium equations are derived in space-time using Lagrange's equations of motion and the implicit time integration schemes for the space-discretized equations of motion based on Newmark's method are introduced.

The well-known locking phenomenon in displacement-based low-order finite element formulations for thin plate and shell finite element models and other shortcomings they may exhibit with regard to low accuracy e.g. element distortion, mesh coarseness, etc. were introduced in Section 1.2. These problems can affect the numerical results, such as in the case of finite element simulation of thin fabric sheet. Although a significant amount of works have been done in FEM to alleviate these problems, as presented in Section 1.2, some inherent issues that are related to element distortion still remain unsolved. Based on the existing standard FEM and the existing gradient/strain smoothing technique, which was proposed by Chen et al. [4] in the context of mesh-free methods [5, 6], Liu and his coworkers [3, 7] recently proposed S-FEM models in which each of the discretized elements is further divided into smoothing domain(s), being the integrals evaluated along the edges of the smoothing domain(s) according to the Green's divergence theorem. This gradient/strain smoothing technique avoids evaluating derivatives of mesh-free shape functions at nodes and therefore eliminates defective modes. Liu et al. [7, 8] detailed the theoretical aspects covering stability, bound property and convergence about the S-FEM models, as well as revealed the majority advanced features resulted from the "softening" effects of the gradient/strain smoothing technique. A brief introduction, covering recently published works and most advanced features of S-FEM in which the smoothing operator plays a key role in this research are presented in Section 3.3.

In order to define the system vectors and matrices, such as mass/stiffness matrix and load vector, needed for the space-discretized equations of motion that are derived in Section 3.2, the FSDT and S-FEM models will be combined to develop quadrilateral plate/shell finite element models taking into account the fabric constitutive laws formulated using FOM data dealt with in the previous chapter. This combination resulting in the concise formulations of the four-node quadrilateral plate bending element, the four-node quadrilateral membrane element and the four-node quadrilateral flat shell element with assumed strain smoothing technique that are, respectively, presented in Sections 3.4, 3.5 and 3.6. Finally, this chapter ends with some final remarks.

3.2 Preliminaries

3.2.1 Domains and boundaries

The equations defined below are generally valid (with distinct definitions of the terms involved) for the textile fabrics, under both static and dynamic loading conditions.

Let us assume that a woven fabric sheet occupying a domain Ω with thickness h is expressed in terms of the elastic material with orthotropic anisotropy and constructed with the plain-weave, in which the interlaced warp and weft yarns and the fabric thickness are, respectively, laid on the direction of the x -, y - and z -axes as shown in Figure 3.1.

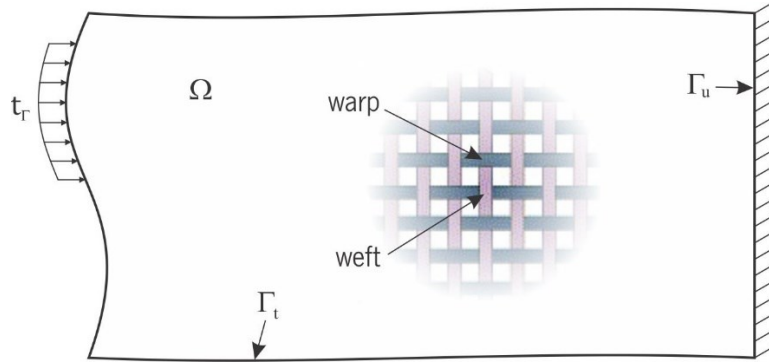


Figure 3.1: Domain, Neumann and Dirichlet boundaries.

The reference configuration Ω is a bounded volume domain in \mathbb{R}^3 . The boundary denotes with Γ , which is formed by the complementary Dirichlet Γ_u and Neumann Γ_t boundary condition parts [9, 10], $\Gamma_u \cup \Gamma_t = \Gamma$ and $\Gamma_u \cap \Gamma_t = \emptyset$. Let us also assume that the displacements and the tractions on the boundary have been prescribed.

Note that this assumption of the woven fabric sheet is set to be the reference configuration domain Ω and boundary Γ through this work.

3.2.2 Governing equations

The dynamic equilibrium equations and compatibility conditions of an infinitesimal cut of the domain Ω can be defined as in [9-14]

$$\nabla \cdot \boldsymbol{\sigma}(x, y, z, t) + \mathbf{b}(x, y, z, t) = \mu \mathbf{v}(x, y, z, t) + \rho \mathbf{a}(x, y, z, t) \quad \text{in } \Omega \quad (3.1)$$

$$\boldsymbol{\varepsilon}(x, y, z, t) = \nabla \mathbf{u}(x, y, z, t) \quad \text{in } \Omega \quad (3.2)$$

where the divergence operator $\nabla \cdot$ and gradient operator ∇ are adjoint in a geometrically linear structure, the vectors $\boldsymbol{\sigma}(x, y, z, t)$, $\boldsymbol{\varepsilon}(x, y, z, t)$ and $\mathbf{u}(x, y, z, t)$ assemble the independent components of the stress fields, strain fields and the displacement components of the structure, respectively, and the vector $\mathbf{b}(x, y, z, t)$ stands for the body force vector, while the symbols μ and ρ denote the damping coefficient and the density. In structural dynamic finite element problems, the effects of velocity $\mathbf{v}(x, y, z, t)$ and acceleration $\mathbf{a}(x, y, z, t)$ can be considered with respect to time as follows

$$\mathbf{v}(x, y, z, t) = \dot{\mathbf{u}}(x, y, z, t) \quad (3.3)$$

$$\mathbf{a}(x, y, z, t) = \ddot{\mathbf{u}}(x, y, z, t) \quad (3.4)$$

The constitutive relations are written in the alternative stiffness and flexibility forms,

$$\boldsymbol{\sigma}(x, y, z, t) = \mathbf{k}\boldsymbol{\varepsilon}(x, y, z, t) \quad \text{in } \Omega \quad (3.5)$$

$$\boldsymbol{\varepsilon}(x, y, z, t) = \mathbf{f}\boldsymbol{\sigma}(x, y, z, t) \quad \text{in } \Omega \quad (3.6)$$

in which matrices \mathbf{k} and \mathbf{f} define the material properties.

In the Neumann boundary conditions,

$$\mathbf{N}\boldsymbol{\sigma}(x, y, z, t) = \mathbf{t}_\Gamma(x, y, z, t) \quad \text{on } \Gamma_t \quad (3.7)$$

where vector \mathbf{t}_Γ collects the applied surface tractions, being the components of the unit outward normal to the boundary organized in matrix \mathbf{N} .

In the Dirichlet boundary conditions,

$$\mathbf{u}(x, y, z, t) = \mathbf{u}_\Gamma(x, y, z, t) \quad \text{on } \Gamma_u \quad (3.8)$$

the domain displacements \mathbf{u} must be compatible with the imposed displacements collected in vector Γ_u .

The initial displacements and velocities of the dynamic system in the time interval $t = [0, \Delta t]$ and their components defined in vectors $\mathbf{u}_0(x, y, z)$ and $\mathbf{v}_0(x, y, z)$ are given by

$$\mathbf{u}(x, y, z, 0) = \mathbf{u}_0(x, y, z) \quad (3.9)$$

$$\mathbf{v}(x, y, z, 0) = \mathbf{v}_0(x, y, z) \quad (3.10)$$

either of which can be replaced by a constraint on the initial acceleration.

In the dynamic problems, the accelerations, velocities, displacements, strains, stresses and loads are all time-dependent. The dynamic equilibrium equation (Eq. 3.1) can be derived using either Lagrange equations or Hamilton's principle. In this study, the Lagrange equations will be used.

3.2.3 Domain discretization and continuity conditions

Consider a fabric sheet with thickness h occupying the volume domain Ω bounded by Γ . The total domain of the undeformed fabric mid-plane is thus the tensor product $\bar{\Omega} \equiv \Omega \times (-h/2, h/2)$. The boundary of the total domain consists of top surface ($z = h/2$) and bottom surface ($z = -h/2$) and the edge $\bar{\Gamma} \equiv \Gamma \times (-h/2, h/2)$. In general, Γ can be either a curved surface or plane surface, with outward normal $\hat{\mathbf{n}} = n_x \hat{\mathbf{e}}_x + n_y \hat{\mathbf{e}}_y$, where n_x and n_y are the direction cosines of the unit normal.

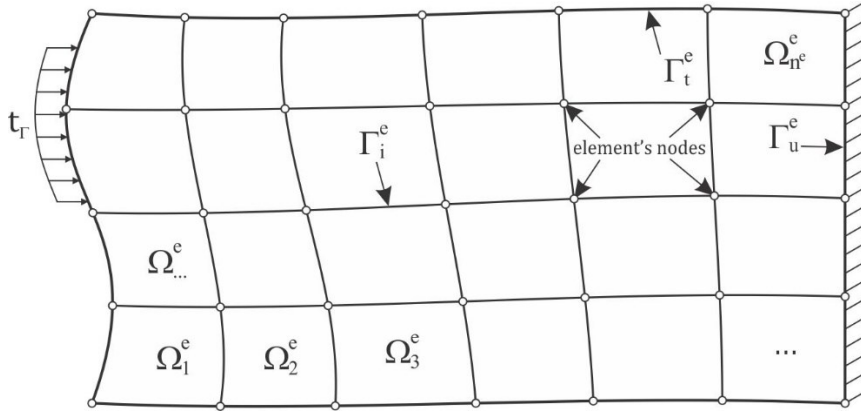


Figure 3.2: Example of finite elements and Neumann and Dirichlet boundaries.

Now let the reference domain Ω be discretized into n^e finite elements and connected by the nodal points on the element boundaries such that $\Omega = \bigcup_{i=1}^{n^e} \Omega_i^e$, $\Omega_i^e \cap \Omega_j^e = \emptyset$, $i \neq j$ ($i = 1, \dots, n^e$; $j = 1, \dots, n^e$), where Ω_i^e and Γ_i^e denote the domain of the i th generic element and its boundary, respectively, as illustrated in Figure 3.2.

Boundary Γ^e is established, in general, by the complementary Neumann Γ_t^e and Dirichlet Γ_u^e parts, where Equations (3.7, 3.8) are prescribed, respectively, and the interior Γ_i^e part, where the boundary equilibrium and compatibility conditions must be satisfied

$$\mathbf{t}_i(x, y, z, t) = \mathbf{t}_j(x, y, z, t) \quad \text{on } \Gamma_i^e \quad (3.11a)$$

$$\mathbf{u}_i(x, y, z, t) = \mathbf{u}_j(x, y, z, t) \quad \text{on } \Gamma_i^e \quad (3.11b)$$

in which the subscripts i and j denote the two finite elements that share the interior boundary Γ_i^e .

Note that the current configuration of domain discretization and its continuity conditions is set to be the reference configuration through the present work. In practice, to develop the finite element computer codes or to implement finite element model, numbering the nodes and elements of a discretized problem domain in order is of paramount importance. For example, with a typical element Ω^e from the mesh shown in Figure 3.2, let the local node numbers for the nodes of the element be denoted by I ($I = 1,2,3,4$) and the mesh node numbers by i , then the nodal coordinates of element Ω^e are denoted with (x_I^i, y_I^i) . It is recommended that the nodes be numbered counterclockwise. The formulations that follow can also be developed with the clockwise numbering, but most FEM/FEA/CAE computer applications, including the ones in this research, use counterclockwise numbering, as otherwise some crucial signs will be wrong. This recommendation is consistent with the smoothing domain(s) used in the formulation of S-FEM models, as presented in the following sections.

3.2.4 Integration in space

The finite element solution \mathbf{u} of a displacement model, for instance, in 3D is expressed as follows

$$\mathbf{u} = \sum_I^{n^n} \begin{bmatrix} N_I & 0 & 0 \\ 0 & N_I & 0 \\ 0 & 0 & N_I \end{bmatrix} \mathbf{q}_I = \mathbf{N}\mathbf{q}(t) \quad (3.12)$$

where n^n is the total number of nodes in the mesh, N_I is shape function matrix associated with node I , $\mathbf{q}_I = [u_{0I} \quad v_{0I} \quad w_{0I}]^T$ stands for the degrees of freedom for node I and \mathbf{q} is the nodal displacement vector and assumed to be a function of time t . Introducing Equation (3.12) to Equation (3.2), the discrete strain field results in

$$\boldsymbol{\varepsilon} = \mathbf{B}\mathbf{q} \quad (3.13)$$

where \mathbf{B} is the discretized gradient matrix. Using Equation (3.6), the stress-strain relation is obtained as

$$\boldsymbol{\sigma} = \mathbf{D}_0\boldsymbol{\varepsilon} \quad (3.14)$$

being \mathbf{D}_0 a matrix that defines the material properties

The dynamic equilibrium condition in Equation (3.1) can be derived by using the following Lagrange's equations of motion [13], which gives

$$\left\{ \frac{\partial L}{\partial \mathbf{q}} \right\} = \frac{d}{dt} \left\{ \frac{\partial L}{\partial \dot{\mathbf{q}}} \right\} + \left\{ \frac{\partial R}{\partial \dot{\mathbf{q}}} \right\} \quad (3.15)$$

in which L is the Lagrange function, R is the dissipation function, \mathbf{q} is the nodal displacement and $\dot{\mathbf{q}}$ is the nodal velocity. The Lagrange function is expressed as

$$L = T - \Pi \quad (3.16)$$

where T is the kinetic energy and Π is the potential energy. The kinetic energy and the potential energy of each element are given by

$$T^e = \frac{1}{2} \iiint_{\Omega^e} \rho \dot{\mathbf{u}}^T \dot{\mathbf{u}} d\Omega \quad (3.17a)$$

$$\Pi^e = \frac{1}{2} \iiint_{\Omega^e} \hat{\boldsymbol{\varepsilon}}^T \hat{\boldsymbol{\sigma}} d\Omega - \left(\iiint_{\Omega^e} \mathbf{u}^T \mathbf{b} d\Omega + \iint_{\Gamma^e} \mathbf{u}^T \mathbf{t}_\Gamma d\Gamma \right) \quad (3.17b)$$

Because at equilibrium the dissipation function for element can be defined by

$$R^e = \frac{1}{2} \iiint_{\Omega^e} \mu \dot{\mathbf{u}}^T \dot{\mathbf{u}} d\Omega \quad (3.17c)$$

By substituting Equations (3.12 to 3.14) into Equation (3.17) and then introducing Equation (3.15) the expressions for T , Π and R can be written as

$$T = \sum_{k=1}^{N_e} T^e = \frac{1}{2} \dot{\mathbf{q}}^T \left(\sum_{k=1}^{N_e} \mathbf{m} \right) \dot{\mathbf{q}} = \frac{1}{2} \dot{\mathbf{q}}^T \mathbf{M} \dot{\mathbf{q}} \quad (3.18a)$$

$$\Pi = \sum_{k=1}^{N_e} \Pi^e = \frac{1}{2} \mathbf{q}^T \left(\sum_{k=1}^{N_e} \mathbf{k} \right) \mathbf{q} - \mathbf{q}^T \left[\left(\sum_{k=1}^{N_e} (\mathbf{f}_b + \mathbf{f}_s) \right) + \mathbf{f}_c(t) \right] = \frac{1}{2} \mathbf{q}^T \mathbf{K} \mathbf{q} - \mathbf{q}^T \mathbf{F} \quad (3.18b)$$

$$R = \sum_{k=1}^{N_e} R^e = \frac{1}{2} \dot{\mathbf{q}}^T \left(\sum_{k=1}^{N_e} \mathbf{c} \right) \dot{\mathbf{q}} = \frac{1}{2} \dot{\mathbf{q}}^T \mathbf{C} \dot{\mathbf{q}} \quad (3.18c)$$

where \mathbf{q} is the global nodal displacement vector, $\dot{\mathbf{q}}$ is the global nodal velocity vector, \mathbf{M} and \mathbf{K} are the global mass matrix and stiffness matrix, \mathbf{C} is the global damping matrix, \mathbf{F} is total load vector and \mathbf{f}_c is the concentrated nodal force vector. The element matrices involving the integrals associated to mass matrix \mathbf{m} , damping matrix \mathbf{c} and stiffness matrix \mathbf{k} are defined as follows

$$\mathbf{m} = \iiint_{\Omega^e} \rho \mathbf{N}^T \mathbf{N} d\Omega \quad (3.19)$$

$$\mathbf{c} = \iiint_{\Omega^e} \mu \mathbf{N}^T \mathbf{N} d\Omega \quad (3.20)$$

$$\mathbf{k} = \iiint_{\Omega^e} \widehat{\mathbf{B}}^T \widehat{\mathbf{D}} \widehat{\mathbf{B}} d\Omega \quad (3.21)$$

and the vector of element nodal forces produced by body forces \mathbf{f}_b and surface tractions \mathbf{f}_s can be written as

$$\mathbf{f}_b = \iiint_{\Omega^e} \mathbf{N}^T \mathbf{b} d\Omega \quad (3.22)$$

$$\mathbf{f}_s = \iint_{\Gamma^e} \mathbf{N}^T \mathbf{t}_\Gamma d\Gamma \quad (3.23)$$

Finally, by substituting Equations (3.18) into Equation (3.16), then the dynamic equilibrium equation can be written in terms of displacements as

$$\mathbf{M}\ddot{\mathbf{q}}(t) + \mathbf{C}\dot{\mathbf{q}}(t) + \mathbf{K}\mathbf{q}(t) = \mathbf{F}(t) \quad (3.24)$$

where $\ddot{\mathbf{q}}$ is the vector of nodal acceleration in the global system. For simplicity, the velocity-dependent damping is not considered, then the semi-discrete dynamic equilibrium equation is written as

$$\mathbf{M}\ddot{\mathbf{q}} + \mathbf{K}\mathbf{q} = \mathbf{F} \quad (3.25)$$

By assuming the external force vector \mathbf{F} to be zero and the displacements to be harmonic [15-21] as

$$\mathbf{q} = \bar{\mathbf{q}} e^{i\omega t} \quad (3.26)$$

where $\bar{\mathbf{q}}$ is n -dimensional vector called a mode shape. The free-vibration equation of motion is then rewritten from Equation (3.25) as follows

$$[\mathbf{K} + \omega^2 \mathbf{M}] \bar{\mathbf{q}} = \mathbf{0} \quad (3.27)$$

The formulation of the buckling analysis whose equation of motion can be expressed as

$$[\mathbf{K} + \lambda_{cr} \mathbf{K}^g] \bar{\mathbf{q}} = \mathbf{0} \quad (3.28)$$

In Equations (3.27, 3.28), $\bar{\mathbf{q}}$ is the eigenvector that contains the vibration/buckling mode shapes, ω is a non-trivial forcing frequency, λ_{cr} is the so-called critical buckling load, \mathbf{K}^g is nonlinear geometric stiffness element matrix presented in Equations (3.72, 3.111). Note that the term $\bar{\mathbf{q}}$ used in Equation (3.28) is not relative to Equation (3.26).

If the loads applied on the solid are static, the dynamic term in Equation (3.26) vanishes. The static equilibrium equation is then as follows

$$\mathbf{K}\mathbf{q} = \mathbf{F} \quad (3.29)$$

It is clear that the above semi-discrete or so-called space-discretized dynamic equilibrium equations can be solved by means of a time integration scheme, as the one introduced in the next section.

3.2.5 Integration in time

Time integration schemes can be classified into two main categories: explicit and implicit. In explicit integration schemes, the dynamic equation of motion (Eq. 3.24) can be solved at time t ; based on that, the solution at time $t + \Delta t$ is obtained without having to solve a set of linear equations at each step. In explicit schemes, the time integration of the discrete momentum equations does not require the solution of any equations. Therefore, explicit solutions are conditionally stable with respect to the size of the time step. Besides, the resulting time increment is generally too small for practical considerations in computer effort and for the response necessary to model slowly varying loads.

In implicit schemes, Equation (3.24) can be solved at time t after the solution at time $t - \Delta t$ is found. Therefore in implicit solutions, the time integration of the discrete momentum equations requires the solution of a set of algebraic equations at each time step; however, larger time steps may be used. Implicit methods can be conditionally or unconditionally stable. A computational model of large real structures generally takes a large number of periods which are smaller than the integration time step, so it is therefore essential to select a numerical integration method that is unconditionally stable for all time steps.

In this research, the implicit integration schemes and unconditionally stable methods are applied for dynamic response analysis of the textile fabrics. Among the numerical integration methods available to integrate second order equations, the single-step integration method developed by Newmark [9, 22] is used.

In 1959 Newmark [23] presented a family of single-step integration methods for solving the structural dynamic problems. During the past 50 years, Newmark's method has been applied to the dynamic analysis of many practical engineering structures. In addition, it has been modified and improved by many other researchers. In 1962, Wilson [24] formulated Newmark's method in matrix notation as shown in Equations (3.30, 3.31). He added stiffness and mass proportional damping and eliminated the need for iteration by introducing the direct solution of equations at each time step.

Newmark's method for the solution of the space-discrete equations of motion (Eq. 3.24) is defined by Newmark's equations as follows

$$\ddot{\mathbf{q}}_t = b_1(\mathbf{q}_t - \mathbf{q}_{t-\Delta t}) + b_2\dot{\mathbf{q}}_{t-\Delta t} + b_3\ddot{\mathbf{q}}_{t-\Delta t} \quad (3.30)$$

$$\dot{\mathbf{q}}_t = b_4(\mathbf{q}_t - \mathbf{q}_{t-\Delta t}) + b_5\dot{\mathbf{q}}_{t-\Delta t} + b_6\ddot{\mathbf{q}}_{t-\Delta t} \quad (3.31)$$

where Δt is the time step size and the constants b_1 to b_6 are given by

$$b_1 = \frac{1}{\beta\Delta t^2}; b_2 = \frac{1}{\beta\Delta t}; b_3 = \beta - \frac{1}{2}; \quad (3.32)$$

$$b_4 = \gamma\Delta t b_1; b_5 = 1 + \gamma\Delta t b_2; b_6 = \Delta t(1 + \gamma b_3 - \gamma)$$

being β and γ are the parameters that determine the stability and accuracy of the scheme.

Newmark's method used Equations (3.24, 3.30, 3.31) iteratively, for each time step, for each displacement DOF of the structural system. The term $\ddot{\mathbf{q}}_t$ was obtained from Equation (3.30) by dividing the equation by the mass associated with the DOF.

By substituting Equations (3.30, 3.31) into Equation (3.24), the Equation (3.24) at time t can be written in terms of the unknown nodal displacements \mathbf{q}_t as follow

$$(b_1\mathbf{M} + b_4\mathbf{C} + \mathbf{K})\mathbf{q}_t = \mathbf{F}_T + \mathbf{M}(b_1\mathbf{q}_{t-\Delta t} - b_2\dot{\mathbf{q}}_{t-\Delta t} - b_3\ddot{\mathbf{q}}_{t-\Delta t}) + \mathbf{C}(b_4\mathbf{q}_{t-\Delta t} + b_5\dot{\mathbf{q}}_{t-\Delta t} - b_6\ddot{\mathbf{q}}_{t-\Delta t}) \quad (3.33)$$

Note that the constants b_i need be calculated only once. Also, for linear systems, the effective dynamic stiffness matrix \mathbf{K} is formed and triangularized only once.

Besides, Newmark's method without damping is conditionally stable if

$$\beta \leq \frac{1}{2}, \gamma \geq \frac{1}{2} \quad (3.34)$$

but it is unconditionally stable if

$$2\beta \geq \gamma \geq \frac{1}{2} \quad (3.35)$$

However, if γ is greater than $1/2$, errors are introduced. These errors are associated with “numerical damping” and “period elongation”. For large multi degree-of-freedom structural systems, the time step limit given by Equation (3.24) can be written as

$$\frac{\Delta t}{t_{min}} \leq \frac{1}{2\pi \sqrt{\frac{\gamma}{2} - \beta}} \quad (3.36)$$

3.3 The strain/gradient smoothing technique

3.3.1 Introduction

S-FEM was recently presented by Liu and his coworkers [3, 7] based on the existing standard FEM and the existing gradient/strain smoothing technique, which was proposed by Chen et al. [4] in the context of the stabilized conforming nodal integration (SCNI) mesh-free methods [5, 6]. It is a strain smoothing stabilization that is to compute the nodal strain as the divergence of a spatial average of the compatible strain field. This technique avoids evaluating derivatives of mesh-free shape functions at nodes and therefore eliminates defective modes. Liu and Nguyen-Thoi [3] presented the most advanced features of the strain/gradient smoothing technique used in the S-FEM models and the major differences in key numerical techniques between S-FEM and FEM, as explained in the book entitled ‘Smoothed Finite Element Methods’ published in 2010 and also in the newest book ‘The Finite Element Method: A Practical Course’ by Liu and Quek [25], published in 2013. The essential idea in S-FEM is to modify the compatible strain field, or construct a strain field using only the displacements in order to ensure stability and convergence to the exact solution. The major techniques used in S-FEM models appear summarized in references [3, 7, 8].

The S-FEM models can well resolve almost the main difficult issues in the standard FEM models through the works of Liu et al [7, 26-32], Nguyen-Thoi et al [33-36], Nguyen-Xuan et al [37-41], Nguyen-Thanh et al [42, 43] and other researchers [44-71], e.g. overly stiff phenomenon leading to the so-called locking behavior for many problems, stress accuracy issues, mesh distortion issues,

meshing issues, solution certificate and computational efficiency. The versions of S-FEM models and properties are summarized in Table 3.1.

Table 3.1 Versions of S-FEM Models and Properties.

Abbreviation	Full Name	Formulation	Features/Properties
CS-FEM (2D) CS-FEM (3D)	Cell-based smoothed finite element method using quadrilateral elements	Smoothed Galerkin Linear or enriched PIM Quadrilateral cell-based smoothing domains	Linearly conforming Good accuracy Softer than FEM Super-convergence Conditionally stable
nCS-FEM (2D) nCS-FEM (3D)	Cell-based smoothed finite element method using n -sided polygonal elements	Smoothed Galerkin Linear or enriched PIM Triangular cell-based smoothing domains	Linearly conforming Good accuracy Super-convergence Spatially and temporally stable
NS-FEM (2D and 3D)	Node-based smoothed finite element method using n -sided polygonal elements (including T3 and T4)	Smoothed Galerkin Linear or enriched PIM Smoothing operation based on nodes	Linearly conforming Volumetric locking free Upper bound Strong super-convergence in energy norm Spatially stable, temporally instable
ES-FEM (2D) FS-FEM (3D)	Edge-based (face-based) smoothed finite element method using n -sided polygonal elements (including T3 and T4)	Smoothed Galerkin Linear or enriched PIM Smoothing operation based on the edges (faces) of cells	Linearly conforming Ultra-accuracy Very efficient Strong super-convergence in displacement/energy norm Spatially and temporally stable
α FEM (2D) α FEM (3D)	Alpha finite element method using T3 and T4 Elements	Smoothed and standard Galerkin Linear or enriched PIM Smoothing operation based on the node and cells	Linearly conforming Nearly "exact" solution Strong super-convergence in displacement/energy norm Upper and lower bounds Spatially and temporally stable

Source: Liu and Nguyen-Thoi [3]

The historical developments of S-FEM and most implementations of the strain smoothing techniques in S-FEM models can be easily found in the above-mentioned book about S-FEM [3, 25], so the reader is referred to them for more details.

3.3.2 The smoothing operator

The strain/gradient smoothing technique is the simplest and most frequently used approach to obtain a smoothed strain field for an S-FEM model. The approach uses two assumptions [3]:

- The strain at a specific location inside the smoothing domain is approximated by smoothing the compatible strain field or the displacement gradient in the smoothing domain, using the strain/gradient smoothing technique.
- The smoothed strain field inside the entire smoothing domain is assumed to be constant and is the approximated strain obtained at first step.

In this work, each of the discretized domain Ω^e is subdivided into $SD \in [1, \infty)$ nonoverlap no-gap quadrilateral smoothing domains, as illustrated in Figure 3.3. Typical types of smoothing domains can be found in Table 3.2.

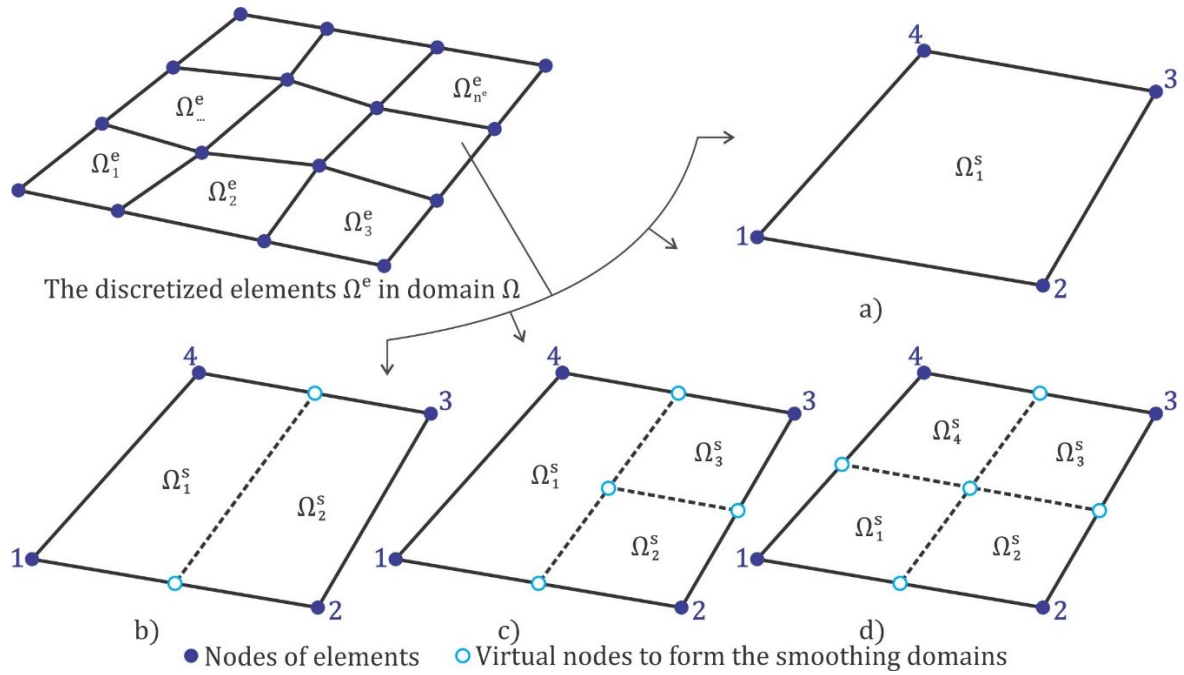


Figure 3.3: Example of the division of a four-node quadrilateral element Ω^e into the smoothing domains in CS-FEM by connecting between the opposite mid-segment points of smoothing domains: a) 1 SD; b) 2 SDs; c) 3 SDs; and d) 4 SDs.

Let the k th smoothing domain and its boundary be denoted with Ω_k^s and Γ_k^s , such that $\Omega^e \equiv \Omega^s = \bigcup_{k=1}^{SD} \Omega_k^s$ and $\Omega_i^s \cap \Omega_j^s = \emptyset$, $i \neq j$ ($i = 1, \dots, n^s; j = 1, \dots, n^s$). The total number of smoothing domain Ω_k^s in the system domain Ω can be computed by $n^s = n^e \times SD$, where n^e is the total number of discretized domains Ω^e in the system domain Ω .

Table 3.2 Typical types of smoothing domains

Name	Method for creation of smoothing domain(s) (number of smoothing domains, n^s)	S-FEM models	Problem domain
Cell-based smoothing domain (CSD)	Based on elements ($n^s = n^e$ for single division) or cells formed by dividing further the elements ($n^s = n^e \times SD$ for multiple division)	CS-FEM (S-FEM) [7, 8, 72]	1D, 2D, 3D
Node-based smoothing domain (NSD)	Based on each of the nodes of the mesh by connecting portions of the surrounding elements sharing the node (in the case of the number of smoothing domains n^s is the same as the number of nodes n^n ; $n^s = n^n$)	NS-FEM [28]	1D, 2D, 3D
Edge-based smoothing domain (ESD)	Based on each edge of the mesh by connecting portions of the element sharing the edge (the problem domain Ω being divided into $n^s = n^{eg}$ nonoverlap no-gap smoothing domains associated with the edges)	ES-FEM [27]	2D
Face-based smoothing domain (FSD)	Based on each face of the element mesh by connecting portions of the surrounding elements sharing the face (in the case of the number of smoothing domains n^s is the same as the number of faces n^f in the mesh; $n^s = n^f$)	FS-FEM [73]	3D

Source: Liu and Nguyen-Thoi [3]

The smoothing operation performed over the smoothing domain Ω_k^s is now expressed in [3]

$$\bar{\mathbf{v}}\mathbf{u}(\mathbf{x}_k) = \int_{\Omega_i^s} \boldsymbol{\varepsilon}(\mathbf{x})\Phi(\mathbf{x} - \mathbf{x}_k)d\Omega \quad (3.37a)$$

or, equivalently,

$$\bar{\mathbf{v}}\mathbf{u}(\mathbf{x}_k) = \int_{\Omega_i^s} \nabla\mathbf{u}(\mathbf{x})\Phi(\mathbf{x} - \mathbf{x}_k)d\Omega \quad (3.37b)$$

where Φ is a smoothing or weight function associated with point \mathbf{x}_i in Ω_k^s . This smoothing function has to satisfy the following basic conditions [74]

$$\Phi \geq 0 \text{ and } \int_{\Omega_i^s} \Phi d\Omega = 1 \quad (3.38)$$

By expanding the corresponding Taylor series for $\boldsymbol{\varepsilon}$ at the point \mathbf{x}_k , it is obtained as follow

$$\boldsymbol{\varepsilon}(\mathbf{x}) = \boldsymbol{\varepsilon}(\mathbf{x}_k) + \nabla \boldsymbol{\varepsilon}(\mathbf{x}_k) \cdot (\mathbf{x} - \mathbf{x}_k) + (\|\mathbf{x} - \mathbf{x}_k\|)^2 \quad (3.39)$$

This expression indicates that the smoothed strain field is defined via the compatibility of several terms of higher order in the Taylor series. For simplicity, a piecewise constant function [3, 7] is applied here, as given by

$$\Phi(\mathbf{x} - \mathbf{x}_k) = \begin{cases} \frac{1}{A_k^s}, & \mathbf{x} \in \Omega_k^s \\ 0, & \mathbf{x} \notin \Omega_k^s \end{cases} \quad (3.40)$$

where the area of smoothing domain $A_k = \int_{\Omega_k^s} d\Omega$. In an S-FEM model, the strain in smoothing domain Ω_k^s can be further assumed to be a constant and equals $\bar{\boldsymbol{\varepsilon}}(\mathbf{x}_k)$, which gives

$$\bar{\boldsymbol{\varepsilon}}_k = \bar{\boldsymbol{\varepsilon}}_k(\mathbf{x}) = \bar{\boldsymbol{\varepsilon}}(\mathbf{x}_k) = \frac{1}{A_k^s} \int_{\Omega_k^s} \boldsymbol{\varepsilon}(\mathbf{x}) d\Omega \quad (3.41)$$

where $\bar{\boldsymbol{\varepsilon}}_k$ is the averaged/smoothed strain. The strain field in an S-FEM model is therefore piecewise constant.

Now, by substituting smoothing function Φ into Equation (3.37), the smoothed gradient of displacement can be defined as

$$\bar{\boldsymbol{\varepsilon}}(\mathbf{x}_k) = \int_{\Omega_k^s} \nabla \mathbf{u}(\mathbf{x}) \cdot \Phi(\mathbf{x} - \mathbf{x}_k) d\Omega = \frac{1}{A_k^s} \int_{\Gamma_k^s} \mathbf{n}(\mathbf{x}) \cdot \mathbf{u}(\mathbf{x}) d\Gamma \quad (3.42)$$

where $\mathbf{u}(\mathbf{x})$ is the generalized displacement vector and $\mathbf{n}(\mathbf{x})$ is the outward unit normal matrix containing the components of the outward unit normal vector to the boundary Γ_k^s .

3.4 Analysis of bending, buckling and vibrational behavior of plate

3.4.1 Introduction

The formulation of the four-node quadrilateral plate bending element with assumed transverse shear strain fields based on the Mindlin-Reissner theory and the integration schemes of S-FEM models will be presented. The formulated plate bending element here is to predict mechanical deformations of thin to moderately thick fabric involved to fabric bending behavior such as buckle and free vibration behavior. The loads and boundary conditions are applied at the reference plane or mid-surface of the structure. Displacements are computed at the reference plane. According to FSDT and the thickness of fabric, the stresses in z direction are not considered in the formulation since the dimensional thickness are too small. The problem is defined in the domain Ω bounded by Γ , as presented in Section 3.2.3 and illustrated in Figure 3.2.

3.4.2 Kinetic equations

Consider a Mindlin-Reissner plate of uniform thickness h , occupying domain Ω bounded by Γ . The in-plane displacements u, v and the transverse displacement w of an arbitrary point (x, y, z) at a distance z to the fabric mid-surface at the time t are expressed as

$$\begin{aligned} u(x, y, z, t) &= z\theta_y(x, y, t) \\ v(x, y, z, t) &= -z\theta_x(x, y, t) \\ w(x, y, z, t) &= w_0(x, y, t) \end{aligned} \quad (3.43)$$

where w_0 is the deflection at the mid-surface, θ_x and θ_y are the rotations about the x - and y -axes, respectively, as illustrated in Figure 3.4.

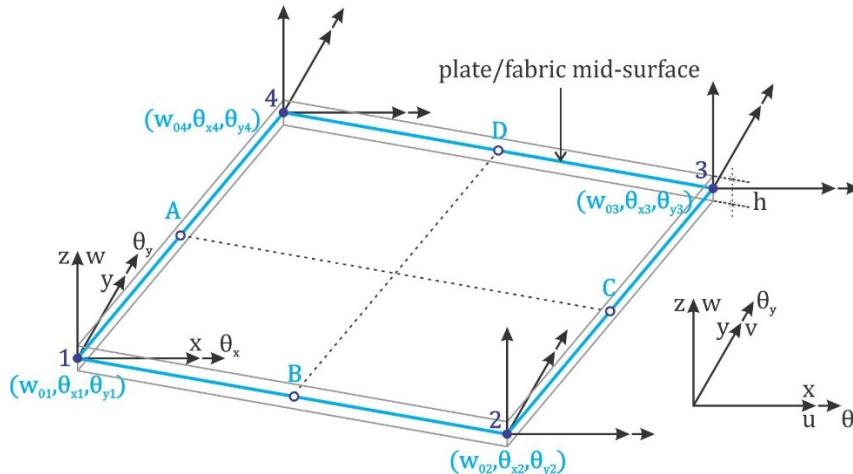


Figure 3.4: A four-node quadrilateral plate bending element.

In view of that displacement field, the strains can be separated into bending strains (in-plane components) and off-plane transverse shear deformations. Bending strains can be written as follows

$$\boldsymbol{\varepsilon} = \begin{Bmatrix} \varepsilon_x \\ \varepsilon_y \\ \gamma_{xy} \end{Bmatrix} = z \begin{bmatrix} \frac{\partial}{\partial x} & 0 \\ 0 & \frac{\partial}{\partial y} \\ \frac{\partial}{\partial y} & \frac{\partial}{\partial x} \end{bmatrix} \begin{Bmatrix} \theta_y \\ -\theta_x \end{Bmatrix} = z \nabla_s \boldsymbol{\theta} = z \boldsymbol{\kappa} \quad (3.44)$$

where ∇_s is the symmetric-gradient operator and $\boldsymbol{\kappa}$ is the curvature strain vector, while those shear deformations are given by

$$\boldsymbol{\gamma} = \begin{Bmatrix} \gamma_{xz} \\ \gamma_{yz} \end{Bmatrix} = \begin{bmatrix} \frac{\partial}{\partial x} \\ \frac{\partial}{\partial y} \end{bmatrix} w_0 + \begin{Bmatrix} \theta_y \\ -\theta_x \end{Bmatrix} = \nabla w_0 + \boldsymbol{\theta} \quad (3.45)$$

where ∇ stands for the gradient operator.

In respect to bending moment applied on the fabric mid-surface, the constitutive relations between bending moment and bending strain are defined by

$$\boldsymbol{\sigma} = \{\sigma_x \quad \sigma_y \quad \tau_{xy}\}^T = \mathbf{D}_0^b \boldsymbol{\kappa} \quad (3.46)$$

where \mathbf{D}_0^b stands for the material matrix, while the average shear stresses relating to the transverse shear strain have the form

$$\boldsymbol{\tau} = \{\tau_{xz} \quad \tau_{yz}\}^T = \mathbf{D}_0^s \boldsymbol{\gamma} \quad (3.47)$$

where \mathbf{D}_0^s is the material matrix related to shear deformation. The stress components σ_x , σ_y , τ_{xy} , τ_{xz} and τ_{yz} lead to the force and moment resultants per unit length.

The bending moment forces in the mid-thickness are defined by

$$\begin{Bmatrix} M_x \\ M_y \\ M_{xy} \end{Bmatrix} = \int_{-\frac{h}{2}}^{\frac{h}{2}} \begin{Bmatrix} \sigma_x \\ \sigma_y \\ \gamma_{xy} \end{Bmatrix} z dz \quad (3.48)$$

in which M_x and M_y are bending moments and M_{xy} is the twisting moment.

The transverse shear forces per unit length that relates to the average shear stresses can be defined by

$$\begin{Bmatrix} Q_x \\ Q_y \end{Bmatrix} = \int_{-\frac{h}{2}}^{\frac{h}{2}} \begin{Bmatrix} \gamma_{xz} \\ \gamma_{yz} \end{Bmatrix} dz \quad (3.49)$$

The total potential energy for the Mindlin-Reissner plate takes form as

$$\Pi = U - W \quad (3.50)$$

where U stands for the strain energy for the Mindlin-Reissner plate, which is defined as

$$U = \frac{1}{2} \iiint_{\Omega} \boldsymbol{\varepsilon}^T \boldsymbol{\sigma} d\Omega + \frac{\alpha}{2} \iiint_{\Omega} \boldsymbol{\tau}^T \boldsymbol{\gamma} d\Omega \quad (3.51)$$

and W is the energy produced by the body forces defined as

$$W = \iiint_{\Omega} \mathbf{u}^T \mathbf{b} d\Omega \quad (3.52)$$

where \mathbf{b} is the distributed load applied on the plate.

The kinetic energy is specified by considering the displacement assumptions for the Mindlin-Reissner plate and Equations (3.17a, 3.43) given as

$$T = \frac{1}{2} \iiint_{\Omega} \rho (\dot{u}^2 + \dot{v}^2 + \dot{w}^2) d\Omega \quad (3.53)$$

The geometric strain energy for the Mindlin-Reissner plate is enforced by in-plane pre-buckling stresses $\sigma_x^0, \sigma_y^0, \sigma_{xy}^0$ is defined by

$$U_{\sigma} = \frac{1}{2} \iiint_{\Omega} (\boldsymbol{\varepsilon}^g)^T \boldsymbol{\tau} \boldsymbol{\varepsilon}^g d\Omega \quad (3.54)$$

where $\boldsymbol{\varepsilon}^g$ stands for the geometrical strains given by

$$\boldsymbol{\varepsilon}^g = \begin{bmatrix} \partial w / \partial x & 0 & 0 \\ \partial w / \partial y & 0 & 0 \\ 0 & \partial \theta_x / \partial x & 0 \\ 0 & \partial \theta_y / \partial y & 0 \\ 0 & 0 & \partial \theta_y / \partial x \\ 0 & 0 & \partial \theta_x / \partial y \end{bmatrix} \quad (3.55)$$

being $\boldsymbol{\tau}$ written as

$$\boldsymbol{\tau} = \begin{bmatrix} \hat{\boldsymbol{\sigma}}_0 & 0 & 0 \\ 0 & \hat{\boldsymbol{\sigma}}_0 & 0 \\ 0 & 0 & \hat{\boldsymbol{\sigma}}_0 \end{bmatrix} \quad (3.56)$$

where $\hat{\boldsymbol{\sigma}}_0$ is the nonlinear strain resulting from the in-plane pre-buckling stresses, which can be written as

$$\hat{\boldsymbol{\sigma}}_0 = \begin{bmatrix} \sigma_x^0 & \sigma_{xy}^0 \\ \sigma_{xy}^0 & \sigma_y^0 \end{bmatrix} \quad (3.57)$$

3.4.3 Four-node quadrilateral plate bending element

Let us assume that each of the discretized element Ω^e with boundary Γ^e in the reference configuration is a four-node quadrilateral element. The generalized displacement vector \mathbf{u} can be approximated as follows

$$\mathbf{u} = \begin{Bmatrix} w_0 \\ \theta_x \\ \theta_y \end{Bmatrix} = \sum_{I=1}^4 \begin{bmatrix} N_I & 0 & 0 \\ 0 & N_I & 0 \\ 0 & 0 & N_I \end{bmatrix} \mathbf{q}_I^p \quad (3.58)$$

where N_I and $\mathbf{q}_I^p = \{w_{0I} \ \theta_{xI} \ \theta_{yI}\}^T$ are, respectively, the bilinear Lagrange shape function and the vector of nodal degrees of freedom associated with node I . The curvature, shear strain and geometrical strain fields can be now approximated as

$$\boldsymbol{\kappa} = \sum_{I=1}^4 \mathbf{B}_I^b \mathbf{q}_I^p = \mathbf{B}^b \mathbf{q}_I^p \quad (3.59)$$

$$\boldsymbol{\gamma} = \sum_{I=1}^4 \mathbf{B}_I^s \mathbf{q}_I^p = \mathbf{B}^s \mathbf{q}_I^p \quad (3.60)$$

$$\boldsymbol{\varepsilon}^g = \sum_{i=1}^4 \mathbf{B}_I^g \mathbf{q}_I = \mathbf{B}^g \mathbf{q}_I^p \quad (3.61)$$

where \mathbf{B}_I^b , \mathbf{B}_I^s and \mathbf{B}_I^g are the discretized gradient matrices and the so-called strain-displacement matrices for node I , respectively, written as

$$\mathbf{B}_I^b = \begin{bmatrix} 0 & 0 & \frac{\partial N_I}{\partial x} \\ 0 & -\frac{\partial N_I}{\partial y} & 0 \\ 0 & -\frac{\partial N_I}{\partial x} & \frac{\partial N_I}{\partial y} \end{bmatrix} \quad (3.62)$$

$$\mathbf{B}_I^s = \begin{bmatrix} \frac{\partial N_I}{\partial x} & 0 & N_I \\ \frac{\partial N_I}{\partial y} & -N_I & 0 \end{bmatrix} \quad (3.63)$$

$$\mathbf{B}_I^g = \begin{bmatrix} \frac{\partial N_I}{\partial x} & 0 & 0 \\ \frac{\partial N_I}{\partial y} & 0 & 0 \\ 0 & \frac{\partial N_I}{\partial x} & 0 \\ 0 & \frac{\partial N_I}{\partial y} & 0 \\ 0 & 0 & \frac{\partial N_I}{\partial x} \\ 0 & 0 & \frac{\partial N_I}{\partial y} \end{bmatrix} \quad (3.64)$$

Substituting Equations (3.58, 3.59 and 3.60) into Equation (3.50), the involved element matrices can be specified as follows. The plate element stiffness matrix is defined by $\mathbf{k}^p = \mathbf{k}^b + \mathbf{k}^s$, where the curvature stiffness \mathbf{k}^b and the shear stiffness \mathbf{k}^s are written as

$$\mathbf{k}^b = \iint_{\Omega^e} (\mathbf{B}^b)^T \mathbf{D}^b \mathbf{B}^b d\Omega \quad (3.65)$$

and

$$\mathbf{k}^s = \iint_{\Omega^e} (\mathbf{B}^s)^T \mathbf{D}^s \mathbf{B}^s d\Omega \quad (3.66)$$

and the load vector \mathbf{f} is defined as

$$\mathbf{f} = \iint_{\Omega^e} h \mathbf{N}^T \mathbf{b} d\Omega + \mathbf{f}_s \quad (3.67)$$

In above expressions, \mathbf{f}_s relates to the prescribed boundary loads, \mathbf{D}^b and \mathbf{D}^s are the bending stiffness constitutive coefficients and the transverse shear stiffness constitutive coefficients, respectively. These coefficients can be written as follows

$$\mathbf{D}^b = \int_{-\frac{h}{2}}^{\frac{h}{2}} \mathbf{D}_0^b dz = \frac{h^3}{12} \mathbf{D}_0^b \quad (3.68)$$

and

$$\mathbf{D}^s = \int_{-\frac{h}{2}}^{\frac{h}{2}} \mathbf{D}_0^s dz = \alpha h G \mathbf{D}_0^s \quad (3.69)$$

in which $\alpha = \frac{5}{6}$ is a shear correction factor and h is the fabric thickness, being \mathbf{D}_0^b and \mathbf{D}_0^s given in Equations (3.39, 3.29).

The mass matrix of plate bending element can be obtained from Equations (3.43, 3.53 and 3.58) as follows

$$\mathbf{m}^p = \frac{1}{2} \iint_{\Omega^e} \mathbf{N}^T \mathbf{I} \mathbf{N} d\Omega \quad (3.70)$$

where \mathbf{N} stands for shape function matrix and

$$\mathbf{I} = \begin{bmatrix} \rho h & 0 & 0 \\ 0 & \frac{\rho h^3}{12} & 0 \\ 0 & 0 & \frac{\rho h^3}{12} \end{bmatrix} \quad (3.71)$$

The geometric stiffness matrix of plate element \mathbf{k}^g is specified by

$$\mathbf{k}^g = \iint_{\Omega^e} (\mathbf{B}^g)^T \boldsymbol{\tau} \mathbf{B}^g d\Omega \quad (3.72)$$

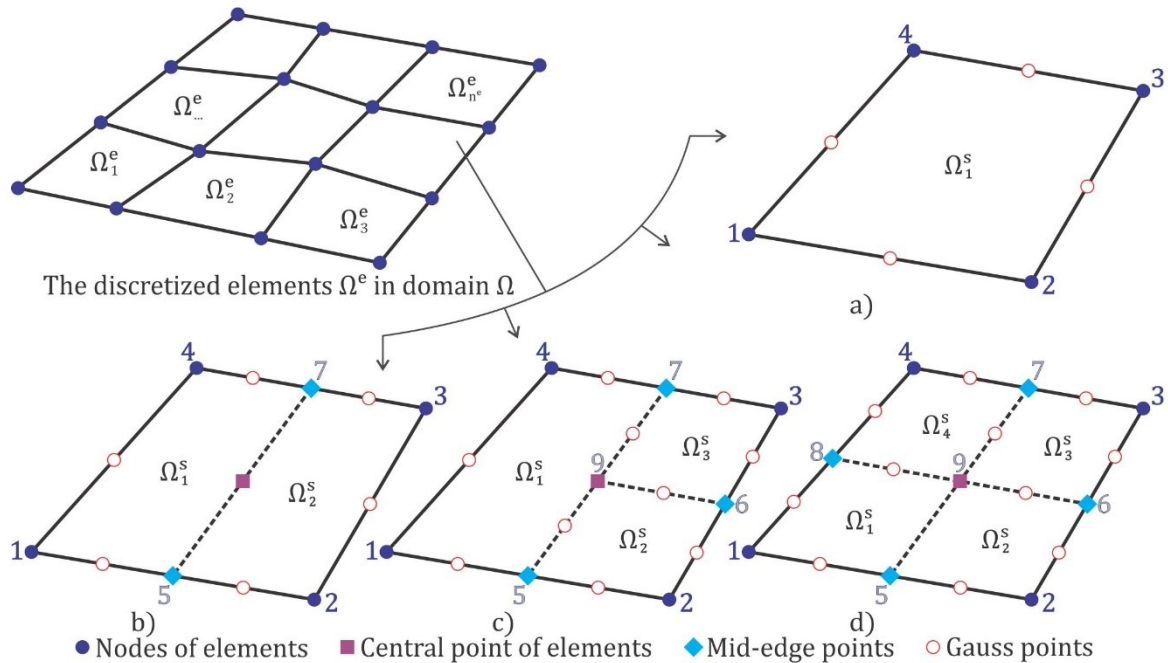
where the gradient strain matrix \mathbf{B}^g is defined in Equation (3.64) and

$$\boldsymbol{\tau} = \begin{bmatrix} h\hat{\boldsymbol{\sigma}}_0 & 0 & 0 \\ 0 & \frac{h^3}{12}\hat{\boldsymbol{\sigma}}_0 & 0 \\ 0 & 0 & \frac{h^3}{12}\hat{\boldsymbol{\sigma}}_0 \end{bmatrix} \quad (3.73)$$

where $\hat{\boldsymbol{\sigma}}_0$ is the nonlinear strain resulting from the in-plane pre-buckling stresses defined in Equation (3.57).

3.4.4 Strain-smoothing operation

In CS-FEM models, each of the discretized element Ω^e in the system domain Ω is further subdivided into $SD \in [1, \infty)$ quadrilateral smoothing domains in a non-overlapping and no-gap manner, such that $\Omega^e = \cup_{k=1}^{SD} \Omega_k^s$ and $\Omega_i^s \cap \Omega_j^s = \emptyset, i \neq j (i = 1, \dots, SD; j = 1, \dots, SD)$, where Ω_k^s indicates the k th smoothing domain of the element Ω^e , as illustrated in Figure 3.5. Each smoothing domain has the total number n_b^s of boundary segments that $\Gamma_k^s = \cup_{b=1}^{n_b^s} \Gamma_{kb}^e$ with $\Gamma_i^s \cap \Gamma_j^s = \emptyset, i \neq j (i = 1, \dots, n_b^s; j = 1, \dots, n_b^s)$. The total number SD of smoothing domains within each discretized element Ω^e can be equal to the total number of discretized elements Ω^e within the system domain Ω . This means that one discretized elements Ω^e can be used as one smoothing domain Ω_k^s .



Examples of a discretized element Ω^e is further subdivided into quadrilateral smoothing domain(s) Ω^s

Figure 3.5: The problem domain Ω is divided into n^e quadrilateral elements Ω^e , each discretized element of domain is further divided into SD smoothing domains Ω^s : a) 1 SD; b) 2 SDs; c) 3 SDs; d) 4 SDs.

Numbering the nodes and elements of smoothing domain(s) within a discretized element Ω^e in order is of paramount importance. To construct smoothing domains within a discretized element Ω^e , this scheme of numbering works as follows:

- Firstly, numbering the mid-edge points of element starting on the first edge (constructed by nodes 1 and 2) and ending on the last edge (constructed by nodes 4 and 1), e.g. in this case, those mid-edge points are {5, 6, 7, 8} as illustrated in Figures 3.5.
- Secondly, numbering the central point of element, e.g. in this case, the central point is {9}, as illustrated in Figures 3.5.

Finally, the numbering of smoothing domain(s) per discretized element Ω^e , e.g. in case of the number of smoothing domain is equal to 1: $SD1 = \{1,2,3,4\}$; 2: $SD1 = \{1,5,7,4\}$, $SD2 = \{5,2,3,7\}$; 3: $SD1 = \{1,5,7,4\}$, $SD2 = \{5,2,6,9\}$, $SD3 = \{9,6,3,7\}$; 4: $SD1 = \{1,5,9,8\}$, $SD2 = \{5,2,6,9\}$, $SD3 = \{9,6,3,7\}$, $SD4 = \{8,9,7,4\}$.

Taking into consideration Equations (3.37, 3.40, 3.41), the averaged/smoothing strain operation for curvature strains in the discrete form for each of the smoothing domains Ω_k^s within the element domain Ω^e can be obtained from Equations (3.44, 3.45, 3.55) as follows

$$\bar{\boldsymbol{\kappa}}(\mathbf{x}_k) = \frac{1}{A_k^s} \int_{\Omega_k^s} \boldsymbol{\kappa}(\mathbf{x}_k) d\Omega = \frac{1}{A_k^s} \int_{\Gamma_k^s} \mathbf{n} \cdot \mathbf{u}(\mathbf{x}_k) d\Gamma = \sum_{I=1}^4 \bar{\mathbf{B}}_{kl}^b(\mathbf{x}_k) \cdot \mathbf{q}_I^p \quad (3.74)$$

where $\bar{\mathbf{B}}_{kl}^b$ is smoothed gradient matrix and \mathbf{n} is the outward normal matrix containing the components of the outward normal vector to the boundary Γ_k^s . Similarly, transverse shear and geometrical strains are obtained as follows

$$\bar{\boldsymbol{\gamma}}(\mathbf{x}_k) = \sum_{I=1}^4 \bar{\mathbf{B}}_{kl}^s(\mathbf{x}_k) \cdot \mathbf{q}_I^p \quad (3.75)$$

and

$$\bar{\boldsymbol{\varepsilon}}^g(\mathbf{x}_k) = \sum_{I=1}^4 \bar{\mathbf{B}}_{kl}^g(\mathbf{x}_k) \cdot \mathbf{q}_I^p \quad (3.76)$$

The smoothed curvature gradient matrix has the following form

$$\bar{\mathbf{B}}_{kl}^b(\mathbf{x}_k) = \begin{bmatrix} 0 & 0 & \bar{b}_{klx} \\ 0 & -\bar{b}_{kly} & 0 \\ 0 & -\bar{b}_{klx} & \bar{b}_{kly} \end{bmatrix} \quad (3.77)$$

where

$$\bar{b}_{kIx} = \frac{1}{A_k^s} \int_{\Gamma_k^s} n_x N_I d\Gamma = \frac{1}{A_k^s} \sum_{b=1}^{n_b^s} n_{xb} \cdot N_I(x_b^G) \cdot l_b \quad (3.78a)$$

$$\bar{b}_{kIy} = \frac{1}{A_k^s} \int_{\Gamma_{k,c}^e} n_y N_I d\Gamma = \frac{1}{A_k^s} \sum_{b=1}^{n_b^s} n_{yb} \cdot N_I(x_b^G) \cdot l_b \quad (3.78b)$$

being $A_k^s = \int_{\Omega_k^s} d\Omega$ the area of the k th smoothing domain $\Omega_k^s \subset \Omega^e$, n_{xb} and n_{yb} indicate the components of the outward unit normal to the b th boundary segment and x_b^G is the coordinate value of Gauss point of the b th boundary segment. The values of shape functions corresponding to the local points in the element are shown in Figure 3.6.

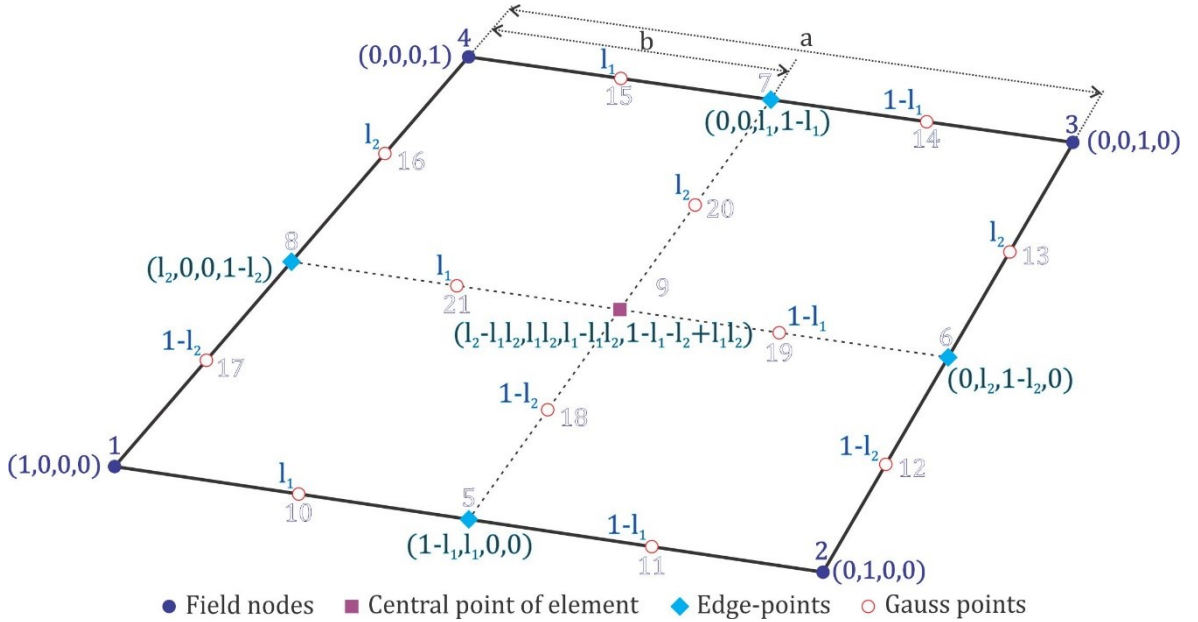


Figure 3.6: The shape function of local point in the element. l_1 is the proportion of b to a and similarly to l_2 .

The smoothed transverse shear gradient matrix of the smoothing domain Ω_k^s can be expressed as

$$\bar{\mathbf{B}}_{kI}^s(x_k) = \begin{bmatrix} \bar{b}_{kIx} & 0 & \bar{b}_{kI} \\ \bar{b}_{kIy} & -\bar{b}_{kI} & 0 \end{bmatrix} \quad (3.79)$$

where

$$\bar{b}_{kI} = \frac{1}{n_n^s} \sum_{n=1}^{n_n^s} N_{In} \quad (3.80)$$

with $n_n^s = n_b^s$ denoting the total number of the nodes of the k th smoothing domain Ω_k^s and N_{In} indicating the shape function value of the i th node of the k th smoothing domain Ω_k^s .

Similarly, the smoothed gradient matrix for the geometrical strain operating over the smoothing domain Ω_k^s can be specified as follows

$$\bar{\mathbf{B}}_{kl}^g(\mathbf{x}_k) = \begin{bmatrix} \bar{b}_{klx} & 0 & 0 \\ \bar{b}_{kly} & 0 & 0 \\ 0 & \bar{b}_{klx} & 0 \\ 0 & \bar{b}_{kly} & 0 \\ 0 & 0 & \bar{b}_{klx} \\ 0 & 0 & \bar{b}_{kly} \end{bmatrix} \quad (3.81)$$

with \bar{b}_{klx} and \bar{b}_{kly} are given as in Equation (3.78).

The relationship between the strain fields and the nodal displacements can be modified by replacing the corresponding gradient matrix \mathbf{B} with the smoothed gradient matrix $\bar{\mathbf{B}}$. Thus, the smoothed stiffness $\bar{\mathbf{k}}^b$, $\bar{\mathbf{k}}^s$ and $\bar{\mathbf{k}}^g$ of elements can be formulated as follows

$$\bar{\mathbf{k}}^b = \iint_{\Omega^e} (\bar{\mathbf{B}}^b)^T \mathbf{D}^b \bar{\mathbf{B}}^b d\Omega = \sum_k^{SD} (\bar{\mathbf{B}}_{kl}^b(\mathbf{x}_k))^T \mathbf{D}^b (\bar{\mathbf{B}}_{kl}^b(\mathbf{x}_k)) A_k^s \quad (3.82)$$

$$\bar{\mathbf{k}}^s = \iint_{\Omega^e} (\bar{\mathbf{B}}^s)^T \mathbf{D}^s \bar{\mathbf{B}}^s d\Omega = \sum_k^{SD} (\bar{\mathbf{B}}_{kl}^s(\mathbf{x}_k))^T \mathbf{D}^s (\bar{\mathbf{B}}_{kl}^s(\mathbf{x}_k)) A_k^s \quad (3.83)$$

$$\bar{\mathbf{k}}^g = \iint_{\Omega^e} (\bar{\mathbf{B}}^g)^T \boldsymbol{\tau} \bar{\mathbf{B}}^g d\Omega = \sum_k^{SD} (\bar{\mathbf{B}}_{kl}^g(\mathbf{x}_k))^T \boldsymbol{\tau} (\bar{\mathbf{B}}_{kl}^g(\mathbf{x}_k)) A_k^s \quad (3.84)$$

The smoothed stiffness matrix of plate bending element can be then obtained as follows

$$\bar{\mathbf{k}}^p = \bar{\mathbf{k}}^b + \bar{\mathbf{k}}^s = \iint_{\Omega^e} (\bar{\mathbf{B}}^b)^T \mathbf{D}^b \bar{\mathbf{B}}^b d\Omega + \iint_{\Omega^e} (\bar{\mathbf{B}}^s)^T \mathbf{D}^s \bar{\mathbf{B}}^s d\Omega \quad (3.85)$$

Note that the element shear stiffness matrix $\bar{\mathbf{k}}^s$ in Equations (3.83, 3.85) will be formulated by using a classical reduced integration and mixed interpolation of tensorial components (MITC) approaches, which proposed by Bathe and Dvorkin [75]. It is used to eliminate the shear locking of shell models that will be presented in Section 3.6. The approximation of the shear strain fields $\boldsymbol{\gamma}$ can be interpolated in the natural coordinates system as follows

$$\boldsymbol{\gamma} = \begin{bmatrix} \gamma_{xz} \\ \gamma_{yz} \end{bmatrix} = \mathbf{J}^{-1} \begin{bmatrix} \gamma_\xi \\ \gamma_\eta \end{bmatrix} \quad (3.86)$$

with

$$\gamma_\xi = \frac{1}{2}[(1 - \eta)\gamma_\xi^B + (1 + \eta)\gamma_\xi^D] \quad (3.87a)$$

$$\gamma_\eta = \frac{1}{2}[(1 - \xi)\gamma_\eta^A + (1 + \xi)\gamma_\eta^C] \quad (3.87b)$$

and $\mathbf{J} \frac{(\xi, \eta)}{(x, y)}$ stands for the Jacobian transformation matrix and superscripts A, B, C and D are the mid-side node, as shown in Figure 3.4. Expressing $\gamma_\eta^A, \gamma_\eta^C$ and $\gamma_\xi^B, \gamma_\xi^D$ in terms of the discretized fields \mathbf{u} , the shear part of the stiffness matrix is then rewritten as

$$\bar{\mathbf{B}}_{sl} = \mathbf{J}^{-1} \begin{bmatrix} \frac{\partial N_I}{\partial \xi} & b_i^{11} \frac{\partial N_I}{\partial \xi} & b_i^{12} \frac{\partial N_I}{\partial \xi} \\ \frac{\partial N_I}{\partial \eta} & b_i^{21} \frac{\partial N_I}{\partial \eta} & b_i^{22} \frac{\partial N_I}{\partial \eta} \end{bmatrix} \quad (3.88)$$

where

$$b_i^{11} = \xi_i \frac{\partial x^M}{\partial \xi}; \quad b_i^{12} = \xi_i \frac{\partial y^M}{\partial \xi}; \quad b_i^{21} = \eta_i \frac{\partial x^L}{\partial \eta}; \quad b_i^{22} = \eta_i \frac{\partial y^L}{\partial \eta} \quad (3.89)$$

The coordinates of the unit square are $\xi_i \in \{-1, 1, 1, -1\}$ and $\eta_i \in \{-1, -1, 1, 1\}$ and the allocation of the mid-side nodes to the corner nodes of element are given as $(i; M; L) \in \{(1; B; A); (2; B; C); (3; D; C); (4; D; A)\}$.

By using Equation (3.88), the shear part of the stiffness matrix $\tilde{\mathbf{k}}^s$ can be evaluated using full integration (2 x 2 Gauss Quadrature). This element is referred as MITC4.

3.5 Analysis of plane-stress problems

3.5.1 Introduction

In this section, a brief review of the strain smoothing approach for the four-node quadrilateral membrane/shell element with normal rotation is presented. The loads and boundary conditions are applied at the reference plane or mid-surface of the structure. Displacements are computed at the reference plane. The problem is defined in the domain Ω bounded by Γ , as represented in Section 3.2.3 and illustrated in Figure 3.2. The four-node quadrilateral membrane/shell element is also a part of the formulation of the four-node quadrilateral flat shell element, which will be introduced below.

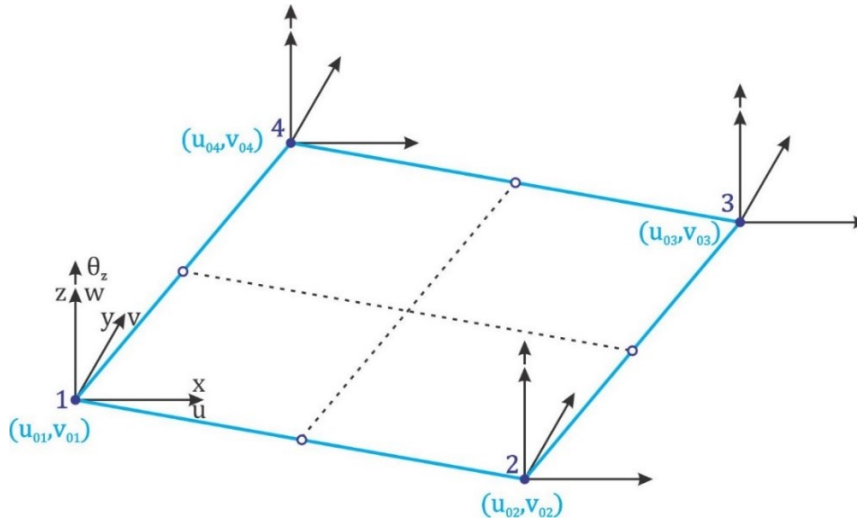


Figure 3.7: A four-node quadrilateral membrane element with normal rotation.

3.5.2 Four-node quadrilateral membrane element with normal rotation

Let us consider a four node quadrilateral element with domain Ω^e bounded by Γ^e , so that the in-plane displacements can be approximated as

$$\mathbf{u} = \sum_{I=1}^4 \begin{bmatrix} N_I & 0 \\ 0 & N_I \end{bmatrix} \mathbf{q}_I = \mathbf{N} \mathbf{q}_I^m \quad (3.90)$$

where $\mathbf{u} = \{u_0 \quad v_0\}^T$ is the displacement vector, \mathbf{N} is the element shape function matrix and $\mathbf{q}_I^m = \{u_{0I} \quad v_{0I}\}^T$ is the vector of nodal degrees of freedom for element node I , as illustrated in Figure 3.7. Then the discrete strain fields are defined as

$$\boldsymbol{\varepsilon}^m = \nabla_s \mathbf{u} = \sum_{I=1}^4 \mathbf{B}_I^m \mathbf{q}_I = \mathbf{B}^m \mathbf{q}_I^m \quad (3.91)$$

where $\mathbf{B}^m = \nabla_s \mathbf{N}$ is the discretized strain–displacement matrix and

$$\mathbf{B}_I^m = \begin{bmatrix} \frac{\partial N_I}{\partial x} & 0 \\ 0 & \frac{\partial N_I}{\partial y} \\ \frac{\partial N_I}{\partial y} & \frac{\partial N_I}{\partial x} \end{bmatrix} \quad (3.92)$$

The constitutive relationship can be expressed as

$$\boldsymbol{\sigma}^m = \{\sigma_x \quad \sigma_y \quad \gamma_{xy}\}^T = \mathbf{D}_0^m \boldsymbol{\varepsilon}^m \quad (3.93)$$

The stress resultants that are in the form of the in-plane membrane forces can be formulated as

$$\begin{Bmatrix} N_x \\ N_y \\ N_{xy} \end{Bmatrix} = \int_{-\frac{h}{2}}^{\frac{h}{2}} \begin{Bmatrix} \sigma_x \\ \sigma_y \\ \gamma_{xy} \end{Bmatrix} dz \quad (3.94)$$

The total potential energy for the membrane element can be defined as

$$\Pi = \frac{1}{2} \iiint_{\Omega^e} (\boldsymbol{\varepsilon}^m)^T \boldsymbol{\sigma}^m d\Omega - \iiint_{\Omega^e} \mathbf{u}^T \mathbf{b} d\Omega - \iint_{\Gamma^e} \mathbf{u}^T \mathbf{t}_\Gamma b d\Gamma \quad (3.95)$$

Substituting Equations (3.90, 3.91, 3.93) into the previous expression, it is obtained the element membrane stiffness matrix \mathbf{k}_m and the vector of element nodal forces produced by body forces \mathbf{f}_b and tractions \mathbf{f}_s , written as

$$\mathbf{k}^m = \iint_{\Omega^e} (\mathbf{B}^m)^T \mathbf{D}^m \mathbf{B}^m d\Omega \quad (3.96)$$

and

$$\mathbf{f} = \mathbf{f}_b + \mathbf{f}_s = \iint_{\Omega^e} h \mathbf{N}^T \mathbf{b} d\Omega + \int_{\Gamma^e} h \mathbf{N}^T \mathbf{t}_\Gamma d\Gamma \quad (3.97)$$

in which \mathbf{D}^m is the membrane stiffness constitutive coefficients defined by

$$\mathbf{D}^m = \int_{-\frac{h}{2}}^{\frac{h}{2}} \mathbf{D}_0^m dz = h \mathbf{D}_0^m \quad (3.98a)$$

where \mathbf{D}_0^m is given in Equation (2.39).

Substituting Equation (3.90) into Equation (3.17a), the element mass matrix is defined as

$$\mathbf{m}^m = \iiint_{\Omega^e} \rho \mathbf{N}^T \mathbf{N} d\Omega = \iiint_{\Omega^e} h \rho \mathbf{N}^T \mathbf{N} d\Omega \quad (3.98b)$$

3.5.3 Strain-smoothing operation

Similarly to the procedure of strain-smoothing operation for plate bending element in Section 3.4.4, the averaged/smoothing strain operation for membrane strains in the discrete form for each of the smoothing domains Ω_k^s within the element domain Ω^e can be obtained from Equations (3.91) as follows

$$\bar{\boldsymbol{\varepsilon}}(\mathbf{x}_k) = \sum_{I=1}^4 \bar{\mathbf{B}}_{kl}^m(\mathbf{x}_k) \cdot \mathbf{q}_I^m \quad (3.99)$$

where $\bar{\mathbf{B}}_{kl}^m(\mathbf{x}_k)$ is the smoothed strain-displacement matrix given by

$$\bar{\mathbf{B}}_{kl}^m(\mathbf{x}_k) = \begin{bmatrix} \bar{b}_{klx} & 0 \\ 0 & \bar{b}_{kly} \\ \bar{b}_{kly} & \bar{b}_{klx} \end{bmatrix} \quad (3.100)$$

and where

$$\bar{b}_{klx} = \frac{1}{A_k^s} \int_{\Gamma_k^s} n_x N_I d\Gamma = \frac{1}{A_k^s} \sum_{b=1}^{n_b^s} n_{xb} \cdot N_I(\mathbf{x}_b^G) \cdot l_b \quad (3.101a)$$

and

$$\bar{b}_{kly} = \frac{1}{A_k^s} \int_{\Gamma_{k,c}^s} n_y N_I d\Gamma = \frac{1}{A_k^s} \sum_{b=1}^{n_b^s} n_{yb} \cdot N_I(\mathbf{x}_b^G) \cdot l_b \quad (3.95a)$$

Finally, we end up having the element smoothed stiffness matrix defined as

$$\bar{\mathbf{k}}^m = \iint_{\Omega^e} (\bar{\mathbf{B}}^m)^T \mathbf{D}^m \bar{\mathbf{B}}^m d\Omega = \sum_k^{SD} (\bar{\mathbf{B}}_{kl}^m(\mathbf{x}_k))^T \mathbf{D}^m (\bar{\mathbf{B}}_{kl}^m(\mathbf{x}_k)) A_k^s \quad (3.102)$$

3.6 Analysis of shell structures

3.6.1 Four-node quadrilateral flat shell element

The four-node isoparametric quadrilateral flat shell element is derived by superposition of the plate bending element with the membrane element or so-called plane-stress element (see Figure 3.8), assuming that all of their four nodes are located at the mid-plane of the shell shown in Figure 3.9 [10, 76, 77].

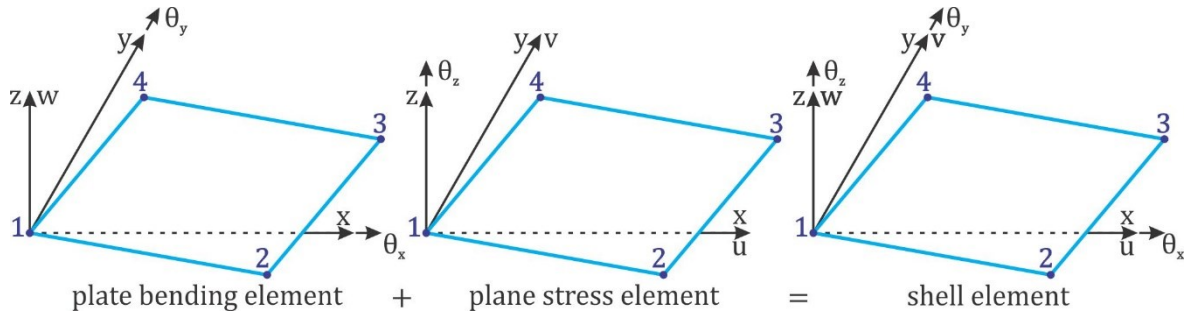


Figure 3.8: Formation of the four-node shell element.

When all four nodes of a quadrilateral flat shell element are placed in the mid-plane of the shell, the generalized displacement vector can be expressed as

$$\mathbf{u} = \{\mathbf{q}_1 \quad \mathbf{q}_2 \quad \mathbf{q}_3 \quad \mathbf{q}_4\}^T \quad (3.103)$$

in which \mathbf{q}_I is the nodal degrees of freedom vector associated to element node I ($I = 1, 2, 3, 4$). Each nodal DOFs vector has three translational displacements in the x , y and z directions and three rotational deformations with respect to the x , y and z axes. Figure 3.9 illustrates the middle plane of a four-node quadrilateral flat shell element and the DOFs at the nodes. Thus, the nodal displacement vector \mathbf{q}_I corresponding with node I is defined as

$$\mathbf{q}_I = \begin{Bmatrix} \mathbf{q}_I^m \\ \mathbf{q}_I^p \\ \theta_{zI} \end{Bmatrix} = \{u_{0I} \quad v_{0I} \quad w_{0I} \quad \theta_{xI} \quad \theta_{yI} \quad \theta_{zI}\}^T \quad (3.104)$$

Note that the sixth degree of freedom θ_z is included in the above equation, which is attached with the shell normal rotation, which is the so-called drilling degree of freedom [78-81].

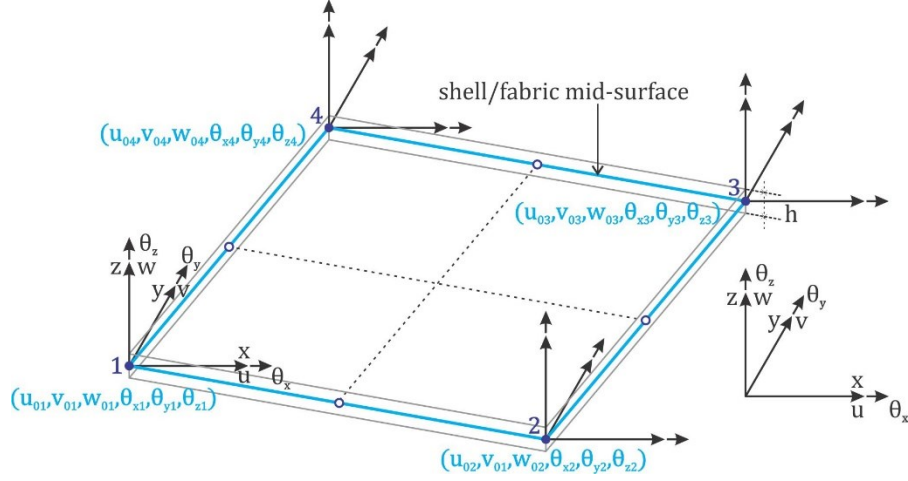


Figure 3.9: A four-node quadrilateral flat shell element undergoes bending and twisting, as well as in-plane deformation.

The generalized stress vector $\tilde{\sigma}$ and strain vector $\tilde{\epsilon}$ are expressed as follows

$$\tilde{\sigma} = \begin{Bmatrix} \mathbf{N} \\ \mathbf{M} \\ \mathbf{Q} \end{Bmatrix} \quad (3.105)$$

$$\tilde{\epsilon} = \begin{Bmatrix} \boldsymbol{\epsilon}^m \\ \boldsymbol{\kappa} \\ \boldsymbol{\gamma} \end{Bmatrix} \quad (3.106)$$

in which $\mathbf{N} = \{N_x \ N_y \ N_{xy}\}^T$ is the in-plane force resultant given in Equation (3.94), $\mathbf{M} = \{M_x \ M_y \ M_{xy}\}^T$ is the out-of-plane moment resultant given in Equation (3.48) and $\mathbf{Q} = \{Q_x \ Q_y\}^T$ is the out-of-plane force resultant given in Equation (3.49), these resultants are defined as acting per unit length. The discretized strain fields $\boldsymbol{\kappa}$, $\boldsymbol{\gamma}$ and $\boldsymbol{\epsilon}^m$ are given in Equations (3.58, 3.59 and 3.91). The constitutive relationship is defined as

$$\tilde{\sigma} = \tilde{\mathbf{D}} \tilde{\epsilon} \quad (3.107)$$

where

$$\tilde{\mathbf{D}} = \begin{bmatrix} \mathbf{D}_0^m & 0 & 0 \\ 0 & \mathbf{D}_0^b & 0 \\ 0 & 0 & \mathbf{D}_0^s \end{bmatrix} \quad (3.108)$$

in which \mathbf{D}_0^m is the membrane stiffness constitutive coefficients, \mathbf{D}_0^b is the bending stiffness constitutive coefficients and \mathbf{D}_0^s is the transverse shear stiffness constitutive coefficients.

The flat shell element stiffness matrix takes form as

$$\mathbf{k} = \iint_{\Omega^e} (\tilde{\mathbf{B}})^T \tilde{\mathbf{D}} \tilde{\mathbf{B}} d\Omega \quad (3.109)$$

with

$$\tilde{\mathbf{B}} = \begin{Bmatrix} \mathbf{B}^m \\ \mathbf{B}^b \\ \mathbf{B}^s \end{Bmatrix} \quad (3.110)$$

and where \mathbf{B}^m , \mathbf{B}^b and \mathbf{B}^s are, respectively, strain-displacement matrices corresponding to membrane, curvature and shear element.

According to the four-node quadrilateral flat shell element, the nodal stiffness matrix \mathbf{k}_I and the nodal mass matrix \mathbf{m}_I at each node I can be formed by the corresponding sub-matrices as follows

$$\mathbf{k}_I = \begin{bmatrix} [\mathbf{k}_I^m]_{2 \times 2} & [0]_{2 \times 3} & [0]_{2 \times 1} \\ [0]_{3 \times 2} & [\mathbf{k}_I^p]_{3 \times 3} & [0]_{3 \times 1} \\ [0]_{1 \times 2} & [0]_{1 \times 3} & [0]_{1 \times 1} \end{bmatrix} \quad (3.111)$$

and

$$\mathbf{m}_I = \begin{bmatrix} [\mathbf{m}_I^m]_{2 \times 2} & [0]_{2 \times 3} & [0]_{2 \times 1} \\ [0]_{3 \times 2} & [\mathbf{m}_I^p]_{3 \times 3} & [0]_{3 \times 1} \\ [0]_{1 \times 2} & [0]_{1 \times 3} & [0]_{1 \times 1} \end{bmatrix} \quad (3.112)$$

Hence, the shell element stiffness and mass matrix have the dimension of 24×24 can be written as follows

$$\mathbf{k} = \begin{bmatrix} [\mathbf{k}_{11}]_{6 \times 6} & [\mathbf{k}_{12}]_{6 \times 6} & [\mathbf{k}_{13}]_{6 \times 6} & [\mathbf{k}_{14}]_{6 \times 6} \\ [\mathbf{k}_{21}]_{6 \times 6} & [\mathbf{k}_{22}]_{6 \times 6} & [\mathbf{k}_{23}]_{6 \times 6} & [\mathbf{k}_{24}]_{6 \times 6} \\ [\mathbf{k}_{31}]_{6 \times 6} & [\mathbf{k}_{32}]_{6 \times 6} & [\mathbf{k}_{33}]_{6 \times 6} & [\mathbf{k}_{34}]_{6 \times 6} \\ [\mathbf{k}_{41}]_{6 \times 6} & [\mathbf{k}_{42}]_{6 \times 6} & [\mathbf{k}_{43}]_{6 \times 6} & [\mathbf{k}_{44}]_{6 \times 6} \end{bmatrix} \quad (3.113)$$

$$\mathbf{m} = \begin{bmatrix} [\mathbf{m}_{11}]_{6 \times 6} & [\mathbf{m}_{12}]_{6 \times 6} & [\mathbf{m}_{13}]_{6 \times 6} & [\mathbf{m}_{14}]_{6 \times 6} \\ [\mathbf{m}_{21}]_{6 \times 6} & [\mathbf{m}_{22}]_{6 \times 6} & [\mathbf{m}_{23}]_{6 \times 6} & [\mathbf{m}_{24}]_{6 \times 6} \\ [\mathbf{m}_{31}]_{6 \times 6} & [\mathbf{m}_{32}]_{6 \times 6} & [\mathbf{m}_{33}]_{6 \times 6} & [\mathbf{m}_{34}]_{6 \times 6} \\ [\mathbf{m}_{41}]_{6 \times 6} & [\mathbf{m}_{42}]_{6 \times 6} & [\mathbf{m}_{43}]_{6 \times 6} & [\mathbf{m}_{44}]_{6 \times 6} \end{bmatrix} \quad (3.114)$$

Note that the geometrical stiffness matrix of plate element \mathbf{k}^g , as given in Equation (3.72), can be used in the case of buckling analysis of shell structures, which gives

$$\mathbf{k}^g = \iint_{\Omega^e} (\mathbf{B}^g)^T \boldsymbol{\tau} \mathbf{B}^g d\Omega \quad (3.115)$$

where the discretized geometric (strain-displacement) matrix associated to element node I must be rewritten according to nodal DOFs of flat shell element as follows

$$\mathbf{B}_I^g = \begin{bmatrix} \partial N_I / \partial x & 0 & 0 & 0 & 0 & 0 \\ \partial N_I / \partial y & 0 & 0 & 0 & 0 & 0 \\ 0 & \partial N_I / \partial x & 0 & 0 & 0 & 0 \\ 0 & \partial N_I / \partial y & 0 & 0 & 0 & 0 \\ 0 & 0 & \partial N_I / \partial x & 0 & 0 & 0 \\ 0 & 0 & \partial N_I / \partial y & 0 & 0 & 0 \end{bmatrix} \quad (3.116)$$

In general, the shell element has five degrees of freedom per node [25, 76, 77], one out-of-plane displacement (w_0) and two in-plane rotations (θ_x, θ_y) from the plate bending element as presented in Section 3.4.2 and two in-plane displacements (u_0, v_0) from the plane stress element as presented in Section 3.5.2. The resulting flat shell has five degrees of freedom per node and the either stiffness or mass matrix of a 4-node quadrilateral flat shell element has size of 20×20 [10, 14, 75]. Using the extended 24×24 stiffness and mass matrix that makes it more advantageous to solve engineering problems in practice [9, 78, 82], i.e. it is more convenient for programming, implement and maintenance and transforming the matrix from the local coordinate system into the global coordinate system. Thus, the simplest approach [14] is to insert an arbitrary stiffness coefficient, $k_{\theta_{zI}}$ at the additional degree of freedom θ_{zI} , as shown in Equation (3.104), which is defined as

$$k_{\theta_{zI}} \theta_{zI} = \mathbf{0} \quad (3.117)$$

However, there is no stiffness value associated with the local rotation degrees of freedom θ_z [14], the global stiffness matrix will be therefore rank deficient when all the elements meeting at a node are coplanar. There are various approaches reported in the literature [14, 83] in order to estimate and improve the performance of the element with drilling degrees of freedom. To improve the performance of the element with drilling degrees of freedom θ_{zI} in this context, the arbitrary stiffness coefficient $k_{\theta_{zI}}$ is chosen to be 10^3 times the maximum diagonal value of the element stiffness matrix [80]. Then the nodal stiffness matrix in Equation (3.111) can be expressed as

$$\mathbf{k}_I = \begin{bmatrix} [\mathbf{k}_I^m]_{2 \times 2} & [0]_{2 \times 3} & [0]_{2 \times 1} \\ [0]_{3 \times 2} & [\mathbf{k}_I^p]_{3 \times 3} & [0]_{3 \times 1} \\ [0]_{1 \times 2} & [0]_{1 \times 3} & \max(k_{\theta_{zI}}) 10^{-3} \end{bmatrix} \quad (3.118)$$

The smoothed stiffness sub-matrices corresponding with each element node I given by

$$\bar{\mathbf{k}}_I = \begin{bmatrix} [\bar{\mathbf{k}}_I^m]_{2 \times 2} & [0]_{2 \times 3} & [0]_{2 \times 1} \\ [0]_{3 \times 2} & [\bar{\mathbf{k}}_I^p]_{3 \times 3} & [0]_{3 \times 1} \\ [0]_{1 \times 2} & [0]_{1 \times 3} & \max(\bar{k}_{\theta_{zI}}) 10^{-3} \end{bmatrix} \quad (3.119)$$

Thus, the smoothed stiffness matrix of shell element is formed from the smoothed stiffness sub-matrices of plate element and membrane element which yields

$$\bar{\mathbf{k}} = \begin{bmatrix} [\bar{\mathbf{k}}_{11}]_{6 \times 6} & [\bar{\mathbf{k}}_{12}]_{6 \times 6} & [\bar{\mathbf{k}}_{13}]_{6 \times 6} & [\bar{\mathbf{k}}_{14}]_{6 \times 6} \\ [\bar{\mathbf{k}}_{21}]_{6 \times 6} & [\bar{\mathbf{k}}_{22}]_{6 \times 6} & [\bar{\mathbf{k}}_{23}]_{6 \times 6} & [\bar{\mathbf{k}}_{24}]_{6 \times 6} \\ [\bar{\mathbf{k}}_{31}]_{6 \times 6} & [\bar{\mathbf{k}}_{32}]_{6 \times 6} & [\bar{\mathbf{k}}_{33}]_{6 \times 6} & [\bar{\mathbf{k}}_{34}]_{6 \times 6} \\ [\bar{\mathbf{k}}_{41}]_{6 \times 6} & [\bar{\mathbf{k}}_{42}]_{6 \times 6} & [\bar{\mathbf{k}}_{43}]_{6 \times 6} & [\bar{\mathbf{k}}_{44}]_{6 \times 6} \end{bmatrix} \quad (3.120)$$

3.6.2 The warped configuration

The flat shell element is placed on the mid-plane of the shell is defined by the input nodal points $I \in \{1,2,3,4\}$ and the local coordinate system xyz is defined via taking the cross product of the diagonal vectors or $V_z = V_{1-3}V_{2-4}$ show in Figure 3.10. The distance vector is defined as the normal distance between the flat shell element node points and input node points at the mid-plane of the shell, denoted as d and calculated by [77]

$$d = \pm \frac{(z_1 + z_3) - (z_2 + z_4)}{2} \quad (3.121)$$

where z_I ($|z_I| = h$) is the warpage offset at each node I perpendicular to the flat shell element.

For most shells, the finite element nodes are generally positioned at the mid-plane nodes of the shell and satisfy force equilibrium at the mid- surface of the shell structure, i.e. the rotations about the local z -axes in the warped and projected planes can be taken as equal and the distance d is zero.

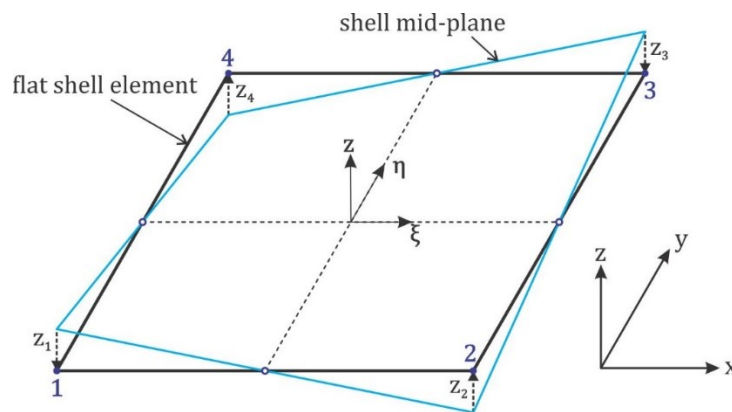


Figure 3.10: Warped and projected quadrilateral shell element to flat geometric transformation.

In the case of the distance d is not equal to zero, e.g. shells with double curvature, the flat shell element stiffness must be modified before the transformation to the global XYZ coordinate system. This can be solved by using the rigid link correction suggested by Taylor [14]. It is a transformation of

the flat shell element stiffness matrix to the mid-surface locations via applying the displacement transformation equation at each node given as follow

$$\begin{Bmatrix} u'_{0I} \\ v'_{0I} \\ w'_{0I} \\ \theta'_{xI} \\ \theta'_{yI} \\ \theta'_{zI} \end{Bmatrix} = \begin{bmatrix} 1 & 0 & 0 & 0 & 0 & 0 \\ 0 & 1 & 0 & 0 & 0 & 0 \\ 0 & 0 & 1 & 0 & 0 & 0 \\ -z_I & 0 & 0 & 1 & 0 & 0 \\ 0 & z_I & 0 & 0 & 1 & 0 \\ 0 & 0 & 0 & 0 & 0 & 1 \end{bmatrix} \begin{Bmatrix} u_{0I} \\ v_{0I} \\ w_{0I} \\ \theta_{xI} \\ \theta_{yI} \\ \theta_{zI} \end{Bmatrix} = \mathbf{w} \mathbf{q}_I \quad (3.122)$$

where \mathbf{w} is the projection matrix in the local coordinate system.

Transformation of the flat shell element stiffness matrix to the mid-plane locations by using the projection matrix is obtained as follow

$$\mathbf{k} = \mathbf{w}^T \mathbf{k}_{flat} \mathbf{w} \quad (3.123)$$

and similarly for the smoothed stiffness matrix of element, which gives

$$\bar{\mathbf{k}} = \mathbf{w}^T \bar{\mathbf{k}}_{flat} \mathbf{w} \quad (3.124)$$

This physically states that the flat shell element nodes are stiffly positioned to the mid-plane nodes and the distance d reaches to zero. Thus, the elements become smaller and the flat shell element results will converge to the shell solution [77].

3.6.3 Elements in the global coordinate system

The global stiffness matrix and force vector associated to the flat shell is constructed by transforming each element matrix into the global coordinate system prior to assembly. The matrices for shell elements in the global coordinates XYZ system can be accomplished by performing the transformations as follows [9, 12]

$$\mathbf{K}^e = \mathbf{T}^T \mathbf{k} \mathbf{T} \quad (3.125)$$

$$\bar{\mathbf{K}}^e = \mathbf{T}^T \bar{\mathbf{k}} \mathbf{T} \quad (3.126)$$

$$\mathbf{M}^e = \mathbf{T}^T \mathbf{m} \mathbf{T} \quad (3.127)$$

in which \mathbf{T} is the transformation matrix according to the four-node quadrilateral flat shell element, defined by

$$\mathbf{T} = \begin{bmatrix} \mathbf{R} & 0 & 0 & 0 & 0 & 0 & 0 & 0 \\ 0 & \mathbf{R} & 0 & 0 & 0 & 0 & 0 & 0 \\ 0 & 0 & \mathbf{R} & 0 & 0 & 0 & 0 & 0 \\ 0 & 0 & 0 & \mathbf{R} & 0 & 0 & 0 & 0 \\ 0 & 0 & 0 & 0 & \mathbf{R} & 0 & 0 & 0 \\ 0 & 0 & 0 & 0 & 0 & \mathbf{R} & 0 & 0 \\ 0 & 0 & 0 & 0 & 0 & 0 & \mathbf{R} & 0 \\ 0 & 0 & 0 & 0 & 0 & 0 & 0 & \mathbf{R} \end{bmatrix} \quad (3.128)$$

where matrix \mathbf{R} stores the direction cosines of $\{x, y, z\}$ with respect to $\{X, Y, Z\}$ and

$$\mathbf{R} = \begin{bmatrix} l_x & m_x & n_x \\ l_y & m_y & n_y \\ l_z & m_z & n_z \end{bmatrix} \quad (3.129)$$

where l_i , m_i and n_i ($i = x, y, z$) are direction cosines (see [9, 12, 80] for more details), which are given as follows

$$\begin{aligned} l_x &= \cos(x, X), & m_x &= \cos(x, Y), & n_x &= \cos(x, Z) \\ l_y &= \cos(y, X), & m_y &= \cos(y, Y), & n_y &= \cos(y, Z) \\ l_z &= \cos(z, X), & m_z &= \cos(z, Y), & n_z &= \cos(z, Z) \end{aligned} \quad (3.130)$$

In practice, it is convenient for the local coordinates xyz to be defined under the global coordinates XYZ system using the four-node quadrilateral flat shell element.

3.7 Final remarks

A smoothed finite element method for mechanical analysis and modelling of the textile fabrics has been proposed in this chapter. Using Lagrange's equations, a set of system equations defining both static and dynamic mechanical analysis and modelling of the textile fabrics was presented. The appropriate time integration schemes using Newmark's methods was also presented. These system equations are applicable for both the existing standard FEM and the developed S-FEM models by replacing the terms \mathbf{K} and \mathbf{K}^g with $\bar{\mathbf{K}}$ and $\bar{\mathbf{K}}^g$, as summarized in Table 3.3.

Table 3.3: List of space-discretized equations of motions

Equations	Space-discretized equations of motions	Analysis and simulation (principle for structural mechanic problems)
(3.24)	$\mathbf{M}\dot{\mathbf{q}} + \mathbf{C}\dot{\mathbf{q}} + \bar{\mathbf{K}}\mathbf{q} = \mathbf{F}$	Linear and non-linear dynamics including the velocity and acceleration effects
(3.25)	$\mathbf{M}\ddot{\mathbf{q}} + \bar{\mathbf{K}}\mathbf{q} = \mathbf{F}$	Linear and non-linear dynamics including the acceleration effects
(3.29)	$\bar{\mathbf{K}}\mathbf{q} = \mathbf{F}$	Linear and non-linear static
(3.27)	$[\bar{\mathbf{K}} + \omega^2\mathbf{M}]\bar{\mathbf{q}} = \mathbf{0}$	Free-vibration behavior
(3.28)	$[\bar{\mathbf{K}} + \lambda_{cr}\bar{\mathbf{K}}^g]\bar{\mathbf{q}} = \mathbf{0}$	Non-linear pre-buckling behavior

For those motion equations shown in Table 3.3, recall that $\dot{\mathbf{q}}$ and $\ddot{\mathbf{q}}$ stand for the vector of global nodal velocity and nodal accelerations; $\bar{\mathbf{q}}$ denotes the eigenvector that contains the vibration/buckling mode shapes; ω is a non-trivial forcing frequency, λ_{cr} expresses critical buckling load; $\bar{\mathbf{K}}$ and $\bar{\mathbf{K}}^g$ are the global stiffness matrix and the global geometric stiffness matrix which are developed using S-FEM models via the strain/gradient smoothing technique; \mathbf{M} is the global mass matrix and \mathbf{F} is total load vector. Note that the term $\bar{\mathbf{q}}$ in Equation (3.27) is defined in Equation (3.26).

Three dimensional problems of mechanical deformation of the textile fabrics are successfully analyzed and modelled by the proposed method. The numerical examples are presented in the next chapter in which each of the discretized elements in the problem domain that played role of fabric samples was further subdivided into the number of appropriate smoothing domains. Theoretically and practically, the dynamic modelling results at last time step can be approximated to the static modelling results.

The implementation and debugging of developed finite element computer codes as well as testing of these developed S-FEM models have produced a significant amount of works. However, the computational implementation served mostly to assess the applicability of theoretical ideas, meaning that, in their current stage of development, the use of S-FEM by an external analyst is hindered by the lack of a unified and fully automatic analysis tool. In fact, this is in general the case for S-FEM, which is still a very rare presence in commercially available FEA computer applications and almost non-existent in general purpose open-source platforms. Good convergence has been observed for finite quantities and numerical values of singular quantities are determined with orders of magnitude that correctly reflect the strengths of material properties.

3.8 References

1. Mindlin, R.D., *Influence of rotary inertia and shear in flexural motion of isotropic, elastic plates*. Journal of Applied Mechanics, 1951. **18**: p. 1031-1036.
2. Reissner, E., *The effect of transverse shears deformation on the bending of elastic plate*. Journal of Applied Mechanics, 1945. **12**: p. 6-77.
3. Liu, G.-R. and T. Nguyen-Thoi, *Smoothed finite element methods*. 2010: Taylor and Francis Group, LLC.
4. Chen, J.-S., et al., *A stabilized conforming nodal integration for Galerkin mesh-free methods*. International Journal for Numerical Methods in Engineering, 2001. **50**(2): p. 435-466.
5. Liu, G.R., *Meshfree methods: moving beyond the finite element method*. 2010, Boca Raton: CRC Press.
6. Liu, G.R. and Y.T. Gu, *An introduction to meshfree methods and their programming*. 2005, Dordrecht; New York: Springer.
7. Liu, G., K. Dai, and T. Nguyen, *A Smoothed Finite Element Method for Mechanics Problems*. Computational Mechanics, 2007. **39**(6): p. 859-877.
8. Liu, G.R., et al., *Theoretical aspects of the smoothed finite element method (SFEM)*. International Journal for Numerical Methods in Engineering, 2007. **71**(8): p. 902-930.
9. Liu, G.R. and S.S. Quek, *The finite element method a practical course*. 2003, Oxford; Boston: Butterworth-Heinemann.
10. Oñate, E., *Structural analysis with the finite element method. Linear statics: Beams, Plates and Shells*. Vol. 2. 2009, Dordrecht; London: Springer.
11. Zienkiewicz, O.C., R.L. Taylor, and J.Z. Zhu, *The Finite Element Method Set*. 6 ed. 2005, Oxford: Butterworth-Heinemann.
12. Logan, D.L., *A First Course in the Finite Element Method: SI Edition*. 2011: Nelson Education Limited.
13. Rao, S.S., *Chapter 12 - Dynamic Analysis*, in *The Finite Element Method in Engineering (Fifth Edition)*. 2011, Butterworth-Heinemann: Boston. p. 427-469.
14. Zienkiewicz, O.C. and R.L. Taylor, *The finite element method*. 5 ed. 2000, Oxford; Boston: Butterworth-Heinemann Ltd.
15. Mukherjee, A., *Free vibration of laminated plates using a high-order element*. Computers & Structures, 1991. **40**(6): p. 1387-1393.
16. Lee, S.J., *Free vibration analysis of plates by using a four-node finite element formulated with assumed natural transverse shear strain*. Journal of Sound and Vibration, 2004. **278**(3): p. 657-684.
17. Mukherjee, S., P. Jafarali, and G. Prathap, *A variational basis for error analysis in finite element elastodynamic problems*. Journal of Sound and Vibration, 2005. **285**(3): p. 615-635.
18. Gorman, D.G. and J. Horáček, *Analysis of the free vibration of a coupled plate/fluid interacting system and interpretation using sub-system modal energy*. Engineering Structures, 2007. **29**(5): p. 754-762.
19. Prokić, A. and D. Lukić, *Dynamic analysis of thin-walled closed-section beams*. Journal of Sound and Vibration, 2007. **302**(4-5): p. 962-980.
20. Kelly, S.G. and S. Srinivas, *Free vibrations of elastically connected stretched beams*. Journal of Sound and Vibration, 2009. **326**(3-5): p. 883-893.
21. Jeong, K.-H., G.-M. Lee, and T.-W. Kim, *Free vibration analysis of a circular plate partially in contact with a liquid*. Journal of Sound and Vibration, 2009. **324**(1-2): p. 194-208.

-
22. Lind, N.C., *Newmark's numerical method*. 1975, Waterloo, Ont.: University of Waterloo Press.
 23. Newmark, N.M., *A Method of Computation for Structural Dynamics*. ASCE Journal of the Engineering Mechanics Division, 1959. **85**(EM3).
 24. Wilson, E.L. and R.W. Clough, *Dynamic Response by Step-by-step Matrix Analysis*. 1962.
 25. Liu, G.R. and S.S. Quek, *The Finite Element Method: A Practical Course*. 2013: Elsevier Science.
 26. Aalto, J., *Built-in field equations for recovery procedures*. Computers & Structures, 1997. **64**(1-4): p. 157-176.
 27. Liu, G.R., T. Nguyen-Thoi, and K.Y. Lam, *An edge-based smoothed finite element method (ES-FEM) for static, free and forced vibration analyses of solids*. Journal of Sound and Vibration, 2009. **320**(4-5): p. 1100-1130.
 28. Liu, G.R., et al., *A node-based smoothed finite element method (NS-FEM) for upper bound solutions to solid mechanics problems*. Computers & Structures, 2009. **87**(1-2): p. 14-26.
 29. Liu, G.R., et al., *A novel Galerkin-like weakform and a superconvergent alpha finite element method (S α FEM) for mechanics problems using triangular meshes*. Journal of Computational Physics, 2009. **228**(11): p. 4055-4087.
 30. Liu, G.R., N. Nourbakhshnia, and Y.W. Zhang, *A novel singular ES-FEM method for simulating singular stress fields near the crack tips for linear fracture problems*. Engineering Fracture Mechanics, 2011. **78**(6): p. 863-876.
 31. Liu, G.R., W. Zeng, and H. Nguyen-Xuan, *Generalized stochastic cell-based smoothed finite element method (GS_CS-FEM) for solid mechanics*. Finite Elements in Analysis and Design, 2013. **63**(0): p. 51-61.
 32. Liu, P., et al., *The singular edge-based smoothed finite element method for stationary dynamic crack problems in 2D elastic solids*. Computer Methods in Applied Mechanics and Engineering, 2012. **233-236**(0): p. 68-80.
 33. Nguyen-Thoi, T., et al., *Static, free vibration and buckling analyses of stiffened plates by CS-FEM-DSG3 using triangular elements*. Computers & Structures, 2013. **125**(0): p. 100-113.
 34. Nguyen-Thoi, T., et al., *A face-based smoothed finite element method (FS-FEM) for visco-elastoplastic analyses of 3D solids using tetrahedral mesh*. Computer Methods in Applied Mechanics and Engineering, 2009. **198**(41-44): p. 3479-3498.
 35. Nguyen-Thoi, T., et al., *A cell-based smoothed discrete shear gap method (CS-DSG3) using triangular elements for static and free vibration analyses of shell structures*. International Journal of Mechanical Sciences, 2013. **74**(0): p. 32-45.
 36. Nguyen-Thoi, T., et al., *A node-based smoothed finite element method (NS-FEM) for upper bound solution to visco-elastoplastic analyses of solids using triangular and tetrahedral meshes*. Computer Methods in Applied Mechanics and Engineering, 2010. **199**(45-48): p. 3005-3027.
 37. Nguyen-Xuan, H. and G.R. Liu, *An edge-based smoothed finite element method softened with a bubble function (bES-FEM) for solid mechanics problems*. Computers & Structures, 2013. **128**(0): p. 14-30.
 38. Nguyen-Xuan, H., et al., *An adaptive singular ES-FEM for mechanics problems with singular field of arbitrary order*. Computer Methods in Applied Mechanics and Engineering, 2013. **253**(0): p. 252-273.
 39. Nguyen-Xuan, H., et al., *An edge-based smoothed finite element method (ES-FEM) with stabilized discrete shear gap technique for analysis of Reissner-Mindlin plates*. Computer Methods in Applied Mechanics and Engineering, 2010. **199**(9-12): p. 471-489.
 40. Nguyen-Xuan, H., et al., *A smoothed finite element method for plate analysis*. Computer Methods in Applied Mechanics and Engineering, 2008. **197**(13-16): p. 1184-1203.
-

-
41. Nguyen-Xuan, H., et al., *Analysis of functionally graded plates using an edge-based smoothed finite element method*. Composite Structures, 2011. **93**(11): p. 3019-3039.
 42. Nguyen-Thanh, N., et al., *A smoothed finite element method for shell analysis*. Computer Methods in Applied Mechanics and Engineering, 2008. **198**(2): p. 165-177.
 43. Nguyen-Thanh, N., et al., *An alternative alpha finite element method (AFEM) for free and forced structural vibration using triangular meshes*. Journal of Computational and Applied Mathematics, 2010. **233**(9): p. 2112-2135.
 44. Bordas, S.P.A., et al., *Strain smoothing in FEM and XFEM*. Computers & Structures, 2010. **88**(23–24): p. 1419-1443.
 45. Cazes, F. and G. Meschke, *An Edge-based Imbricate Finite Element Method (EI-FEM) with full and reduced integration*. Computers & Structures, 2012. **106–107**(0): p. 154-175.
 46. Cui, X.Y. and G.Y. Li, *Smoothed Galerkin methods using cell-wise strain smoothing technique*. Engineering Analysis with Boundary Elements, 2012. **36**(5): p. 825-835.
 47. Cui, X.Y., G.R. Liu, and G.Y. Li, *A cell-based smoothed radial point interpolation method (CS-RPIM) for static and free vibration of solids*. Engineering Analysis with Boundary Elements, 2010. **34**(2): p. 144-157.
 48. Cui, X.Y., et al., *Analysis of elastic–plastic problems using edge-based smoothed finite element method*. International Journal of Pressure Vessels and Piping, 2009. **86**(10): p. 711-718.
 49. Dai, K.Y. and G.R. Liu, *Free and forced vibration analysis using the smoothed finite element method (SFEM)*. Journal of Sound and Vibration, 2007. **301**(3–5): p. 803-820.
 50. Dai, K.Y., G.R. Liu, and T.T. Nguyen, *An n-sided polygonal smoothed finite element method (nSFEM) for solid mechanics*. Finite Elements in Analysis and Design, 2007. **43**(11–12): p. 847-860.
 51. Feng, S.Z., X.Y. Cui, and G.Y. Li, *Analysis of transient thermo-elastic problems using edge-based smoothed finite element method*. International Journal of Thermal Sciences, 2013. **65**(0): p. 127-135.
 52. Feng, S.Z., X.Y. Cui, and G.Y. Li, *Transient thermal mechanical analyses using a face-based smoothed finite element method (FS-FEM)*. International Journal of Thermal Sciences, 2013. **74**(0): p. 95-103.
 53. He, Z., et al., *An improved modal analysis for three-dimensional problems using face-based smoothed finite element method*. Acta Mechanica Solida Sinica, 2013. **26**(2): p. 140-150.
 54. He, Z.C., et al., *An ES-FEM for accurate analysis of 3D mid-frequency acoustics using tetrahedron mesh*. Computers & Structures, 2012. **106–107**(0): p. 125-134.
 55. He, Z.C., et al., *A coupled edge-/face-based smoothed finite element method for structural–acoustic problems*. Applied Acoustics, 2010. **71**(10): p. 955-964.
 56. He, Z.C., et al., *An edge-based smoothed finite element method (ES-FEM) for analyzing three-dimensional acoustic problems*. Computer Methods in Applied Mechanics and Engineering, 2009. **199**(1–4): p. 20-33.
 57. He, Z.C., et al., *Coupled analysis of 3D structural–acoustic problems using the edge-based smoothed finite element method/finite element method*. Finite Elements in Analysis and Design, 2010. **46**(12): p. 1114-1121.
 58. Herath, M.T., et al., *Smoothed finite element and genetic algorithm based optimization for shape adaptive composite marine propellers*. Composite Structures, 2014. **109**(0): p. 189-197.
 59. Jiang, Y., et al., *A singular ES-FEM for plastic fracture mechanics*. Computer Methods in Applied Mechanics and Engineering, 2011. **200**(45–46): p. 2943-2955.
-

-
60. Kazemzadeh-Parsi, M.J. and F. Daneshmand, *Solution of geometric inverse heat conduction problems by smoothed fixed grid finite element method*. Finite Elements in Analysis and Design, 2009. **45**(10): p. 599-611.
 61. Kazemzadeh-Parsi, M.J. and F. Daneshmand, *Three dimensional smoothed fixed grid finite element method for the solution of unconfined seepage problems*. Finite Elements in Analysis and Design, 2013. **64**(0): p. 24-35.
 62. Li, E., Z.C. He, and X. Xu, *An edge-based smoothed tetrahedron finite element method (ES-T-FEM) for thermomechanical problems*. International Journal of Heat and Mass Transfer, 2013. **66**(0): p. 723-732.
 63. Li, W., et al., *Analysis of coupled structural-acoustic problems based on the smoothed finite element method (S-FEM)*. Engineering Analysis with Boundary Elements, (0).
 64. Li, Y., G.R. Liu, and G.Y. Zhang, *An adaptive NS/ES-FEM approach for 2D contact problems using triangular elements*. Finite Elements in Analysis and Design, 2011. **47**(3): p. 256-275.
 65. Lim, J.H., et al., *Variable-node finite elements with smoothed integration techniques and their applications for multiscale mechanics problems*. Computers & Structures, 2010. **88**(7-8): p. 413-425.
 66. Natarajan, S., et al., *Analysis of composite plates by a unified formulation-cell based smoothed finite element method and field consistent elements*. Composite Structures, 2013. **105**(0): p. 75-81.
 67. Nguyen, T.T., et al., *Selective Smoothed Finite Element Method*. Tsinghua Science & Technology, 2007. **12**(5): p. 497-508.
 68. Thai, C.H., et al., *Analysis of laminated composite plates using higher-order shear deformation plate theory and node-based smoothed discrete shear gap method*. Applied Mathematical Modelling, 2012. **36**(11): p. 5657-5677.
 69. Wu, C.T. and W. Hu, *Meshfree-enriched simplex elements with strain smoothing for the finite element analysis of compressible and nearly incompressible solids*. Computer Methods in Applied Mechanics and Engineering, 2011. **200**(45-46): p. 2991-3010.
 70. Wu, S.C., et al., *An edge-based smoothed point interpolation method (ES-PIM) for heat transfer analysis of rapid manufacturing system*. International Journal of Heat and Mass Transfer, 2010. **53**(9-10): p. 1938-1950.
 71. Yao, L.Y., et al., *Numerical treatment of acoustic problems with the smoothed finite element method*. Applied Acoustics, 2010. **71**(8): p. 743-753.
 72. Liu, G.R., et al., *On the essence and the evaluation of the shape functions for the smoothed finite element method (SFEM)*. International Journal for Numerical Methods in Engineering, 2009. **77**(13): p. 1863-1869.
 73. Nguyen-Thoi, T., et al., *A face-based smoothed finite element method (FS-FEM) for 3D linear and nonlinear solid mechanics problems using 4-node tetrahedral elements*. International Journal for Numerical Methods in Engineering, 2009. **78**: p. 324-353.
 74. Yoo, J.W., B. Moran, and J.-S. Chen, *Stabilized conforming nodal integration in the natural-element method*. International Journal for Numerical Methods in Engineering, 2004. **60**(5): p. 861-890.
 75. Bathe, K.-J. and E.N. Dvorkin, *A four-node plate bending element based on Mindlin/Reissner plate theory and a mixed interpolation*. International Journal for Numerical Methods in Engineering, 1985. **21**(2): p. 367-383.
 76. Chapelle, D. and K.-J. Bathe, *The Finite Element Analysis of Shells - Fundamentals (Computational Fluid and Solid Mechanics)*. 2003, Berlin; New York: Springer.
 77. Wilson, E.L., *Three-Dimensional Static and Dynamic Analysis of Structures: A Physical Approach with Emphasis on Earthquake Engineering*. 3 ed. 1999: Computers and Structures.
-

-
78. Cook, R.D., *Four-node 'flat' shell element: Drilling degrees of freedom, membrane-bending coupling, warped geometry, and behavior*. Computers & Structures, 1994. **50**(4): p. 549-555.
 79. Hughes, T.J.R. and F. Brezzi, *On drilling degrees of freedom*. Comput. Methods Appl. Mech. Eng., 1989. **72**(1): p. 105-121.
 80. Kansara, K., *Development of membrane, plate and flat shell elements in java*, in *Civil Engineering*. 2004-05-13.
 81. Zienkiewicz, O.C. and R.L. Taylor, *The Finite Element Method for Solid and Structural Mechanics*. 6 ed. Vol. 2. 2005: Butterworth-Heinemann Ltd.
 82. Geyer, S. and A.A. Groenwold, *A New 24 D.O.F. Assumed Stress Finite Element for Orthotropic Shells*, in *Structural Engineering, Mechanics and Computation*, A. Zingoni, Editor. 2001, Elsevier Science: Oxford. p. 647-654.
 83. Cook, R.D., et al., *Concepts and applications of finite element analysis*. 4 ed. 2002: John Wiley & Sons, Inc.

Numerical examples and discussions

In order to spot the advantages of the proposed techniques, this chapter carries out a series of numerical tests and experiments in order to compare numerical modelling results of the developed S-FEM models to those of the corresponding standard FEM models. This aims to examine the applicability of S-FEM models to macro-mechanical modelling of textile fabrics.

4.1 Numerical examples

In this respect, the 4-node isoparametric quadrilateral membrane, plate and flat shell finite elements were implemented to solve problems of plane-stress, bending, buckling and free-vibration behavior of woven fabric sheet. The number of degrees of freedom (DOFs) per Q4 element corresponding to the 4-node isoparametric quadrilateral membrane, plate and flat shell element are, respectively, 8, 12 and 24 (as presented Sections 3.4, 3.5, 3.6). For convenience, a 4-node isoparametric quadrilateral plate/shell element with assumed strain/gradient smoothing technique will be denoted by Q4SDSDs for S-FEM in which SDs stands for the number of smoothing domains per 4-node quadrilateral flat shell element and a 4-node isoparametric quadrilateral flat shell element will be denoted by MITC4 for standard FEM. It is clear that SDs is in range of $\{1,2,3,4\}$.

For numerical examples, a plain-woven fabric sheet of which both length and width is taken as $L = 100\text{cm}$ and $l = L\sqrt{2}$ stands for the bias direction. These dimensional quantities are applied to fabric samples in terms of quadrilateral mesh (Q4 mesh), as illustrated in Figure 4.1.

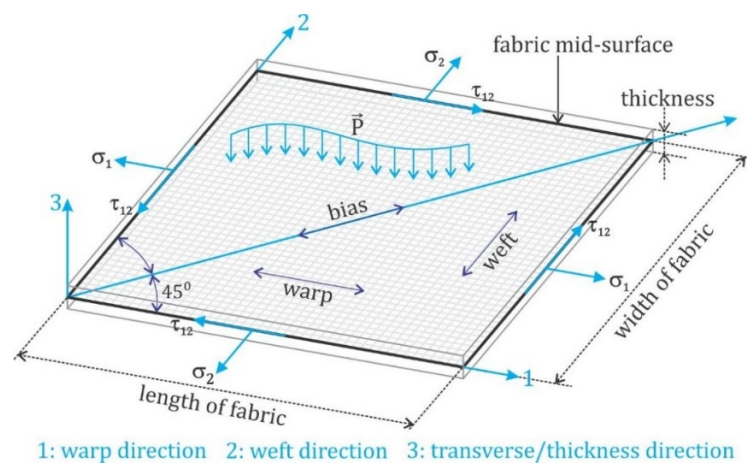


Figure 4.1: General configuration of geometrical and mechanical properties of fabric sample.

The low-stress mechanical properties of two plain-woven fabric samples are listed in Table 4.2. Note that shear modulus and transverse shear modulus are computed by using Equations (2.20, 2.29). Both uniform pressure and uniaxial applied force are taken as $P = 1$.

Table 4.1: Mechanical properties of plain-woven fabric samples

Parameter	Symbol	Sample 1	Sample 2	Measurement unit
Thickness	h	0.2834	0.7484	[mm]
Mass per unit area	ρ	10.6775	24.2720	[mg/cm ²]
Elastic modulus	E_{warp}	13034.4108	3823.7993	[gf/cm]
	E_{weft}	8278.1457	14092.4464	[gf/cm]
	E_{bias}	2313.7436	6896.5517	[gf/cm]
Poisson's ratio	ν_{warp}	0.2500	0.0210	
	ν_{weft}	0.1600	0.0780	
Bending rigidity	B_{warp}	0.0239	0.1237	[gf.cm ² /cm]
	B_{weft}	0.0177	0.1333	[gf.cm ² /cm]
	B_{bias}	0.0172	0.0880	[gf.cm ² /cm]

According to finite element procedure, woven fabric sheet will be divided into a number of 4-node isoparametric quadrilateral finite elements in terms of Q4 mesh that is referred as mesh density, as listed in Table 4.2.

Table 4.2: Geometrical configurations for numerical examples

Index	Meshes	Total elements	Total nodes
1	5x5	25	36
2	10x10	100	121
3	15x15	225	256
4	20x20	400	441
5	25x25	625	676
6	30x30	900	961
7	35x35	1225	1296
8	40x40	1600	1681

The mixed boundary conditions including simply-supported (S) and clamped (C) are listed in Table 4.3 [1].

Table 4.3: Dirichlet boundary conditions

1	CCCC	Sides and ends clamped
2	SSSS	Sides and ends simply-supported
3	CSCS	Ends clamped, sides simply-supported
4	SCSF	One side free, one side clamped, end simply-supported
5	SFSF	Ends simply-supported, sides free
6	SSFF	Ends simply-supported, sides free
7	CFFF	End clamped, sides free
8	SFFF	End simply-supported, sides free

Numerical examples in modeling of low-stress mechanical deformation of fabric samples will be presented in case of buckling behavior of woven fabric, buckling behavior of woven fabric in terms of free-vibration behavior, as well as bending and plane-stress behavior.

4.1.1 Buckling behavior of woven fabric

Fabric wrinkles generally appear in fabric and cloth products in common use. Wrinkles pop up because fabric sheet is very flexible in bending and can easily buckle in space when bent under its own weight or compressive stresses arise. The formation of wrinkle phenomenon is one of buckling and post-buckling deformation behaviors in terms of structural mechanics. Thus, it is of interest to examine the ability of the developed numerical models in previous chapter in modelling of buckling and post-buckling deformations of fabric sheets.

Let us consider a configured fabric sheet as illustrated in Figure 4.1. The numerical modelling results of post-buckling deformation phenomenon of fabric sheet, which was implemented for all mesh indices as listed in Table 4.2 and $SDs = \{1,2,3,4\}$, are presented for a CCCC/SSSS/SCSF/CFFF plain-woven fabric sheet with different ratio of length to thickness $h_1/l = 0.0002$ and $h_2/l = 0.0005$, and buckling factor $k_b = L^2\lambda/\pi^2D_{f11}$.

In order to expose the numerical error between S-FEM and standards FEM, twelve eigenbuckling modes are listed in Tables 4.4 and 4.5 for both S-FEM and FEM. However, only the numerical results for twelve eigenbuckling modes of S-FEM using 1 SD are listed in these tables, because the numerical

results for twelve eigenbuckling modes of S-FEM using 4 SDs are identical to that of FEM. These tables contain numerical output of CS-FEM that is denoted by Q4SD1 according to $SDs = 1$ and the numerical output of the corresponding standard FEM finite element model is denoted by MITC4.

Table 4.4: Numerical output of twelve eigenbuckling modes for a CCCC/SSSS/SCSF/CFFF plain-woven fabric sheet with h_1/l , using 20×20 Q4 elements and 1 smoothing domain per element (Q4SD1)

h_1/l	CCCC		SSSS		SCSF		CFFF	
	Q4SD1	MITC4	Q4SD1	MITC4	Q4SD1	MITC4	Q4SD1	MITC4
1	10.0032	10.0033	4.3717	4.3732	3.6874	3.6886	0.9311	0.9314
2	12.2498	12.2622	6.8545	6.8587	6.5634	6.5660	1.7699	1.7705
3	20.6561	20.6767	11.9583	11.9669	9.3715	9.3776	4.8148	4.8162
4	26.1402	26.2036	17.5648	17.5903	14.0151	14.0327	8.4654	8.4747
5	28.3047	28.3810	19.5110	19.5261	15.5930	15.6046	9.2844	9.2948
6	29.4193	29.4490	21.0477	21.0910	19.9731	20.0043	10.0052	10.0077
7	39.8011	39.9302	23.6448	23.6600	23.7719	23.8234	13.0735	13.0840
8	41.4700	41.5552	27.9898	28.0589	24.3559	24.3750	16.1340	16.1607
9	43.8303	43.8734	29.7920	29.8158	31.7338	31.8245	17.5818	17.5862
10	51.7327	51.7366	38.0381	38.0422	32.2944	32.3758	23.0635	23.0666
11	53.4177	53.4304	39.9132	39.9452	36.1490	36.1781	23.6570	23.7147
12	56.6439	56.8089	43.2551	43.2903	42.7123	42.7292	23.8194	23.8697

Table 4.5: Numerical output of twelve eigenbuckling modes for a CCCC/SSSS/SCSF/CFFF plain-woven fabric sheet with h_2/l , using 20×20 Q4 elements and 1 smoothing domain per element (Q4SD1)

h_2/l	CCCC		SSSS		SCSF		CFFF	
	Q4SD1	MITC4	Q4SD1	MITC4	Q4SD1	MITC4	Q4SD1	MITC4
1	10.9780	10.9869	4.9312	4.9329	3.9818	3.9833	1.0605	1.0608
2	12.0399	12.0520	6.9720	6.9763	7.4434	7.4464	1.8177	1.8183
3	19.0377	19.0557	11.4406	11.4489	9.4400	9.4456	4.7365	4.7378
4	25.0535	25.0773	17.6095	17.6230	14.3444	14.3635	8.8534	8.8617
5	26.7768	26.8396	18.9345	18.9616	14.5756	14.5861	9.4520	9.4547
6	27.3419	27.4159	20.7583	20.8002	21.2437	21.2764	9.5542	9.5650

7	34.6371	34.6748	25.2165	25.2360	21.3109	21.3272	14.8002	14.8092
8	34.6437	34.7375	25.6169	25.6782	22.9439	22.9904	15.5404	15.5637
9	38.8888	38.9973	29.1894	29.2071	28.8293	28.8987	15.7637	15.7675
10	43.5578	43.5954	32.2585	32.3429	29.5418	29.5646	21.0346	21.0685
11	48.4511	48.4913	34.0603	34.0766	30.0226	30.0499	22.7324	22.7842
12	48.5332	48.5550	40.0134	40.0397	35.7162	35.7197	22.8255	22.8286

From the results listed in Tables 4.4 and 4.5, it can be found that the present method is of high accuracy and the number of smoothing domains per Q4 element in range of $\{1,2,3,4\}$ was approximated for each of eigenbuckling modes with mixed boundary conditions, clearly showing the stable and well-balanced feature of the CS-FEM for both the thin and moderately thick fabric sheets.

In fact, the numerical results for strain energy of twelve buckling modes between S-FEM and FEM are identical as illustrated in Figures 4.2, 4.3, 4.4 for thin fabric sample (h_1/l) and Figures 4.5, 4.6, 4.7 for moderately thick fabric sample (h_2/l). These figures of strain energy indicate that S-FEM possesses strain energy convergence for both the thin (h_1) and moderately thick (h_2) fabric sheets with different boundary conditions and mesh density.

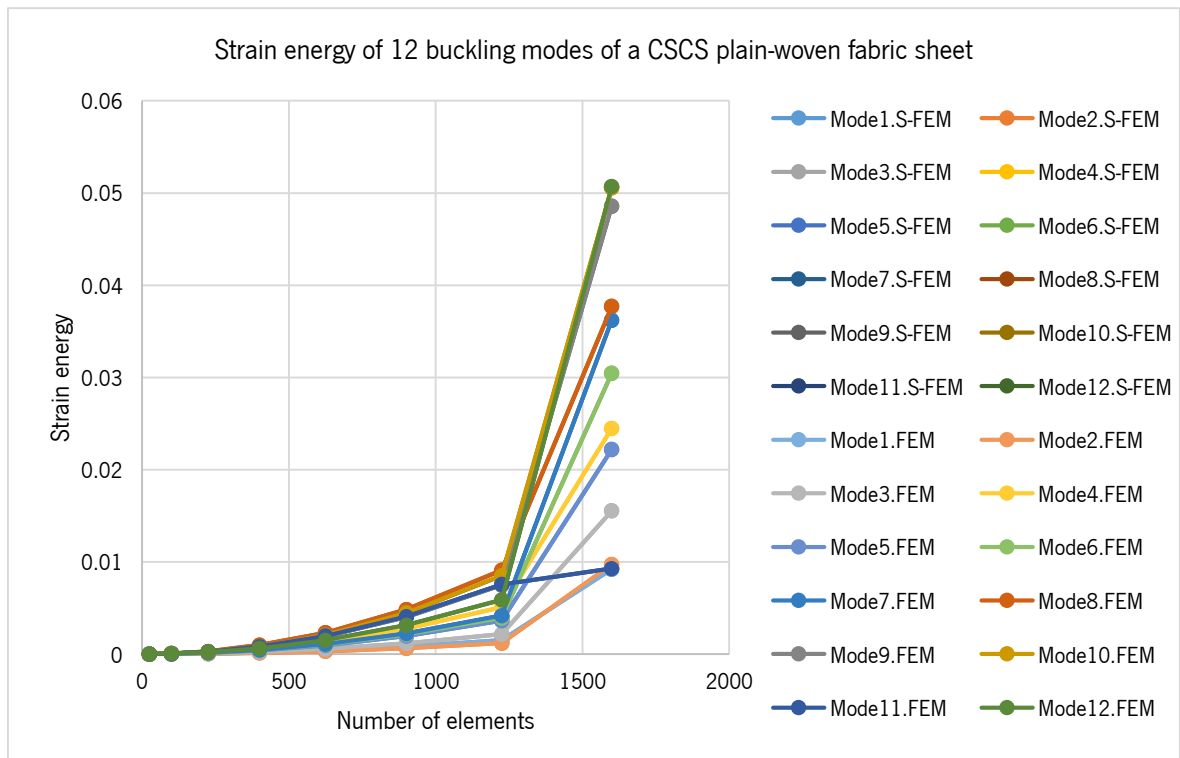


Figure 4.2: Numerical results for strain energy of twelve buckling modes of a CSCS plain-woven fabric sheet (h_1/l) with different mesh density subjected uniform load.

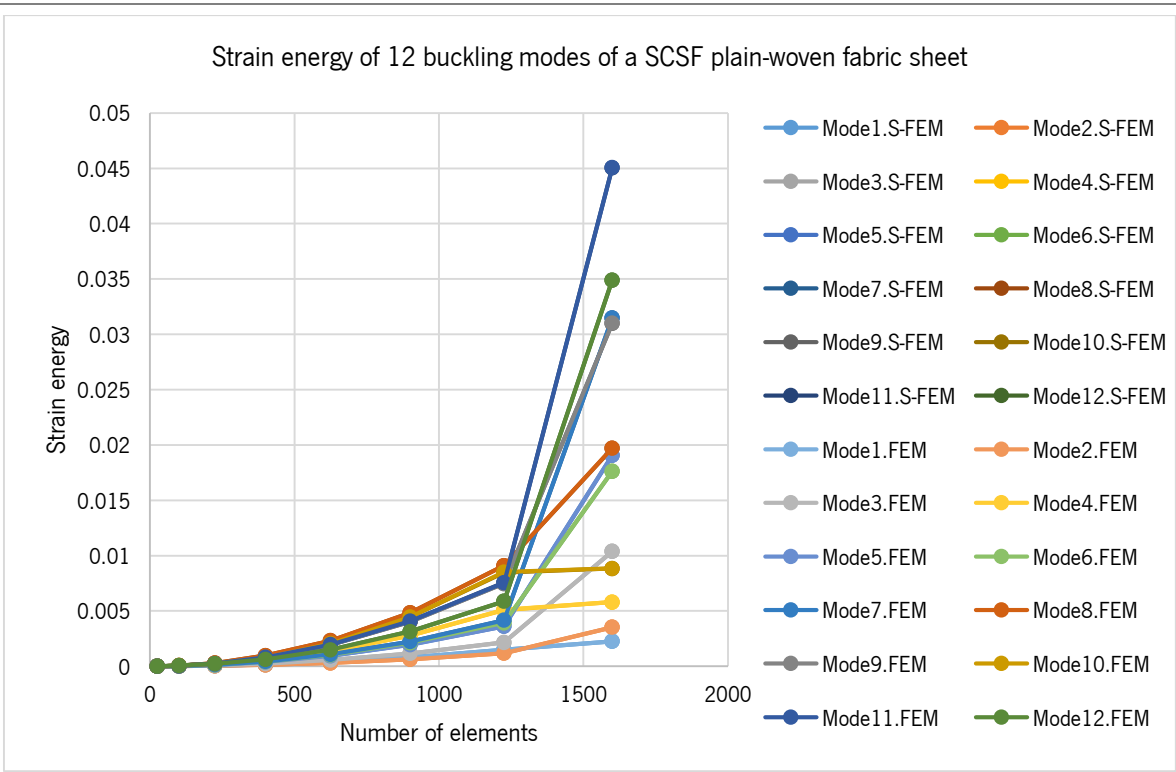


Figure 4.3: Numerical results for strain energy of twelve buckling modes of a SCSF plain-woven fabric sheet (h_1/l) with different mesh density subjected uniform load.

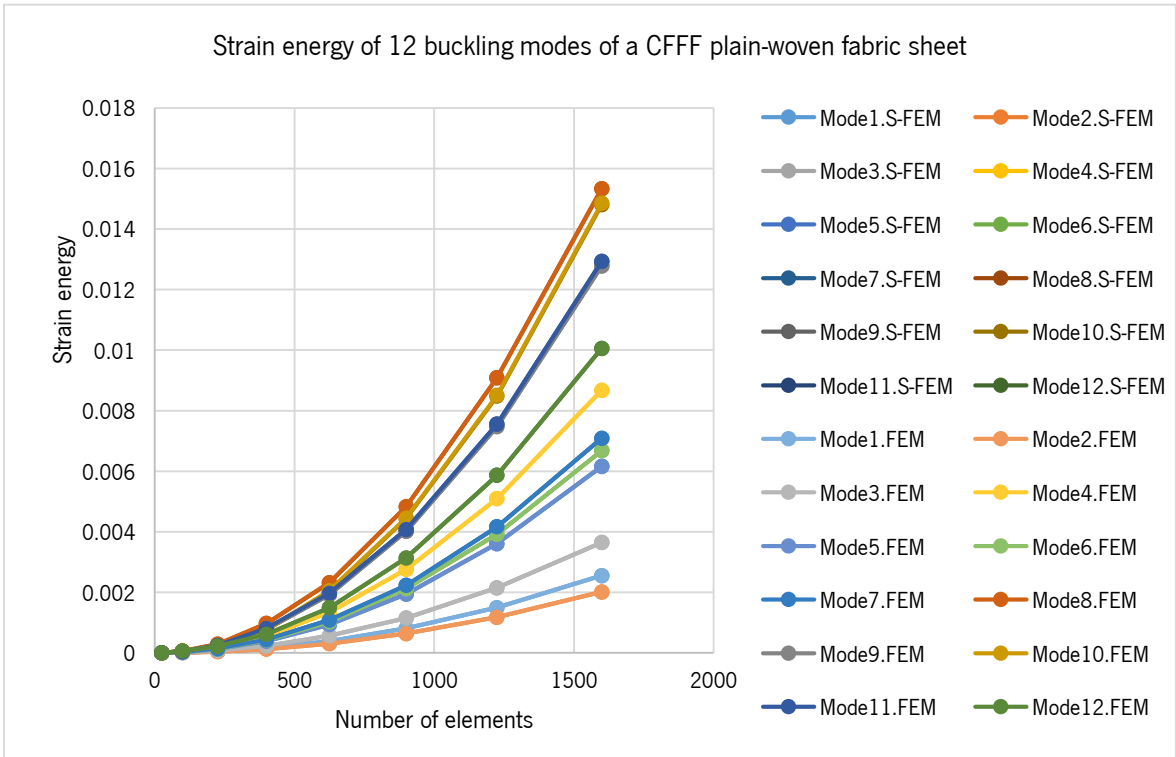


Figure 4.4: Numerical results for strain energy of twelve buckling modes of a CFFF plain-woven fabric sheet (h_1/l) with different mesh density subjected uniform load.

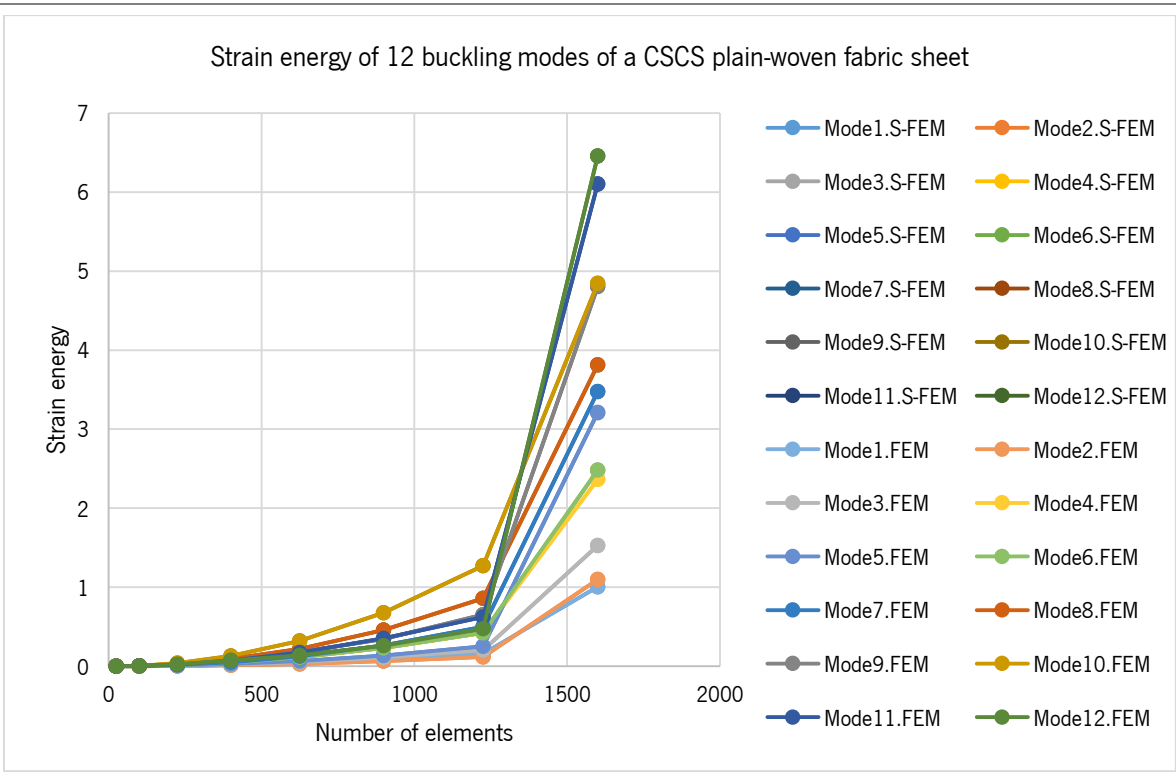


Figure 4.5: Numerical results for strain energy of twelve buckling modes of a CSCS plain-woven fabric sheet (h_2/l) with different mesh density subjected uniform load.

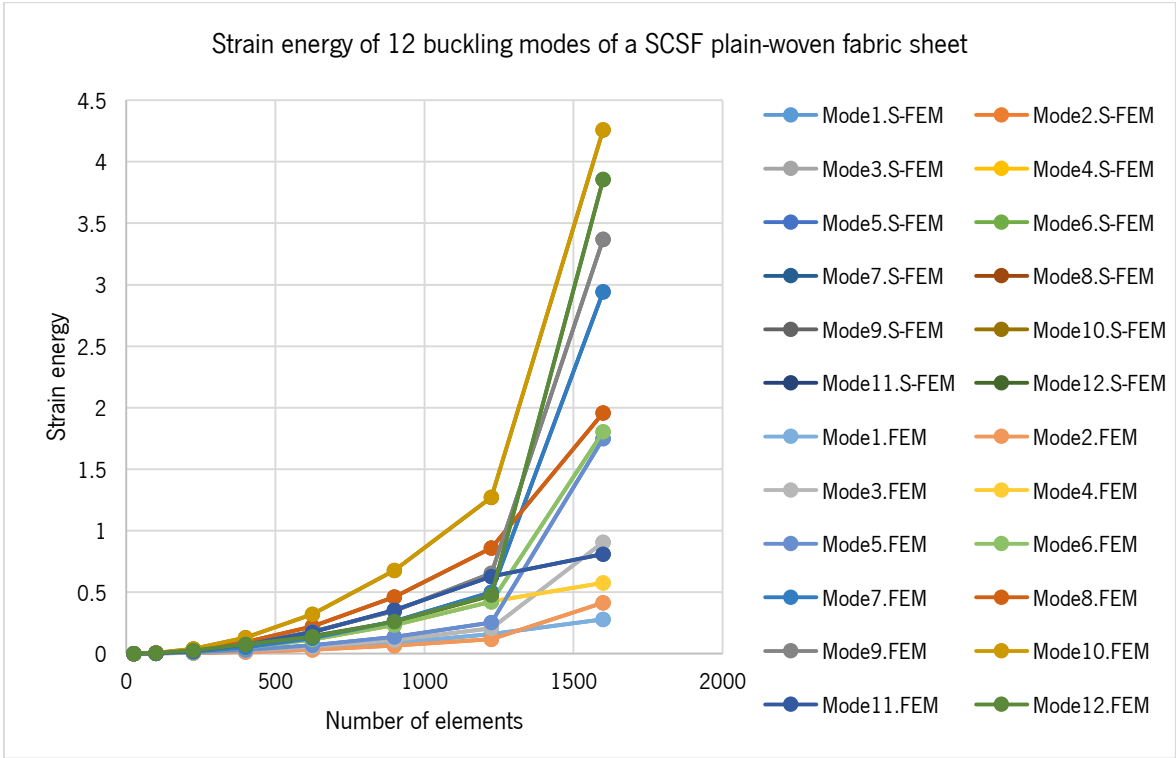


Figure 4.6: Numerical results for strain energy of twelve buckling modes of a SCSF plain-woven fabric sheet (h_2/l) with different mesh density subjected uniform load.

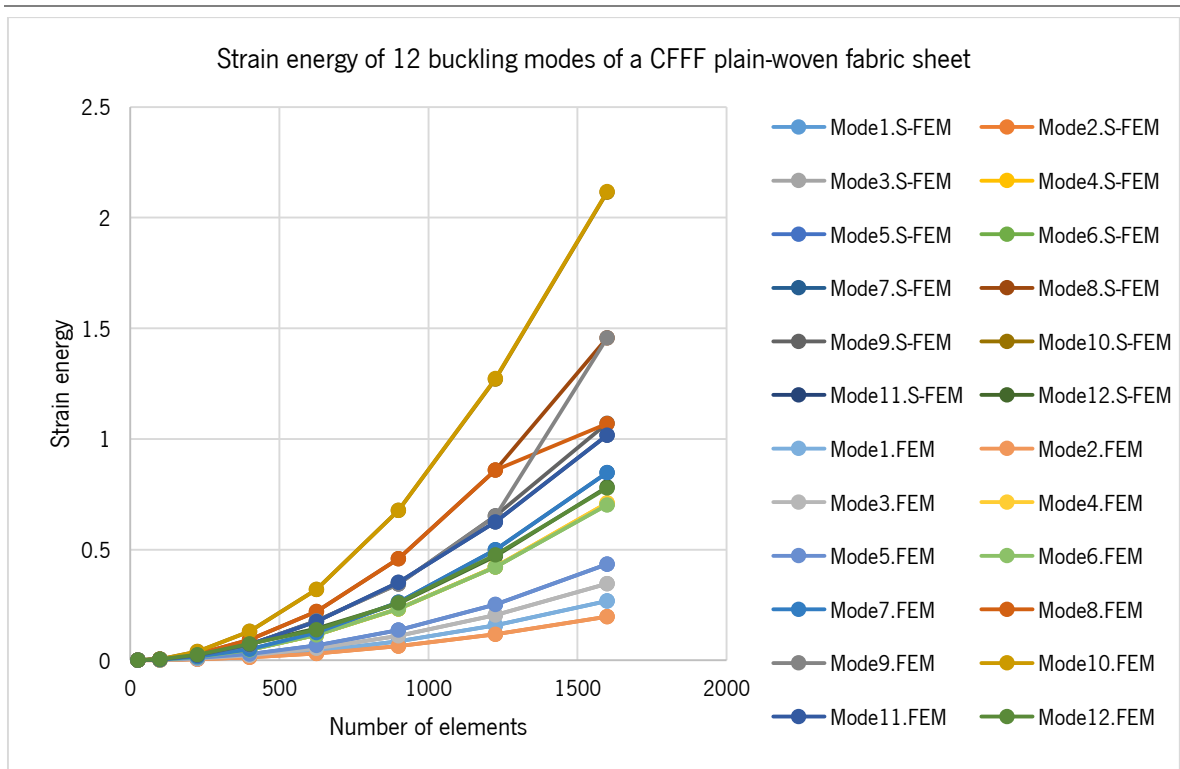


Figure 4.7: Numerical results for strain energy of twelve buckling modes of a CFFF plain-woven fabric sheet (h_2/l) with different mesh density subjected uniform load.

Note that, compared to the standard FEM, the present method S-FEM is straightforward to in implementation and no extra sampling points are introduced. It is found that the smoothed strain gradient matrix of the Q4SD1 element is approximated to the strain gradient matrix of the MITC4 element using the reduced integration of one Gauss point. Although the present solution of S-FEM can be solved by using one smoothing domain per Q4 element (1 SD), four smoothing domains (4 SDs) can produce more accurate numerical results.

According to the output numeric results presented in above tables and figures, there are also geometrical results to illustrate the low-stress mechanical deformation of fabric samples. The post-buckling geometry of twelve buckling modes and the corresponding resultant displacement magnitude of twelve buckling modes for a CSCS/SCSF/CFFF plain-woven fabric sheet with both h_1/l and h_2/l are illustrated in Figure 4.8 to 4.15. Although fabric samples underwent complex deformation under different buckling modes and boundary conditions, these figures indicate that the Q4 elements (Q4 mesh) implemented by S-FEM is well refined, less distorted and not coarse even with low mesh density.

The post-buckling geometry of twelve buckling modes and the corresponding resultant displacement magnitude of twelve buckling modes for a CFFF plain-woven fabric sheet with h_1/l are illustrated in Figures 4.8 and 4.9 as follows

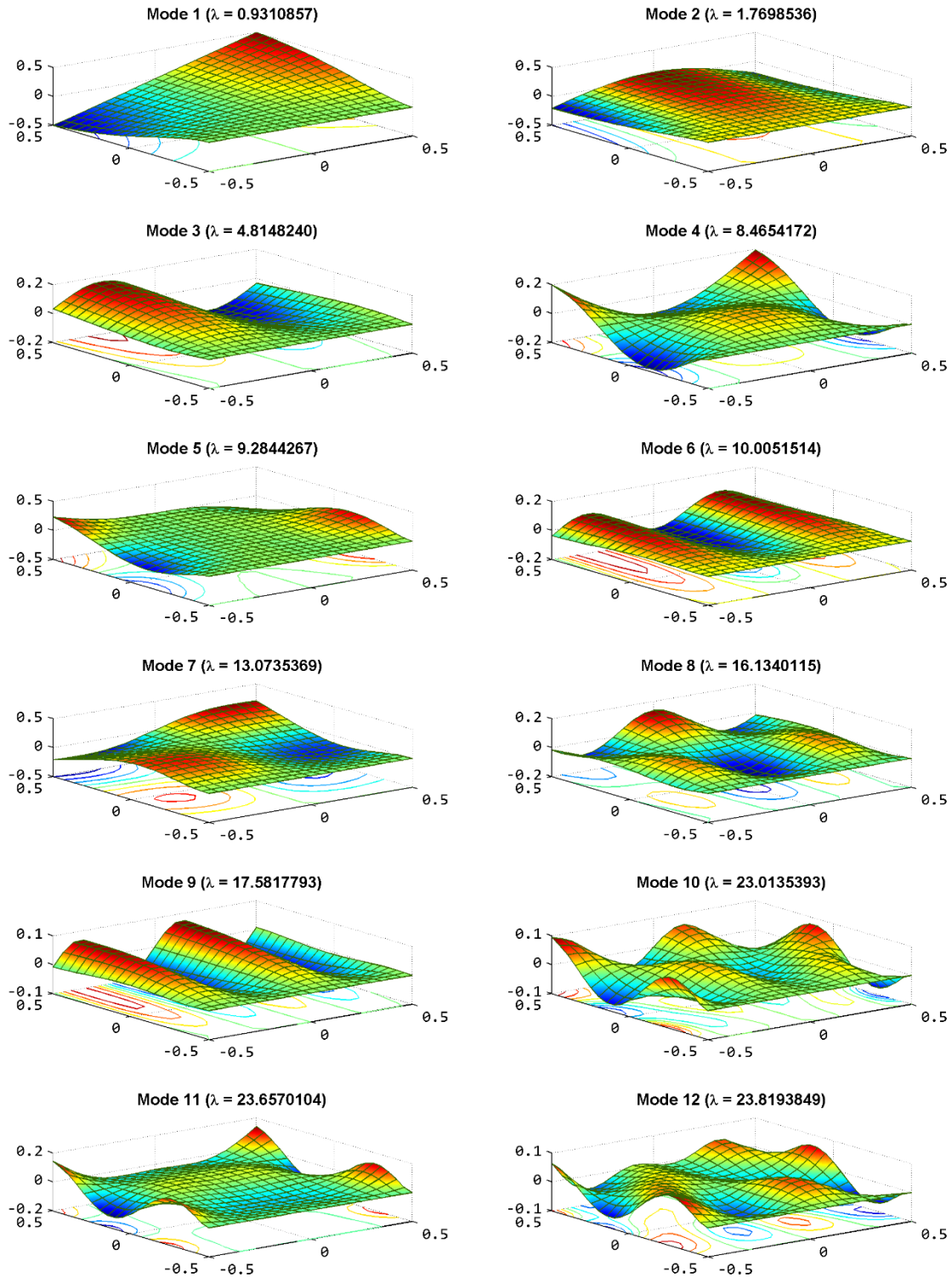


Figure 4.8: Buckling modes of a CFFF plain-woven fabric sheet with h_1/l , using 20×20 Q4 elements and 1 smoothing domain per element.

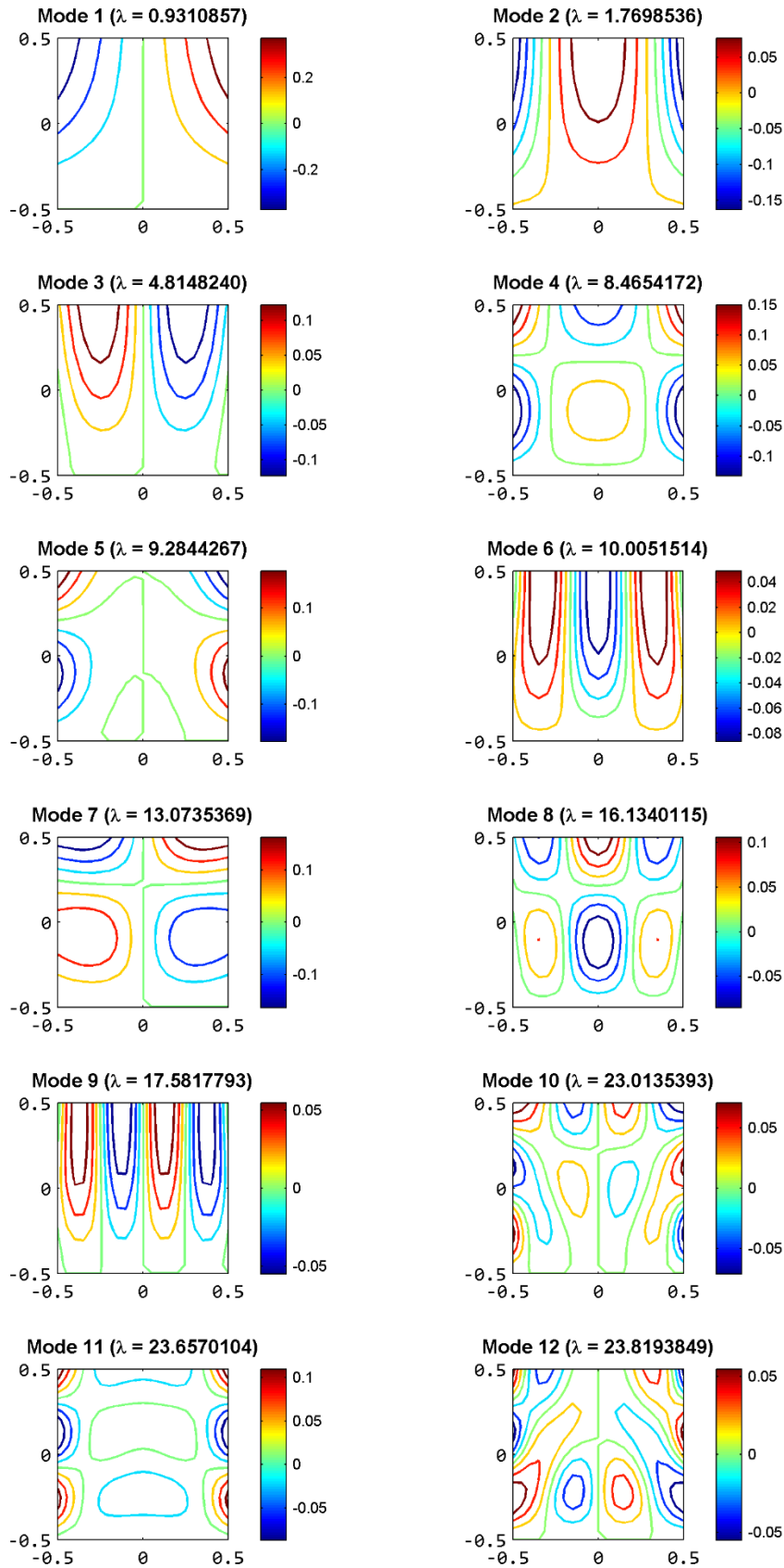


Figure 4.9: Resultant displacement magnitude for buckling modes of a CFFF plain-woven fabric sheet with h_1/l .

The post-buckling geometry of twelve buckling modes and the corresponding resultant displacement magnitude of twelve buckling modes for a CSCS plain-woven fabric sheet with h_1/l are illustrated in Figures 4.10 and 4.11 as follows

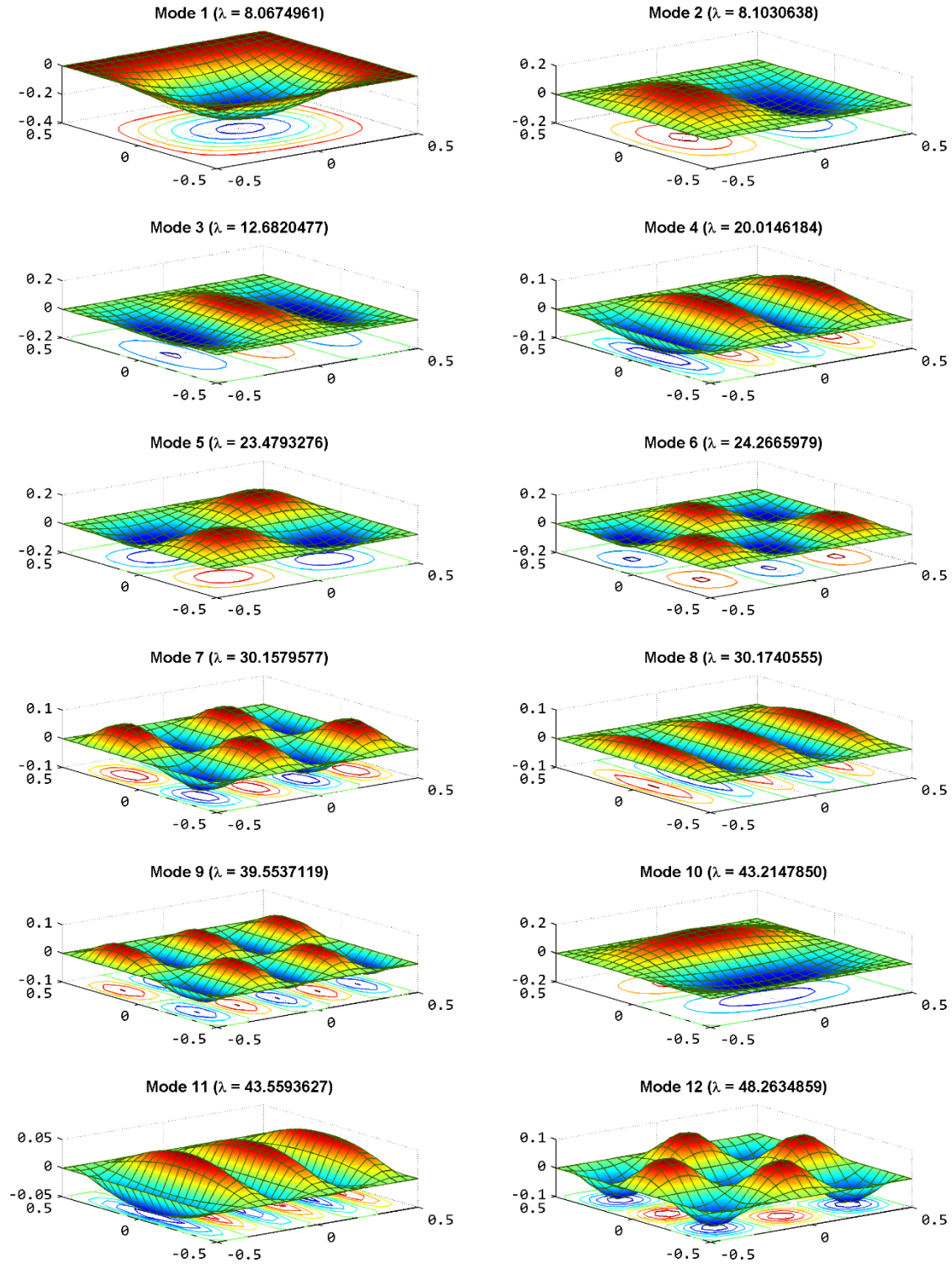


Figure 4.10: Buckling modes of a CSCS plain-woven fabric sheet with h_1/l , using 20×20 Q4 elements and 1 smoothing domains per element.

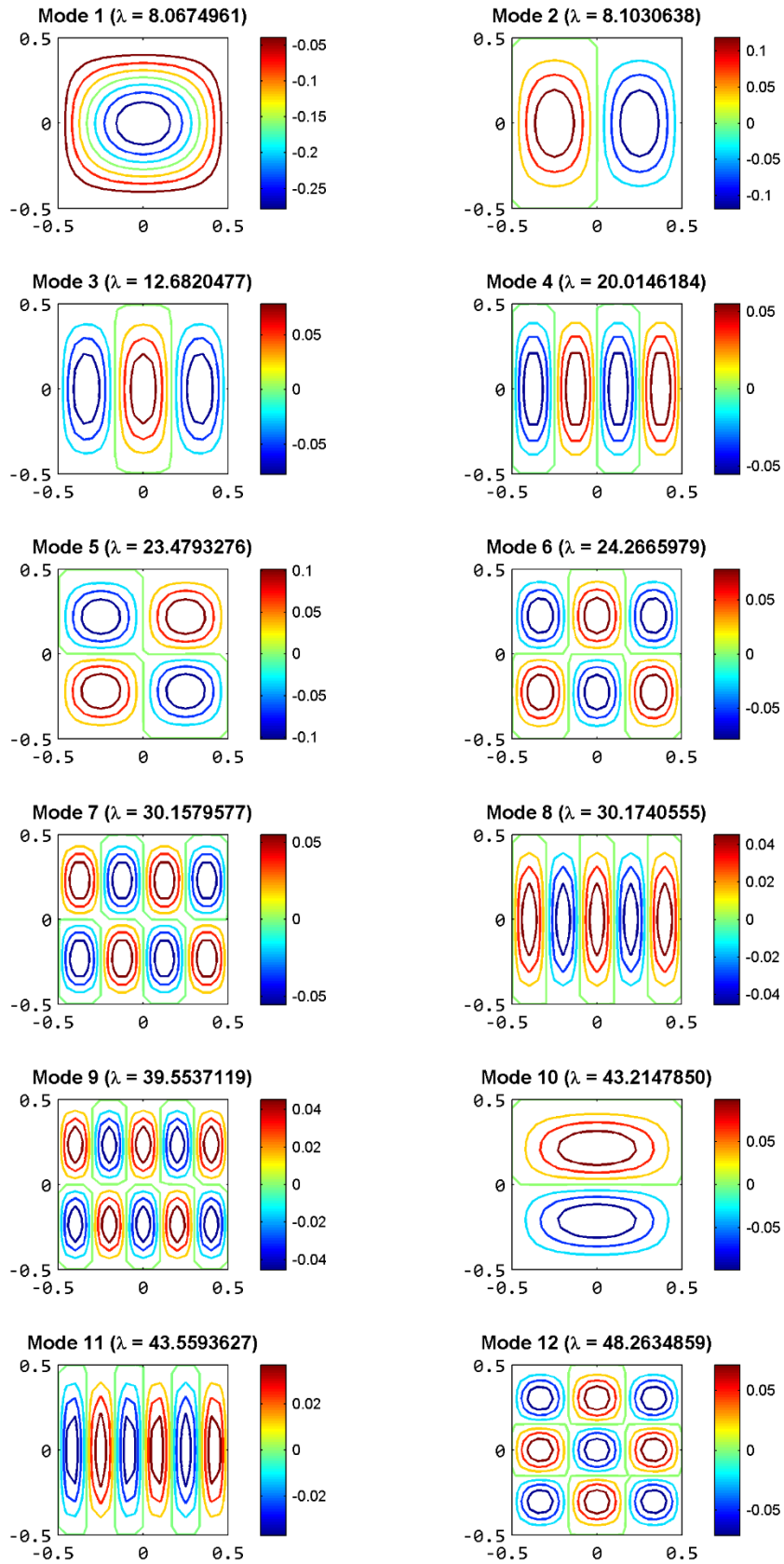


Figure 4.11: Resultant displacement magnitude for buckling modes of a CSCS plain-woven fabric sheet with h_1/l .

The post-buckling geometry of twelve buckling modes and the corresponding resultant displacement magnitude of twelve buckling modes for a SCSF plain-woven fabric sheet with h_2/l are illustrated in Figures 4.12 and 4.13 as follows

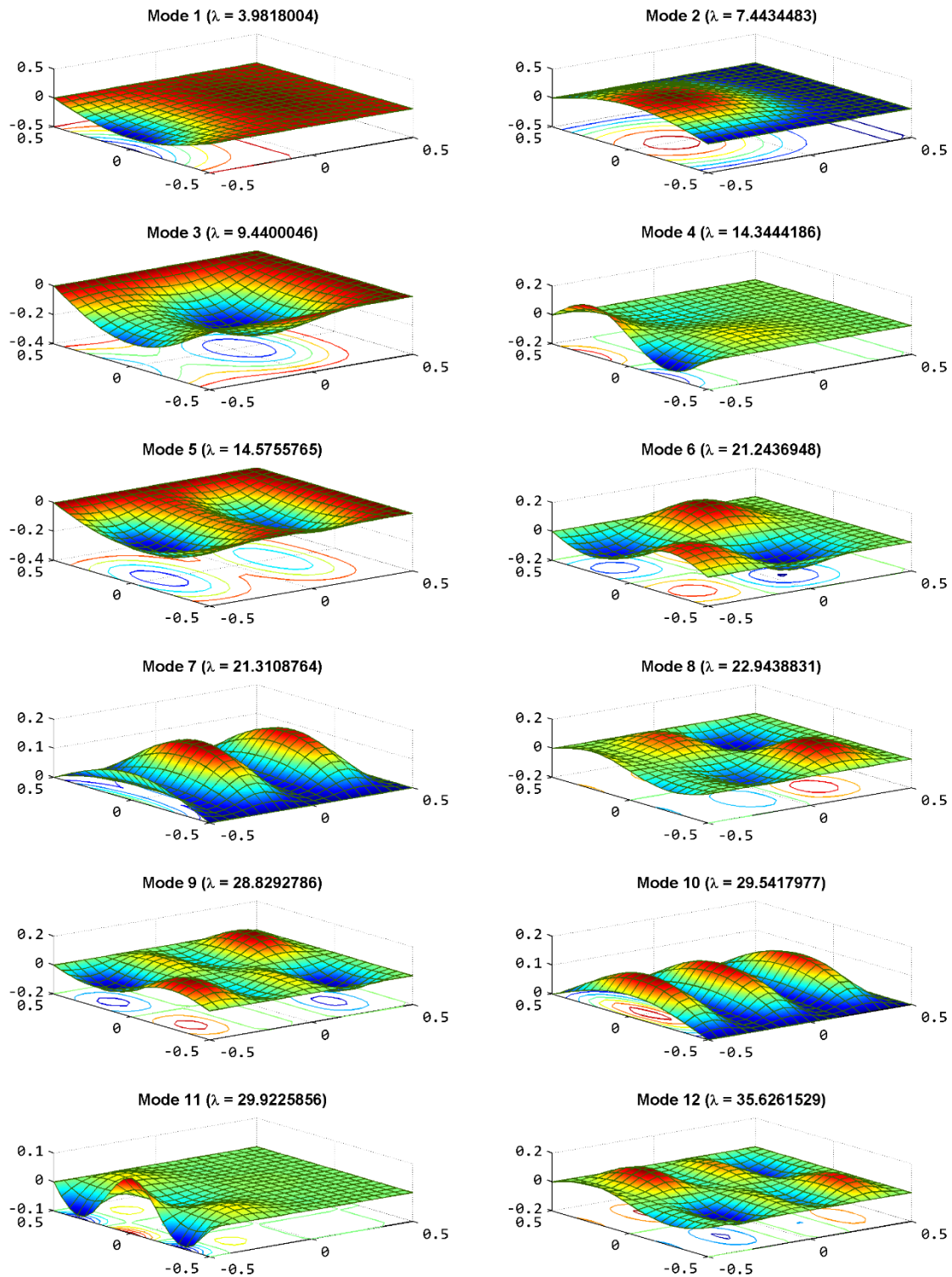


Figure 4.12: Buckling modes of a SCSF plain-woven fabric sheet with h_2/l , using 20×20 Q4 elements and 1 smoothing domains per element.

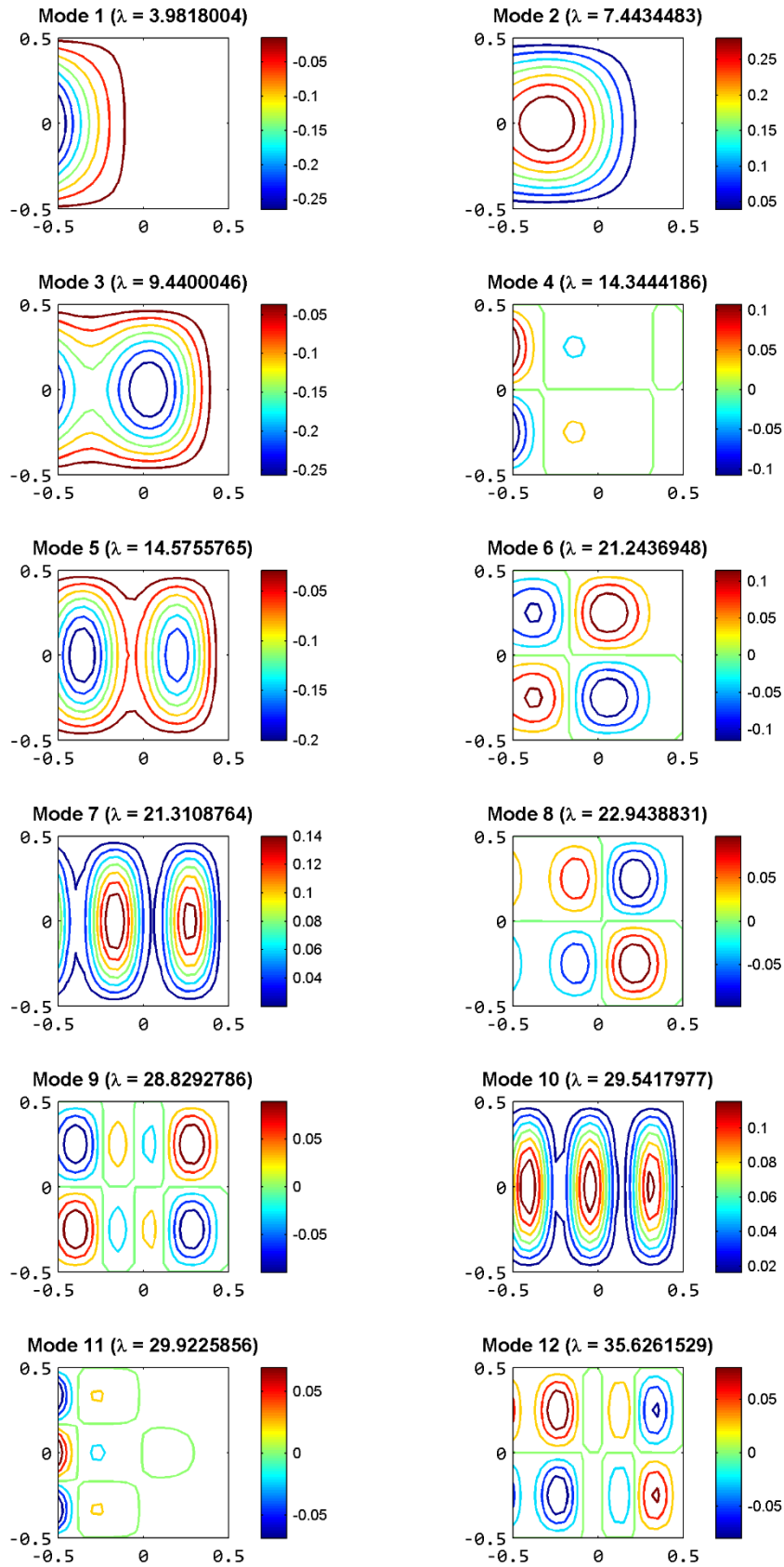


Figure 4.13: Resultant displacement magnitude for modes of buckling of a SCSF plain-woven fabric sheet with h_2/l .

The post-buckling geometry of twelve buckling modes and the corresponding resultant displacement magnitude of twelve buckling modes for a CFFF plain-woven fabric sheet with h_2/l are illustrated in Figures 4.14 and 4.15 as follows

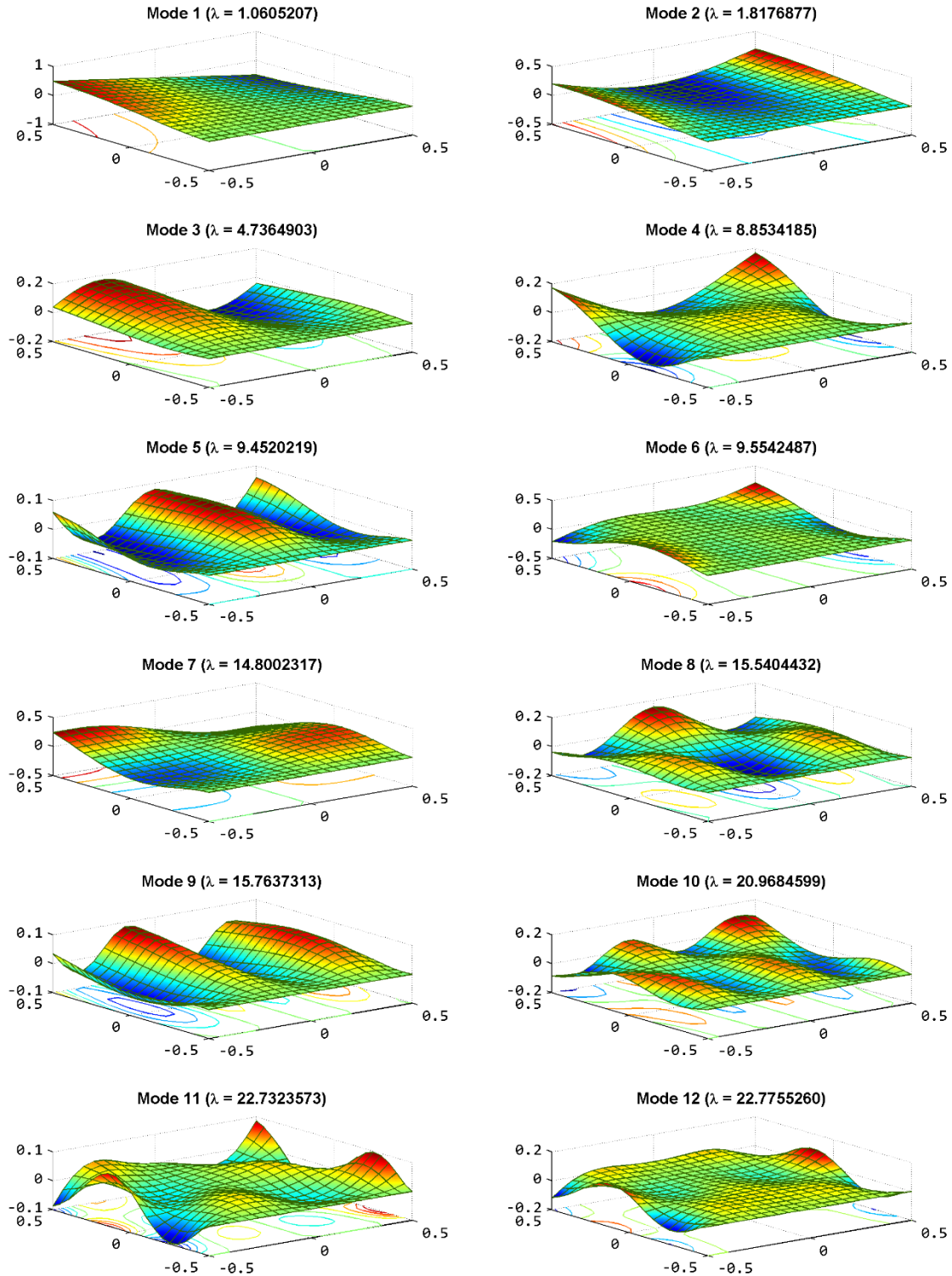


Figure 4.14: Buckling modes of a CFFF plain-woven fabric sheet with h_2/l , using 20×20 Q4 elements and 1 smoothing domains per element.

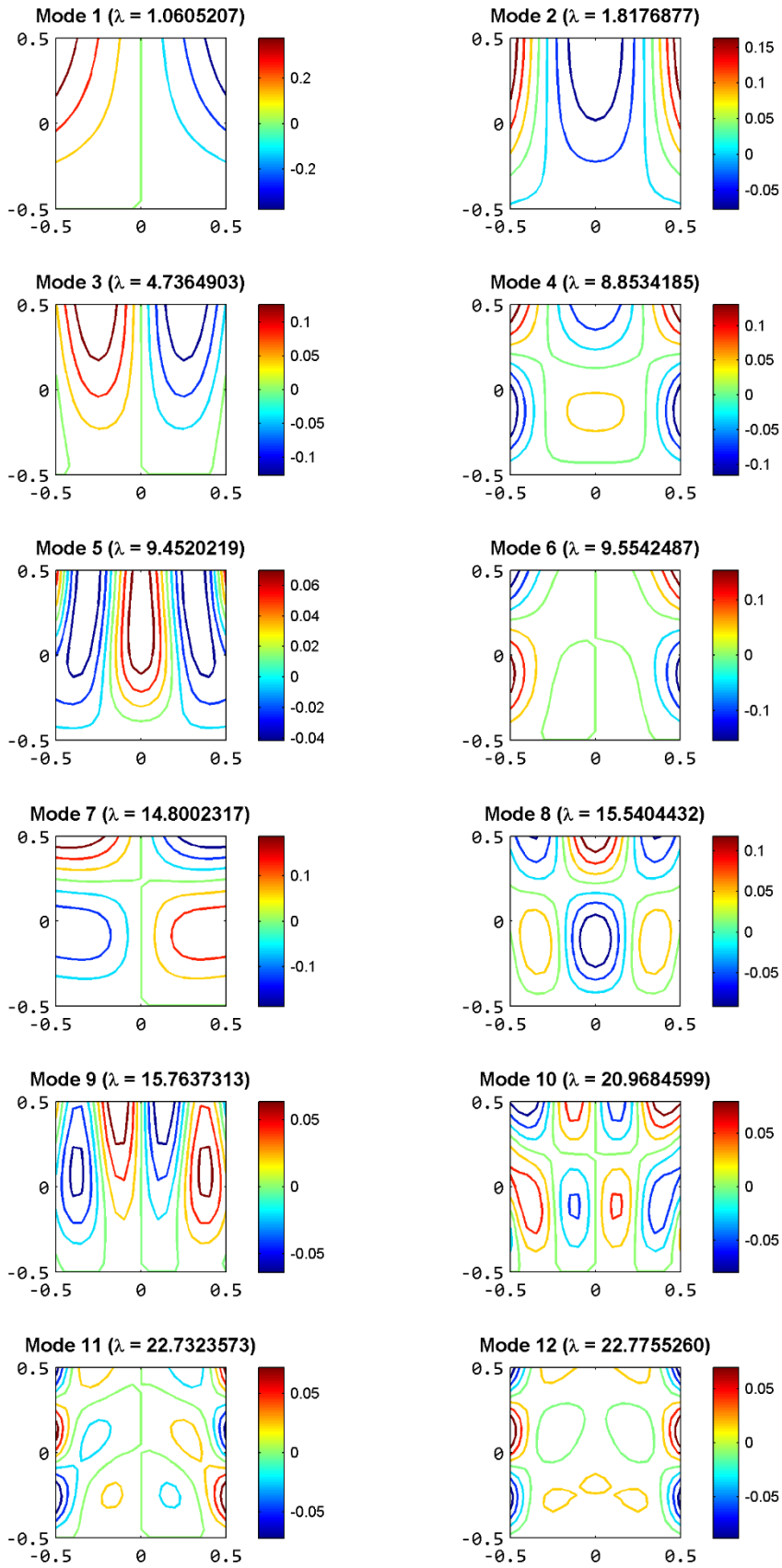


Figure 4.15: Resultant displacement magnitude for modes of buckling of a CFFF plain-woven fabric sheet with h_2/l .

4.1.2 Buckling behavior of woven fabric in terms of free-vibration behavior

Let us consider a configured fabric sheet as illustrated in Figure 4.1. The numerical modelling results of post-buckling deformation phenomenon of fabric sheet in terms of free-vibration behavior, which was implemented for all mesh indices, as listed in Table 4.2 and $SDs = \{1,2,3,4\}$, are presented for a CSCS/SCSF/CFFF plain-woven fabric sheet with different ratio of length to thickness $h_1/l = 0.0002$ and $h_2/l = 0.0005$.

Similar to the previous example, the numeric error between S-FEM and standards FEM for twelve eigenvibration modes are listed in Tables 4.6 and 4.7 for both S-FEM and FEM. Only the numerical results for twelve eigenbuckling modes of S-FEM using 1 SD and 4 SD are listed in these tables in order to find the numerical errors between the implemented number of soothing domains per Q4 element. In Tables 4.6 and 4.7, numerical results of CS-FEM is denoted by Q4SD1 and Q4SD4 according to $SDs = \{1,4\}$ and the numerical output of the corresponding standard FEM finite element model is denoted by MITC4.

Table 4.6: Numerical output of twelve eigenvibration modes for a CSCS/SCSF/CFFF plain-woven fabric sheet with h_1/l , using 20×20 Q4 elements and $SDs = \{1,4\}$ smoothing domains per element

h_1/l	CSCS			SCSF			CFFF		
	Q4SD1	Q4SD4	MITC4	Q4SD1	Q4SD4	MITC4	Q4SD1	Q4SD4	MITC4
1	0.0020	0.0020	0.0020	0.0009	0.0009	0.0009	0.0002	0.0002	0.0002
2	0.0040	0.0040	0.0040	0.0026	0.0026	0.0026	0.0007	0.0007	0.0007
3	0.0046	0.0046	0.0046	0.0027	0.0028	0.0028	0.0014	0.0014	0.0014
4	0.0068	0.0068	0.0068	0.0047	0.0048	0.0048	0.0021	0.0021	0.0021
5	0.0075	0.0076	0.0076	0.0055	0.0055	0.0055	0.0024	0.0024	0.0024
6	0.0085	0.0085	0.0085	0.0059	0.0059	0.0059	0.0038	0.0038	0.0038
7	0.0104	0.0104	0.0105	0.0080	0.0080	0.0080	0.0045	0.0045	0.0045
8	0.0109	0.0109	0.0109	0.0080	0.0080	0.0080	0.0048	0.0048	0.0048
9	0.0127	0.0127	0.0127	0.0099	0.0099	0.0099	0.0050	0.0050	0.0050
10	0.0138	0.0138	0.0138	0.0104	0.0104	0.0104	0.0074	0.0075	0.0075
11	0.0146	0.0147	0.0148	0.0115	0.0116	0.0116	0.0076	0.0076	0.0076
12	0.0156	0.0156	0.0157	0.0125	0.0125	0.0125	0.0076	0.0076	0.0076

Table 4.7: Numerical output of twelve eigenvibration modes for a CSCS/SCSF/CFFF plain-woven fabric sheet with h_2/l , using 20×20 Q4 elements and $SDs = \{1,4\}$ smoothing domains per element

h_2/l	CSCS			SCSF			CFFF		
Mode	Q4SD1	Q4SD4	MITC4	Q4SD1	Q4SD4	MITC4	Q4SD1	Q4SD4	MITC4
1	0.0028	0.0028	0.0028	0.0013	0.0013	0.0013	0.0003	0.0003	0.0003
2	0.0052	0.0052	0.0052	0.0034	0.0034	0.0034	0.0010	0.0010	0.0010
3	0.0066	0.0066	0.0066	0.0040	0.0040	0.0040	0.0020	0.0020	0.0020
4	0.0092	0.0093	0.0093	0.0064	0.0064	0.0064	0.0027	0.0027	0.0027
5	0.0096	0.0096	0.0096	0.0069	0.0070	0.0070	0.0034	0.0034	0.0034
6	0.0124	0.0124	0.0124	0.0086	0.0087	0.0087	0.0057	0.0057	0.0057
7	0.0136	0.0137	0.0137	0.0104	0.0105	0.0105	0.0059	0.0059	0.0059
8	0.0152	0.0152	0.0152	0.0111	0.0111	0.0111	0.0061	0.0061	0.0061
9	0.0159	0.0159	0.0160	0.0123	0.0124	0.0124	0.0071	0.0071	0.0071
10	0.0197	0.0198	0.0199	0.0153	0.0154	0.0154	0.0096	0.0097	0.0097
11	0.0199	0.0200	0.0201	0.0155	0.0155	0.0156	0.0103	0.0104	0.0104
12	0.0203	0.0203	0.0203	0.0160	0.0161	0.0161	0.0114	0.0114	0.0114

The numerical results of free-vibration deflection for two fabric samples under natural frequency are listed in Tables 4.6 and 4.7, from where we again conclude that the present method is highly accurate and the number of smoothing domains per Q4 element is approximated for each of eigenvibration modes for both the thin and moderately thick fabric sheets with different boundary conditions.

For studied cases of buckling modes of woven fabric in terms of free-vibration behavior, the number of smoothing domains per Q4 element in range of $\{1,2,3,4\}$ once again was approximated for each of eigenbuckling modes with mixed boundary conditions, which clearly show the stable and well-balanced feature of the CS-FEM. It is also found that the stiffness matrix of the Q4SD1 element is identical to that one of FEM using the reduced integration (one Gauss point).

The numerical results for strain energy of twelve buckling modes between S-FEM and FEM are identical as illustrated in Figures 4.16, 4.17, 4.18 for thin fabric sample (h_1/l) and Figures 4.19, 4.20, 4.21 for moderately thick fabric sample (h_2/l). These figures also indicate that strain energy of deformed fabric sheet implemented by S-FEM possesses convergence for both the thin (h_1) and moderately thick (h_2) fabric sheets with different boundary conditions and mesh density.

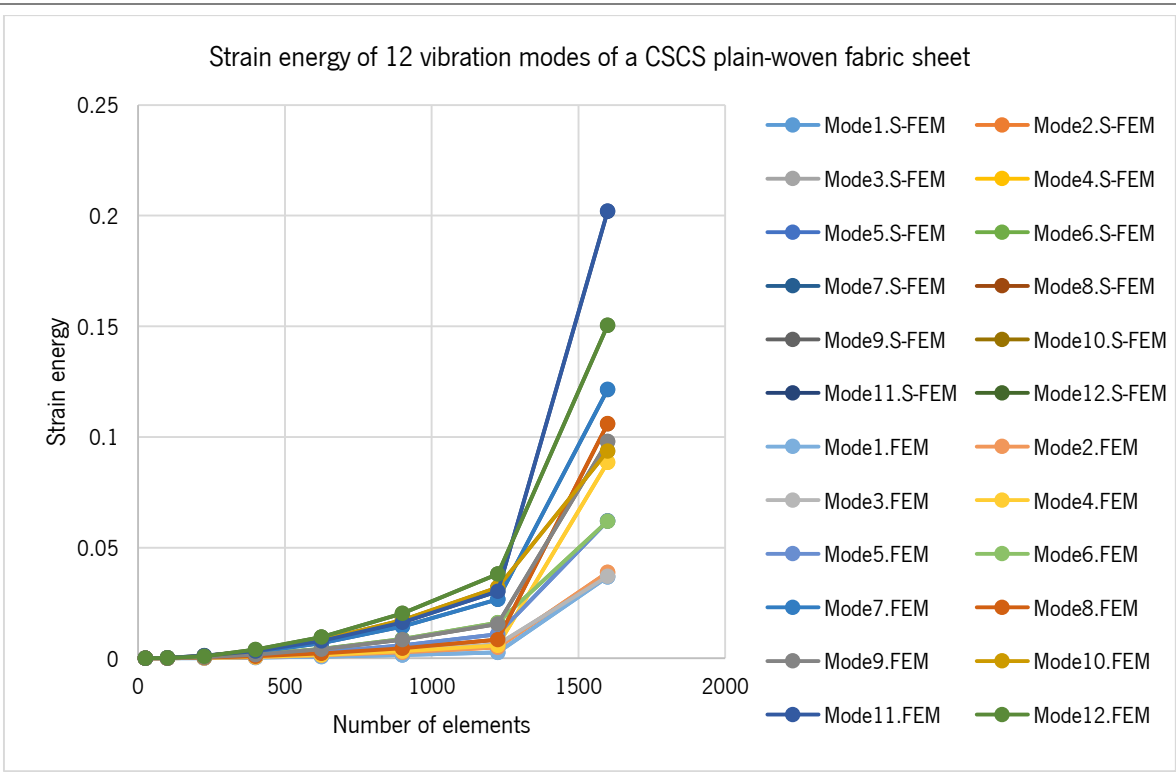


Figure 4.16: Numerical results for strain energy of twelve vibration modes of a CSCS plain-woven fabric sheet (h_1/l) with different mesh density subjected natural frequency.

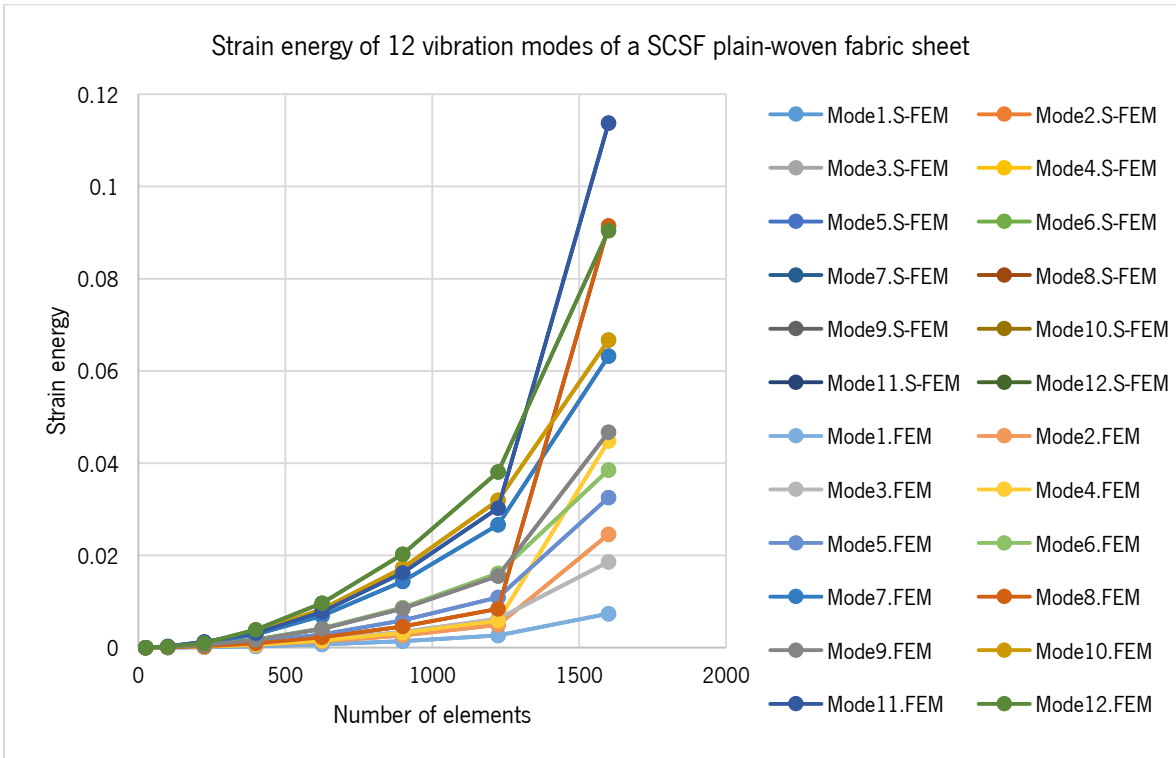


Figure 4.17: Numerical results for strain energy of twelve vibration modes of a SCSF plain-woven fabric sheet (h_1/l) with different mesh density subjected natural frequency.

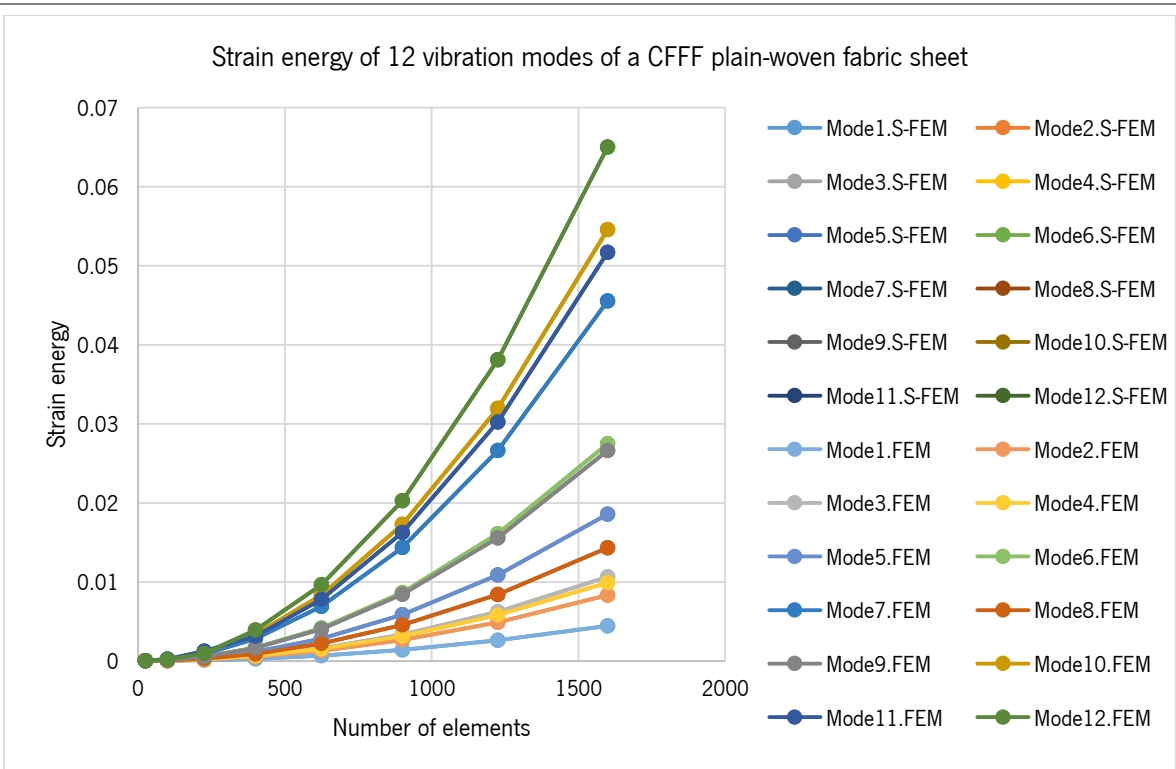


Figure 4.18: Numerical results for strain energy of twelve vibration modes of a CFFF plain-woven fabric sheet (h_1/l) with different mesh density subjected natural frequency.

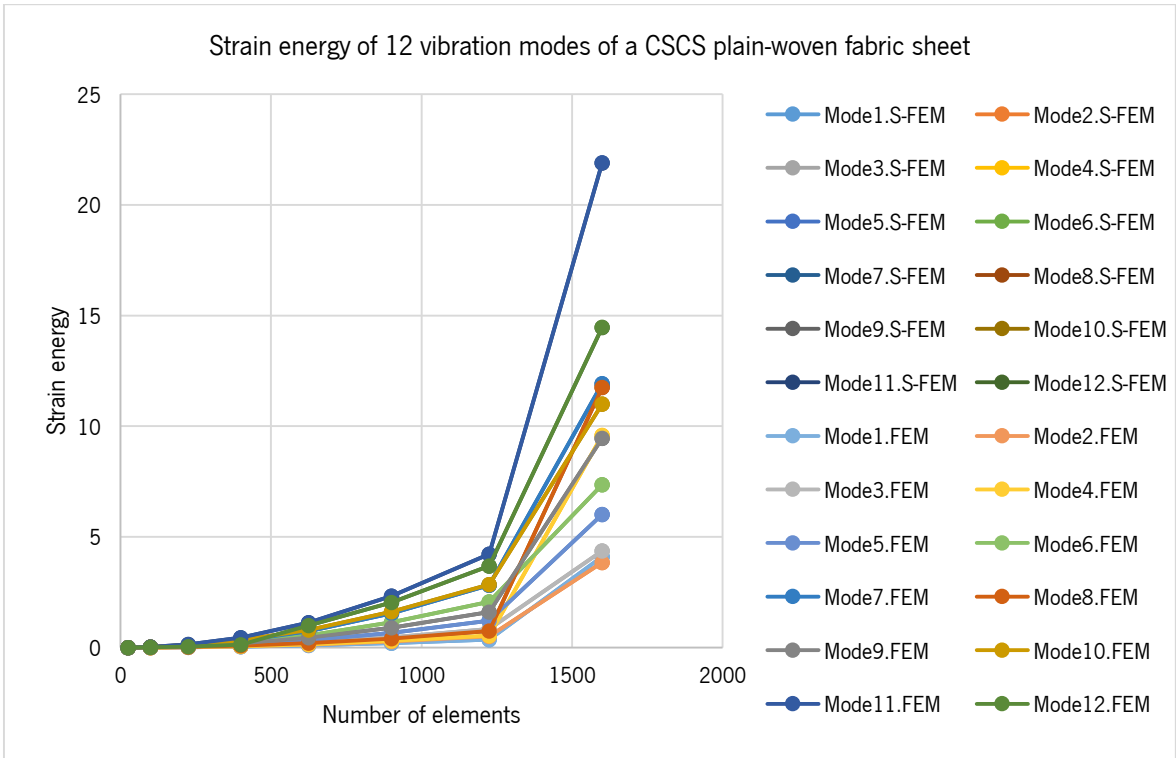


Figure 4.19: Numerical results for strain energy of twelve vibration modes of a CSCS plain-woven fabric sheet (h_2/l) with different mesh density subjected natural frequency.

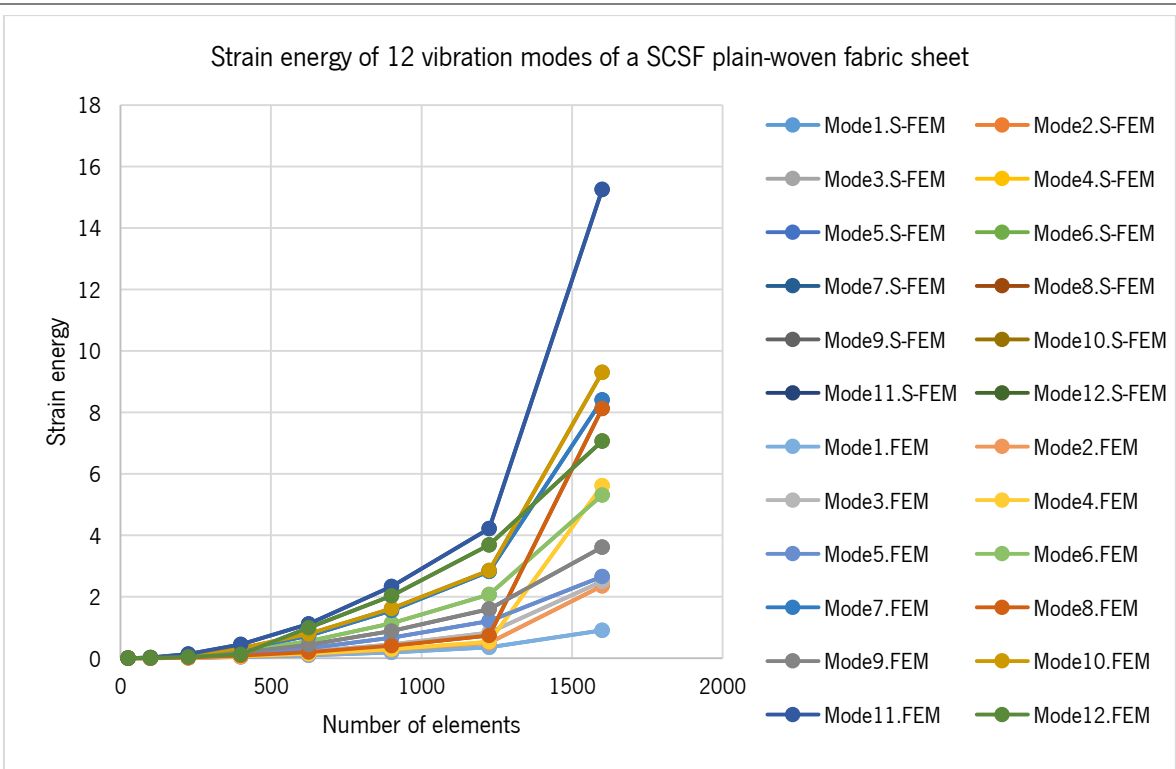


Figure 4.20: Numerical results for strain energy of twelve vibration modes of a SCSF plain-woven fabric sheet (h_2/l) with different mesh density subjected natural frequency.

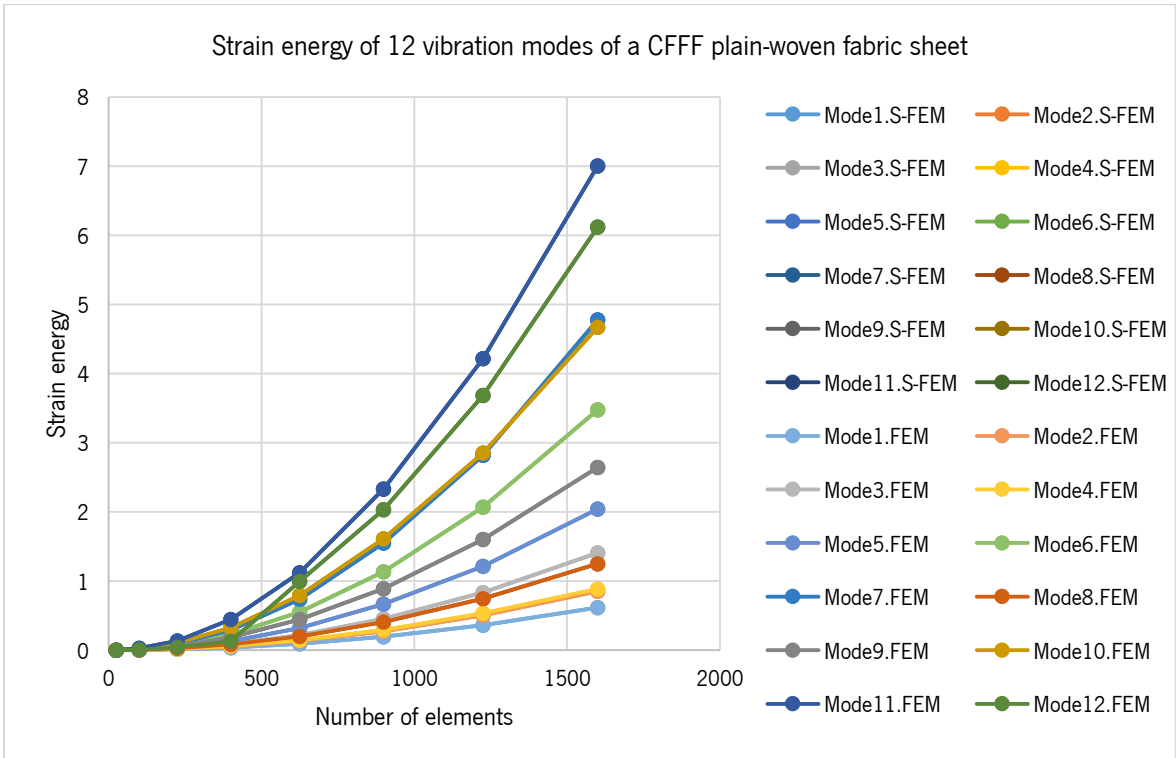


Figure 4.21: Numerical results for strain energy of twelve vibration modes of a CFFF plain-woven fabric sheet (h_2/l) with different mesh density subjected natural frequency.

Taking into consideration output numeric results presented in above tables and figures, the geometrical results of low-stress mechanical deformation of a CSCS/SCSF/CFFF plain-woven fabric

sheet with both h_1/l and h_2/l are, respectively, illustrated in Figures 4.22 to 4.29. These figures once again indicate that the Q4 elements (Q4 mesh) implemented by S-FEM is well refined, less distorted and not coarse even with low mesh density and complex deformed.

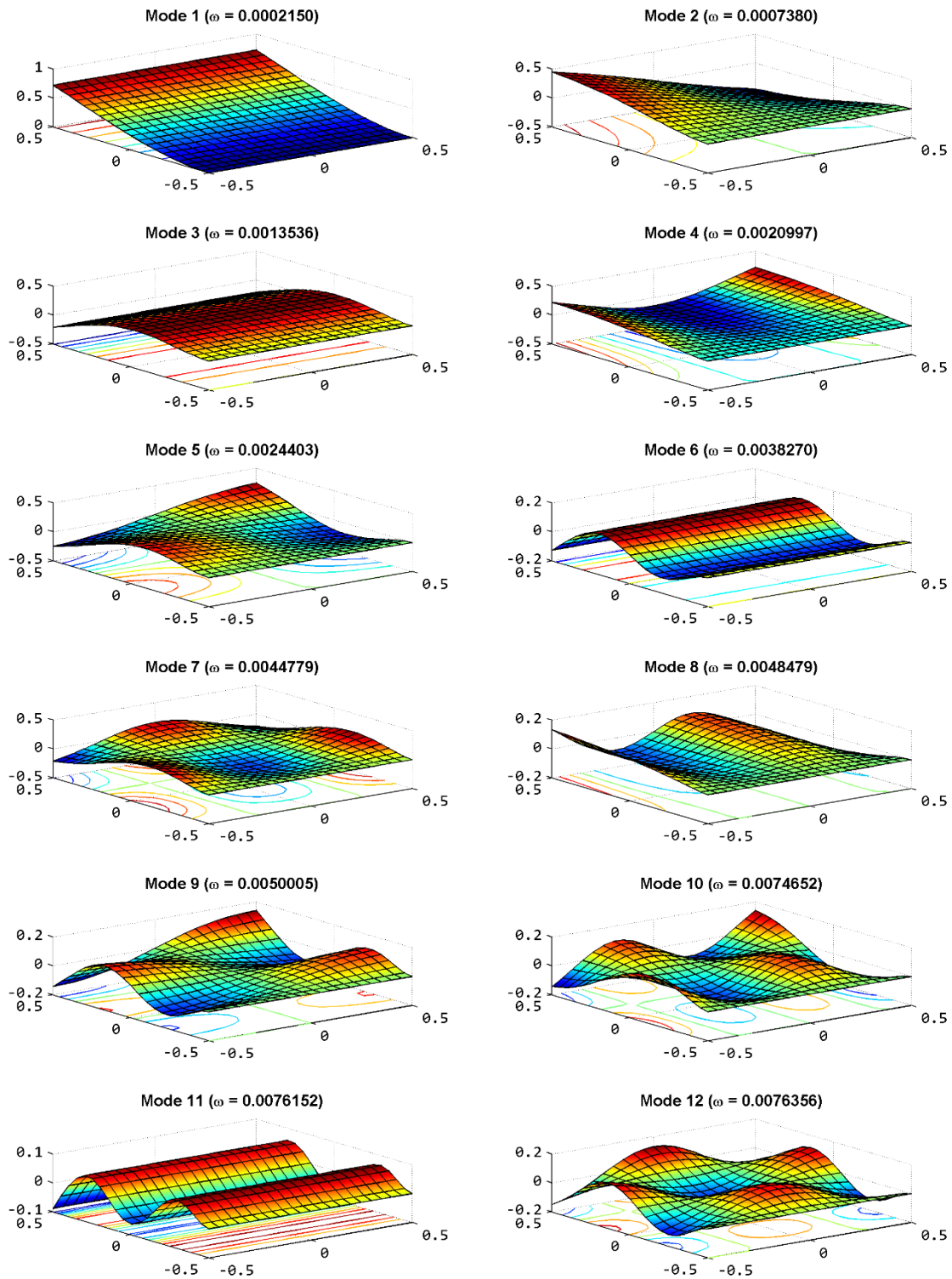


Figure 4.22: Modes of vibration for a CFFF plain-woven fabric sheet with h_1/l , using 20×20 Q4 elements and 1 smoothing domains per element.

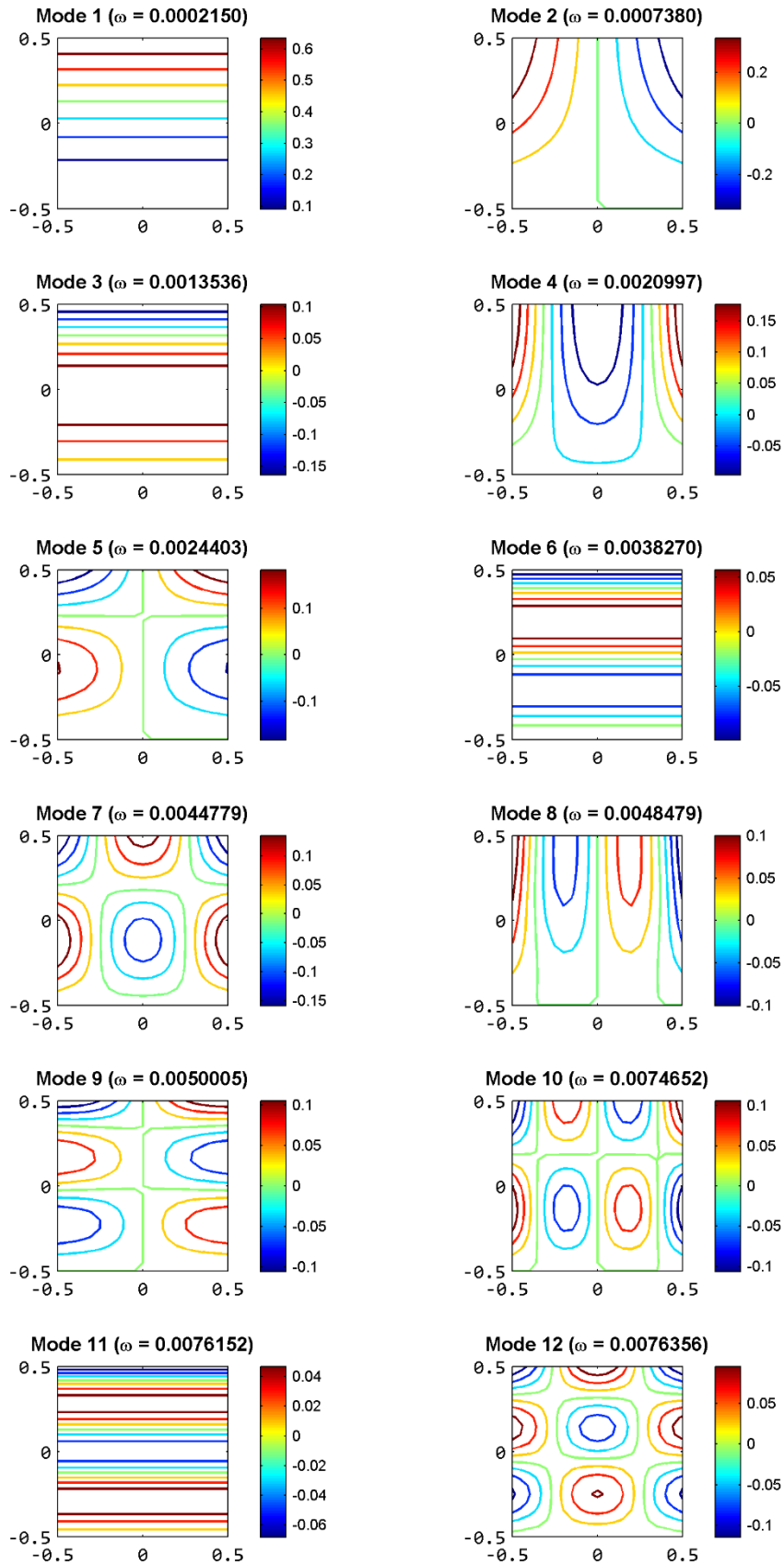


Figure 4.23: Resultant displacement magnitude for modes of free-vibration for a CFFF plain-woven fabric sheet with h_1/l .

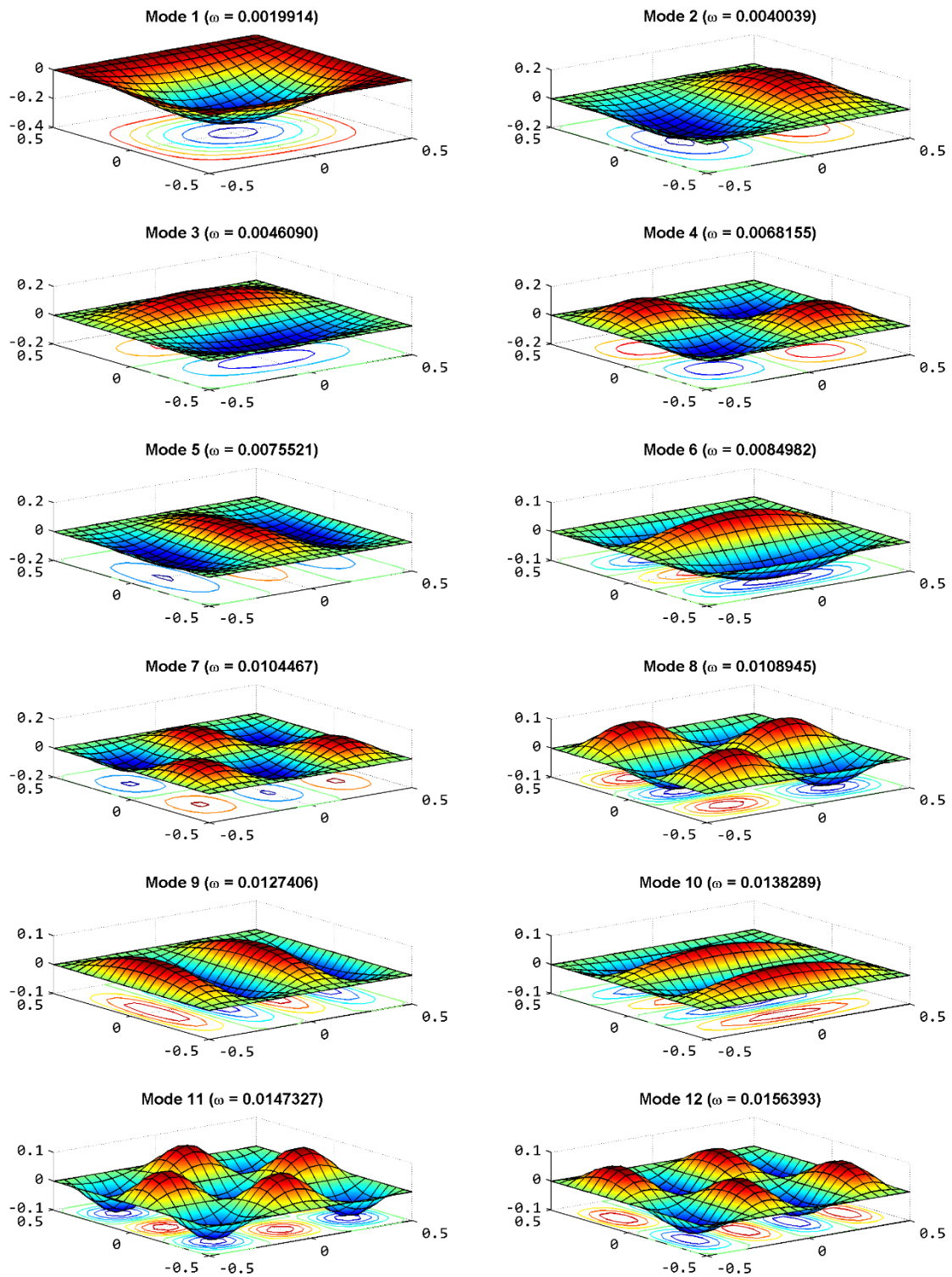


Figure 4.24: Modes of vibration for a C/SCS plain-woven fabric sheet with h_1/l , using 20×20 Q4 elements and 1 smoothing domains per element.

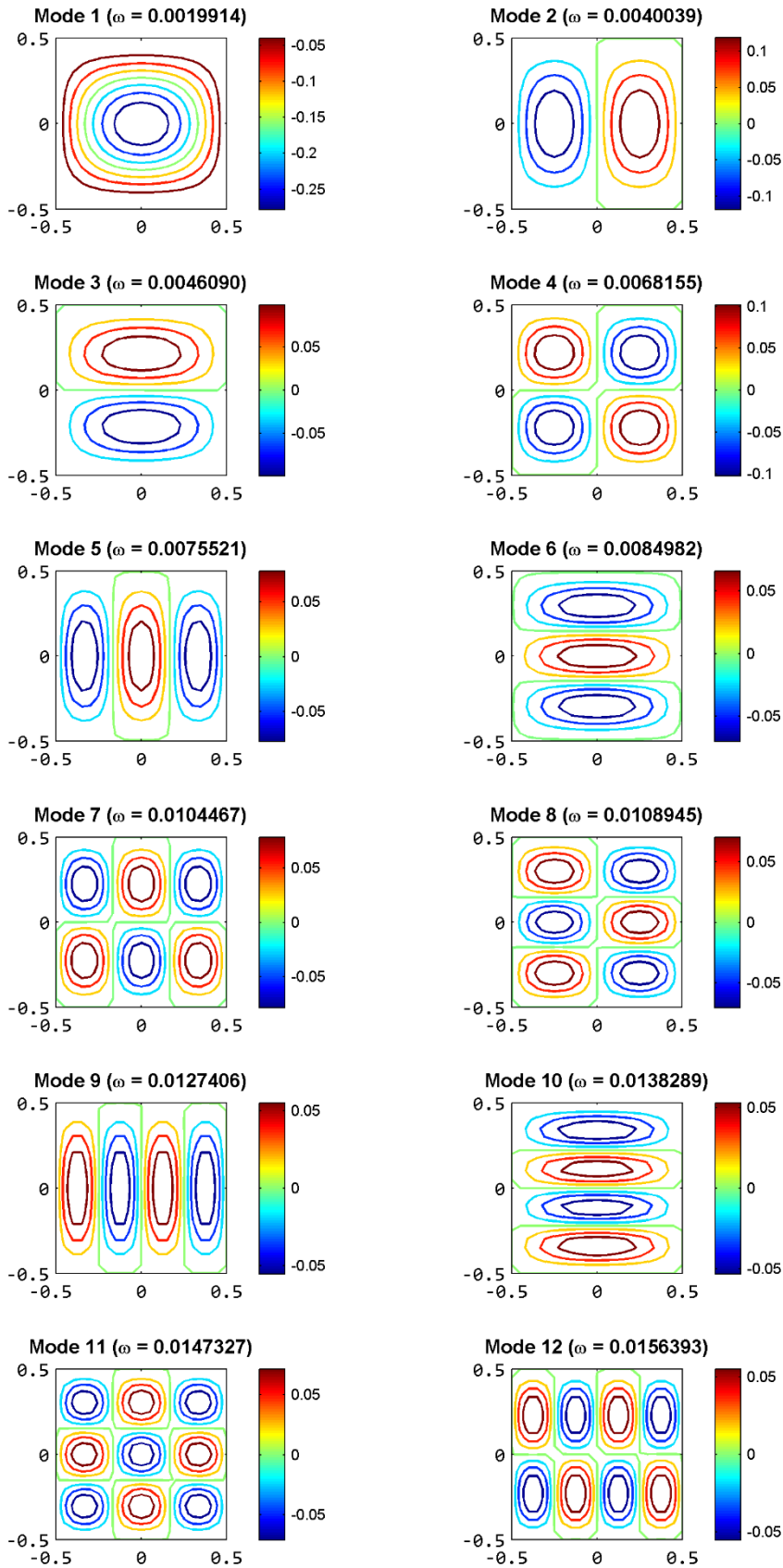


Figure 4.25: Resultant displacement magnitude for modes of free-vibration for a CSCS plain-woven fabric sheet with h_1/l .

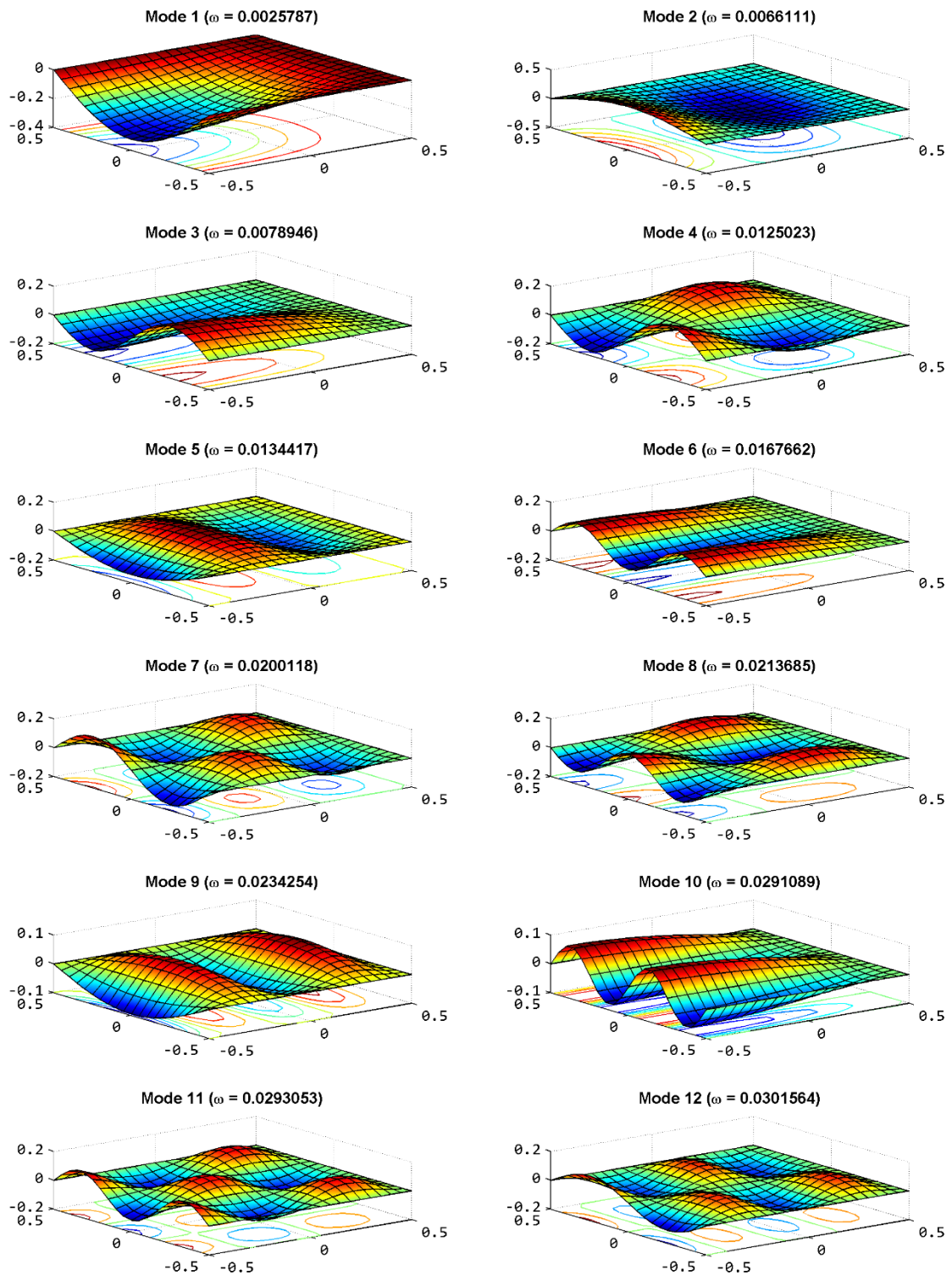


Figure 4.26: Modes of vibration for a SCSF plain-woven fabric sheet with h_2/l , using 20×20 Q4 elements and 1 smoothing domains per element.

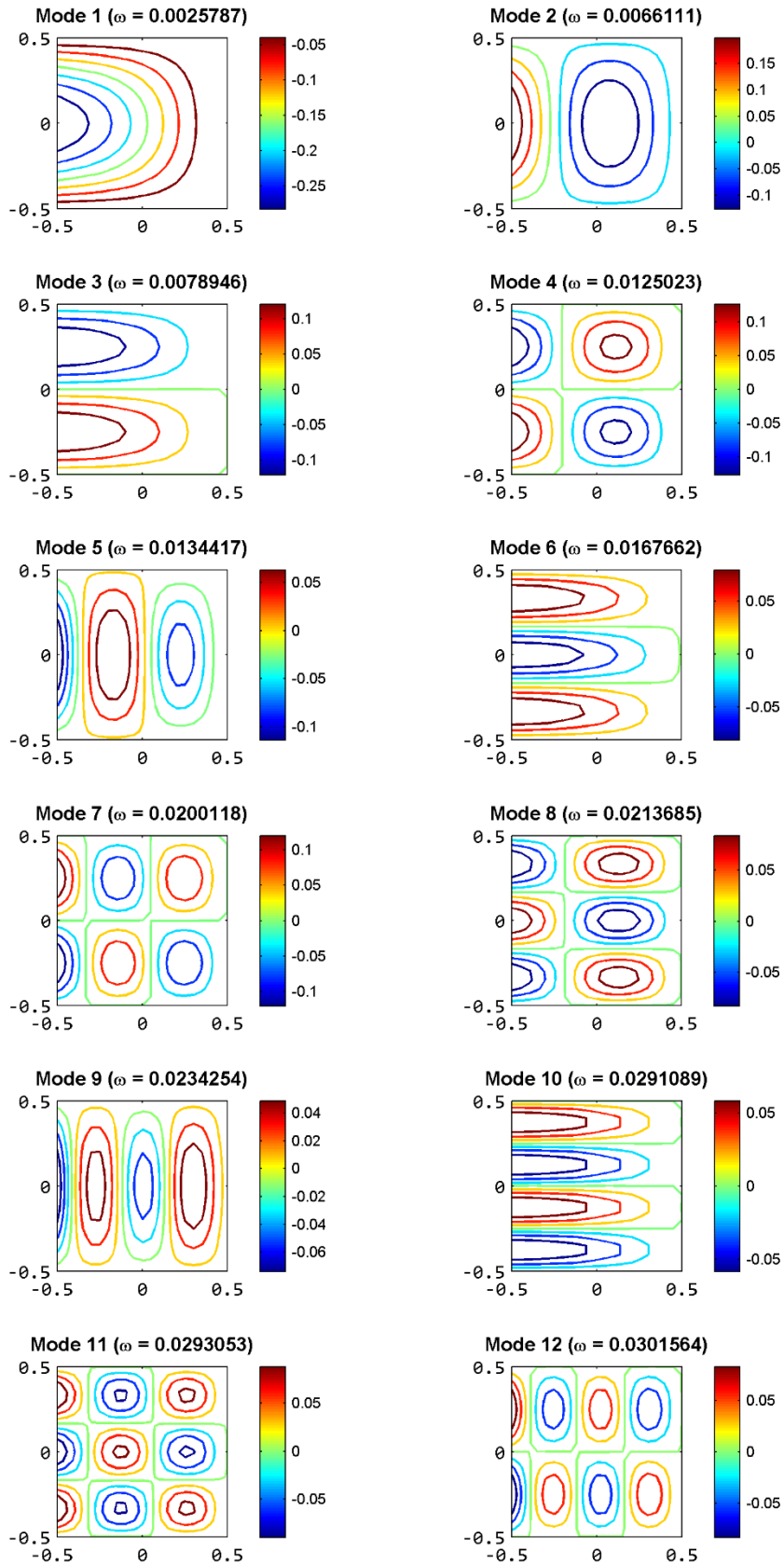


Figure 4.27: Resultant displacement magnitude for modes of free-vibration of a SCSF plain-woven fabric sheet with h_2/l .

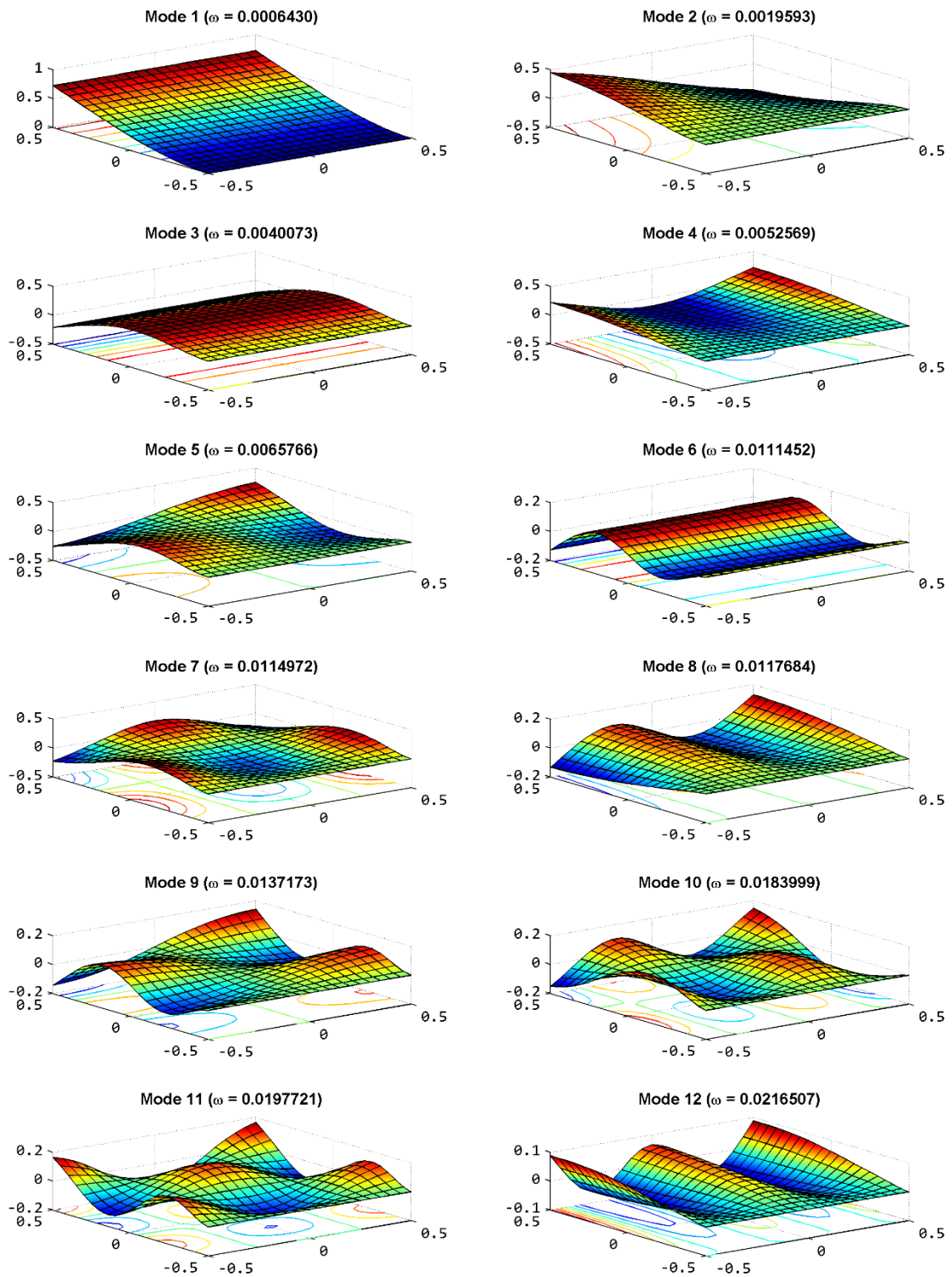


Figure 4.28: Modes of vibration for a CFFF plain-woven fabric sheet with h_2/l , using 20×20 Q4 elements and 1 smoothing domains per element.

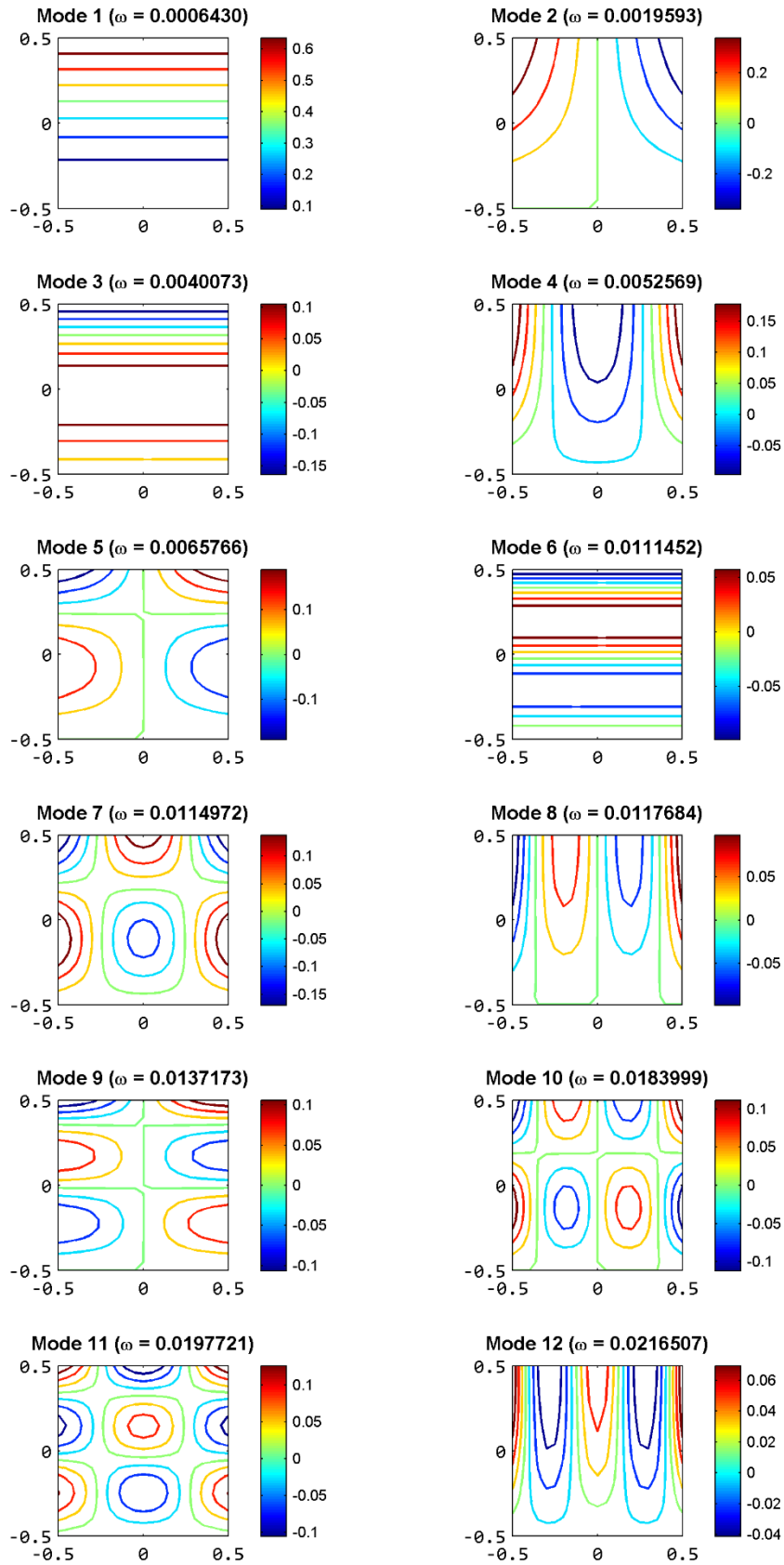


Figure 4.29: Resultant displacement magnitude for modes of free-vibration of a CFFF plain-woven fabric sheet with h_2/l .

4.1.3 Bending behavior of woven fabric

Mechanical bending properties of textile fabrics govern many aspects of fabric appearance and performance, such as wrinkle/buckle, hand and drape [2-4]. These are one of the most important characteristics in complex deformation analysis and modelling of textile fabrics. Numerical modelling of large-deflection elastic structural mechanics from numerical models have been widely applied to examine specific textile fabric engineering and apparel industry problems [5-7]. For example, the prediction of the robotic movement to control the laying of fabric onto a preset work surface [8, 9]. It requires the combination of the relationship between the structural features of the fabric, fabric bending rigidity and the tensile/bending properties of the constituent yarns.

The applicability of mechanical modelling of the bending behavior of textile fabrics is very limited because it requires a large number of mechanical parameters and is, therefore, difficult to express in a closed form [5, 10, 11]. The most detailed analysis of the bending behaviour of plain-woven fabrics can be found in the typical works of Abbott et al. [12], De Jong and Postle [13], Ghosh et al. [14-16], Lloyd et al. [17]. The bending properties of woven fabrics have, therefore, received considerable attention in both literature and model experiments.

Let us consider a configured fabric sheet as illustrated in Figure 4.1. The numerical modelling results for non-dimensional transverse displacement results of a woven fabric sheet under uniform pressure, which was implemented for all mesh indices as listed in Table 4.2 and SDs = {1,2,3,4}, are presented for a SSSS/CCCC/SCSF plain-woven fabric sheet in case of length-to-thickness ratio for the first sample h_1/l and the second sample h_2/l .

The non-dimensional transverse displacement \bar{w} of the SSSS/CCCC/SCSF plain-woven fabric sheet is taken as follows

$$\bar{w} = w \frac{B}{Pl^4} \quad (4.1)$$

where w stands for transverse displacement, B is bending rigidity, P is uniform pressure and l is length in the bias direction of fabric sheet.

The numerical results for non-dimensional transverse displacements of the woven fabric sheet with various length-to-thickness ratio and boundary conditions, as well as various mesh densities are listed in Table 4.8, where S-FEM finite element are denoted by Q4SDSDs, with SDs standing for the number of smoothing domains per Q4 element, being that the corresponding standard FEM model that was implemented with MITC technique is denoted by MITC4.

Table 4.8: Non-dimensional bending displacement of a square fabric sheet with various mesh densities, under uniform pressure, simply-supported (SSSS), clamped (CCCC) and (SCSF) boundary conditions.

h/l	Mesh	CCCC			SSSS			SCSF		
		Q4SD1	Q4SD4	MITC4	Q4SD1	Q4SD4	MITC4	Q4SD1	Q4SD4	MITC4
0.0002	5x5	2.5373	2.4392	2.4082	7.5432	7.4077	7.3636	19.9474	19.755	19.6916
	10x10	2.9613	2.9352	2.9266	8.2677	8.2326	8.2210	21.2488	21.199	21.1824
	15x15	3.0041	2.9931	2.9894	8.2517	8.2364	8.2313	21.4161	21.3945	21.3872
	20x20	3.1766	3.1704	3.1684	8.4387	8.4300	8.4272	21.8543	21.8422	21.8381
	25x25	3.3213	3.3175	3.3162	8.5460	8.5405	8.5387	22.1843	22.1767	22.1742
	30x30	3.5313	3.5286	3.5277	8.7457	8.7419	8.7406	22.6472	22.6419	22.6402
	35x35	3.7455	3.7435	3.7429	8.9305	8.9277	8.9268	23.0973	23.0935	23.0923
	40x40	4.0077	4.0062	4.0058	9.1785	9.1763	9.1756	23.6419	23.6391	23.6381
0.0005	5x5	0.0264	0.0256	0.0253	0.0725	0.0712	0.0708	0.1732	0.1718	0.1713
	10x10	0.0421	0.0419	0.0418	0.0900	0.0896	0.0895	0.2069	0.2065	0.2064
	15x15	0.0603	0.0602	0.0601	0.1072	0.1071	0.1071	0.2395	0.2394	0.2393
	20x20	0.0869	0.0869	0.0869	0.1339	0.1339	0.1338	0.2846	0.2845	0.2845
	25x25	0.1198	0.1197	0.1197	0.1665	0.1664	0.1664	0.3380	0.3379	0.3379
	30x30	0.1607	0.1607	0.1607	0.2074	0.2074	0.2074	0.4029	0.4029	0.4029
	35x35	0.2082	0.2082	0.2082	0.2549	0.2548	0.2548	0.4776	0.4775	0.4775
	40x40	0.2638	0.2637	0.2637	0.3104	0.3104	0.3104	0.5639	0.5639	0.5639

Similar to the previous numerical examples, it can be found that the numerical results for non-dimensional transverse displacements of the woven fabric sheet with various length-to-thickness ratio and boundary conditions, as well as various mesh densities are approximated and accurate for the number of smoothing domains per Q4 element in range of $\{1,2,3,4\}$ with various boundary conditions. It clearly show the stable and well-balanced feature of the CS-FEM.

The numerical results for strain energy of non-dimensional transverse displacements between S-FEM and FEM are identical as illustrated in Figures 4.30 for thin fabric sample (h_1/l) and Figures 4.31 for moderately thick fabric sample (h_2/l). These figures indicate that S-FEM has a highly strain energy convergence for both the thin and moderately thick fabric sheets with different boundary conditions and mesh density under uniform pressure.

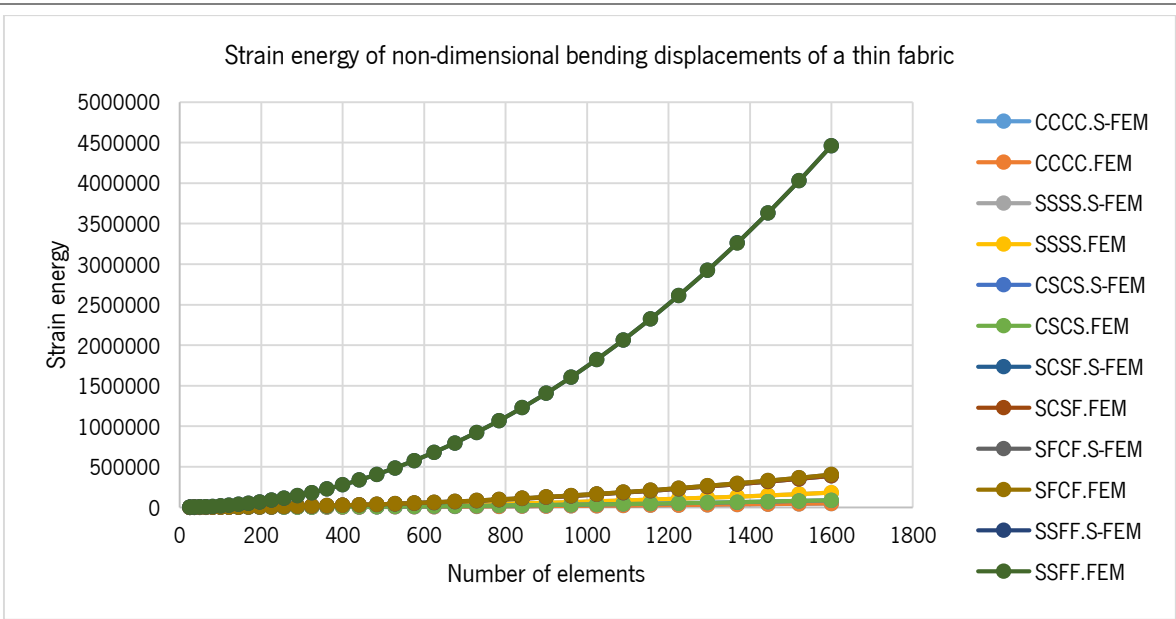


Figure 4.30: Numerical results for strain energy of non-dimensional transverse displacements of the plain-woven fabric sheet (h_1/l) with different mesh density and boundary conditions subjected uniform load.

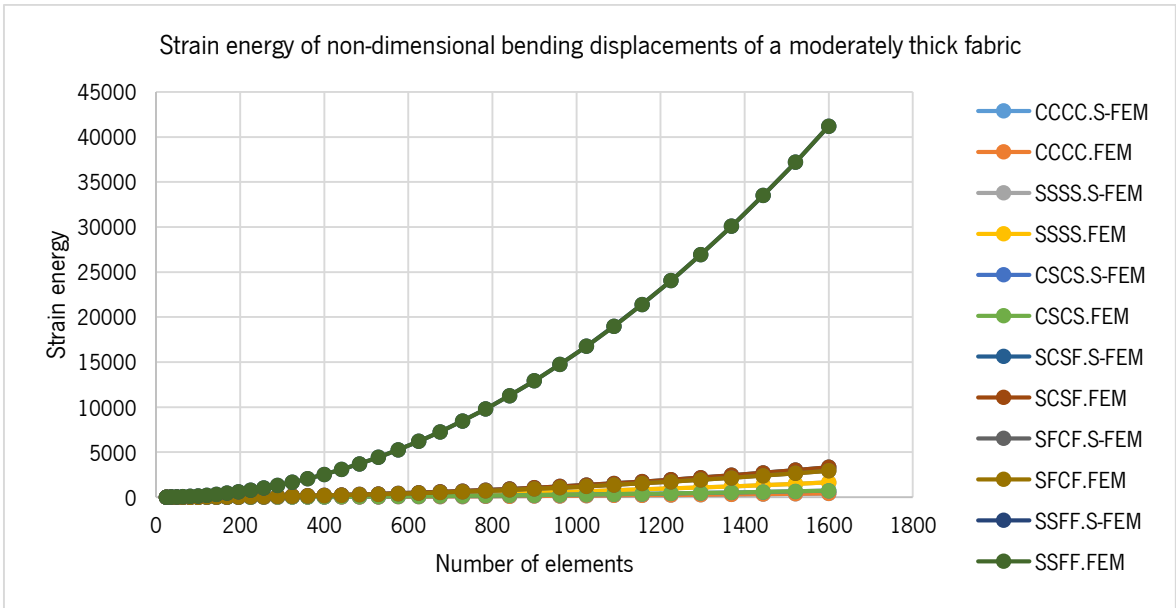


Figure 4.31: Numerical results for strain energy of non-dimensional transverse displacements of a plain-woven fabric sheet (h_2/l) with different mesh density and boundary conditions subjected uniform load.

Following the output numeric results as presented in above tables and figures, the low-stress mechanical deformation of fabric samples for a CCCC/SSSS/CSCS/SCSF/SFCF/SSFF plain-woven fabric sheet is illustrated in Figures 4.32 and 4.33. Similar to buckling modes and free-vibration modes in previous numerical examples, these figures once again express that the Q4 elements (Q4 mesh) implemented by S-FEM is well refined, less distorted and not coarse even with low mesh density and various boundary conditions under uniform pressure.

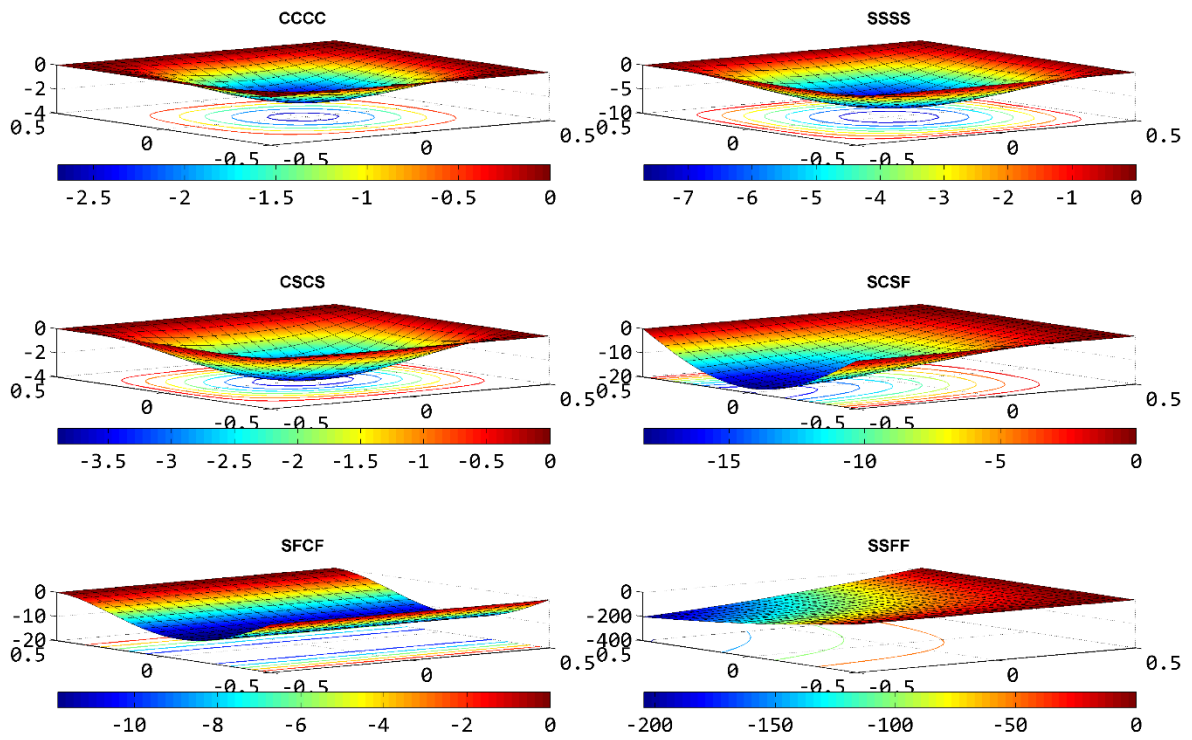


Figure 4.32: Bending behavior of plain-woven fabric sheet with h_2/l , using 20×20 Q4 elements and 1 smoothing domains per element with different boundaries.

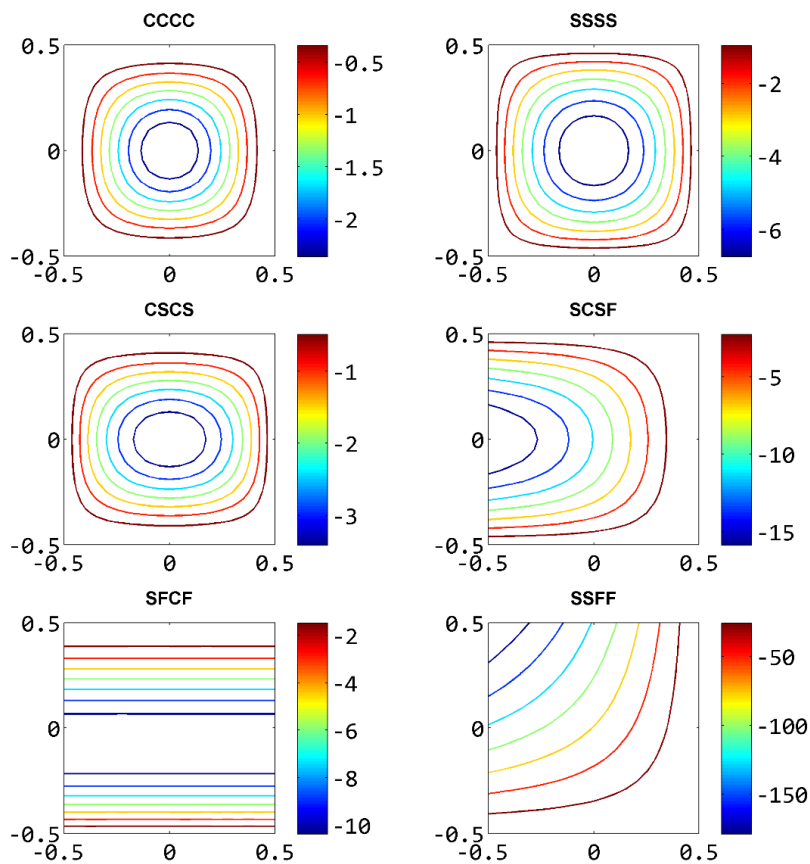


Figure 4.33: Resultant displacement magnitude for bending behavior of plain-woven fabric sheet with h_2/l .

4.1.4 Plane-stress problems of woven fabric

Tensile properties are considered as the most important factor that govern the performance characteristics of textile fabrics [18]. The investigation of tensile properties encounters many difficulties due to the complexity of fabric structure leading to variation strain during deformation [19]. In general, each fabric sheet consists of a large amount of constituent fibers and yarns which will response subsequently to a series of complex movements under any deformation state. This makes the mechanical properties of textile fabrics more complicated due to both fibers and yarns behaving in a non-Hookean law during deformation and presenting hysteresis effect [20].

Peirce (1937) [21] was the pioneer in the investigation of tensile properties of woven fabrics. He proposed a geometrical model in which the cross-section of the yarns in the fabrics is assumed as circular, but this assumption is highly theoretical. This model was modified by many researchers in order to analyze tensile behaviour of woven fabric. For example, Grosberg and Kedia (1966) [22] analyzed the small strain under the initial load-extension curve, while Weissenberg (1949) [23] introduced the trellis model in which the theory of strain, stress and the relationship between them and the Poisson's effect are defined.

Chadwick et al. (1949) [24] studied the deformation of a woven fabric in the bias direction applying the trellis model under a simple pull. Their study indicated that the warp and weft yarns deforms not only in the principal direction of pull but also in length and spacing under bias extension. Cooper (1963) [25] examined the relationship between extension and shear in bias direction of yarns. Kilby (1963) derived elasticity moduli of woven fabric in any direction other than the directions of warp and weft yarns. He showed that bias extension is related to shear modulus. Spivak et al. (1968) [26] presented an analysis of the geometrical tests of bias extension and simple shear for plain woven fabric which indicated that it is impossible to predict the complete stress-strain properties of a fabric in simple shear from measurements of bias extension.

Anandjiwala and Leaf (1991) [27, 28] mainly focused on the tensile and shear moduli of plain-woven fabrics. There are no numerical models to be found in prediction of the anisotropic properties of fabric tensile using mechanical properties obtained from KES-FB (Kawabata Evaluation System for Fabric), such as tensile work (WT), tensile elongation (EMT), tensile linearity (LT) and tensile resilience (RT).

Kawabata and Bassett used a numerical linearization method for modelling of the biaxial tensile stress-strain relation of fabrics and Kageyama et al. (1988) verified this validity [29]. Bassett (1988) [30]

determined constitutive laws of fabrics and used these properties to calculate stress-strain in garment-like systems. The work of Kawabata and Bassett uses very complicated procedures and it is still related to implementation of function between tensile stress and tensile strain for deformation of woven fabrics.

In this numerical example, macro-mechanical modelling of tensile deformation of woven fabrics aims to examine the proposed CS-FEM models via evaluation of the distortion and coarseness of Q4 membrane element, as presented in Section 3.5. Let us consider a configured fabric sheet as illustrated in Figure 4.34.

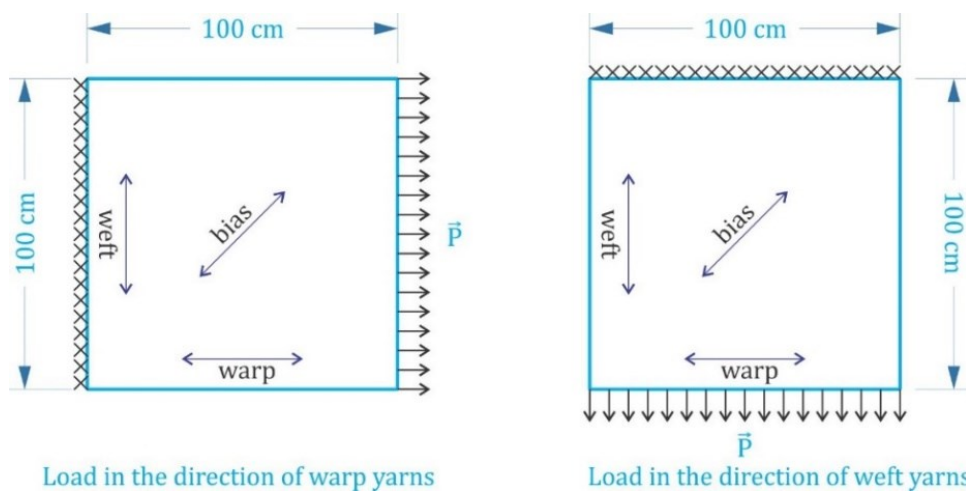


Figure 4.34: Configuration of tensile stress and tensile strain, uniaxial applied force in the direction of warp and weft yarns.

For numerical examples of modelling of tensile behavior of plain-woven fabric sheet, Figure 4.1 is reconfigured according to uniaxial applied force in the direction of warp and weft yarns as shown in Figure 4.34.

Numerical examples for modelling of tensile behavior also produced a highly accurate numerical results implemented by the number of smoothing domains per Q4 element in range of {1,2,3,4}, which clearly show the stable and well-balanced feature of the S-FEM. Besides, S-FEM also possesses fast strain energy convergence for both the thin and moderately thick fabric sheets with the prescribed boundary conditions and various mesh densities. In order to demonstrate mesh density, only geometrical results are presented in this experiment.

Numerical results for the plane-stress deformations, resultant load vectors and magnitude of the plane-stress of a plain-woven fabric sheet with h_1/l , under uniaxial applied force in warp direction, using 70×70 Q4 elements and 4 smoothing domains per element are presented in Figure 4.35 to 4.40.

For a plain-woven fabric sheet with h_2/l , numerical results for the plane-stress deformations, resultant load vectors and magnitude of the plane-stress are presented in Figure 4.41 to 4.46.

Figures 4.35, 4.38, 4.41 and 4.44 exhibit that the Q4 membrane elements implemented by S-FEM are well refined, less distorted and not coarse even with low mesh density and complex deformed. Note that fabric samples are deformed according to uniaxial applied force in the direction of warp and weft yarns in this experiment, while fabric samples are deformed according to uniform pressure, as in previous experiments of fabric buckling and bending.

The numerical results also show that more mesh density is refined, more the numerical modelling are accurately and realistic, as well as CPU time increases exponentially with the DOFs (Degrees of Freedom), as presented in Section 4.2.2.

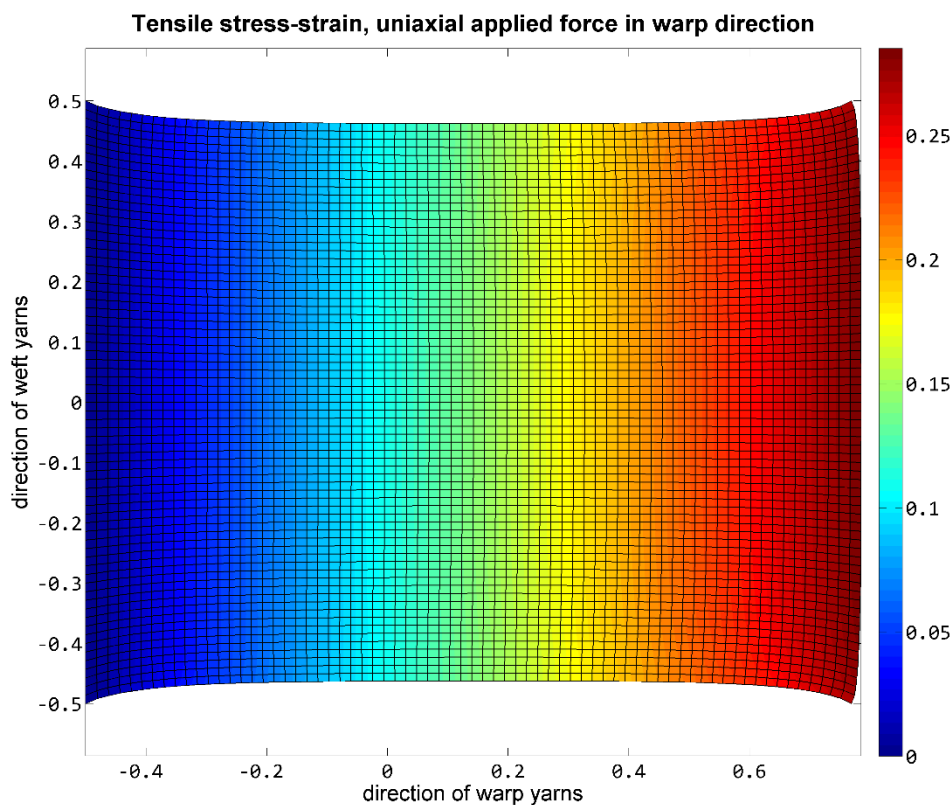


Figure 4.35: The plane-stress deformation of a plain-woven fabric sheet with h_1/l , under uniaxial applied force in warp direction, using 70×70 Q4 elements and 1 smoothing domains per element.

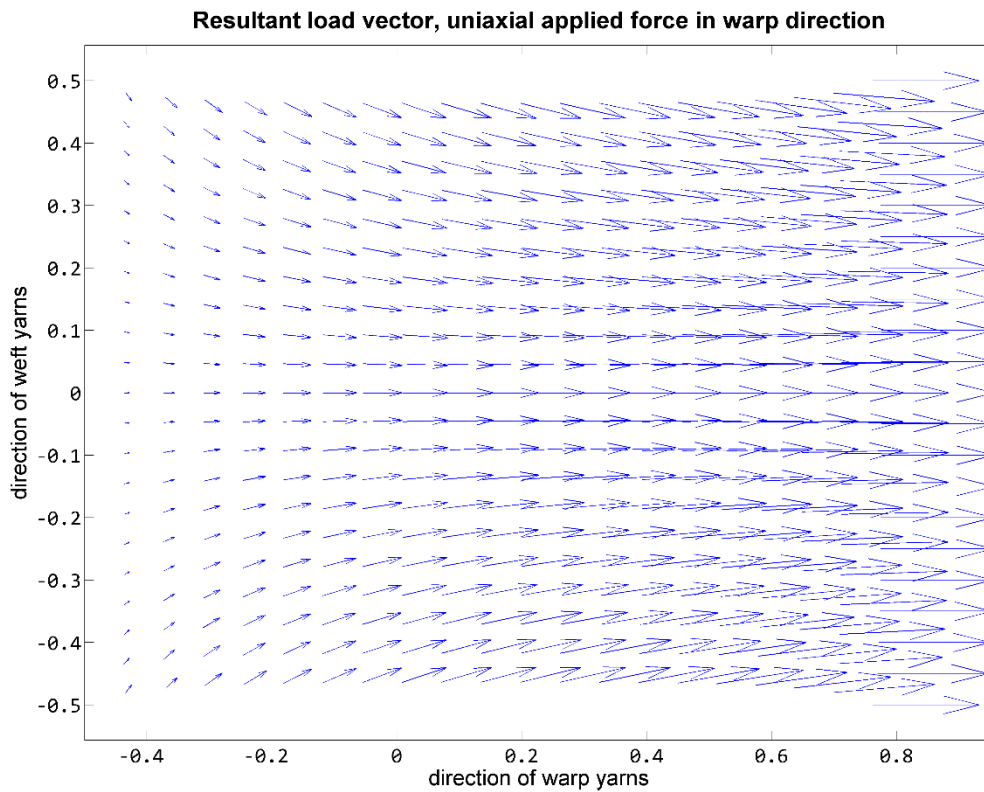


Figure 4.36: Resultant load vector for plane-stress deformation of a plain-woven fabric sheet with h_1/l , under uniaxial applied force in warp direction.

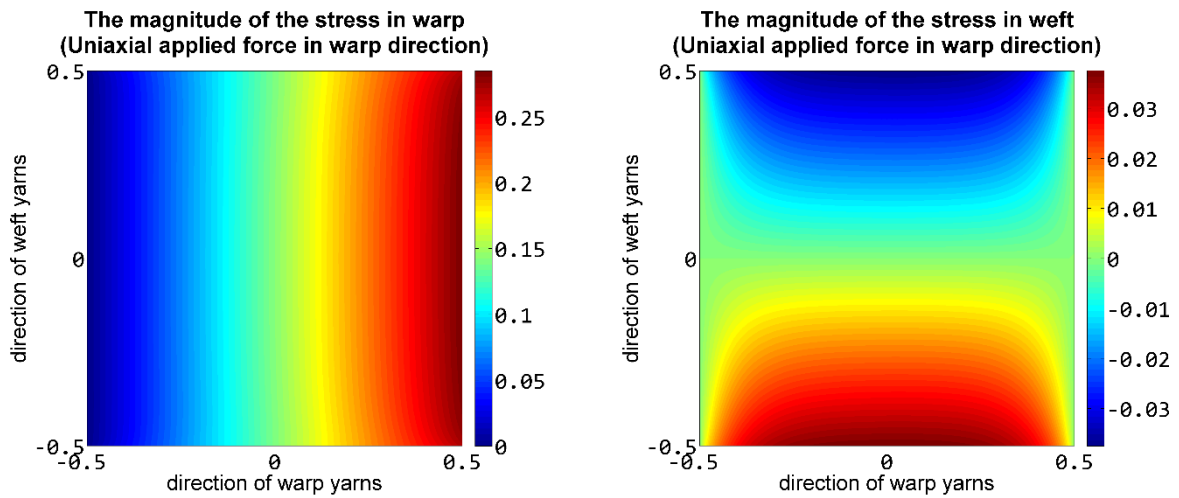


Figure 4.37: The magnitude of the stress of a plain-woven fabric sheet with h_1/l , under uniaxial applied force in warp direction.

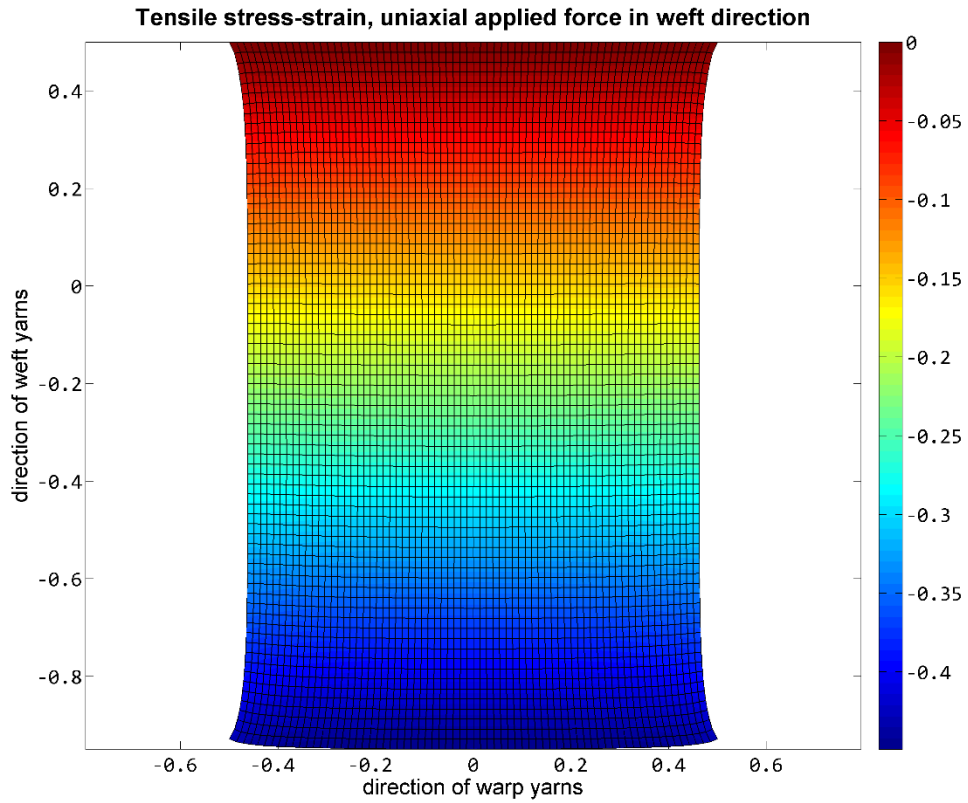


Figure 4.38: The plane-stress deformation of a plain-woven fabric sheet with h_1/l , under uniaxial applied force in weft direction, using 70×70 Q4 elements and 1 smoothing domains per element.

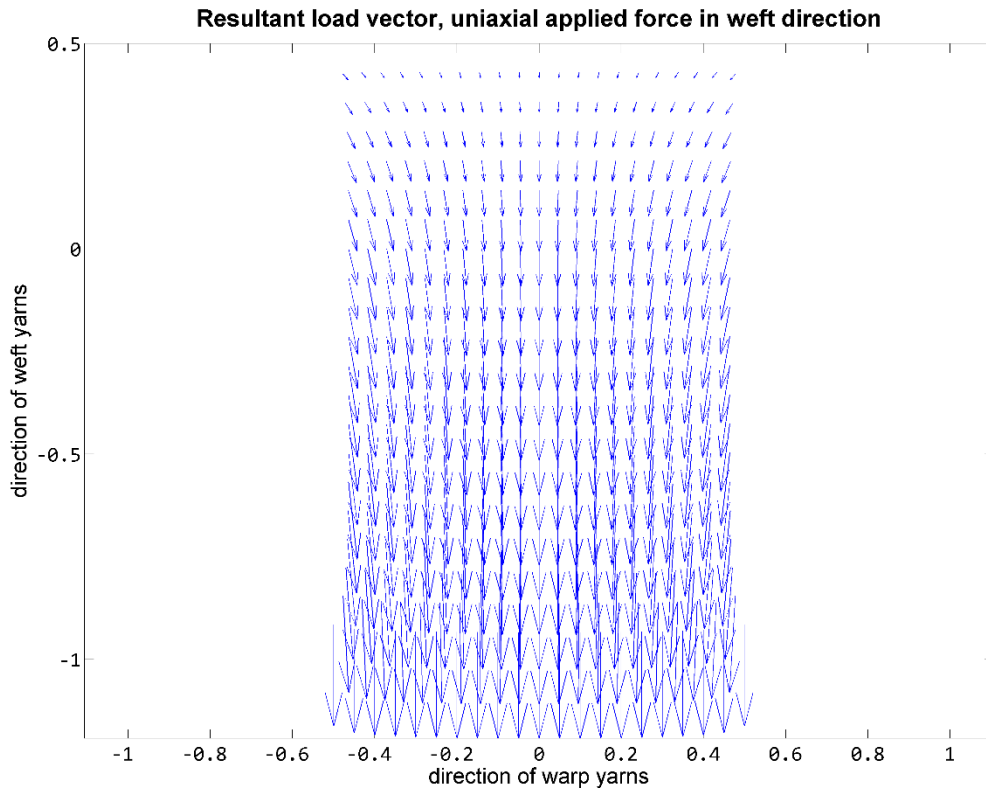


Figure 4.39: Resultant load vector for plane-stress deformation of a plain-woven fabric sheet with h_1/l , under uniaxial applied force in weft direction.

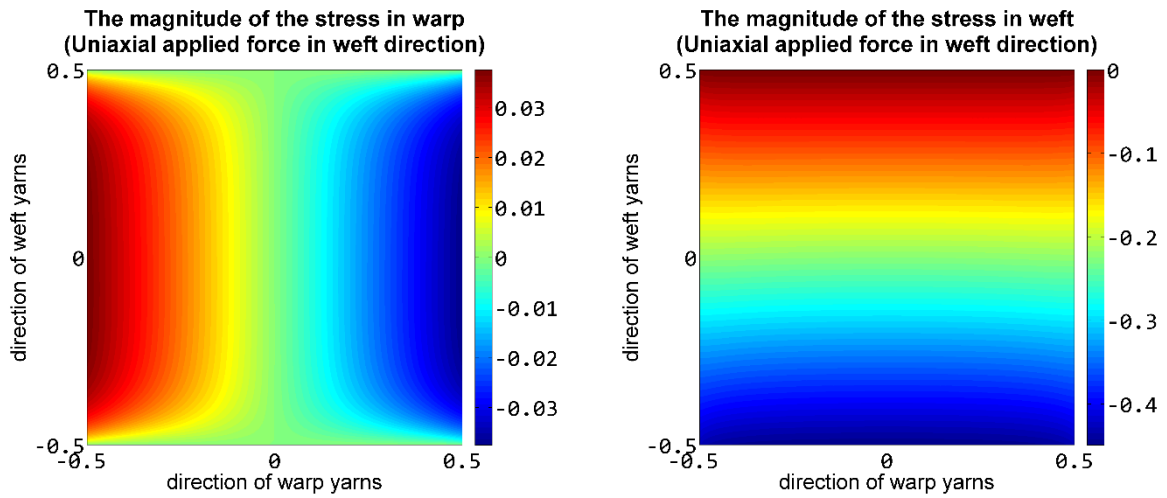


Figure 4.40: The magnitude of the stress of a plain-woven fabric sheet with h_1/l , under uniaxial applied force in weft direction.

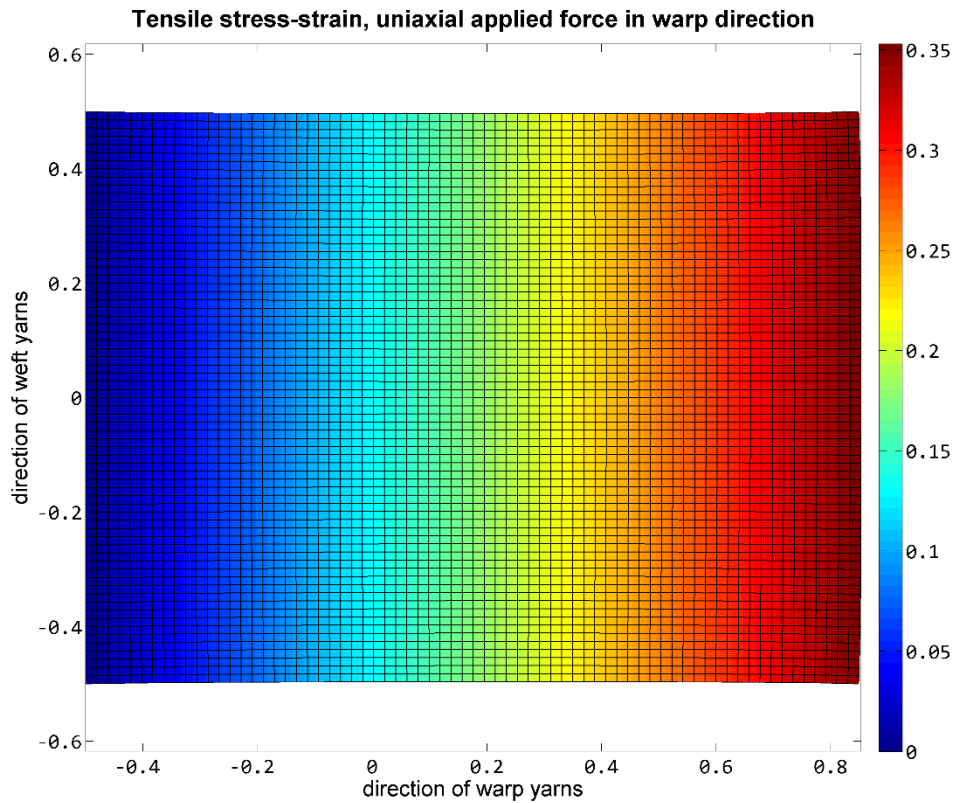


Figure 4.41: The plane-stress deformation of a plain-woven fabric sheet with h_2/l , under uniaxial applied force in warp direction, using 70×70 Q4 elements and 1 smoothing domains per element.

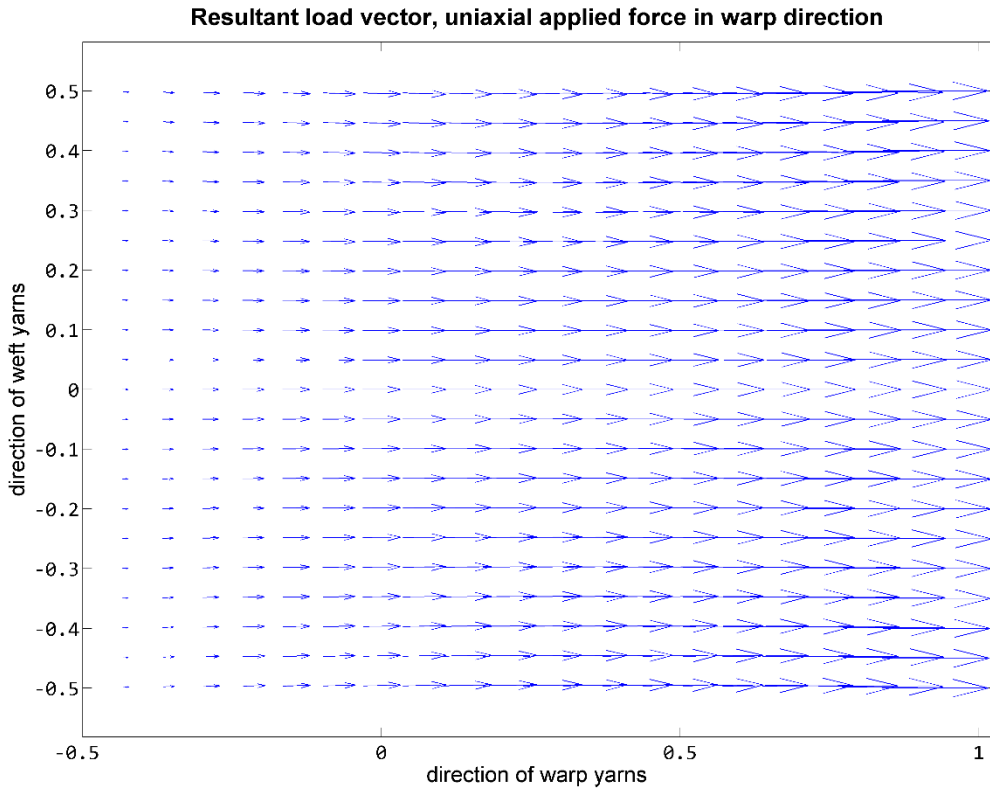


Figure 4.42: Resultant load vector for plane-stress deformation of a plain-woven fabric sheet with h_2/l , under uniaxial applied force in warp direction.

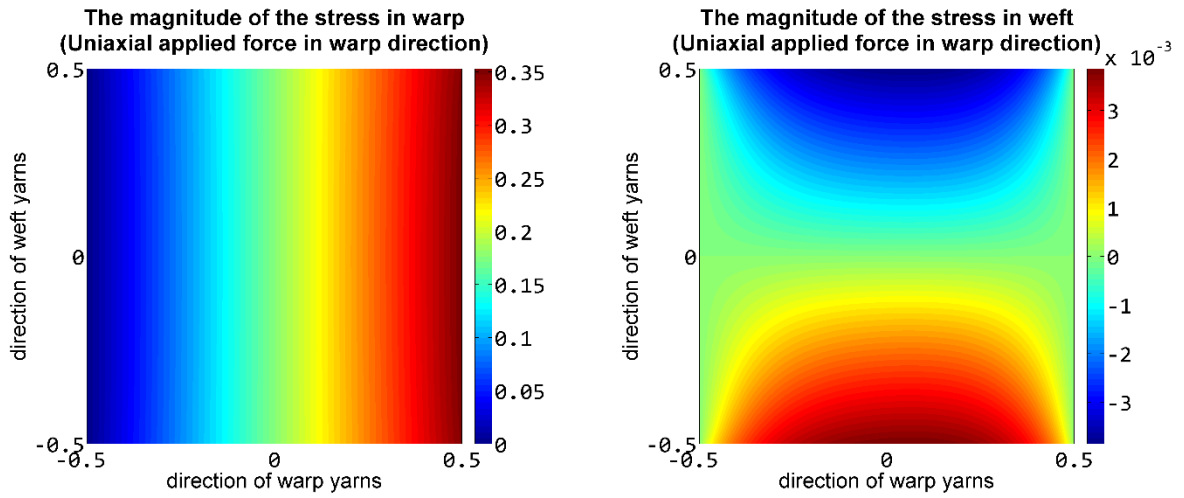


Figure 4.43: The magnitude of the stress of a plain-woven fabric sheet with h_2/l , under uniaxial applied force in warp direction.

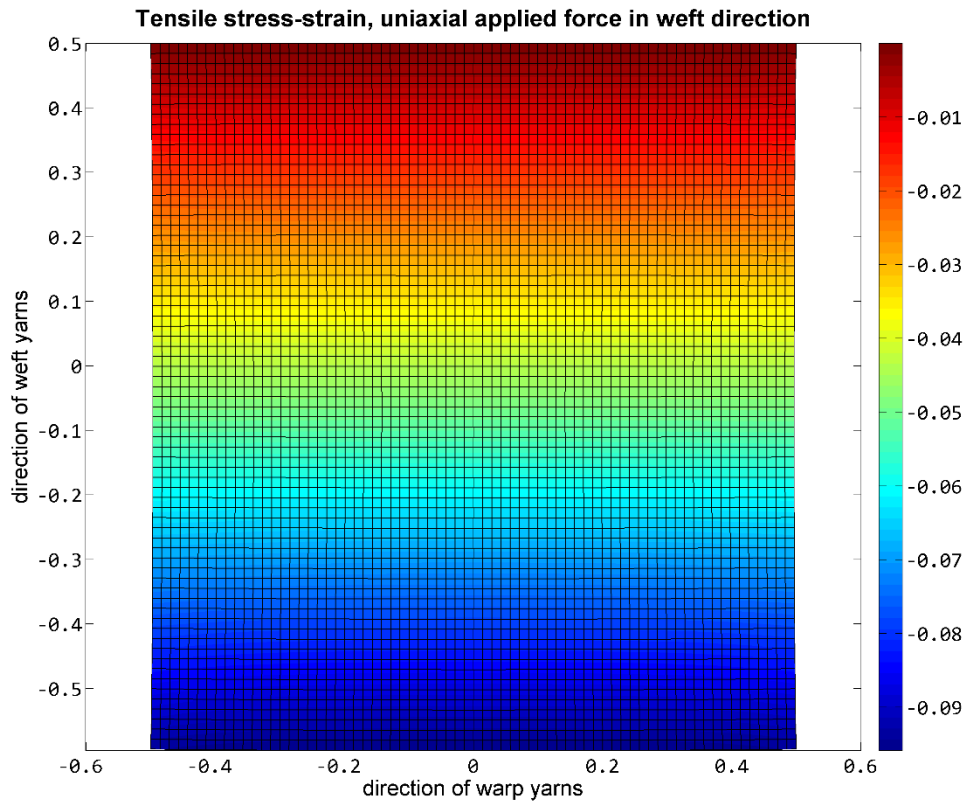


Figure 4.44: The plane-stress deformation of a plain-woven fabric sheet with h_2/l , under uniaxial applied force in weft direction, using 40×40 Q4 elements and 1 smoothing domains per element.

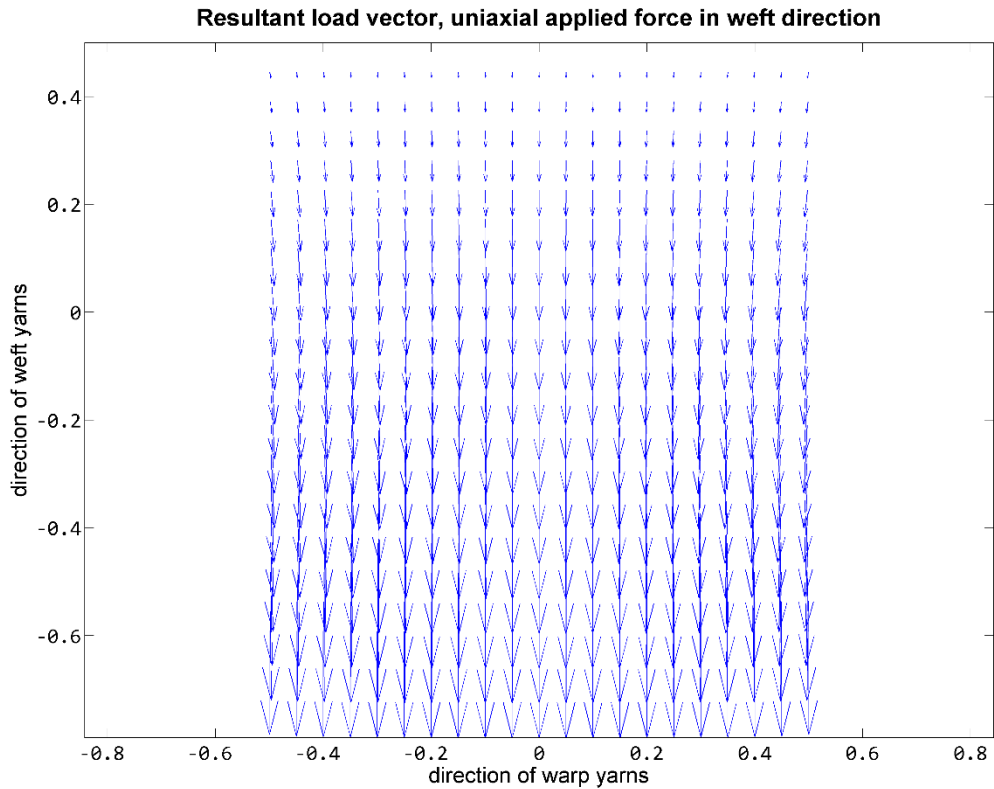


Figure 4.45: Resultant load vector for plane-stress deformation of a plain-woven fabric sheet with h_2/l , under uniaxial applied force in weft direction.

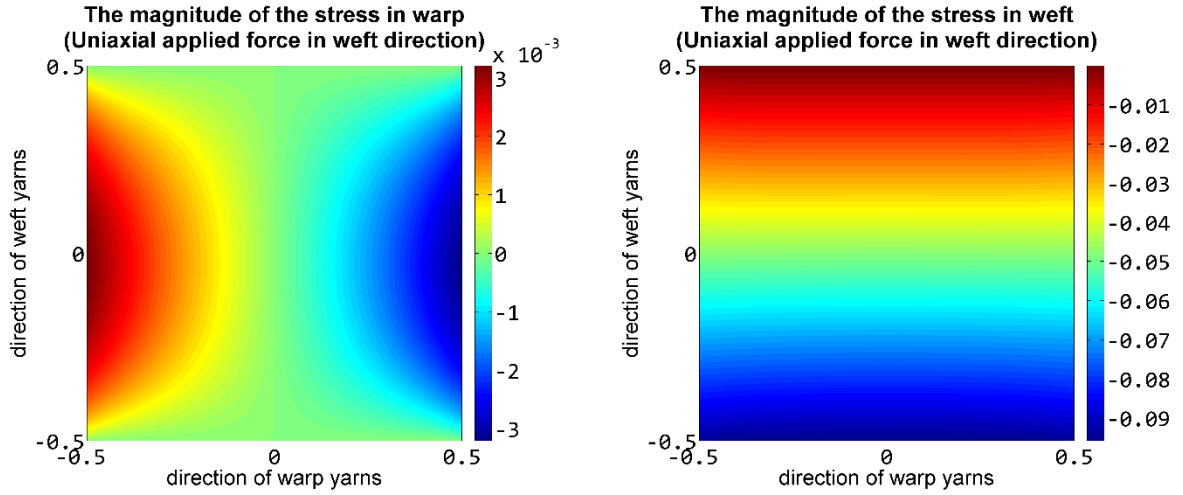


Figure 4.46: The magnitude of the stress of a plain-woven fabric sheet with h_2/l , under uniaxial applied force in weft direction.

4.2 Discussions

4.2.1 Number of smoothing domains

Numerical examples indicated that the used number of smoothing domains per 4-node isoparametric quadrilateral element in range of $\{1,2,3,4\}$ is approximated to that one of 4-node isoparametric quadrilateral element with one-point quadrature in evaluation of element strain-displacement matrix. Through numerical examples, it is found that from one to four smoothing domains for bending strain energy integration and one for shear strain energy integration per element produces identical solutions compared with the existing FEM techniques.

Numerical examples also indicated that the stiffness matrix of 4-node quadrilateral element implemented with 1 smoothing domain per Q4 element (Q4SD1) in CS-FEM is identical to the corresponding standard FEM using the reduced integration that is evaluated by one Gauss point. Therefore, the non-local strain displacement components as given in Equations (3.77, 3.100) can be rewritten as follows

$$\bar{b}_{klx} = \frac{1}{2A^e} (n_{xi}l_i + n_{xj}l_j) \quad (4.2a)$$

$$\bar{b}_{kly} = \frac{1}{2A^e} (n_{yi}l_i + n_{yj}l_j) \quad (4.2b)$$

where A^e stands for the area of element Ω^e , n_{xi} and n_{yi} stand for the normal vector on edge l_i , the indices i and j are defined by a recursive rule such that $ij = \{14, 21, 32, 43\}$. Thus, the smoothed

strain/gradient matrix in Equations (3.82, 3.102) can be implemented and evaluated in terms of one smoothing domain per 4-node Q4 element as follows

$$\bar{\mathbf{B}}^b = \frac{1}{2A^e} \begin{bmatrix} 0 & 0 & y_{24} & 0 & 0 & y_{31} & 0 & 0 & y_{42} & 0 & 0 & y_{13} \\ 0 & x_{24} & 0 & 0 & x_{31} & 0 & 0 & x_{42} & 0 & 0 & x_{13} & 0 \\ 0 & y_{42} & x_{42} & 0 & y_{13} & x_{13} & 0 & y_{24} & x_{24} & 0 & y_{31} & x_{31} \end{bmatrix} \quad (4.3)$$

$$\bar{\mathbf{B}}^m = \frac{1}{2A^e} \begin{bmatrix} y_{24} & 0 & y_{31} & 0 & y_{42} & 0 & y_{13} & 0 \\ 0 & x_{42} & 0 & x_{13} & 0 & x_{24} & 0 & x_{31} \\ x_{42} & y_{24} & x_{13} & y_{31} & x_{24} & y_{42} & x_{31} & y_{13} \end{bmatrix} \quad (4.4)$$

where $x_{ij} = x_i - x_j$ and $y_{ij} = y_i - y_j$.

Note that Equations (4.3, 4.4) applies to 4-node Q4 element that is implemented with one smoothing domain.

4.2.2 CPU time variation

To better expose the influence of the cost of computation times on the numerical simulation results of bending behavior of a plain-woven fabric sheet using S-FEM, it was implemented a series of 4-node isoparametric quadrilateral plate/shell elements with varying number of system DOFs (System Degrees of Freedom) while recording the CPU-time variation for different number of smoothing domains per element such that $SDs = \{1,2,3,4\}$, as shown in Figure 4.47. Besides, it was also implemented the corresponding standard FEM models in order to indicate the difference of the cost of computation times between the developed S-FEM models and standard FEM models.

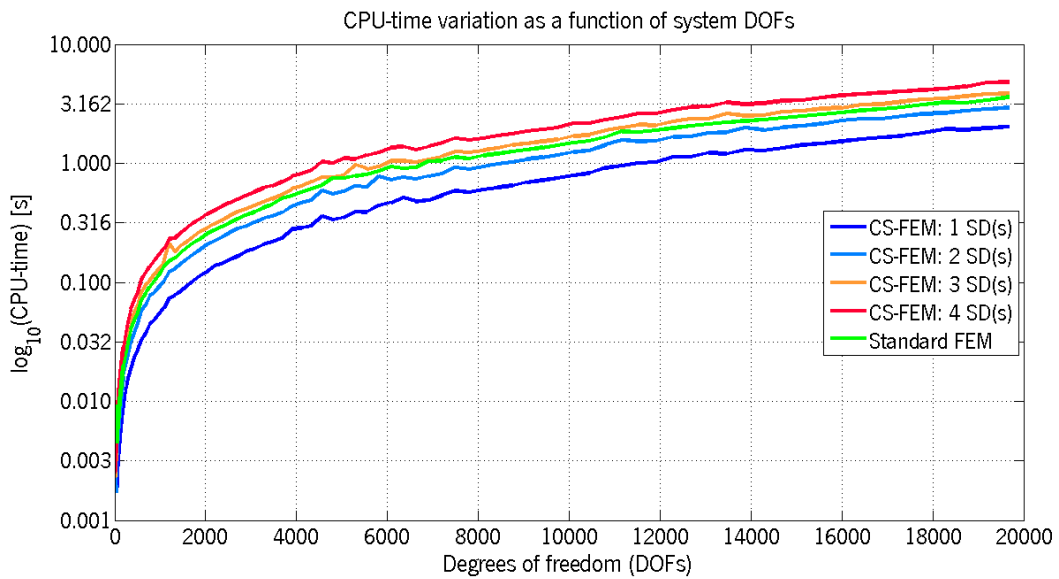


Figure 4.47: Recorded of CPU time on the numerical simulation results of bending behavior of a plain-woven fabric sheet using S-FEM and standard FEM.

The benchmark results have numerically indicated that one smoothing domain ($SDs = 1$) per Q4 element is the best solution in terms of CPU time when compared with standard FEM, while four smoothing domains ($SDs = 4$) per Q4 element is more expensive in CPU time.

A decrease occurs in cost of computation time for the evaluation of gradient matrix, stiffness and geometric matrices of membrane, and curvature element can be applied by the fact that the shape functions of a 'smoothed' Q4 element are constant, while the shape functions of an Q4 element are those of bilinear Lagrange shape functions in natural coordinates (ξ, η, ζ) that are needed to be transformed into Cartesian coordinates (x, y, z) when one evaluates strain gradient matrix. This requires a Jacobian transformation matrix and needs to be evaluated by one or more Gauss points. Thus S-FEM gives a better solution in terms of CPU time and high accuracy when compared with standard FEM.

4.3 Final remarks

Numerical results of low-stress mechanical deformations of woven fabric have confirmed the following features of our method:

- Although the transverse shear contribution for the geometric stiffness matrix is negligible for thin woven fabric sheet, its effects can be significant for thick woven fabric.
- S-FEM shows that field gradients of smoothing domains of elements are evaluated directly only using their shape functions without derivative such that reduce the requirement on the smoothness of shape functions. Moreover, the shape functions are established in a trivial, simple and explicit manner.
- S-FEM gives a better solution in terms of CPU time, and has a higher accuracy and strain energy convergence for both the thin and moderately thick fabric sheet when compared with standard FEM. One smoothing domain ($SDs = 1$) per Q4 element is the best solution in terms of CPU time when compared with standard FEM. However, depending on the requirement on the accuracy and stability, each finite element may be further subdivided into a finite number of smoothing domains; in particular, dividing a quadrilateral element can be divided into four smoothing domains can avoid the spurious zero-energy mode.
- Q4 elements, including membrane element, plate and flat shell elements, that are implemented by S-FEM is well refined, less distorted and not coarse even with low mesh density and complex deformed.

-
- S-FEM via CS-FEM models are well appropriate for numerical modelling and simulation in predicting the mechanical deformation behaviour of the textile fabrics, as needed in cloth simulation, which will lead to the perspective of widely accepted and integrated S-FEM models into FEA/CAE environment for textile fabric engineering.

So, the application of FOM and S-FEM to displacement-based low-order finite element formulations based on quadrilateral plate/shell finite element models are well appropriate for numerical modelling and simulation in predicting the mechanical deformation behaviour of the textile fabrics.

4.4 References

1. Beskos, D.E., G.D. Manolis, and D. Polyzos, *Recent Advances in Boundary Element Methods: A Volume to Honor Professor Dimitri Beskos*. 2009: Springer.
2. Saville, B.P., *Physical testing of textiles*. Woodhead Textiles Series. 1999: Woodhead Publishing Ltd.
3. Sherburn, M., *Geometric and Mechanical Modelling of Textiles*. 2007, University of Nottingham.
4. Behery, H.M., *Effect of mechanical and physical properties on fabric hand*. 2005, North America by CRC Press LLC: Woodhead Publishing Limited
5. Hu, J., *Structure and mechanics of woven fabrics*. 2004, Cambridge: Woodhead Publishing Ltd.
6. Hu, J., *Fabric Testing*. Woodhead Textiles Series. 2008: Woodhead Publishing Ltd.
7. Lutz Walter, G.-A.K., Stefano Carosio, *Transforming Clothing Production into a Demand-driven, Knowledge-based, High-tech Industry*. 2009: Springer-Verlag London Limited.
8. Brown, P.R.B., D. R, and T.G. Clapp, *Large-deflection Bending of Woven Fabric for Automated Material-Handling*. Textile Research Journal, 1990(81): p. 1-14.
9. Eischen, J.W. and D. Dawson, *Automated Three Dimensional Fabric Part Handling*.
10. Veit, D., *Simulation in textile technology: Theory and applications*. 1 ed. Woodhead Publishing Series in Textiles. 2012: Woodhead Publishing.
11. Patanaik, A., *Modeling and Simulation in Fibrous Materials*. 1 ed. 2012: Nova Science Publishers, Inc.
12. Abbott, G.M., P. Grosberg, and G.A.V. Leaf, *The elastic resistance to bending of plain-woven fabrics*. The Journal of The Textile Institute, 1973. **64**(6): p. 346-362.
13. de Jong, S. and R. Postle, *An energy analysis of woven-fabric mechanics by means of optimal-control theory part II: Pure-bending properties*. The Journal of The Textile Institute, 1977. **68**(11): p. 362-369.
14. Ghosh, T.K., S.K. Batra, and R.L. Barker, *The Bending Behaviour of Plain-woven Fabrics Part I: A Critical Review*. The Journal of The Textile Institute, 1990. **81**(3): p. 245-254.
15. Ghosh, T.K., S.K. Batra, and R.L. Barker, *The Bending Behaviour of Plain-woven Fabrics Part II: The Case of Linear Thread-bending Behaviour*. The Journal of The Textile Institute, 1990. **81**(3): p. 255-271.
16. Ghosh, T.K., S.K. Batra, and R.L. Barker, *The Bending Behaviour of Plain-woven Fabrics Part III: The Case of Bilinear Thread-bending Behaviour and the Effect of Fabric Set*. The Journal of The Textile Institute, 1990. **81**(3): p. 272-287.
17. Lloyd, D.W., W.J. Shanahan, and M. Konopasek, *The folding of heavy fabric sheets*. International Journal of Mechanical Sciences, 1978. **20**(8): p. 521-527.
18. Fan, J., W. Yu, and L. Hunter, *Clothing appearance and fit: Science and technology*. Woodhead Publishing in Textiles. 2004: CRC.
19. Hearle, J.W.S., J.J. Thwaites, and J. Amirbayat, *Mechanics of flexible fibre assemblies*. NATO advanced study institutes series: Applied sciences. 1980: Sijthoff & Noordhoff.
20. Konopasek, M.H.J.W.S.U.D.o.T., *Improved procedures for calculating the mechanical properties of textile structures*. 1970, UMIST: Manchester.
21. Peirce, F.T., *The geometry of cloth structure*. Journal of the Textile Institute, 1937. **28**: p. 43-77.
22. Grosberg, P. and S. Kedia, *The Mechanical Properties of Woven Fabrics: Part I: The Initial Load Extension Modulus of Woven Fabrics*. Textile Research Journal, 1966. **36**(1): p. 71-79.

-
23. Weissenberg, K., *The use of a trellis model in the mechanics of homogeneous materials*. Journal of the Textile Institute Transactions, 1949. **40**(2): p. T89-T110.
 24. Chadwick, G.E., S.A. Shorter, and K. Weissenberg, *A trellis model for the application and study of simple pulls in textile materials*. Journal of the Textile Institute Transactions, 1949. **40**(2): p. T111-T160.
 25. Cooper, D.N.E., *A Bias Extension Test*. Textile Research Journal, 1963. **33**(4): p. 315-317.
 26. Spivak, S.M., *The Behavior of Fabrics in Shear: Part I: Instrumental Method and the Effect of Test Conditions*. Textile Research Journal, 1966. **36**(12): p. 1056-1063.
 27. Anandjiwala, R.D. and G.A.V. Leaf, *Large-Scale Extension and Recovery of Plain Woven Fabrics: Part I: Theoretical*. Textile Research Journal, 1991. **61**(11): p. 619-634.
 28. Anandjiwala, R.D. and G.A.V. Leaf, *Large-Scale Extension and Recovery of Plain Woven Fabrics: Part II: Experimental and Discussion*. Textile Research Journal, 1991. **61**(12): p. 743-755.
 29. Kageyama, M., S. Kawabata, and M. Niwa, *The Validity of a "Linearizing Method" for Predicting the Biaxial-extension Properties of Fabrics*. The Journal of The Textile Institute, 1988. **79**(4): p. 543-567.
 30. Bassett, R.J., *The Biaxial Tensile and Shear Properties of Textile Fabrics and Their Application to the Study of Fabric Tailorability*. 1982: The Author.

In this thesis, the formulation of fabric constitutive laws based on the fabric objective measurement technology (FOM) and Kawabata evaluation system for fabric (KES-FB) have been presented. In addition, a class of novel and robust displacement-based low-order finite element formulations for mechanical modelling of textile fabric at sheet level have been also formulated and proposed. The finite elements are based on the Mindlin-Reissner theory (i.e., the so-called first-order shear deformation theory) and smoothed finite element methods (S-FEM) via the strain smoothing technique of the stabilized conforming nodal integration mesh-free method.

5.1 Research outcomes

In respect to fabric objective measurement (FOM), a major research outcome has been attained with the successful formulation and implementation of fabric constitutive laws using low-stress mechanical properties that are applicable for macro-mechanical modelling of the textile fabrics of both non-woven and woven fabrics in terms of elastic material with both isotropy and orthotropic anisotropy. In particular, the transverse shear modulus is approximated by using low-stress compression properties via KES-FB. These constitutive equations are used for displacement-based low-order finite element formulations of plate and shell finite element.

In the numerical modelling and simulation of the textile fabrics, another important research outcome is the successful formulation and implementation of two simple, robust, and high-performance low-order quadrilateral plate and flat shell elements for macro-mechanical modelling of general textile fabric sheet that have the advantage of being applicable to thin to moderately thick fabric, being at the same time less time-consuming, but even so accurate.

The new displacement-based low-order flat quadrilateral plate/shell finite elements have some advanced properties due to be inherited from the strain smoothing technique of the stabilized conforming nodal integration mesh-free method and the mixed interpolation of tensorial components approach as follows:

-
- The formulated finite elements are reliable and have good predictive capability in modelling arbitrary deformed geometries of thin to moderately thick fabric because they are based on the equivalent single-layer and first-order shear deformation theory.
 - The decrease in cost of computation time for the evaluation of gradient matrix, stiffness and geometric matrices of membrane and curvature element is mainly due to be computed by integration along the boundary of smoothing elements, what is in contrast to domain integration.
 - The developed thin plate/shell elements are free from membrane and shear locking without any spurious zero-energy modes. These elements not only optimize shape distortion but also optimize accuracy even with coarse meshes or warping geometries. Besides, these elements also imply the convergence of solutions with mesh refinement.

Numerical simulations have been studied and demonstrated in textile engineering involving analysis of mechanical deformation of fabric sheet in terms of plate/shell structures with various geometric shapes and materials. The numerical results have demonstrated the robustness and accuracy of numerical methods for various applications of macro-mechanical modelling of textile fabric, including plane-stress, bending, buckling and free vibration analysis. The numerical results also have provided a definitive and better understanding of the effect of modulus ratios, yarn orientations and different mixed boundary conditions on the mechanical behaviour of woven fabric. Finally, the smoothed finite element methods (S-FEM), together with fabric objective measurement technology (FOM) that satisfies to low-stress mechanical properties of fabric via Kawabata evaluation system for fabric (KES-FB) are in agreement with objectives of this study, which is to find a numerical solution that offer a lower computational cost but effective performance in comparison with more conventional finite elements for modelling and simulation of mechanical behavior of textile fabrics.

5.2 Limitations

Despite FOM technology via KES-FB system is able to meet the requirements in the formulation of fabric constitutive laws in this research, there are some limitations in experimental analysis of mechanical properties of fabric such as the lack of tester for measuring the Poisson's effect, which is important in many engineering applications and computer simulations of technical textile fabrics. Besides, there is also the lack of a tester for measuring the damping effect factor of fabric.

The computational implementation of S-FEM served mostly to assess the applicability of theoretical ideas, meaning that, in its current stage of development, the use of S-FEM by an external analyst is hindered by the lack of a unified and fully automatic analysis tool. In fact, this is in general the case for S-FEM, which is still a very rare presence in commercially available FEA computer applications and almost non-existent in general purpose open-source platforms.

5.3 Future works

Despite the objectives of this research has been attained, there are many issues that must continue to develop and improve in the future. In respect to fabric objective measurement (FOM), we have in mind the following research goals (or specific objectives):

- For numerical modelling of mechanical deformation behavior of both single and multilayer woven fabric composite materials, we will continue to develop fabric constitutive laws that are based on fabric objective measurement via high-stress mechanical properties.
- For numerical modelling of heat transfer properties of woven fabrics and woven fabric composite materials, fabric constitutive laws will be developed by using mechanical properties measured via ASTM's textile standards.

We also intend to pursue the following research lines to the future development of S-FEM models of this work:

- To adapt the developed finite element computer codes for modelling and simulation of draping behavior of textile fabric, especially for wearing models.
- To continue to develop the finite element computer codes for S-FEM models that bases on GPU computing in order to save computer time for complex analysis of fabric and cloth.
- To continue to improve the developed CS-FEM models and the other S-FEM models, e.g. NS-FEM and ES-FEM, for geometrical non-linear finite element analysis of textile fabrics under the complex boundary conditions.

5.4 Final remarks

The application of FOM and S-FEM to displacement-based low-order finite element formulations based on quadrilateral plate/shell finite element models offer a lower computational cost but effective performance and higher accurate in comparison with more conventional finite elements for modelling and simulation of mechanical behavior of thin to moderately thick textile fabric.

The application of FOM and S-FEM are well appropriate for numerical modelling and simulation in predicting the mechanical deformation behaviour of the textile fabrics, as needed in cloth simulation, which will lead to the perspective of widely accepted and integrated S-FEM models into FEA/CAE environment for textile fabric engineering.

In conclusion, we are able to state that application of FOM and S-FEM to displacement-based low-order finite element formulations based on quadrilateral plate/shell finite element models are well appropriate for numerical modelling and simulation in predicting the mechanical deformation behaviour of the textile fabrics, as needed in cloth simulation, which will lead to the perspective of widely accepted and integrated S-FEM models into FEA/CAE environment for textile fabric engineering.